

NO ECHT-102-
FRAC-URE-
D-10502A
SO-2A10M

LEHIGH UNIVERSITY



HYDROGEN ADSORPTION AND DIFFUSION, AND SUBCRITICAL-CRACK GROWTH IN HIGH-STRENGTH STEELS AND NICKEL BASE ALLOYS

Final Report

November 1, 1971 to May 31, 1974

by

R. P. Wei
K. Klier
W. Simmons
R. P. Gangloff
E. Chornet
R. Kellerman

June 1974

PRICES SUBJECT TO CHANGE

National Aeronautics and Space Administration

Reproduced by
**NATIONAL TECHNICAL
INFORMATION SERVICE**
U.S. Department of Commerce
Springfield, VA. 22151

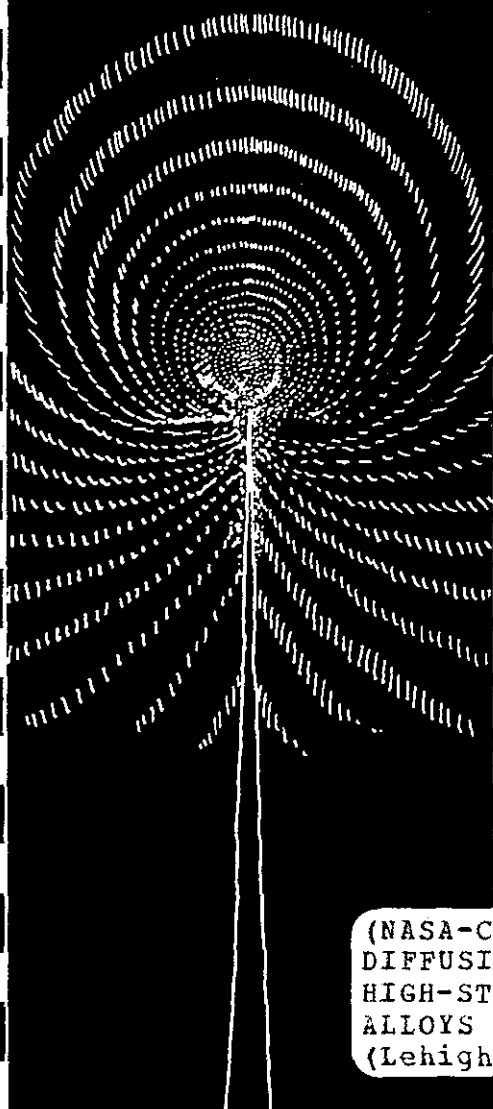
Grant NGR 39-007-067

(NASA-CR-140008) HYDROGEN ADSORPTION AND
DIFFUSION, AND SUBCRITICAL-CRACK GROWTH IN
HIGH-STRENGTH STEELS AND NICKEL BASE
ALLOYS Final Report, 1 Nov. 1971 - 31
(Lehigh Univ.) 158 p HC

N74-32963

Unclas
63/17 48414

CSCL 11F



1. The first part of the report deals with the general situation of the country and the progress of the work during the year.

2. The second part contains a detailed account of the work done in each of the various districts.

3. The third part contains a summary of the work done during the year and a statement of the results.

4. The fourth part contains a list of the names of the persons who have been employed during the year.

FINAL REPORT

SUBJECT: NASA Grant NGR 39-007-067
"Hydrogen Adsorption and Diffusion, and Subcritical-
Crack Growth in High-Strength Steels and Nickel
Base Alloys"

Final Report - November 1, 1971 to
May 31, 1974

ATTENTION: Mr. John Misencik
NASA Lewis Research Center
21000 Brookpark Road
Cleveland, Ohio 44135

PREPARED BY: R. P. Wei, K. Klier, G. W. Simmons,
R. P. Gangloff, E. Chornet, and
R. Kellerman
LEHIGH UNIVERSITY
Bethlehem, Pennsylvania 18015

u



TABLE OF CONTENTS

	<u>Page</u>
ABSTRACT	iii
I. INTRODUCTION	1
II. KINETICS OF SUBCRITICAL CRACK GROWTH	5
A. Materials	5
B. Procedures	6
C. Results and Discussions	10
C.1 Inconel 718 Alloy	11
C.2 18Ni Maraging Steels	12
C.2.1 Effect of Stress Intensity Factor	12
C.2.2 Effect of Temperature	14
C.2.2.1 Stage II Crack Growth	14
C.2.2.2 Apparent Threshold Stress Intensity	18
C.2.3 Effect of Hydrogen Pressure	19
C.2.4 Effect of Yield Strength	22
C.2.5 Fractography	22
C.2.5.1 18Ni(250) Maraging Steel	23
C.2.5.1.1 Fracture Morphology for Stage II Cracking in Region A (Low Temperature Region)	23
C.2.5.1.2 Fracture Morphology for Stage II Cracking in Region B/C (High Temperature Region)	25
C.2.5.1.3 Effect of Stress Intensity (Stretch Zone, Stage I, and Stage II)	27
C.2.5.2 18Ni(200) Maraging Steel	29
C.2.5.2.1 Fracture Morphology for Stage II Cracking in Region A (Low Temperature Region)	29
C.2.5.2.2 Fracture Morphology for Stage II Cracking in Region B/C (High Temperature Region)	30
C.2.5.2.3 Effect of Stress Intensity (Stretch Zone, Stage I, and Stage II)	31
III. HYDROGEN ADSORPTION AND DIFFUSION	32
A. Experimental Arrangement and Procedure	32
B. Materials	35
C. Results and Discussion	36

	<u>Page</u>
IV. DISCUSSIONS	41
V. SUMMARY	46
REFERENCES	49
TABLES	53
FIGURES	59
APPENDIX I	87
APPENDIX II	114

FINAL REPORT
NASA GRANT NGR 39-007-067HYDROGEN ADSORPTION AND DIFFUSION, AND SUBCRITICAL-CRACK
GROWTH IN HIGH-STRENGTH STEELS AND NICKEL BASE ALLOYS

by

R. P. Wei, K. Klier, G. W. Simmons, R. P. Gangloff
E. Chornet, and R. KellermanLEHIGH UNIVERSITY
Bethlehem, PennsylvaniaABSTRACT

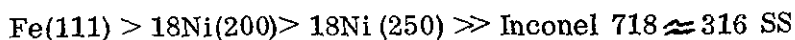
Embrittlement, or the enhancement of crack growth by gaseous hydrogen in high-strength alloys, is of primary interest in selecting alloys for various components in the Space Shuttle. Embrittlement is known to occur at hydrogen gas pressures ranging from fractions to several hundred atmospheres, and is most severe in the case of martensitic high-strength steels. Coordinated studies of the kinetics of crack growth and of hydrogen adsorption and diffusion were initiated under this grant to develop information that is needed for a clearer determination of the rate controlling process and possible mechanism for hydrogen enhanced crack growth, and for estimating behavior over a range of temperatures and pressures. Inconel 718 alloy and 18Ni(200) maraging steel were selected for these studies. 18Ni(250) maraging steel, 316 stainless steel, and iron single crystal of (111) orientation were also included in the chemistry studies. Crack growth data on 18Ni(250) maraging steel from another program are included for comparison.

No sustained-load crack growth was observed for the Inconel 718 alloy in gaseous hydrogen (~ 1000 torr or 133 kN/m^2) at about -50°C , 25°C and $+300^\circ\text{C}$ for stress intensities up to $99 \text{ MN}\cdot\text{m}^{-3/2}$ ($90 \text{ ksi}\sqrt{\text{in.}}$). The rate of fatigue crack growth at room temperature, with $R = K_{\text{min}}/K_{\text{max}} = 0.5$ and $f = 5.0 \text{ Hz}$, was also unaffected by gaseous hydrogen (at ~ 1000 torr or 133 kN/m^2).

Gaseous hydrogen assisted crack growth in the 18Ni maraging steels were characterized by K-independent (Stage II) extension over a wide range of hydrogen pressures (86 to 2000 torr or 12 kN/m^2 to 266 kN/m^2) and test temperatures (-60°C to $+100^\circ\text{C}$). The higher strength 18Ni(250) maraging steel was more susceptible than the lower strength 200 grade. A transition temperature was observed, above which crack growth rates became diminishingly small. This transition temperature was dependent on the alloy and the hydrogen pressure. At low temperatures, Stage II crack growth was found to be thermally activated with an activation energy of $4.4 \pm 0.4 \text{ kcal/mole}$ ($18.2 \pm 1.7 \text{ kJ/mole}$). This activation energy was independent

of hydrogen pressure and yield strength. Within the low temperature region, Stage II crack growth rates were proportional to the square root of hydrogen pressure for both steels. The wide variations in the pressure dependence reported in the literature can be explained in terms of the interactive effect of temperature with hydrogen pressure. Companion fractographic examinations were made and were correlated with the observed crack growth behavior.

The surface activity toward hydrogen exchange reactions of the 18Ni(250) maraging steel, 18Ni(200) maraging steel, Inconel 718 alloy, 316 stainless steel, and iron single crystal of (111) orientation was investigated. The rates of hydrogen atomization by the maraging steels are high and probably sufficient to sustain the crack growth through a mechanism limited by hydrogen atom formation. Aged specimens were found to be more active than non-aged specimens, and highly perturbed surfaces were more active than annealed surfaces. The rates of hydrogen atomization by Inconel 718 and 316 stainless steel were comparable, but were substantially lower than those for iron and for the maraging steels. The order of activities for the formation of surface hydrogen atoms from the gas molecules has been found to be:



The reduced activity for Inconel 718 and 316 stainless steel appears to be related to the presence of chromium in these alloys.

Plausible mechanistic explanations for the observed crack growth behavior in the 18Ni maraging steels were discussed. Surface chemistry experiments at pressures comparable to those used in the crack growth experiments are needed to substantiate and further develop these suggested explanations.

FINAL REPORT
NASA GRANT NGR 39-007-067

HYDROGEN ADSORPTION AND DIFFUSION, AND SUBCRITICAL-CRACK
GROWTH IN HIGH-STRENGTH STEELS AND NICKEL BASE ALLOYS

I. INTRODUCTION

The embrittling effect of hydrogen on the fracture behavior of steels and certain nickel-base alloys is well known and is of great technological importance. In general, hydrogen embrittlement problems may be broadly separated into those that are caused by dissolved hydrogen* (introduced by prior treatments or chemical reactions) and those that result from the exposure to gaseous hydrogen environment during service, at pressures ranging from fractions to several hundred atmospheres.

The problems of embrittlement by hydrogen in solution have been investigated extensively and several mechanisms have been proposed to explain the observed behavior. The first mechanism, the pressure mechanism, suggests that embrittlement is caused by the development of high pressures within internal voids. The pressure build-up results from the accumulation of molecular hydrogen formed from hydrogen that diffuses into these voids [1-4]. The second, the lattice-interaction mechanism suggests that hydrogen would diffuse to regions of high hydrostatic tension within the lattice, under the influence of a strong stress gradient near the crack tip, and interact with the metal and reduce its cohesive strength [5-8]. The precise nature of the hydrogen-metal interaction is not clearly defined. The third proposed mechanism is the stress-sorption mechanism which suggests the reduction in fracture stress, vis-a-vis, embrittlement arises from a reduction in surface energy caused by the adsorption of

* Dissolved hydrogen includes hydrogen dissolved in the crystal lattice, as well as hydrogen trapped at dislocations, intergranular space, and voids.

hydrogen on the surfaces of internal voids [9]. A model, similar in concept to the second mechanism, has been suggested by Oriani recently to account for embrittlement by hydrogen [10]. This lattice-decohesion model suggests that the maximum cohesive strength between iron atoms is reduced by the interaction with hydrogen.

These proposed mechanisms vary widely in rigor and acceptability. The pressure mechanism has been well documented and is generally accepted for explaining problems such as quench cracking of steel ingots and forgings, and embrittlement under hydrogen charging conditions [2-4]. Its applicability to cracking of high-strength steels in mildly corrosive environments, such as distilled water, has been seriously questioned [4, 11] (although it appears to be the most plausible mechanism for moisture-enhanced fatigue crack growth in aluminum and aluminum alloys [12-15]). It fails also to address itself to the fundamental mechanism of embrittlement. The other mechanisms are less established and still need to be tested critically.

Embrittlement by gaseous hydrogen began to receive increasing attention during the past ten years [16-32]. The effect of gaseous hydrogen at low pressures (that is, below 266 kN/m^2 or 2000 torr) on subcritical crack growth in high-strength steels was examined by a number of investigators for sustained loading [16, 17, 19-29, 32] and for fatigue [17, 18, 29, 32]. Hydrogen embrittlement caused by gaseous hydrogen at pressures up to 68.9 MN/m^2 (10,000 psi) on smooth and notched bars, and hydrogen enhanced crack growth at these same pressures for a variety of materials were investigated by Walter and Chandler [30, 31]. These investigations indicated that the high-strength martensitic steels are severely embrittled by gaseous hydrogen at pressures ranging from about 10 kN/m^2 to 70 MN/m^2 [16-32]. Nickel-base alloys, such as Inconel 718, are also embrittled, particularly at high hydrogen pressures [30, 31]. Stable austenitic steels, on

the other hand experience little or no embrittlement [30-32]. The crack growth rate, usually characterized as a function of crack tip stress intensity factor (K), was shown to vary as a function of hydrogen pressure, test temperature, alloy strength level, alloy composition, and hydrogen purity [16-32]. Unfortunately, the interrelated effects of these variables on the kinetics of hydrogen assisted crack growth are, at present, not well understood. The mechanism of gaseous hydrogen embrittlement can be conceptually separated into those processes that control the transport of hydrogen from the molecular gas phase to the point of local mechanical instability, and that process by which hydrogen weakens atomic bonds at the critical point of fracture. At present, the mechanism of gaseous hydrogen embrittlement cannot be defined because of a lack of understanding of these elemental processes involved in hydrogen transport and in hydrogen interaction at the fracture process zone. Definition of a fundamental embrittling mechanism and of the rate limiting process has been further complicated by the paucity of systematic data on the kinetics of hydrogen assisted crack growth and on hydrogen adsorption and diffusion.

Since chemical composition and microstructure can affect hydrogen enhanced crack growth and hydrogen adsorption and diffusion [34], coordinated crack growth and surface chemistry studies utilizing identical materials are needed to develop quantitative information on the mechanism for gaseous hydrogen embrittlement. Such coordinated studies of the kinetics of crack growth in gaseous hydrogen and studies of hydrogen adsorption and diffusion under conditions comparable to those used in the crack growth studies were initiated under this grant. Inconel 718 alloy and 18Ni(200) maraging steel were selected for these studies, and were supplemented by studies on a 18Ni(250) maraging steel in a companion program sponsored by the American Iron and Steel

Institute (AISI). Principal attention was directed to the 18Ni maraging steels in the chemical studies. Iron single crystal of (111) orientation and Inconel 718, and 316 stainless steel were also examined to provide comparative information. These studies were intended to provide not only a better understanding of the gaseous hydrogen embrittlement phenomenon, but also fundamental information on adsorption and diffusion, and crack growth information directly useful for design.

Crack growth experiments were carried out within the framework of linear elastic fracture mechanics, using the crack-tip stress intensity factor K to characterize the mechanical crack driving force. Experiments were conducted over a range of temperatures from about -60°C to $+300^{\circ}\text{C}$, at hydrogen gas pressures of 86 to 2000 torr. Companion examinations of fracture surfaces from selected specimens were made by scanning electron microscopy to identify changes in fracture morphology with environmental conditions. A hydrogen-deuterium exchange technique was used in the surface chemistry studies. By following the exchange kinetics between adsorbed and absorbed hydrogen and gaseous deuterium, the mechanism of adsorption and the magnitude of the diffusion coefficients in the test material could be determined. The deuterium labelling method was selected after careful consideration of tritium labelling, X-ray absorption and electron probe methods.

Progress over the duration of this grant and pertinent results from the AISI program are summarized herein. The crack growth and the chemical experiments are discussed separately.

II. KINETICS OF SUBCRITICAL CRACK GROWTH

A. Materials

A 3.2 mm (1/8 in.) thick Inconel 718 alloy sheet and a 6.4 mm (1/4 in.) thick 18Ni(200) maraging steel plate were used in these studies. Both of these alloys were vacuum melted. A 4.6 mm thick, vacuum melted 18Ni(250) maraging steel was used in a companion AISI program, and is included here for the purpose of comparison.

The Inconel 718 alloy sheet was obtained from the Huntington Alloy Products Division of INCO in the cold rolled and pickle annealed condition, and was heat treated. Chemical composition and heat treatment for this alloy are given in Table 1. Longitudinal and transverse tensile properties are given in Table 2. These results show that this material generally conforms to AMS 5596C specifications and is acceptable. Crack growth resistance curves for this alloy (for monotonically increasing loads) in the longitudinal (LT) and transverse (TL) directions were determined using 76.2 mm (3 in.) wide SEN specimens, Figure 1. These crack growth resistance curves are shown in Figure 2.

The 18Ni(200) maraging steel was obtained as 12.7 mm (1/2 in.) thick plate from the United States Steel Corporation. It was hot rolled straight-away into 6.4 mm (1/4 in.) thick plate and heat treated. Chemical composition and heat treatment for this steel are given in Table 3. A 16-hour aging treatment was used in an attempt to develop yield strength of approximately 1380 MN/m^2 (200 ksi) in this alloy. Longitudinal tensile properties of this steel are given in Table 4. Because of the considerable warpage of this steel from heat treatment, crack growth resistance curves were not determined. This steel, however, had been tested by Dabkowski et al.[35] and is representative of this grade of maraging steel.

The 18Ni(250) maraging steel was obtained as 8.9 mm (0.35 in.) thick hot-rolled (straight-away) plate. It was heat treated as specimen blanks and surface ground to 4.6 mm (0.18 in.) thickness. Chemical composition, heat-treatment, and longitudinal tensile properties of this steel are given in Table 5.

B. Procedures

The kinetics of subcritical crack growth under sustained-load in dehumidified hydrogen were examined over a range of temperatures from -60 to +300°C. 76.2 mm (3-in.) wide center-cracked specimens, Figure 3, oriented in the longitudinal (LT) direction were used for the Inconel 718 alloy sheet in this investigation. Because of the warpage problem, modified wedge-opening-load (WOL) specimens, Figure 4, oriented in the longitudinal (LT) direction were used for the 18Ni(200) maraging steel plate.* Both 70 mm (2.75 in.) wide center-cracked specimens and modified WOL specimens, oriented in the longitudinal (LT) direction, were used for the 18Ni(250) maraging steel plate. All specimens contain starter notches introduced by electro-discharge machine (EDM) and were precracked in fatigue in dehumidified argon or in vacuum (at $\sim 10^{-3}$ torr or 0.133 N/m^2) before testing. The precrack was extended from the end of the starter notch by approximately 2.54 mm (0.1 in.). Fatigue precracking and testing were carried out in a 445 kN (100 KIP) capacity MTS closed-loop electrohydraulic testing machine operated in load control. Load control was estimated to be better than ± 1 percent. The stress intensity factor K for the center-cracked specimens is computed from Equation 1; where P = applied load, B = specimen thickness, W = specimen width, and a = half-crack length.

* Preliminary data were obtained on 76.2 mm (3 in.) wide center-cracked specimens of this material.

$$K = \frac{P}{BW} \sqrt{\pi a \sec (\pi a/W)} \quad (1)$$

A secant correction for finite specimen width was used [36]. This correction closely approximates the series correction given by Isida [36, 37]. The stress intensity factor K for the WOL specimens is computed from Equation 2 [38]:

$$K = \frac{P \sqrt{a}}{BW} \left[30.96 - 195.8 \left(\frac{a}{W}\right) + 730.6 \left(\frac{a}{W}\right)^2 - 1186.3 \left(\frac{a}{W}\right)^3 + 754.6 \left(\frac{a}{W}\right)^4 \right] \quad (2)$$

Equation 2 was developed for a specimen with height to width ratio (H/W), Figure 4, of 0.486, and is valid for a/W from about 0.3 to 0.7.

A continuous recording electrical potential system was used for monitoring crack growth [39]. This system monitors crack growth by measuring changes in electrical potential (vis-a-vis, resistance) across the crack and gives a measure of the change in average (through-thickness average) crack length. The detailed experimental procedure for this method has been described elsewhere [39]. For the center-cracked specimens, an analytical calibration curve developed by Johnson was used [39, 40]. For the WOL specimens, an experimental calibration curve, Figure 5, was used. Resolution at room temperature for the center-cracked Inconel 718 alloy and 18Ni(250) maraging steel specimens was better than 0.025 mm (0.001 in.) in half-crack length (a). Resolution for the 18Ni maraging steel (WOL) specimens at room temperature was also better than 0.025 mm (0.001 in.) in crack length (a). Based on overall system stability and sensitivity, the lower limit for rate measurement was estimated to be about 5×10^{-8} m/sec. (or about 2×10^{-6} inch per second).

Dehumidified high purity hydrogen was used as the test environment. The dehumidified hydrogen environment was maintained around the crack by clamping stainless steel chambers to the faces of the test specimens. Dehumidification and additional

purification were accomplished by one of two procedures. Schematic diagrams of the overall environment control systems are shown in Figures 6 and 7. In the first procedure, hydrogen (99.999% purity) was passed through a gas purifier (Matheson Model 460 purifier with Model 461-R cartridge for moisture), through a series of cold traps at -196°C , then through a heated palladium membrane purifier at P before admission to the test chambers, Figure 6. To reduce back diffusion of impurities, an additional cold trap and a silicone fluid back-diffusion trap are used on the discharge side. A rigorous purging procedure was followed. The gas system was purged for about two hours before each test using 99.999% purity argon. During this initial purging operation, the various components of the gas system upstream from the back-diffusion trap (Figure 6) were heated to at least 100°C . The cold traps were then filled with liquid nitrogen, and the environment-specimen assembly was again heated to a minimum of 100°C while maintaining argon flow. The system was then evacuated with a mechanical pump and back-filled with hydrogen. Hydrogen was then allowed to flow through the palladium purifier and the system for at least 15 minutes prior to the start of the experiment. Continuous flow at a chamber pressure of about 34.5 kN/m^2 gage (5 psig) was maintained throughout the experiment for experiments at ~ 1000 torr ($\sim 133 \text{ kN/m}^2$). Experiments at other hydrogen pressures were carried out by using hydrogen-helium mixtures. With this procedure, the impurity level in the environment was estimated to be less than 5 ppm (on the basis of mass spectroscopic analysis of argon purified in a similar manner in the system.) This procedure was used principally with the center-cracked specimens.

An alternate purification procedure was used for the WOL specimens, Figure 7. To ensure hydrogen purity, the environmental system was modified to provide capability for pumping residual impurities from the specimen chambers [25, 43]. A cryogenic

pump, containing zeolite (Linde 13X molecular sieve), was connected to the discharge side of the test chamber through a high-conductance coupling. When chilled to liquid nitrogen temperatures, the molecular sieve physisorbs CO, CO₂, O₂, H₂O, N₂ and A molecules with high efficiency, while having only a small pumping propensity for H₂ molecules [41, 42]. Jewett et al.[43] estimated that selective cryogenic pumping reduces contaminant levels to below 1 ppm in a flowing hydrogen system, while even lower levels can be achieved in a static environment. Reproducibility of results between duplicate test specimens, and close agreement with previous data obtained on center-cracked specimens [22] suggest that the cryogenic pump was effective in minimizing contamination. A cold trap and a silicone fluid trap were placed downstream of the cryopump to prevent back streaming of contaminants from the gas discharge system. A range of hydrogen pressure from 86 torr (12 kN/m²) to 2,000 torr (266 kN/m²) was used. For tests at hydrogen pressures above one atmosphere (760 torr or 101 kN/m²), hydrogen was passed continually through the gas train and discharged through the silicone oil trap. A static environment was employed for all sub-atmospheric tests. The gas train and chamber assembly was subjected to a vigorous purging and bakeout procedure prior to each test to minimize contamination. All gas lines, cold traps, and the specimen and chamber assembly were heated at about 110°C for two hours while flowing ultra-high purity (UHP) (99.999% pure) argon through the system. Concurrently the Matheson gas purifier was heated to 160°C, and the cryogenic pump to 300°C to remove adsorbed moisture from the zeolite. While continuing with the bakeout on the rest of the system, the Matheson gas purifier was cooled to room temperature, and the cold traps were chilled to about -150°C. The system was then alternately evacuated with a mechanical pump and backfilled with dehumidified UHP argon during the final hours of bakeout.

After the bakeout was completed, the entire system was cooled to room temperature and evacuated with a mechanical pump. All cold traps and the cryogenic pump were immersed in liquid nitrogen (-196°C). Concurrently, the fatigue precrack was extended by about 1 mm (0.04 in.) in vacuum to ensure a "clean" surface for the subsequent static load crack growth tests. After precracking, the selected test temperature was established. Typically a period of two to three hours was required to establish thermal stability. Dehumidified hydrogen was admitted into the system to the desired pressure during the later portion of this period.

Electrical resistance heating tapes were used to heat the specimens for tests above room temperature. Cooling with chilled dry nitrogen was used for the low temperature tests. Temperature stability of better than $\pm 2^{\circ}\text{C}$ was maintained during each test.

Fracture surfaces produced under selected conditions of temperature and hydrogen pressure were examined by scanning electron microscopy. An ETEC Autoscan scanning electron microscope was used and was operated in the secondary electron imaging mode at 20 kV. Typical working distance was about 11 mm. All specimens were tilted 20 degrees about an axis parallel to the direction of crack growth. In all cases, the complete broken-half of the specimen was placed in the scanning electron microscope to avoid potential artifacts introduced by sectioning of the fracture surface. Most of the fractographs were taken in the mid-thickness region of the specimens. Areas for photography were chosen at random, and were representative of fracture morphology for specific values of temperature, pressure, and range of K.

C. Results and Discussions

As a part of this program, crack growth experiments in gaseous hydrogen were carried out on 3.2 mm (1/8 in.) thick Inconel 718 alloy and on 6.4 mm (1/4 in.) thick

18Ni(200) maraging steel plate specimens. These experiments were supplemented by tests on a 4.6 mm (0.18 in.) thick 18Ni(250) maraging steel plate. Because of the apparent insensitivity of this Inconel 718 alloy plate to hydrogen, most of the work was directed to the 18Ni maraging steels. Data on the Inconel 718 alloy will be reported and discussed separately from those of the 18Ni maraging steels in the following sections.

C.1 Inconel 718 Alloy

Crack growth experiments were carried out on the Inconel 718 alloy at about -50, +25 and + 300°C in 1000 torr hydrogen. Increasing K levels for the sustained-load crack growth tests were obtained by increases in the applied load, or by further extension of the crack by fatigue. By the latter procedure some fatigue crack growth data in gaseous hydrogen were obtained. The results showed that there was no detectable crack growth under sustained loading at these temperatures for K levels up to about $99 \text{ MN}\cdot\text{m}^{-3/2}$ (90 ksi $\sqrt{\text{in.}}$) (the lower limit of detectability for crack growth being about 5×10^{-8} m/sec). Fatigue crack growth data obtained during these tests also show the absence of hydrogen effect at room temperature for K_{max} up to $99 \text{ MN}\cdot\text{m}^{-3/2}$ (90 ksi $\sqrt{\text{in.}}$), at $R = K_{\text{min}}/K_{\text{max}} = 0.5$ and a test frequency of 5.0 Hz. (Figure 8). These results are consistent with fatigue test results obtained previously on a 1.5 mm (0.06 in.) thick Inconel 718 alloy sheet [44]. These results suggest that there is little effect of hydrogen under these conditions of temperature and pressure (~ 1000 torr or 133 KN/m^2). The absence of gaseous hydrogen embrittlement under these conditions, however, does not preclude the possibility of embrittlement at other temperatures and pressures. Embrittlement of this alloy in high pressure hydrogen has been observed by Walter and Chandler using smooth and notched round tensile specimens [30] and precracked specimens [45]. Evaluation of the crack

growth characteristics, coupled with surface chemistry studies, at other conditions would be desirable. Fatigue crack growth was shown to be a function of temperature (see Figure 8); decreasing by about a factor of 3 from +300°C to -50°C. This temperature dependence is of importance to service performance and needs to be considered in design.

C.2 18Ni Maraging Steels

It is most convenient to consider the results of the 18Ni(200) and 18Ni(250) maraging steels as a group. The influences of stress intensity factor, temperature, hydrogen pressure, and yield strength on crack growth will be discussed separately. Fractographic results on selected specimens, tested over a range of test conditions, will be considered also. Mechanistic implications of the crack growth and fractographic results will be discussed.

C.2.1 Effect of Stress Intensity Factor

The results from sustained-load tests of 18Ni(200) maraging steel at a hydrogen pressure of 2000 torr (266 kN/m²) and -5°C, and of 18Ni(250) maraging steel at 1240 torr (165 kN/m²) and +23°C are shown in Figures 9 and 10 respectively. These data are typical of hydrogen-enhanced subcritical crack growth in the 18Ni maraging steels, and exhibit two distinct stages of crack growth in agreement with previous results on high-strength steels and titanium alloys tested in hydrogen and in other aggressive environments [21, 22, 26, 27, 39, 46, 47]; that is Stages I and II. In Stage I, the rate of crack growth is strongly dependent on the stress intensity factor (K), whereby a small change in K produces a large change in the rate of crack growth. Stage I data further suggest the existence of an apparent threshold stress intensity (K_{th}) below which hydrogen-enhanced crack growth would not occur under a given condition of temperature and

pressure. In Stage II, the rate of crack growth becomes independent, or nearly independent of the mechanical crack driving force characterized by K . Stage III growth, in which the rate of crack growth once again increases rapidly with K , as K approaches K_c , is expected to follow. This stage of growth, however, was not observed in the present program since all of the tests were terminated before total specimen failure.

The character of these curves is a consequence of the fact that the driving force for subcritical crack growth contains a chemical component as well as a mechanical component. The growth rate for any point on the curve must be controlled by either the rate at which mechanical energy is supplied to the moving crack, or the rate of delivery of hydrogen to that portion of the lattice where embrittlement occurs, or by a combination of these rates. For Stage I growth, the strong dependence on K suggests that the rate of delivery of mechanical energy is important so that kinetic control must lie either entirely or partially in this component. (The rate of production of fresh crack surfaces by the mechanical driving force to interact with the environment is implicitly considered as a part of the delivery of mechanical energy). On the other hand, the fact that Stage II crack growth is independent of the mechanical driving force suggests that the rate controlling process resides in one of the chemical processes that supply active hydrogen to the crack tip. These chemical processes may involve conversion of the "inert" molecular hydrogen into its active form (e.g., atomic hydrogen in the surface or subsurface layers), and various transport processes for the active hydrogen (e.g., surface diffusion, or diffusion into the bulk). In other words, the rate limiting speed results from the inability of the "transport mechanism" or "activation mechanism" to maintain a critical concentration of hydrogen at the embrittlement site at growth rates above this level. It is most appropriate, therefore, to focus attention on the crack

growth kinetics in Stage II in the development of information for relating crack growth to the relevant physio-chemical process(es). Stage III crack growth commences when the K levels become sufficiently high such that crack growth can be sustained by the mechanical process alone. The growth rate is expected to "out run" the supply of aggressive environment (hydrogen) to the crack tip, and would be unaffected by hydrogen.

Data on the kinetics of crack growth on the 18Ni(200) and 18Ni(250) maraging steels, at various hydrogen pressures and temperatures, are given in tabular and graphical form in Appendix I. Mean Stage II growth rates, the associated statistical information, and other pertinent information are also included.

C. 2. 2 Effect of Temperature

Crack growth experiments were conducted over a range of temperatures on the 18Ni(250) maraging steels at hydrogen pressures of 1000, 430, 210, and 86 torr (133, 57, 28, and 12 kN/m²) and on the 18Ni(200) maraging steel at 2000 and 1000 torr (266 and 133 kN/m²). In all cases, a distinct stage of K -independent (Stage II) crack growth was observed for temperatures below some critical value. Apparent threshold stress intensities (K_{th}) for hydrogen-enhanced crack growth were also indicated. The influence of temperature on the mean Stage II growth rates and on K_{th} are discussed separately.

C. 2. 2. 1 Stage II Crack Growth

The influence of temperature on the mean Stage II (K -independent) crack growth rates for the 18Ni(250)* and 18Ni(200) maraging steels are shown in Figures 11 and 12 in a standard Arrhenius representation. The error bands indicate the 95% confidence interval estimates of the mean Stage II crack growth rate for each of the test conditions

* Comparison experiments indicated that data obtained with WOL specimens are in excellent agreement with those from tests of center-cracked specimens [48]. No distinctions between these data, therefore, have been made.

(See Appendix I). The K range over which each of the mean rate values was determined extended typically from the apparent K_{th} to $61 \text{ MN}\cdot\text{m}^{-3/2}$ (55 ksi $\sqrt{\text{in.}}$) for the 18Ni(250) maraging steel, and to $88 \text{ MN}\cdot\text{m}^{-3/2}$ (80 ksi $\sqrt{\text{in.}}$) for the 18Ni(200) maraging steel. Mean Stage II growth rates exhibit three distinct regions of temperature dependence similar to that reported previously by Williams and Nelson [19] for an AISI 4130 steel. Each of these regions will be considered separately.

In Region A (the low temperature branch), the mean Stage II growth rate, $\overline{(da/dt)}_{II}$, conforms to an Arrhenius type relationship:

$$\overline{(da/dt)}_{II} = A \exp (-\Delta H/RT) \quad (3)$$

A is a constant for a given hydrogen pressure; ΔH is the activation energy; R is the universal gas constant; and T is the absolute temperature. Least square analyses of the data in this region were made to determine the activation energy for crack growth. The activation energies for the 18Ni(250) maraging steel were found to be 4.4 ± 0.6 kcal/mole (18.4 ± 2.6 kJ/mole) and 4.2 ± 1.7 kcal/mole (17.5 ± 6.9 kJ/mole) on a 95% confidence level at 1000 and 430 torr (133 and 57 kN/m^2) respectively, and for the 18Ni(200) maraging steel at 2000 torr (266 kN/m^2) to be 4.4 ± 1.3 kcal/mole (18.4 ± 5.5 kJ/mole). (These values of activation energy are statistically equal on a 95% confidence level.) Data at the remaining pressures were not sufficient for the determination of activation energies. These data, however, are consistent with an activation energy of 4.4 kcal/mole (18.4 kJ/mole). These results indicate that in Region A, Stage II hydrogen assisted crack growth in 18Ni maraging steel is thermally

activated with a pooled value* of activation energy equal to 4.4 ± 0.4 kcal/mole (18.2 ± 1.7 kJ/mole) that is independent of hydrogen pressure, and of alloy composition and/or yield strength level on a 95% confidence level.

In Region B, the mean Stage II growth rates become essentially insensitive to changes in temperature, and attain the maximum value for each hydrogen pressure (Figures 11 and 12). The temperature range for Region B and the maximum growth rate depend on the hydrogen pressure and on the alloy. This region represents a transition zone between Regions A and C, and is indicative of a change in the rate controlling process for hydrogen enhanced crack growth.

Region C is characterized by an abrupt decrease in the rate of crack growth with increasing temperature, and is associated with an apparent change in hydrogen susceptibility in these two alloys. The transition in behavior occurred over a temperature range of less than 5°C at each of the pressures (Figures 11 and 12). The actual transition temperature ranges were dependent on the hydrogen pressure and on the alloy. Below the transition temperatures, the rates of crack growth were finite and were quite rapid. Above the transition temperatures, however, no discernible crack growth was observed; that is, the rate of crack growth was below the limit of resolution of the measurement system (approximately 5×10^{-8} m/sec). The possibility that this abrupt decrease in susceptibility to gaseous hydrogen embrittlement with small increases in temperature was caused by oxygen or water vapor contamination

* The pooled value of activation energy (ΔH) was computed on the basis of nine data points (Figures 11 and 12) -- data on 18Ni(250) maraging steel at 1000 and 430 torr, and on 18Ni(200) maraging steel at 2000 torr. Usage of this value resulted in a significant reduction in the uncertainty interval for ΔH [49].

was ruled out by experiments designed to start a stationary crack by a small decrease in temperature, or to arrest a moving crack with a small temperature increase [50]. These experiments were carried out at all pressures at K levels compatible with those for Stage II crack growth in Regions A and B. In addition, tests carried out in the 18Ni(250) maraging steel at 1000 torr (133 kN/m^2) at 50°C and at 80°C for K levels up to 79 and $92 \text{ MN-m}^{-3/2}$ (72 and $84 \text{ ksi } \sqrt{\text{in.}}$) respectively, indicated no crack extension for several hours. These results indicate that the observed transition represents a real change in hydrogen susceptibility in these maraging steels. This behavior is, however, different from the Region C behaviors reported by Nelson and Williams for AISI 4130 steel [23] and by Sawicki for H-11 steel [21]. For these medium-carbon, high-strength steels, a gradual drop off in growth rate with increasing temperature was observed in Region C. The observed Region C transition behavior for the 18Ni maraging steels has significant mechanistic implications, and will be discussed later.

Because of the obvious influences of hydrogen pressure, and of alloy composition and/or yield strength on the kinetics of crack growth, care must be exercised in defining the pressure, composition, and yield strength dependencies for hydrogen enhanced crack growth. To avoid ambiguities, crack growth isotherms must be selected such that they fall within a given region of the temperature response curves (Figures 11 and 12). The effects of hydrogen pressure and of alloy composition/yield strength will be considered in Sections C. 2.3 and C. 2.4.

C. 2. 2. 2 Apparent Threshold Stress Intensity

The effect of test temperature on the apparent threshold stress intensity (K_{th}) for crack growth in both grades of 18Ni maraging steels tested in gaseous hydrogen at 1000 torr (133 kN/m^2) is shown in Figure 13. These results were obtained by extrapolation, and represent only best estimates of the asymptotic values of stress intensity indicated by the Stage I kinetics data in Appendix I and [22,48]. The results must be tempered by the inherent uncertainties associated with the extrapolation procedure [50], but are nevertheless interesting. Within Region A (that is, below -40°C for the 200-grade material and below -20°C for the 250-grade material), K_{th} is relatively insensitive to temperature. This behavior is in agreement with results on other high strength steels reported in the literature [21]. Within Region B (that is, between about -40°C and -10°C , and about -20°C and $+40^\circ\text{C}$ for the 200- and 250-grade materials, respectively), K_{th} increased with increasing temperature. As the temperature is increased into Region C, K_{th} is expected to approach the apparent threshold K for creep-controlled crack growth [39, 51, 52]. (This threshold K would be an appreciable fraction of the critical K for fracture, K_c , and would be dependent on the alloy and temperature. The actual values, however, were not determined in this investigation.) These results are consistent with a change in hydrogen susceptibility at a critical temperature, and have the same mechanistic implications as that for Stage II crack growth. A similar behavior (Figure 13) is expected for both steels at the other hydrogen pressures.

C. 2. 3 Effect of Hydrogen Pressure

The effect of hydrogen pressure on Stage II crack growth in the 18Ni maraging steels is shown in Figures 11 and 12, and has been considered in the previous discussion on the influence of temperature on crack growth. It is worthwhile to recapitulate the salient points of the previous discussions relating to pressure dependence before going on to a quantitative consideration of the influence of hydrogen pressure on crack growth. It was observed that the functional form of the relationship between Stage II crack growth rate and temperature remains unaffected by changes in pressure (Figures 11 and 12). The ranges of temperature for the various regions of Stage II crack growth (that is, Regions A, B, and C) were affected by hydrogen pressure. There was a general reduction in the rate of crack growth with decreases in pressure. The transition temperature, indicative of a transition in hydrogen susceptibility, decreased with decreasing hydrogen pressure. The results suggested that, in Region A, Stage II crack growth is rate limited by a single chemical or transport process with an activation energy of about 4.4 kcal/mole (18.2 kJ/mole). This activation energy appears to be independent of the hydrogen pressure. Transition from Region A to Regions B and C suggests a change in this rate controlling mechanism. To derive meaningful mechanistic information from data on crack growth kinetics, therefore, the pressure dependence for Stage II crack growth must be obtained within a specified region (Figures 11 and 12). In other words, a selected isotherm should not be allowed to intersect more than one region in the Arrhenius plots.

Results obtained during the current study indicate that mean Stage II crack growth rate in Region A is directly proportional to the square root of hydrogen environment pressure for both grades of maraging steel. Figures 11 and 12 show that, at a test temperature of -45°C , both steels exhibit Region A behavior over the complete range of hydrogen pressures. 95% confidence interval estimates of the mean Stage II crack growth rates determined at this temperature, for both grades of 18Ni maraging steel (Appendix I), are well characterized by a straight line with a slope equal to 0.5 as shown in Figure 14. (Least squares analysis of the data obtained for the 250 grade steel indicated that the best estimate of the slope of the straight line relation was 0.53 ± 0.08 on a 95% confidence level.) Because the activation energy for Stage II crack growth in Region A was found to be independent of hydrogen pressure, this one-half power pressure dependence is valid over the entire region.

The interactive effects of test temperature on the pressure dependence of the mean Stage II crack growth rate for 18Ni(250) maraging steel are clearly seen in Figure 15. The Region A relationship at -45°C is shown for reference. Points with 95% confidence interval error flags represent actual data, and those without error flags are determined from lines shown in Figure 11. At a constant temperature of -5°C , crack growth rates at all pressures fall within Region B of the temperature dependence, Figure 11. Figure 15 indicates that the mean Stage II growth rate at this temperature is proportional to $P_{\text{H}_2}^{0.8}$. At a constant temperature of $+20^{\circ}\text{C}$, Stage II

growth rates are characterized by Region B temperature dependence over the pressure range from 1000 torr (133 kN/m²) to about 150 torr (20kN/m²), with Region C behavior at the lower pressure levels. The corresponding pressure dependence (Figure 15) ranges from 1.2-power over the Region B pressure range to increasingly higher power within the Region C range, as indicated by the increasing slope of the pressure dependence curve with decreasing hydrogen pressure.

These results are consistent with the established effects of hydrogen pressure on gaseous hydrogen embrittlement. The pressure dependence suggested by Hudak's [22] preliminary low pressure data are confirmed. In those cases [23, 26, 53] where the crack growth may be inferred as being in Stage II and being entirely within Region A, the growth rate was proportional to the square root of hydrogen pressure. For those cases [21, 23, 27, 54, 55] in which the possibility of temperature-pressure interactive effects was not considered, the pressure dependence exponent was found to increase with increasing temperature, in agreement with current results.

In summary, the wide variations in pressure dependence reported in the literature can be explained on the basis of an interactive temperature effect. Stage II crack growth rate is proportional to the square root of gaseous hydrogen pressure at all temperatures within Region A. The mechanistic significance of this result is considered in Section C.2.6. Within Region B, the Stage II growth rate was more sensitive to hydrogen pressure. The exponent for pressure dependence was found to increase with increasing temperature within the range from 0.5 to about 1.5. This range of exponent values is characteristic of the values reported in the literature. Mixed Region B - Region C pressure dependence are highly irregular, and are of no mechanistic significance.

C. 2. 4 Effect of Yield Strength

Characterization of crack growth kinetics during the current investigation showed that, at constant temperature and hydrogen pressure, the higher strength 18Ni(250) grade maraging steel was more susceptible to gaseous hydrogen embrittlement than the lower strength 200 grade, in agreement with preliminary results presented by Hudak [22]. For example, Figure 16 shows that the threshold stress intensity (K_{th}) was reduced by a factor of three, while the Stage II (K-independent) crack growth rate increased by a factor of 2.5 in response to a 30% increase in yield strength. Similar results, observed over a range of temperature and hydrogen pressure conditions, verify the trend illustrated in Figure 17. These results have been integrated into Section C. 2. 1. It should be noted that in spite of the difference in susceptibility, the activation energies and pressure dependencies for Stage II crack growth for these two steels in Region A were the same ($\Delta H = 4.4$ kcal/mole or 18.2 kJ/mole, with a one-half power pressure dependence). It is not clear whether the difference in susceptibility is the result of differences in yield strength per se, or is the consequence of changes in local chemical composition (say along the prior-austenite grain boundaries). Further investigation to clarify this issue is warranted.

C. 2. 5 Fractography

Scanning electron fractographic examinations of the 18Ni (250) and 18Ni (200) maraging steel have been made to identify those features of the microstructure that are susceptible to hydrogen enhanced cracking. Because of the high value of K_c ($> 220 \text{ MN}\cdot\text{m}^{-3/2}$) for these steels and the relatively low K levels required to produce crack growth in gaseous hydrogen, studies of the fracture morphology associated with embrittlement would not be complicated by a large component related to purely mechanical separation (such as tear ridges and dimples).

Because of the rate-limited nature of Stage II crack growth, primary emphasis will be placed on the considerations of fracture morphology for this stage. Comparisons between the fracture morphologies in the various regions of the Arrhenius diagram and in the various stages will be made and discussed. Each alloy will be considered separately, and similarities between the two alloys will be discussed.

C. 2. 5. 1 18Ni(250) Maraging Steel

C. 2. 5. 1. 1 Fracture Morphology for Stage II Cracking in Region A (Low Temperature Region)

Scanning electron (SEM) fractographs from specimens of 18Ni(250) maraging steel tested in Region A (the low temperature region) of Figure 11 are shown in Figure 18 and 19. The fracture morphology is typical of specimens fractured in this region, and is representative of the entire range of temperatures and pressures for this region.

Figure 18 illustrates the five components that are commonly observed:

- (1) A predominant component of intergranular separation along the prior-austenite grain boundaries.
- (2) Deformation markings and apparent phase decohesion on otherwise featureless intergranular facets.
- (3) Subcracks or secondary cracks out of the plane of macroscopic fracture. These subcracks apparently lie along prior-austenite grain boundaries.
- (4) A small amount of transgranular quasi-cleavage, with respect to the prior austenite grains.
- (5) A small amount of mixed ductile tearing and quasi-cleavage.

Each of these components is indicated numerically on Figure 18 in accordance with the listing above.

The existence of a bimodal fracture morphology composed of a large component of intergranular separation combined with a small amount of transgranular quasi-cleavage is in agreement with previous fractographic results. Typically, 18Ni maraging steels fractured in hydrogen producing environments exhibit a predominantly

intergranular fracture morphology, with grain facet markings and secondary cracking [17, 56-58]. The susceptibility of prior austenite boundaries to hydrogen induced failure has already been documented in several studies [60-63]. It is reasonable to expect transgranular quasi-cleavage to occur along massive martensite lath boundaries in the 18Ni maraging steels [58], however, such interfaces are apparently less susceptible to hydrogen than prior austenite boundaries [61]. Cleavage features illustrated in Figure 18 should not be interpreted as true crystallographic separation along low indice planes, as observed in pure iron [60, 62, 63], but rather as either transgranular quasi-cleavage or transgranular interboundary fracture. (The term quasi-cleavage will be used to refer to both of these features in the following discussions.) The mixed ductile tearing/quasi-cleavage component illustrated in Figure 18 is considered to be the result of highly localized mechanical rupture of remaining ligaments of material partially eroded by hydrogen embrittlement. The ductile features are consistent with the fracture mode observed on specimens broken under monotonically increasing loads in inert environments [64, 65], and are the only ones not associated directly with embrittlement.

Figure 19 provides amplification of the five components of the Region A fracture morphology, and contains an extreme example of grain facet deformation markings and apparent phase boundary separation. The density of these markings exhibited no simple relation to stress intensity, hydrogen pressure or temperature. Grain facet deformation markings (e.g. Feature A, Figure 19) were defined as tear ridges by Beachem and Pelloux[66], and were considered to be plastic tearing of ligaments of material between microscopic segments of the environmentally assisted crack front. This explanation implies that boundary failures nucleate ahead of the microscopic crack front, and has mechanistic implication for defining the exact location of the fracture process zone. No

information was obtained during the current study which pertains to the location of the fracture process zone. Substructures on the prior austenite boundaries could be related to hydrogen enhanced cracking of other boundaries that intersect the prior-austenite surface. For example, the large feature (B) in the center of Figure 19 could be interpreted as a subcrack along a transgranular massive martensite boundary which intersected the austenite grain face. Smaller features, such as the void (C) in Figure 19, could be explained in a like manner, or they could represent hydrogen cracking of residual Ti (C, N) phase boundaries which by chance intersected the austenite grain boundary.

Examination of specimens tested in Region A, over a wide range of K levels, indicate that there is no essential change in fracture morphology for Stage II crack growth with stress intensity (up to a K level of $55 \text{ MN}\cdot\text{m}^{-3/2}$). This observation should be tempered by the fact that this K level is well below the fracture toughness of the material. At higher K levels and as the crack growth proceeds into Stage III, greater amounts of ductile tearing and dimpled rupture (micro-void coalescence) can be expected.

C.2.5.1.2 Fracture Morphology for Stage II Cracking in Regions B/C (Higher Temperature Region)

The dramatic effect of test temperature on the rate of Stage II crack growth, illustrated in Figure 11, suggests that there may be an attendant transition in fracture morphology in going from the low temperature region (Region A) into Regions B/C. As such, fractographic analyses were carried out on specimens tested in the transition region between Regions B and C; that is, the region just to the high temperature side of the maximum Stage II growth rate, Figure 11. Figure 20 shows a typical example of the fracture morphology in this region, which is characterized by the following four

components:

- (1) A finite (but small) amount of intergranular separation, with attendant faceted deformation markings and phase boundary separation features.
- (2) Transgranular quasi-cleavage, apparently along massive martensite boundaries. This component is present in larger amounts than that observed on specimens fractured in Region A.
- (3) A large amount of plastically torn material with no identifiable crack path orientation. This component was by-and-large absent from specimens tested in Region A.
- (4) Subcracks or secondary cracks out of the macroscopic fracture plane. Such cracks often exceeded 50 microns in length, and were apparently both intergranular and transgranular in character.

The four components of the Stage II fracture morphology illustrated in Figure 20 were essentially invariant in appearance over a stress intensity range of 44 to 83 $\text{MN}\cdot\text{m}^{-3/2}$ (40 to 75 $\text{ksi}\sqrt{\text{in}}$) (all Stage II) at a hydrogen pressure of 1000 torr (133 kN/m^2). The only noticeable changes in fracture surface morphology with K were a small increase in the amount of plastically torn material, and an increase in the density of long ($> 50\ \mu$) subcracks. Fracture morphologies of specimens tested at the other pressures in Region B/C were similar to those illustrated in Figure 20, and exhibited a similar K independence.

Comparison between Figures 18 and 20 clearly demonstrates the dramatic change in fracture morphology associated with a change in Stage II crack growth from Region A to Regions B/C. The predominantly intergranular crack morphology for Stage II crack growth in Region A transformed to a fracture morphology that is characterized by increased amounts of transgranular quasi-cleavage, dramatically decreased amounts of intergranular separation, and the appearance of a large component of plastic tearing. Although the observed transition in fracture morphology was made on specimens tested

at K levels that differed by a factor of 1.6, the difference in crack path was not produced by this difference in mechanical driving force. (Data obtained during the current study showed that the mechanical driving force had little effect on fracture morphology over the range of K levels investigated). Rather, the change in fracture morphology is integrally related to the temperature induced change in susceptibility to gaseous hydrogen embrittlement; that is, the Region A to Region B transition. This observation is confirmed by results at the other hydrogen pressures.

C.2.5.1.3 Effect of Stress Intensity (Stretch Zone, Stage I, and Stage II)

McIntyre [26] had suggested that "stretch zone" formation is a necessary precursor to cracking in hydrogen and in hydrogen producing environments. Stretch zones are formed as a result of slip deformation at the crack tip during load application. Examination of fracture surfaces produced during this program showed that the boundary between the fatigue precrack and the hydrogen assisted crack was distinctly discontinuous, with no resolvable stretch zone (Figure 21). This observation suggests that the stretch zone is merely incidental to the cracking process (being more discernible in the lower strength steels used in McIntyre's studies), and that embrittlement occurs in a region very close to the crack tip.

Two mutually exclusive effects of stress intensity have been presented in the literature. The majority of results [21, 23, 25, 67] indicate that, as stress intensity increases, the percentage of ductile tearing (general micro-void coalescence) increases from threshold (K_{th}) to fast fracture (K_c) as a result of competition between the chemical and mechanical components of the fracturing process. Kerns [27], however, hypothesized that a marked transition in fracture morphology would occur at that K value corresponding

to the transition between Stage I and Stage II crack growth. Fractographic results obtained during the current study of 18Ni(250) maraging steel specimens, tested in Region A over a range of hydrogen pressures, are consistent with the majority view on the effect of stress intensity, and do not support Kern's hypothesis. Figure 22 illustrates typical fracture morphologies observed at locations within Stage I (Figure 22a, $K = 13 \text{ MN-m}^{-3/2}$) and within Stage II (Figure 22b, $K = 28 \text{ MN-m}^{-3/2}$) of crack growth for a specimen that exhibited a transition at $K = 17 \text{ MN-m}^{-3/2}$. The fracture morphologies for the two stages of growth are comparable in every respect, each containing those five components described in the previous section. These micrographs support the important conclusion that, within Region A, there is no discernible change in fracture morphology attendant with the Stage I to Stage II growth rate transition. This conclusion lends credit to the hypothesis that the same mechanism of embrittlement is operative over the complete range of K . Stage I is considered as being limited by the mechanical component of cracking, while Stage II is governed by the rate limiting transport step involved in the chemical component of embrittlement. Similarly, changes in fracture morphology between Stage I and Stage II crack growth in Region B were absent.

Fractographic analysis of 18Ni(250) maraging steel specimens tested in Region A revealed that changes in the mechanical driving force (K) from threshold to $45 \text{ MN-m}^{3/2}$ had little effect on the density of the ductile tear component present in the fracture morphology. This observations does not contradict the concept of increased mechanical rupture with increased mechanical driving force [21, 23, 25, 67]. Rather, the maximum K value investigated at low temperatures was $45 \text{ MN-m}^{-3/2}$, a value equal to about 20% of the critical stress intensity for fracture.

(Stress intensity levels above about $45 \text{ MN}\cdot\text{m}^{3/2}$ often resulted in macroscopic crack branching at low temperatures, and were not studied extensively). It is considered likely that, at stress intensity levels above about 50% of K_{Ic} , the ductile component of the fracture morphology would become more pronounced.

C.2.5.2 18Ni(200) Maraging Steel

C.2.5.2.1 Fracture Morphology for Stage II Cracking in Region A (Low Temperature Region)

Typical fracture morphology for Stage II crack growth in an 18Ni(200) maraging steel specimen, tested in Region A of the Arrhenius diagram (Figure 12) is illustrated in Figure 23. The fracture morphology was essentially invariant with respect to temperature and hydrogen pressure within this region, and is represented by six features. Five of these features are analogous to those observed on the 18Ni(250) maraging steel (see Section C.2.5.1.1 and Figure 18), and are identified accordingly in Figure 23. The sixth feature (Feature A in Figure 23), not present in the 18Ni(250) maraging steel, occupied a large percentage of the fracture surface for this lower strength material (see Figures 18 and 23). This feature indicates that there was extensive mechanical rupturing over regions encompassing several grains that were apparently not embrittled.

The observed difference in fracture morphology between the two grades of maraging steel is consistent with the decreased susceptibility of the lower strength material to gaseous hydrogen embrittlement. Specifically, the presence of large regions of plastically ruptured material (ductile failure) in the 18Ni(200) maraging steel implies that a substantial component of localized, high-stress creep crack growth [39, 52]

accompanied environment-enhanced cracking. This component would tend to reduce the overall rate of crack growth; a trend that is consistent with the results on crack growth kinetics (Figure 17). The observed fracture morphology further suggests that the prior-austenite boundaries are less susceptible in the lower strength grade of maraging steel. Analyses of grain boundary composition will contribute towards the understanding of this difference in susceptibility, and are under investigation.

Similar to the higher strength material, the fracture surface morphology for the 18Ni(200) maraging steel, tested in Region A, was essentially unaffected by changing K within Stage II, and was independent of hydrogen pressure. Some increase in the plastic component was observed with increasing K, consistent with the expected competition between the mechanical and chemical driving forces for crack growth.

C.2.5.2.2 Fracture Morphology for Stage II Cracking in Regions B/C (High Temperature Region)

The temperature induced transition in fracture morphology observed for the 18Ni(250) maraging steel was characterized by the appearance of a large component of plastic rupture, an increase in the amount of transgranular quasi-cleavage, and a decrease in intergranular separation. An analogous transition in fracture morphology was observed in the 18Ni(200) maraging steel as the temperature for Stage II crack growth was moved from Region A into Regions B/C for both hydrogen pressures, Figure 12.

A comparison of the appearance of fracture surfaces obtained in Region A and Regions B/C, at a hydrogen pressure of 1000 torr (133 kN/m^2), is given in Figure 24. The Fracture morphology for Region A (Figure 24a) is analogous in all respects to that illustrated in Figure 23, and has been described already in Section C.2.5.2.1. In contrast,

the Region B/C morphology is characterized by increased amounts of transgranular quasi-cleavage and a large component of plastically ruptured material, while maintaining a substantial component of intergranular separation. The change in fracture morphology for Stage II cracking between the various regions was found to be essentially independent of K and of hydrogen pressure. The transition, however, was not as obvious as that for the 18Ni (250) maraging steel because of the fact that a large component of plastic rupture was already present in Region A. Nonetheless, the observed change in fracture morphology tends to support a temperature induced transition in hydrogen susceptibility in the maraging steels.

C.2.5.2.3 Effect of Stress Intensity (Stretch Zone, Stage I, and Stage II)

Fractographic results on the 18Ni(200) maraging steel tend to confirm the results on the higher strength 250-grade materials. There was no evidence to support the presence of a stretch zone between the fatigue precrack and the hydrogen induced crack in this alloy. Furthermore, the fracture morphology for Stage I and Stage II crack growth was found to be the same in the low temperature region (Region A), as well as in the higher temperature regions (Regions B and C). These results provide additional support to the concept of a single embrittling process over the complete K range from Stage I on through Stage II. They do not support the hypothesis of a discontinuous transition in fracture morphology between Stages I and II [27], or the hypothesis that the formation of a stretch zone is requisite for environment enhanced crack growth [26].

III. HYDROGEN ADSORPTION AND DIFFUSION

A. Experimental Arrangement and Procedure

Hydrogen adsorption and diffusion in metals and alloys were studied using a hydrogen-deuterium exchange technique. Based on a statistical treatment of the exchange reactions in which diatomic molecules react with solids containing the same kind of atoms [70], the mechanism of adsorption and the diffusion coefficients can be determined by monitoring the following quantities with time. The reduced concentrations

$$\frac{[H_2] - [H_2]_\infty}{[H_2]_0 - [H_2]_\infty}, \quad \frac{[HD] - [HD]_\infty}{[HD]_0 - [HD]_\infty}, \quad \frac{[D_2] - [D_2]_\infty}{[D_2]_0 - [D_2]_\infty}, \quad \text{and the quantities}$$

$$K = \frac{[HD]^2}{[D_2][H_2]} \quad (4)$$

$$W = 2 [D_2] + [HD] \quad (5)$$

$[D_2]$, $[H_2]$, and $[HD]$ are the molecular fractions of the D_2 , H_2 and HD molecules, respectively, in the gaseous phase at a time t . The reduced concentrations are normalized measures of the rates of change of the individual molecular species. In the case of surface-catalyzed homomolecular exchange, the reduced concentrations follow the same time course [70]. At equilibrium, the quantity K assumes the value of 4, and becomes equal to the equilibrium constant. Deviation of K from this equilibrium value provides a direct measure of the proportion of different possible mechanisms of the exchange, and identification of the likely process associated with gaseous hydrogen embrittlement [70]. Measurements of the change in atomic deuterium concentration (W) in the gaseous phase give information regarding the extent of hydrogen diffusion into the bulk material and the relative contribution of this process to crack growth.

An ultrahigh vacuum (UHV) apparatus for the hydrogen deuterium exchange experiment has been constructed. A schematic diagram of this apparatus is shown in Figure 25. Ultrahigh vacuum is obtained by cryostatic roughing, followed by pumping with a titanium sublimation pump and a titanium sputter ion pump. The total pressures in the apparatus are measured by an ionization gage (low pressures) and by a Pirani gage (intermediate and high pressures). A quadrupole residual gas analyzer is used to monitor the D_2 , H_2 and HD components in the gaseous phase during the exchange experiments through a calibrated capillary. To provide a reaction cell that is free of metal deposits, a separate cleaning cell is provided. (Details of the cleaning cell and of the reaction cell are given in Figures 26 and 27 respectively). The cleaning cell is isolated from the reaction cell by a ground glass valve during the exchange experiments, so that the specimen is the only metal in contact with the experimental gases. For exchange experiments at high temperatures, the specimen is heated by an external, 1 kilowatt, 300 kHz R. F. generator. Experiments at low temperatures are carried out by cooling the reaction cell with a stream of chilled nitrogen regulated by a variable temperature controller.

Specimens were cut from materials used in the crack growth studies. These specimens are polished mechanically, and then chemically. After rinsing in distilled water and in methanol, they are dried and transferred to the cleaning cell, Figure 26, in the UHV apparatus. The specimens are heated by electron bombardment and sputter cleaned by argon ($\sim 10^{-4}$ torr) ion bombardment in this cell by applying the proper potentials to the electrodes as shown in Figure 27. After a number of ion bombardment and heating cycles, reproducible surface conditions can be obtained. Chemical cleaning

may be appropriate in some cases, and can be accomplished by heating the specimens in hydrogen at low pressures.

Following cleaning, the specimen is transferred into the reaction cell. Hydrogen (or deuterium) at selected pressure is admitted and allowed to react with the clean specimen for a predetermined length of time. Hydrogen (or deuterium) is then pumped out rapidly, and is replaced by deuterium (or hydrogen). Valves 1 and 2, Figure 27, are then closed so that the exchange reactions can be carried out in a small volume, isolated from the rest of the vacuum apparatus. To permit continuous sampling of the reaction mixture at relatively high pressures ($\sim 10^{-3}$ torr) with the quadrupole analyzer, and to prevent contact with the metal walls of the analyzer, a small amount of the reaction mixture is admitted directly into the ionization chamber of the analyzer through a calibrated capillary leak, C, Figure 27. The amounts of deuterium (D_2), hydrogen (H_2) and the mixed molecules (HD) are monitored as functions of time to determine the time variation of K and W.

In the apparatus described above, the activity of a metal surface can be investigated in three ways:

1. By mass spectrometric monitoring of an exchange reaction between hydrogen (H_2) and deuterium (D_2) molecules catalyzed by the metal surface. This rate is a measure of the ability of the metal to atomize hydrogen in its surface.

2. By mass-spectrometric monitoring of a replacement reaction in which hydrogen is placed in the material first and then isothermally replaced by deuterium from the gas phase. The total rate of production of hydrogen in the gaseous phase is a measure of the extent of adsorption and diffusion. The rates of appearance of the individual molecules

H_2 and HD and of disappearance of D_2 from the gas phase are measures of the mechanism by which hydrogen enters the surface layer.

3. By flash desorption of hydrogen from the metal surfaces. This technique enables the determination of the total adsorbed amounts and approximate binding strength of hydrogen to the surface.

B. Materials

The materials studied were the 18Ni(250) maraging steel, 18Ni(200) maraging steel, a single crystal of iron, cut and polished to expose the (111) plane, Inconel 718, and 316 stainless steel. Some of these materials were not included in the original proposal but their activities are reported here because they provide a useful comparison. The samples were 0.6 mm thick rectangular slabs of total surface area of about 1.5 cm^2 for the maraging steels and iron, and 0.5 mm of 4.17 cm^2 for the Inconel 718 and 316 stainless steel.

The following pretreatments were employed:

1. The metal surface was cleaned by argon ion bombardment (denoted as AB) under the conditions specified in section III-A. According to the results of Auger spectroscopic analyses, the surface composition of the ion bombarded material was the same as the nominal bulk composition (within the limits of accuracy of Auger spectroscopy). This cleaning procedure was employed prior to any of the subsequent treatments.

2. Some specimens were then surface-annealed at $400^\circ - 650^\circ\text{C}$ by electron bombardment for 5-10 minutes. This treatment is denoted A (annealed sample); absence of this treatment is denoted NA (non-annealed sample).

3. Prior to any cleaning procedure, the maraging steel specimens were always

heated to 850°C in vacuo and subsequently cooled to room temperature without aging at 500°C. Experiments on these annealed, non-aged specimens are marked by the symbol NAG. However, some specimens were aged at 500°C for 3 hrs. after the first argon ion bombardment, and subsequently ion bombarded again. These specimens are denoted AG (aged).

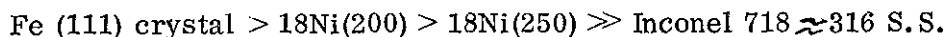
C. Results and Discussion

The replacement reactions (process #2, page 34) were attempted by loading the specimens with deuterium (D₂) at 10⁻² torr and 25°C and replacing the gas phase by hydrogen (H₂) at 10⁻⁴ torr from a volume of 1.5 liter. No replacement reactions were observed at temperatures between -190°C and 200°C. This result indicates that not much hydrogen was picked up by the materials studied, at least not in excess of 10-20 layers. Further experiments should be made at lower pressures of hydrogen to pursue the replacement reaction with a greater sensitivity.

The exchange reactions (process #1, page 34) were then investigated to provide a measure of the activity of the steel and iron crystal surfaces towards atomization of hydrogen. The ranges of pressures 10⁻³ to 10⁻² torr and temperatures between -190°C and +300°C were investigated. Measurable rates of the exchange
$$\text{H}_{2(g)} + \text{D}_{2(g)} \rightleftharpoons 2\text{HD}_{(g)}$$
 were obtained at temperatures between 0°C and 300°C. The results of the measurements of the total homomolecular rate of exchange (R + R' + R'') for the different materials and treatments are summarized in Table 6. The experimental material substantiating these data is presented in Appendix II. Comparison of the rates of H₂/D₂ exchange for the five materials is shown in Figure 28.

The rates (R + R' + R'') are those of overall adsorption, atomization, and re-

combination of hydrogen molecules on the given surface, irrespective of the mechanism by which the surface atomization takes place. These rates are therefore representative of the ability of the given material to atomize and recombine hydrogen. The data in Table 6 demonstrate the following order of chemical activities:



The effect of pretreatments is such that non-annealed surfaces are more active than annealed surfaces, and that aged specimens of maraging steels are more active than non-aged specimens (Inconel 718 and 316 stainless steel were not subjected to aging). The activation energies for the exchange reaction on all samples are between 0.45 and 4.0 kcal/mole, and are higher on 18Ni(250) specimens than on 18Ni(200) specimens. The activation energy for 316 stainless steel was very low, although this material has overall low activity. This result indicated that relatively few centers of very high activity are involved in hydrogen exchange for the 316 stainless steel. No activation energy data are available for Inconel 718. The kinetic data presented in Table 6 are based on the initial rates. The rates themselves are not constant with time as shown in the last column of Table 6, and indicate some decay of the surface activity with time. This phenomenon is most likely caused by hydrogen self-poisoning of the surface.

The initial rates ($R + R' + R''$) on the iron crystal ($\approx 10^{17}$ molecules $\text{cm}^{-2} \text{sec}^{-1}$ at 25°C and 10^{-2} torr) are quite comparable to the adsorption rates of hydrogen on polycrystalline iron, obtained by extrapolation of data reported by Chornet and Coughlin [71]. One out of 143 collisions with the surface results in an exchange event on Fe(111) crystal; while the reaction efficiency drops to one reaction event in 43,000 collisions

on the surface of annealed 316 stainless steel. We can conclude that the exchange rates on pure iron are kinetically limited by and coincide with the adsorption rates, and conversely, that the adsorption rates are determined by the rates of surface atomization of the impinging hydrogen molecules. The surface annealed 18Ni(200) maraging steel exhibits an activity about one-half order of magnitude lower, and the surface-annealed 18Ni(250) steel one order of magnitude lower than that of pure iron. The surface composition of these alloys, determined by Auger spectroscopy under conditions comparable to those of the exchange reactions, is close to the bulk composition with about 18% Ni, 7-8% Co, and 3-5% Mo. It appears that the alloying elements Ni, Co, and Mo have some effect on the activity but not a very profound one. On the other hand, Inconel 718 and 316 stainless steel exhibit activities amounting to less than one-half percent of that for pure iron (Figure 28). Both these materials have different amounts of Fe (18 and 63-65%, respectively) and Ni (54 and 12-14%, respectively). They have the same content of Cr (18%) and Mo (3%). Since Mo is also present in the maraging steels in about the same concentrations, it is unlikely to have different poisoning effects in Inconel 718 and in 316 stainless steel.

Since chromium is present in nearly equal concentrations in Inconel and 316 stainless and is absent in the maraging steels, it appears that the inhibition of the activity toward hydrogen exchange may be connected with enrichment of chromium on the surface, or with alloying effects that alter the electronic structure of the metal surface as to render it substantially less active toward hydrogen. Surface analyses are not available but will be performed to establish whether the inhibition effects are caused by concentration of chromium at the surface or by alloying effects.

The dissociation of hydrogen molecules into atoms is the most common mechanism for activation of hydrogen for chemical reactions, and may be suggested as a prerequisite for hydrogen embrittlement. The hydrogen atoms adsorbed in the vicinity of a crack tip may weaken the metal-metal bond and cause an enhancement of the crack growth rate (stress sorption cracking), or may diffuse ahead of the crack tip and form a composite zone whose mechanical cohesion is weaker than that of the hydrogen-free material. This involves the possible "hydride phase" discussed in Section IV. Either of these processes will be arrested when the surface does not produce atomic hydrogen at a sufficiently fast rate. This model is in agreement with the observations that the alloys not susceptible to hydrogen embrittlement (Inconel 718 and 316 stainless steel) are also poor catalysts for hydrogen exchange which requires surface atomization of hydrogen.

When an alloy is an active catalyst for hydrogen exchange, there may still exist a number of mechanisms which do not allow the hydrogen atoms to cause embrittlement. To list a few such possibilities, the ductility of the metal, structure and texture of the surface, surface diffusivity of hydrogen, and surface phase transformations [68-69] may influence the susceptibility of a metal to hydrogen embrittlement.

The effects of texture and surface roughness can be crudely estimated from the comparison of argon bombarded, non-annealed surfaces with argon bombarded and annealed surfaces. There is a distinct difference in the reactivities of the non-annealed and annealed surfaces, although their chemical composition is approximately the same. The non-annealed surfaces have in average about half order of magnitude higher activity than the annealed surfaces (Table 6). This effect is easily understood in terms of

higher activity of atoms displaced from their regular positions, increased concentration of vacancies, and generally higher energy content of the non-annealed, highly perturbed surfaces. The difference in the activity of the annealed and non-annealed surfaces is not great, however, and one can expect that slightly perturbed surfaces will have their activity close to that of the annealed surface. It would be desirable to know what kind of surface perturbations occur at the crack surface, and therefore the hydrogen adsorption and exchange experiments should be carried out on the actual crack surface which will yield additional kinetic information for comparison with that presently obtained for pure iron and steel surfaces cleaned by argon bombardment.

The effects of structure are perhaps reflected in the differences in the activities of the aged and non-aged specimens of the 18Ni(250) maraging steel (Table 6, rows 6 and 7). The aged specimens exhibit about one order greater activity than the non-aged specimens, indicating a higher reactivity of the aged martensitic structure over the annealed structure. These results should be compared with crack growth data on the aged and the annealed maraging steels.

IV. DISCUSSIONS

Both the 18Ni(200) and 18Ni(250) maraging steels exhibited K-independent (Stage II) sustained-load crack growth in gaseous hydrogen over the stress intensity ranges investigated. This Stage II crack growth was observed over a wide range of hydrogen pressure and temperature conditions. Apparent threshold stress intensity factors (K_{th}) for hydrogen assisted crack growth were also observed. Excellent agreement was obtained with a previous study on the same heat of 18Ni(250) maraging steel, attesting to the fact that specimen type and environment control procedure did not affect the observed behavior. The existence of a K-independent stage (Stage II) of crack growth suggests the operation of a chemical rate limiting process, and provides an essential link between the phenomenological observations of cracking and the mechanism for embrittlement. The basic correlative information is to be deduced from kinetic data on Stage II crack growth as functions of temperature and hydrogen pressure.

The general response to changes in temperature and hydrogen pressure were the same for these two grades of maraging steels. Three distinct regions of temperature response were observed. The general form of the temperature dependence was independent of the hydrogen pressure, and of the yield strength or chemical composition. Decreasing the yield strength or the hydrogen pressure, however, shifted the boundaries of each region to lower temperatures. Within Region A (the low temperature region), Stage II crack growth in both steels appears to be rate limited by the same thermally activated hydrogen transport process independent of the hydrogen pressure. This process is characterized by an activation energy of 4.4 ± 0.4 kcal/mole (18.2 ± 1.7 kJ/mole) on a pooled basis. Identification of this transport process has not been made at this time.

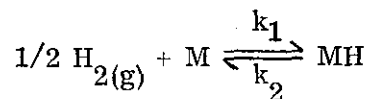
An abrupt temperature induced decrease in the susceptibility to gaseous hydrogen was observed in both steels in Region C. The transition temperature was found to be influenced by hydrogen pressure, and by alloy composition or yield strength level. This behavior implies that either a unit process in the transport of hydrogen from the gas phase to the fracture process zone, or the process involved in the weakening of inter-atomic bonds by hydrogen was deactivated by an extremely small increase in temperature (that is, about 5°C). One can only speculate at this time as to the identity of that mechanism that is abruptly affected by temperature. Two of the possible mechanisms are discussed later on in this section.

Region B represents the zone between Regions A and C, in which the mean Stage II crack growth rates attain their maximum value. Fracture morphology within this region reflects the gradual change from the embrittled condition at low temperatures to one of reduced embrittlement.

The isothermal pressure dependence for Stage II crack growth was found to be affected by temperature; that is, different pressure dependence may be obtained in accordance with the positions of the crack growth isotherms in the Arrhenius diagrams, Figures 11 and 12. Within Region A (for all pressures), the mean Stage II growth rate was proportional to the one-half power of hydrogen pressure. The pressure dependence for Region B ranged between one-half power to second power of hydrogen pressure as the temperature was increased. Mixed region pressure dependence were irregular and are of little value. These findings accounts for the wide range of pressure dependence that have been reported in the literature. The mechanistic basis for the pressure dependence will need to be investigated.

Fractographic examinations showed that there were no changes in fracture morphology between Stage I and Stage II of crack growth, and suggest that there is a single mechanism for hydrogen embrittlement over the entire range of K values. The processes controlling hydrogen enhanced cracking in the various temperature regions, however, are likely to be different, and require further examination. No detectable stretch zones were observed on the specimens tested during this program. This observation indicates that stretch zone formation is incidental to the fracturing process, and is not a prerequisite for embrittlement.

The simplest model to account for the observed cracking behavior might be one in which a "hydride phase" is formed according to the reaction



where M is the metal or active component of the alloy and MH is a separate hydride phase, either bulk or surface. At low temperatures (Region A), the process characterized by k_2 is negligibly slow and the hydride formation is controlled by k_1 ; and since hydrogen dissociates, the rate of that process is proportional to the square root of P_{H_2} . At equilibrium, both processes characterized by k_1 and k_2 become equally fast. Moreover, the phase rule allows only one degree of freedom in this system, so that for each equilibrium pressure there is only one equilibrium temperature above which the "hydride phase" cannot coexist with the metal phase, and below which the metal phase should all be converted into the hydride phase. The important point is that the experiment or practical exposure always starts from the metal-molecular hydrogen system, and therefore the conversion of the metal into the hydride is kinetically limited at the low temperatures.

Although attractive at first sight, the implementation of the phase rule for the bulk equilibria is almost certainly oversimplified in the interpretation of hydrogen embrittlement observed here. Notably, the phase rules in the presence of surfaces and external forces are more complicated and cannot be discarded in their complex form, since both the surfaces and the external forces are present. It must therefore first be experimentally determined which surfaces in the alloy are attacked by hydrogen.

Fractography shows that the principal mode of fracture is intergranular, and therefore alloy components appearing at the interfaces between the grains are the likely candidates for "hydride phase" formation.

Alternative to the metal hydride phase formation, a surface phase transformation between an "active hydrogen surface phase" and an "inactive surface phase" may be considered. Examples of such surface phase transformation may be a two-dimensional liquid-gas first order transition [68, 69], the 2-D liquid being the "active phase" and the 2-D gas being the inactive phase. There are some difficulties with such an interpretation, namely that the two-dimensional liquid-gas transitions ordinarily occur at substantially lower pressures (10^{-8} to 10^{-1} torr) for most metals, giving rise to saturation at pressures of the fracture experiment.

Further experimental work is needed to document the existence of such a phase transition for the hydrogen-martensitic steel system, and to investigate other possible mechanisms for this transition behavior. Fractographic evidence indicated that the change in hydrogen susceptibility was accompanied by a change from predominantly intergranular fracture to transgranular quasi-cleavage and ductile rupture, and suggests the reduction of sensitivity of the prior austenite grain boundaries to hydrogen. Future chemical investigations should incorporate considerations of grain boundary compositions

on the surface reaction kinetics.

Because of the early termination of this program, surface chemistry experiments at the higher pressures (100 to 1000 torr or 13.3 to 133 kN/m²) could not be carried out to provide direct comparisons with the crack growth experiments. Data from experiments at low pressures (10^{-3} - 10^{-2} torr) suggest that those alloys which are active catalysts for hydrogen atomization tend to be more susceptible to gaseous hydrogen embrittlement (18Ni maraging steels versus Inconel 718 and 316 stainless steel). These data also suggest that chromium may act as a poison for the catalytic activity of alloy surfaces for hydrogen atomization. More extensive surface chemistry studies are urgently needed to help elucidate the mechanism for hydrogen embrittlement.

V. SUMMARY

1. No sustained-load crack growth was observed for the Inconel 718 alloy in gaseous hydrogen (~ 1000 torr or $\sim 133 \text{ kN/m}^2$) at about -50°C , 25°C and $+300^\circ\text{C}$ for stress intensities up to $99 \text{ MN-m}^{-3/2}$ ($90 \text{ ksi } \sqrt{\text{in.}}$). The rate of fatigue crack growth at room temperature, with $R = K_{\text{min}}/K_{\text{max}} = 0.5$ and $f = 5.0 \text{ Hz}$, was also unaffected by gaseous hydrogen (at ~ 1000 torr or $\sim 133 \text{ kN/m}^2$).

2. Gaseous hydrogen assisted crack growth in the 18Ni maraging steels from -60°C to $+100^\circ\text{C}$, were characterized by K-independent (Stage II) extension over a wide range of hydrogen pressure and test temperature conditions. Apparent thresholds for hydrogen assisted crack growth were also observed. The higher strength 18Ni(250) maraging steel was more susceptible to embrittlement than the 200-grade material. The concept of a chemical or transport process limited Stage II crack growth rate was verified as consistent with current results, and as such, provided the interface between phenomenological result and mechanistic inference.

3. Three distinct Regions of temperature dependence were observed. The general form of this dependence is independent of yield strength and hydrogen pressure. Decreased yield strength and decreased hydrogen pressure, however, shifted the boundaries of each Region to lower temperatures. These three regions have been designated as Regions A, B, and C. (that is, low-, intermediate-, and high temperature regions). Within Region A, Stage II crack growth was thermally activated with an activation energy equal to $4.4 \pm 0.4 \text{ kcal/mole}$ ($18.2 \pm 1.7 \text{ kJ/mole}$), independent of yield strength and hydrogen pressure. Within Region B, the Stage II crack growth tended to become slower than that predicted by extrapolation from Region A. Region C was characterized by an abrupt

decrease in susceptibility to gaseous hydrogen embrittlement attendant with a small increase ($<5^{\circ}\text{C}$) in test temperature. This effect was verified as not being an artifact, and was observed at the various yield strengths and pressures.

4. The mean Stage II crack growth rate was proportional to the square root of hydrogen pressure within Region A of the temperature dependence. The pressure dependence of Stage II crack growth rate varied within Region B over the range of exponent values from 0.5 to about 2.0 as test temperature increased. Mixed region isothermal pressure dependence were irregular and of little mechanistic value. The wide variation in reported Stage II isothermal pressure dependence can be explained on the basis of the interactive effect of test temperature with hydrogen pressure.

5. Fractographic examination showed that there were no changes in fracture morphology between Stage I and Stage II of crack growth, and suggests that there is a single mechanism for hydrogen embrittlement over the entire range of K values. (The processes controlling hydrogen enhanced cracking in the various temperature regions, however, are likely to be different, and require further examination.) A transition from predominately intergranular failure (with respect to the prior-austenite grains) to mixed intergranular quasi-cleavage and ductile tearing accompanied a change from Region A to Region B/C. This change in fracture morphology is consistent with the reduced susceptibility to gaseous hydrogen embrittlement. No detectable stretch zones were observed on the specimens tested during this program. This observation indicates that stretch zone formation is incidental to the fracturing process, and is not a prerequisite for embrittlement.

6. The rates of hydrogen atomization by the maraging steels investigated are

high and probably sufficient to sustain the crack growth through a mechanism limited by hydrogen atom formation.

7. Pure iron is a very good catalyst for hydrogen activation. Nickel, cobalt, and small amounts of molybdenum in the maraging steels reduce the activity of iron only slightly. On the other hand, chromium in Inconel 718 and in 316 stainless steel appears to have large inhibiting effect on both the activity of hydrogen exchange reactions and on hydrogen embrittlement.

8. Aged specimens are more active for hydrogen atomization than non-aged specimens.

9. Surface roughness induced by ion bombardment increases the activity of all materials studied.

10. It appears that prevention of hydrogen embrittlement in maraging steels should be sought in adding alloying elements (such as chromium) which would poison the catalytic activity of the surface for hydrogen atomization, or which would act as traps for hydrogen atoms preventing their surface diffusion. The effects of gaseous poisons such as O_2 , N_2O , CS , and CS_2 should also be considered if the presence of these gases can be accepted on technological grounds. The experiments on poisoning of the steel surfaces by these gases with respect to hydrogen adsorption and exchange can be carried out in our present system without modification.

11. Plausible mechanistic explanations for the observed crack growth behavior in the 18Ni maraging steels were discussed. Surface chemistry experiments at pressures comparable to those used in the crack growth experiments are needed to substantiate and further develop these suggested explanations.

REFERENCES

1. C. Zapffe and C. Sims, Trans. TMS-AIME, 145, 225 (1941).
2. F. Garofalo, Y. T. Chou, and V. Ambegaokar, Acta Met., 8, 504 (1960).
3. B. A. Bilby and J. Hewitt, Acta Met., 10, 587 (1962).
4. A. S. Tetelman, Proceedings - Fundamental Aspects of Stress Corrosion Cracking, Natl. Assoc. Corr. Engrs., Houston, 446 (1969).
5. R. P. Frohberg, W. J. Barnett, and A. R. Troiano, Trans. ASM, 47, 892 (1955).
6. H. H. Johnson, J. G. Morlet, and A. R. Troiano, Trans. TMS-AIME, 212, 528 (1958).
7. E. A. Steigerwald, F. W. Schaller, and A. R. Troiano, Trans. TMS-AIME, 215, 1048 (1959).
8. A. R. Troiano, Trans. ASM, 52, 54 (1960).
9. N. O. Petch and P. Stables, Nature, 169, 842 (1952).
10. R. A. Oriani, Proc. Intl. Conf. on Stress Corrosion Cracking and Hydrogen Embrittlement of Iron Based Alloys, Firminy, France (to be published by NACE) (1974).
11. H. H. Johnson, Proceedings - Fundamental Aspects of Stress Corrosion Cracking, Natl. Assoc. Corr. Engrs., Houston, 439 (1969).
12. R. P. Wei, Intl. J. Fract. Mech., 4, 159 (1968).
13. R. P. Wei, J. Eng'g. Fract. Mech., 1, 633 (1970).
14. F. J. Bradshaw and C. Wheeler, RAE Tech. Memo. No. MAT 26 (1968).
15. T. Bloom and A. J. Nicholson, J. Inst. Metals, 89, 183 (1960).
16. G. G. Hancock and H. H. Johnson, Trans. TMS-AIME (1966).
17. R. P. Wei and J. D. Landes, Matl. Res. & Std., ASTM, Vol. 9, No. 7, 25 (1969).
18. W. A. Spitzig, P. M. Talda, and R. P. Wei, J. Eng'g. Fract. Mech., 1, 155 (1968).
19. D. P. Williams and H. G. Nelson, Met. Trans., 1, 63 (1970).

20. H. G. Nelson, D. P. Williams, and A. S. Tetelman, *Met. Trans.*, 2, 953 (1971).
21. V. R. Sawicki, Jr., Ph. D. Dissertation, Cornell University (1971).
22. S. J. Hudak, Jr., M. S. Thesis, Lehigh University (1972).
23. H. G. Nelson and D. P. Williams, Proc. Intl. Conf. on Stress Corrosion Cracking and Hydrogen Embrittlement of Iron Based Alloys, Firminy, France (to be published by NACE) (1974).
24. R. A. Oriani, Proc. Intl. Conf. on Stress Corrosion Cracking and Hydrogen Embrittlement of Iron Based Alloys, Firminy, France (to be published by NACE) (1974).
25. R. A. Oriani and P. H. Josephic, to be published in Acta Met. (1974).
26. P. McIntyre, Proc. Intl. Conf. on Stress Corrosion Cracking and Hydrogen Embrittlement of Iron Based Alloys, Firminy, France (to be published by NACE) (1974).
27. G. E. Kerns, Ph. D. Dissertation, Ohio State University (1973).
28. R. W. Staehle, M. T. Wang and G. E. Kerns, Proc. Intl. Conf. on Stress Corrosion Cracking and Hydrogen Embrittlement of Iron Based Alloys, Firminy, France (to be published by NACE) (1974).
29. H. H. Johnson, Proc. Intl. Conf. on Stress Corrosion Cracking and Hydrogen Embrittlement of Iron Based Alloys, Firminy, France (to be published by NACE) (1974).
30. R. J. Walter and W. T. Chandler, "Effect of High-Pressure Hydrogen on Metals," paper presented at the Symposium on Effects of Gaseous Hydrogen on Metals, 1968, Materials Eng'g. Congress, Detroit, Mich., 13-17 October 1968.
31. R. J. Walter and W. T. Chandler, NASA CR-124410 (1973).
32. R. P. Wei, unpublished results (1973).
33. R. P. Wei, "The Effects of Temperature and Environment on Subcritical Crack Growth," presented at the WESTEC Conference (1972); Rept. IFSM-72-14, Lehigh University (April 1972).
34. R. A. Oriani, Proceedings - Fundamental Aspects of Stress Corrosion Cracking, Natl. Assoc. Corr. Engrs., Houston, 32 (1969).

35. D. S. Dabkowski, L. F. Porter, and G. E. Loveday, "Evaluation of Vacuum Induction Melted 18Ni(180) and 18Ni(250) Maraging Steels," Rept. 39.018-007(3), Applied Research Laboratory, U. S. Steel Corporation, January 1, 1967.
36. W. F. Brown, Jr. and J. E. Strawley, ASTM STP 410 (1966).
37. M. Isida, "Crack Tip Stress Intensity Factors for the Tension of an Eccentrically Cracked Strip," Lehigh University, Dept. of Mechanics Report (1965).
38. W. K. Wilson, Westinghouse Research Laboratories Rept. No. 67-7D7-BTLPV-R1 (1967).
39. J. D. Landes, Ph. D. Dissertation, Lehigh University, (1970).
40. Che-Yu Li and R. P. Wei, Mat'l. Res. and Stds., ASTM 6, 392 (1966).
41. F. Turner, "Cryosorption Pumping," presented at Varian Vacuum Division 10th Annual Vacuum Technology Seminar (1972).
42. S. A. Stern, J. T. Mullhaupt, R. A. Hempstreet, and F. S. D. Paolo, J. Vac. Sci. Tech. 2, 165 (1965).
43. R. P. Jewett, R. J. Walter, W. T. Chandler, and R. P. Frohberg, NASA CR-2163 (1973).
44. R. P. Wei, unpublished results.
45. R. J. Walter and W. T. Chandler, Rocketdyne Report, NASA CR-124410 (1973).
46. C. S. Carter, J. Eng. Frac. Mech. 3, 1 (1971).
47. S. Mostovoy, H. R. Smith, R. G. Lingwall, and E. J. Ripling, J. Eng. Frac. Mech., 3, 291, (1971).
48. S. J. Hudak, Jr. and R. P. Wei, "The Kinetics of Hydrogen Enhanced Crack Growth 18Ni Maraging Steels," to be published.
49. A. Hald, Statistical Theory with Engineering Applications, John Wiley and Sons, Inc., New York (1952).
50. R. P. Gangloff, Ph. D. Dissertation, Lehigh University, in preparation (1974).
51. J. D. Landes and R. P. Wei, J. Eng. Matls. Tech., 95 H, 2 (1973).
52. Che-Yu Li, P. M. Talda and R. P. Wei, "Subcritical-Crack Growth in an Inert Environment Under Constant Load," Applied Research Laboratory, U. S. Steel Corp. (1966).

53. H. G. Nelson and D. P. Williams, *Met. Trans.*, 3, 2107, (1972).
54. G. E. Kerns and R. W. Staehle, *Scripta Met.*, 6, 631 (1972).
55. G. E. Kerns and R. W. Staehle, *Scripta Met.*, 6, 1189, (1972).
56. J. P. Fidelle, J. Legrand, and C. Couderc: "A Fractographic Study of Hydrogen Gas Embrittlement in Steels," TMS-AIME Paper No. F71-8 (1971).
57. A. J. Stavros and H. W. Paxton, *Met. Trans.*, 1, 3049, (1970).
58. D. P. Dautovich and S. Floreen, Proc. Intl. Conf. on Stress Corrosion Cracking and Hydrogen Embrittlement of Iron Based Alloys, Firminy, France (to be published by NACE) (1974).
59. D. P. Williams and A. G. Evans, *J. Test. Matls.*, 1, 264 (1973).
60. I. M. Bernstein, *Met. Trans.*, 1, 3143, (1970).
61. M. L. Wayman and G. C. Smith, *Met. Trans.*, 1, 1189, (1970).
62. B. B. Rath and I. M. Bernstein, *Met. Trans.*, 2, 2845, (1972).
63. I. M. Bernstein, *Matls. Sci. Eng.*, 6, 1, (1970).
64. G. J. Spaeder, *Met. Trans.*, 1, 2011, (1970).
65. T. B. Cox and J. R. Low, Jr., "Investigation of the Plastic Fracture of High Strength Steels," NASA Technical Report No. 5, Grant NGR 39-087-003, (1973).
66. C. D. Beachem and R. M. N. Pelloux, Fracture Toughness Testing, ASTM STP 381, Am. Soc. Testing Matls., 210 (1964).
67. C. D. Beachem, Proc. Intl. Conf. on Stress Corrosion Cracking and Hydrogen Embrittlement of Iron Based Alloys, Firminy, France (to be published by NACE) (1974).
68. E. W. Hart, *Scripta Met.*, 2, 179, (1968).
69. E. W. Hart, Nature and Behavior of Grain Boundaries, Plenum Publishing Corporation, New York, 155 (1970).
70. K. Klier, J. Novakova, and P. Jiru, *J. Catalysis*, 2, 479 (1963).
71. E. Chornet and R. W. Coughlin, *J. Catalysis* 27, 246 (1972).

TABLE 1
 CHEMICAL COMPOSITION AND HEAT TREATMENT
 FOR INCONEL 718 ALLOY SHEET

Chemical Composition, Weight Percent
 (INCO Huntington Alloy Products Div. Heat No. HT94B1ES)

	AMS 5596 C		Supplier's Analysis	Check Analysis
	min.	max.		
C	---	0.10	0.05	0.03
Mn	---	0.35	0.07	0.40
Si	---	0.35	0.19	0.17
P	---	0.015	0.009	0.007
S	---	0.015	0.007	0.004
Ni	50.0	55.0	53.81	54.2
Cr	17.0	21.0	18.40	17.9
Mo	2.8	3.3	2.96	2.94
Cu	---	0.1	0.04	0.05
Cb+ Ta	5.0	5.5	5.19	3.68
Ti	0.65	1.15	1.00	1.00
Al	0.4	0.8	0.58	0.43
Co	---	1.0	0.03	0.12
B	---	---	0.0028	ND*
Fe	Balance		17.65	ND*(~19.1)

*ND - Not Determined

Heat Treatment

Solution Anneal - 1800°F, 1 hour + Air Cool

Age - 1325°F, 8 hours + Furnace Cool to 1150°F + Hold
 at 1150°F for total aging time of 18 hours + Air Cool

TABLE 2

Tensile Properties of Inconel 718 Sheet
(Heat No. HT94B1ES)

<u>Source</u>	<u>Orientation</u>	<u>Tensile Strength</u> ksi	<u>Yield Strength</u> ksi	<u>Elongation</u> in 2 in. percent
Lehigh University	Longitudinal	203.4	166.8	18.0
		205.1	168.5	18.0
		<u>202.8</u>	<u>166.2</u>	<u>17.5</u>
	(Average)	203.8	167.2	17.8
	Transverse	200.5	167.4	17.0
		201.9	168.4	17.0
		<u>201.7</u>	<u>168.5</u>	<u>17.0</u>
201.4		168.1	17.0	
Huntington Alloy (Supplier)	Transverse	202.0	177.0	18.0
AMS 5596C	Transverse	180.0 (min.)	150.0 (min.)	12 (min.)

TABLE 3

CHEMICAL COMPOSITION AND HEAT TREATMENT
FOR 18Ni(200) MARAGING STEEL PLATE

Chemical Composition, Weight Percent
(U. S. Steel Corporation Heat No. L-50446)

	<u>Supplier's</u> <u>Analysis [35]</u>	<u>Check</u> <u>Analysis</u>
C	0.002	ND*
Mn	<0.02	ND
Si	0.003	ND
P	0.003	ND
S	0.007	ND
Ni	17.50	17.89
Co	7.60	7.50
Mo	2.93	2.75
Ti	0.20	0.18
Al (sol.)	0.007	ND
N	0.004	ND
O	0.0011	ND
Fe	Balance	Balance

* ND - Not Determined

Heat Treatment

Solution Anneal - 1650°F, 1/2 hour + Air Cool

Re-solution Anneal - 1500°F, 1/2 hour + Water Quench

Age - 900°F, 16 hours + Water Quench

TABLE 4

Tensile Properties of 18Ni(200) Maraging Steel Plate
(U. S. Steel Heat No. L-50446)

<u>Orientation</u>	<u>Tensile Strength</u> ksi	<u>Yield Strength</u> ksi	<u>Elongation</u> in 2 in. percent
Longitudinal	193.1	185.7	13.0
	192.8	185.5	13.0
	<u>193.2</u>	<u>185.0</u>	<u>12.5</u>
(Average)	193.0	185.4	12.8

TABLE 5

CHEMICAL COMPOSITION, HEAT TREATMENT, AND MECHANICAL PROPERTIES
OF 18Ni (250) MARAGING STEEL

<u>Chemical Composition, Weight Percent</u>										
<u>C</u>	<u>Mn</u>	<u>P</u>	<u>S</u>	<u>Si</u>	<u>Ni</u>	<u>Co</u>	<u>Mo</u>	<u>Ti</u>	<u>Al</u>	<u>Fe</u>
0.003	0.002	0.002	0.004	0.017	17.8	7.6	5.0	0.45	0.01	Balance

Heat Treatment

- (1) Solution anneal for 1 hour at 1700°F in a protective atmosphere and air cool
- (2) Age for 3 hours at 900°F and air cool

Room Temperature Mechanical Properties

<u>Direction</u>	<u>0.2% Yield Strength, ksi</u>	<u>Tensile Strength, ksi</u>	<u>Elong. in 1 in., %</u>
Longitudinal (LT)	239	250	10

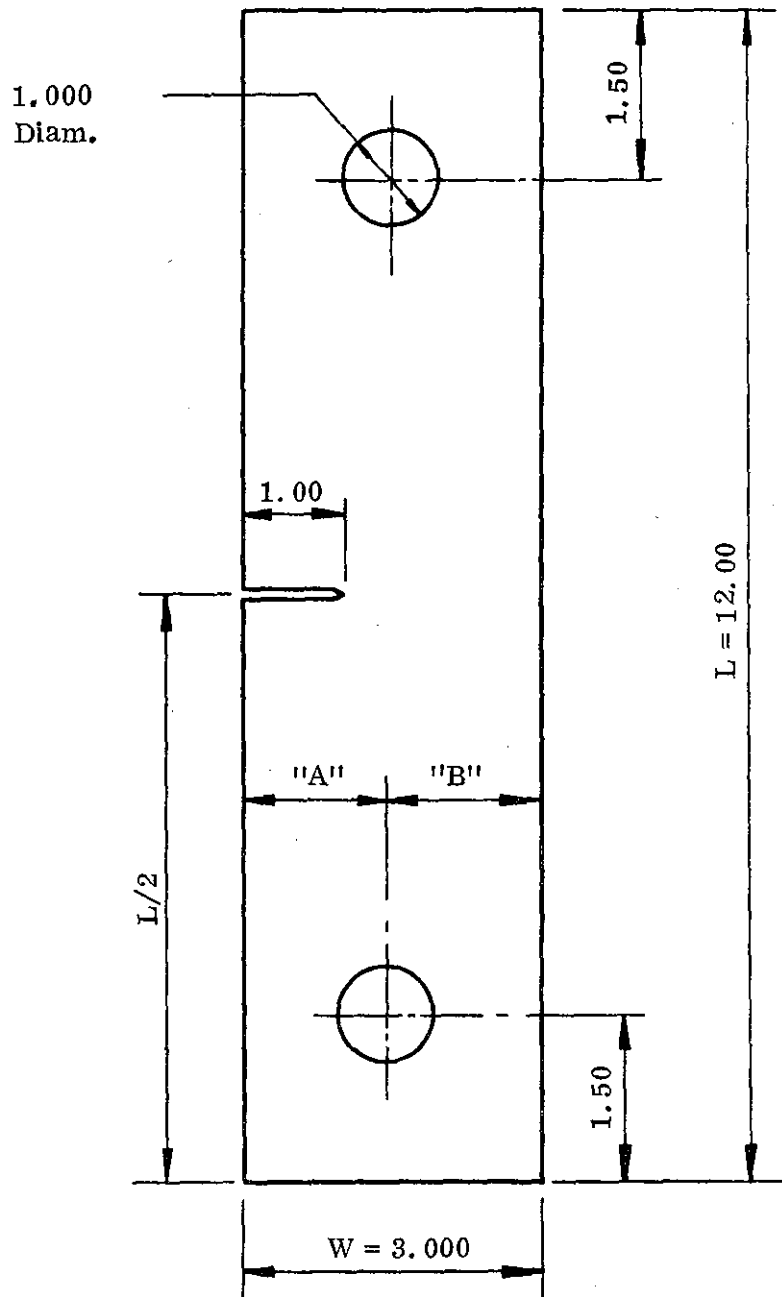
TABLE 6

Summary of the Rates, Activation Energies, and Time Dependences of the H_2/D_2 Exchange on Iron Crystal of (111) Orientation, $^{18}Ni(200)$ Maraging Steel, $^{18}Ni(250)$ Maraging Steel, Inconel 718, and 316 Stainless Steel

Material	Treatment ^a	Rate of homomolecular exchange $R + R' + R''$ at 25°C ^b	E_A (kcal/mole)	Time Dependence
Iron single crystal, (111) plane	AB-A (750°C)	1×10^{17}		$10^{17} \rightarrow 4 \times 10^{16}$ in 10 min
$^{18}Ni(200)$ maraging steel	AG-AB-A	5×10^{16}	1.1-1.4	$5 \times 10^{16} \rightarrow 1 \times 10^{16}$ in 10 min
	AG-AB-NA	1×10^{17}	1.7	
$^{18}Ni(250)$ maraging steel	AG-AB-A	1×10^{16}	2.2	$3 \times 10^{16} \rightarrow 10^{16}$ in 10 min (200°C) $1.5 \times 10^{16} \rightarrow 6 \times 10^{15}$ in 10 min (100°C)
	AG-AB-NA	4×10^{16}	1.2-1.8	
	NAG-AB-NA	4.5×10^{15}	1.0-4.0	
Inconel 718	AB-A	4.75×10^{14}		
316 Stainless Steel	AB-A	3.4×10^{14}	0.43	
	AB-NA	4.9×10^{14}		

^a AG = aged, NAG = non-aged, AB = argon bombarded, A = annealed at 700 - 800°C after argon bombardment, NA = non-annealed.

^b Rates are in molecules/cm² sec. Homomolecular exchange is the reaction $H_{2(g)} + D_{2(g)} \rightleftharpoons 2HD_{(g)}$ catalyzed by the surface.



Note: $"A" = "B" \pm 0.001$

Figure 1: SEN Fracture Toughness Test Specimen

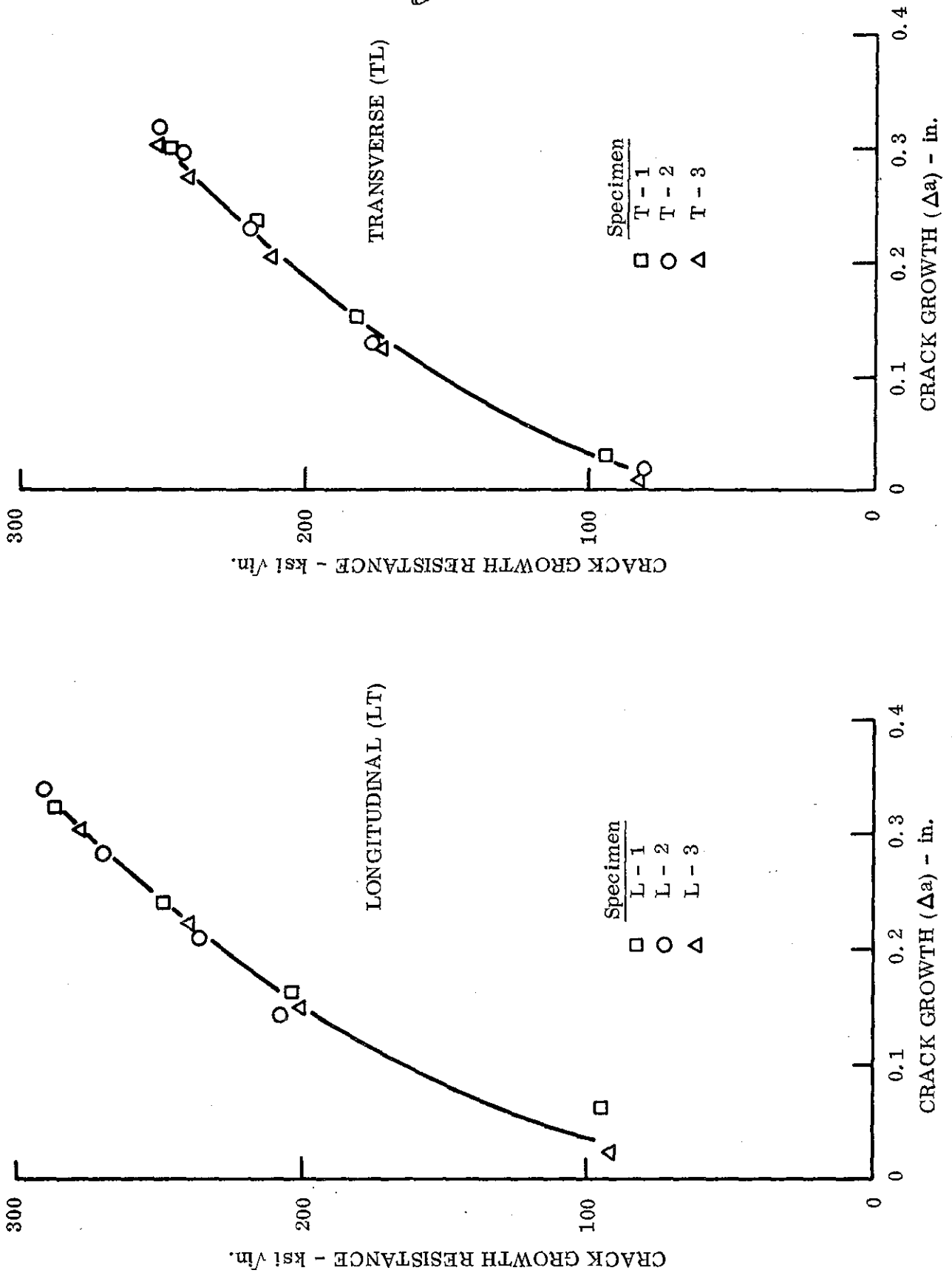


Figure 2: Crack growth resistance curves for 1/8-inch-thick Inconel 718 alloy sheet (solution annealed and aged)

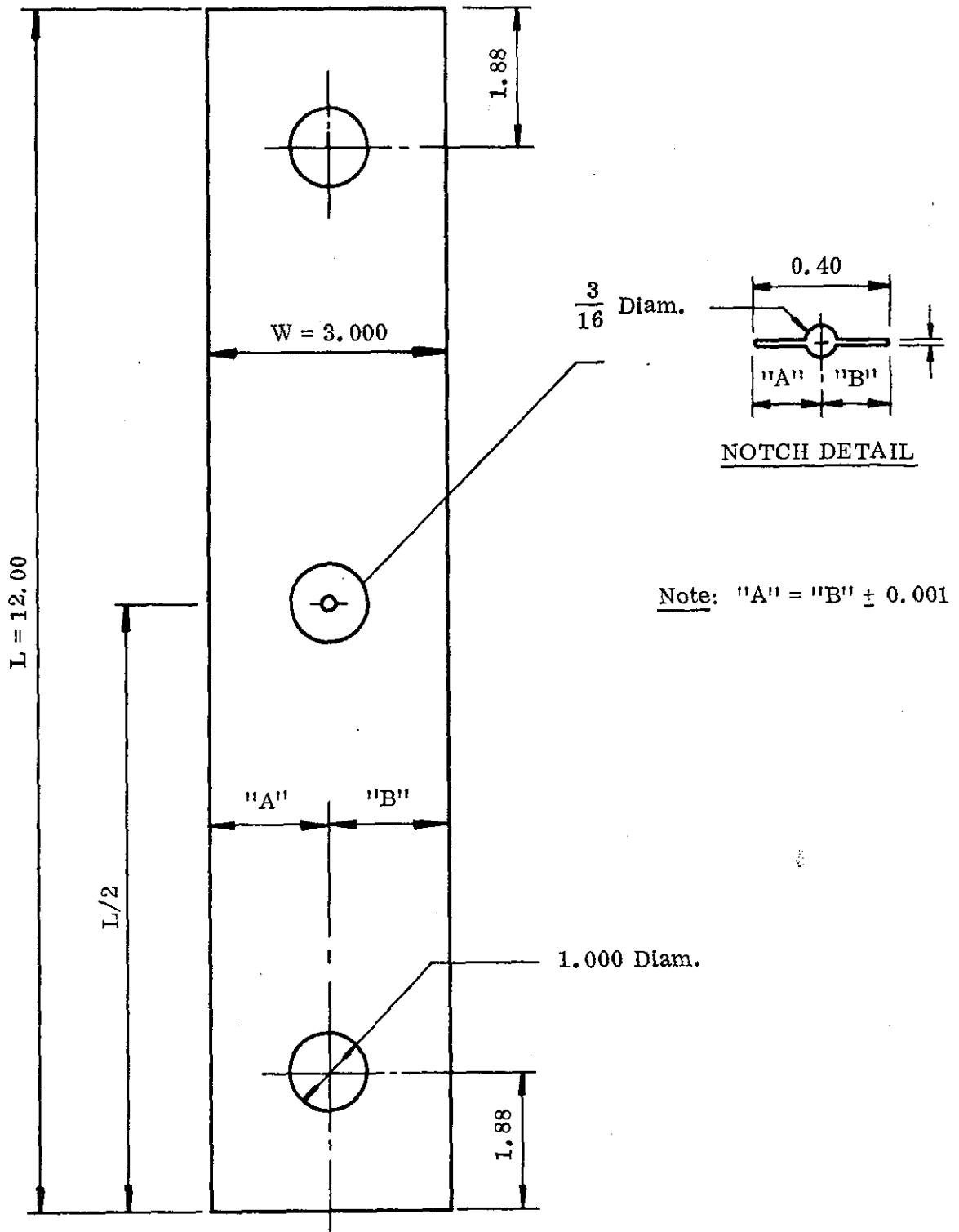


Figure 3: Center-Cracked Crack Growth Test Specimen

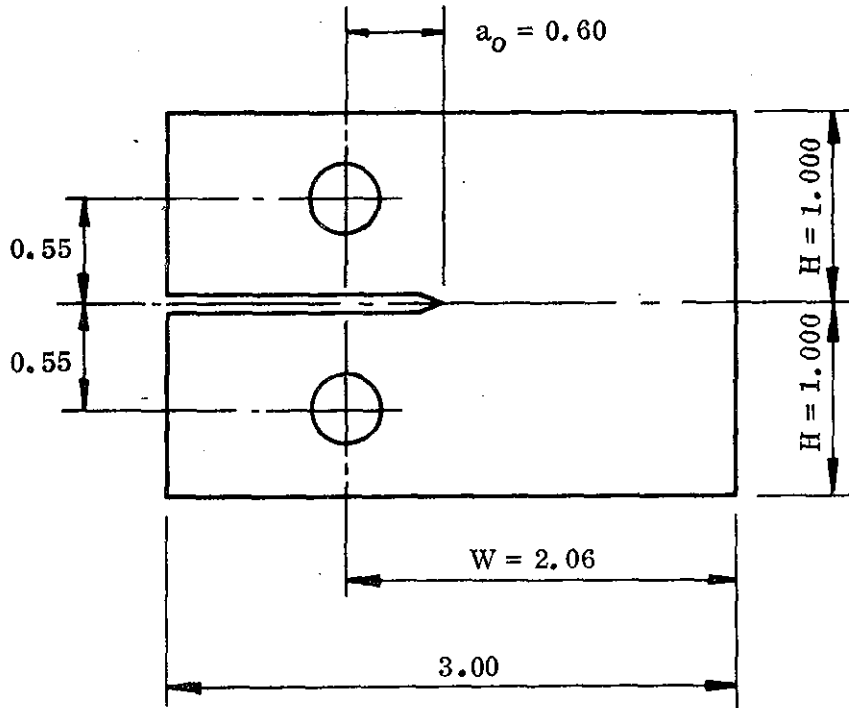


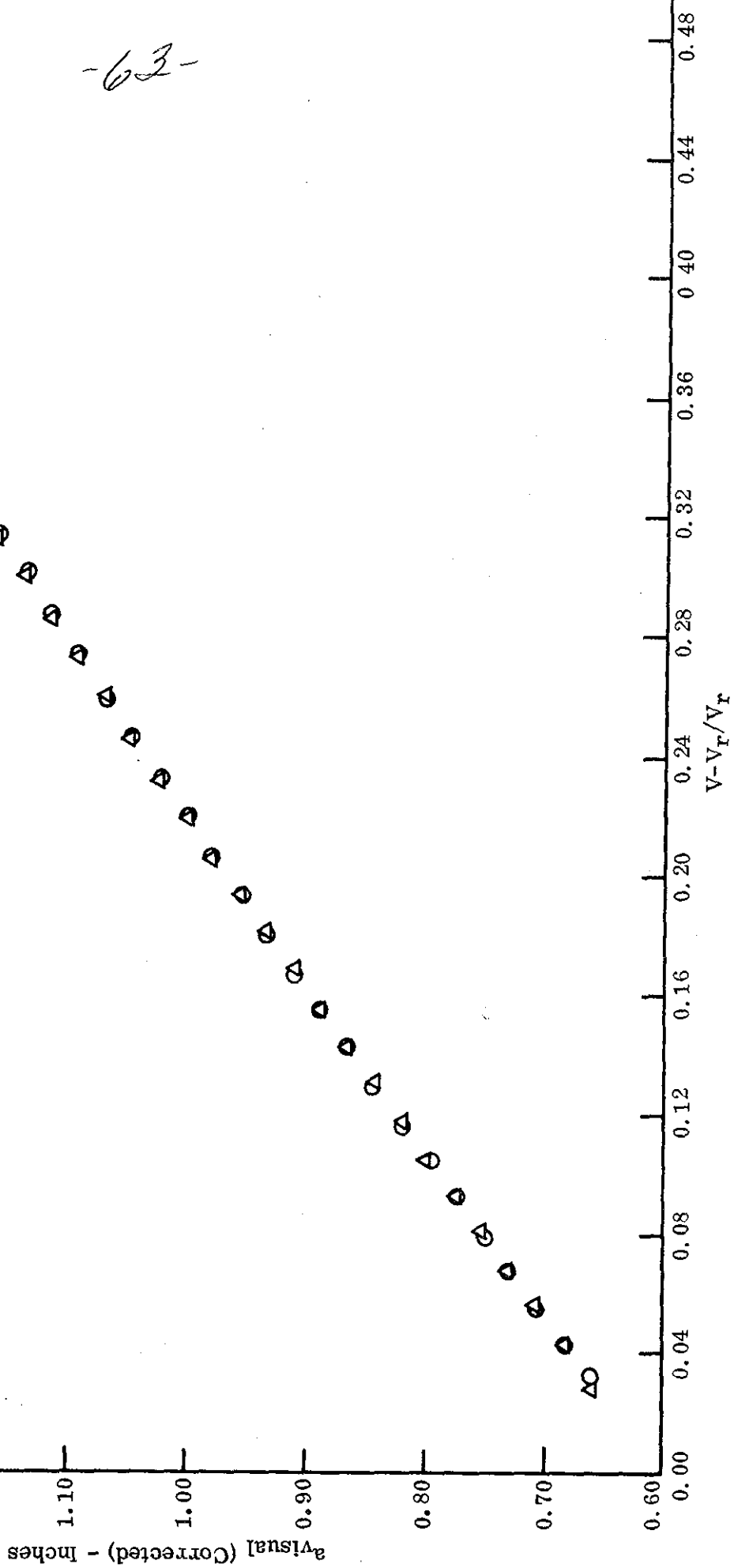
Figure 4: Modified Wedge-Opening-Load (WOL) Specimen

-63-

○ Specimen S3-CAL [I = 2.1 amp., $V_r = 443.2 \mu\text{v}$ at $a = 0.602 \text{ in.}$]

△ Specimen S4-CAL [I = 3.3 amp., $V_r = 708.2 \mu\text{v}$ at $a = 0.602 \text{ in.}$]

Figure 5: Calibration curve for 2.06-inch-wide modified WOL specimens.



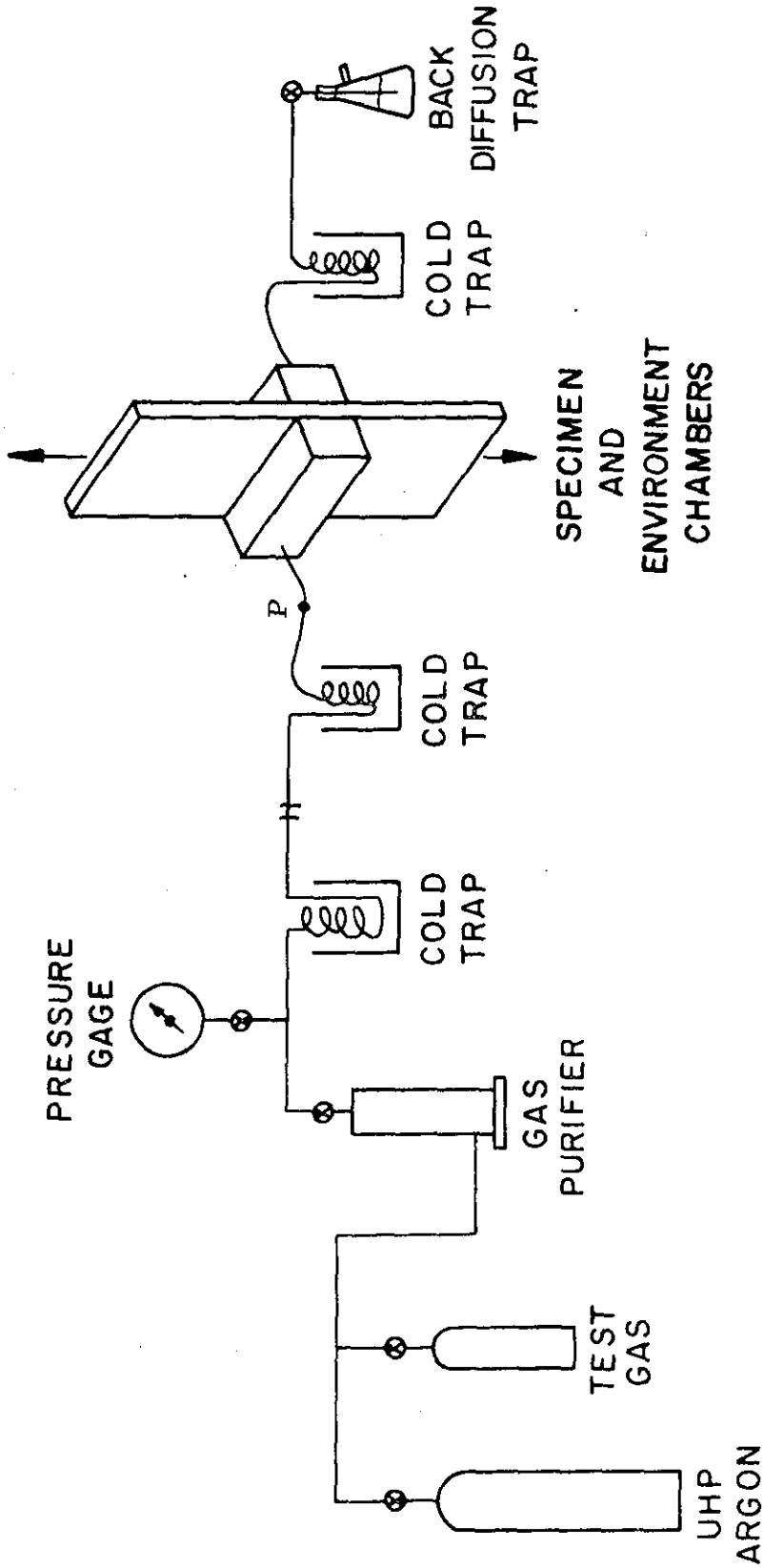


Figure 6: Schematic Diagram of Environmental Control System for Center Cracked Specimen.

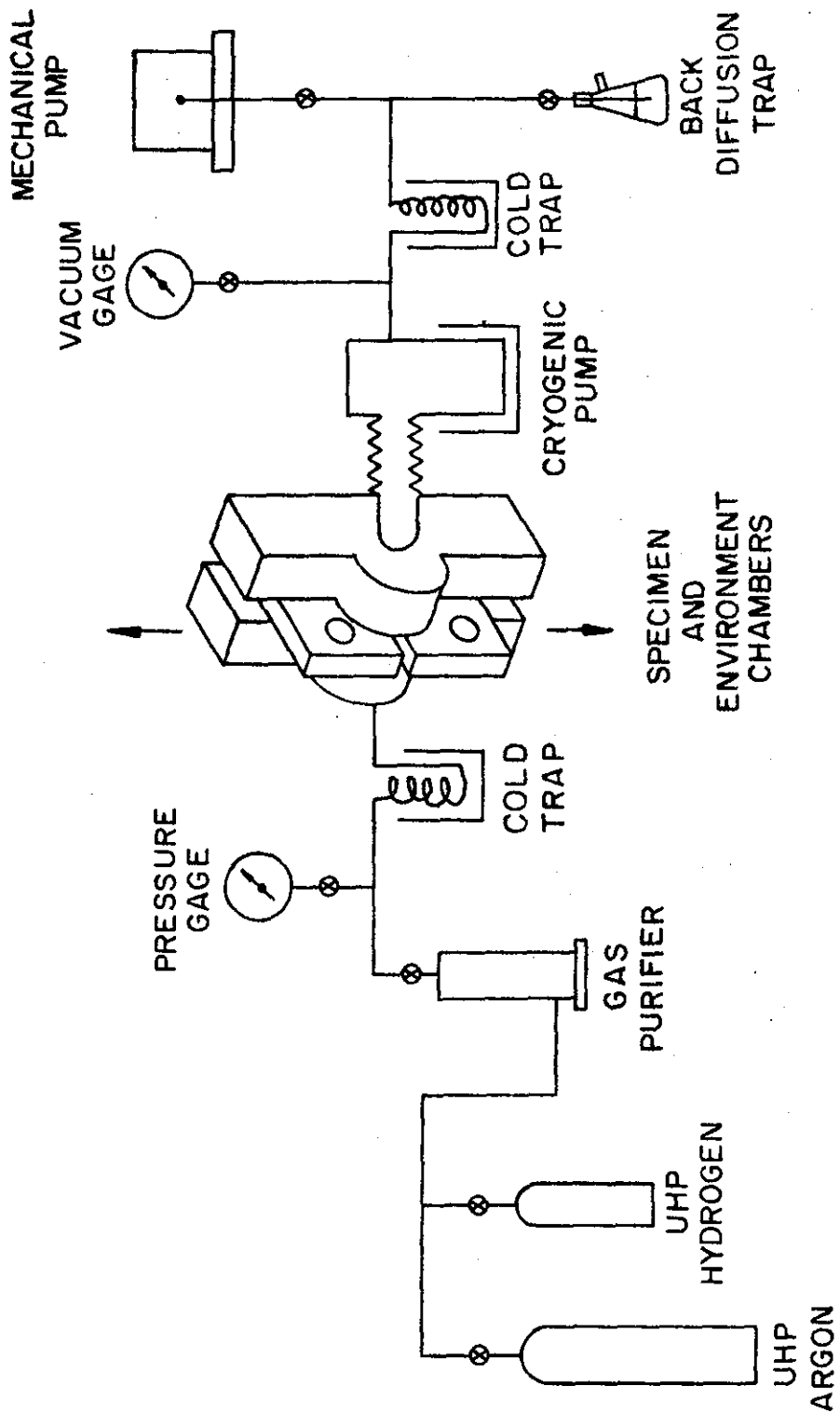


Figure 7: Schematic Diagram of Environmental Control System for WOL Specimen.

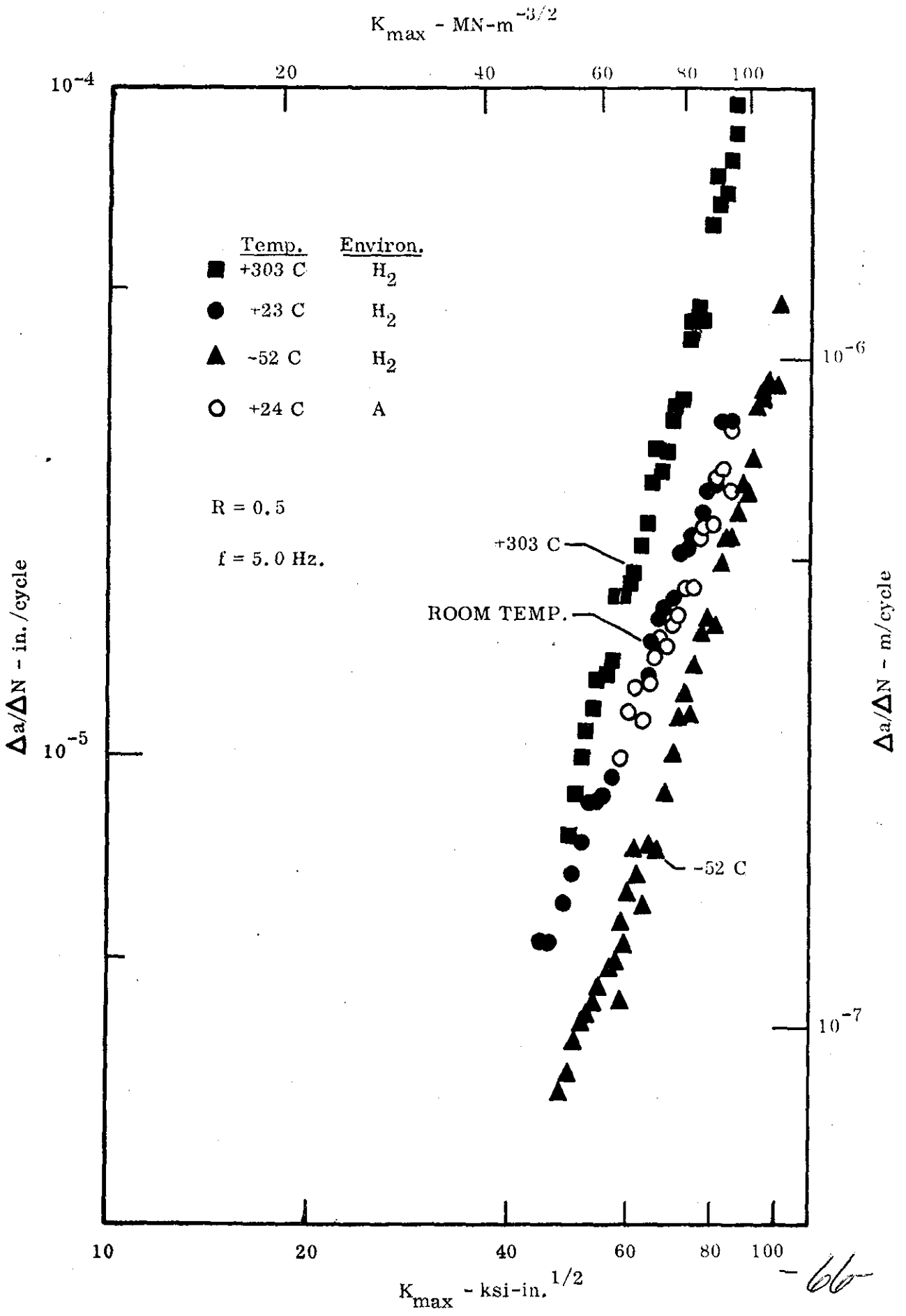


Figure 8: Fatigue crack growth in Inconel 718 alloy sheet in dehumidified hydrogen and argon at ≈ 1000 torr

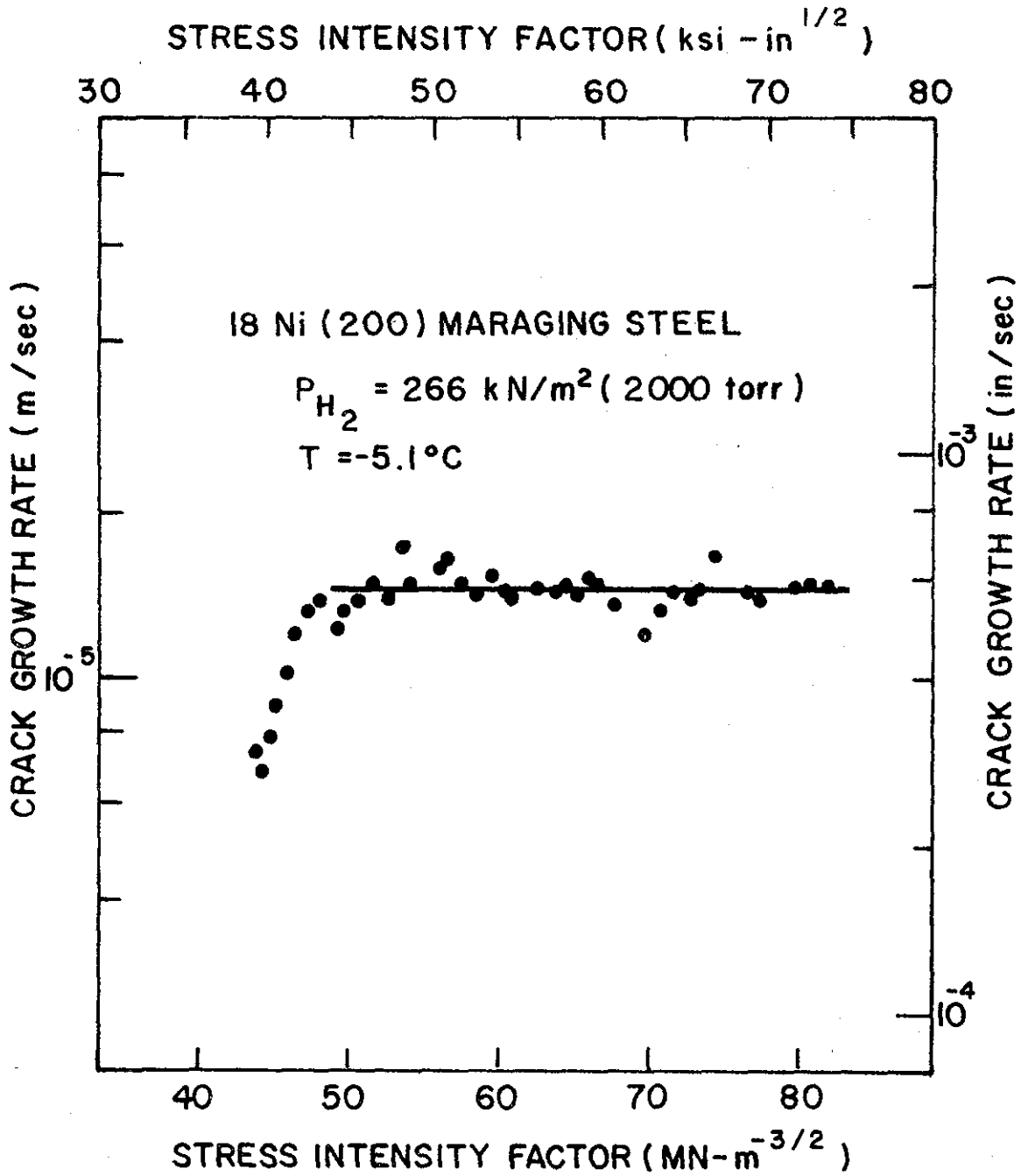


Figure 9: Sustained-load crack growth kinetics for 18Ni(200) maraging steel tested in $266 \text{ kN/m}^2 \text{ H}_2$ at -5.1°C .

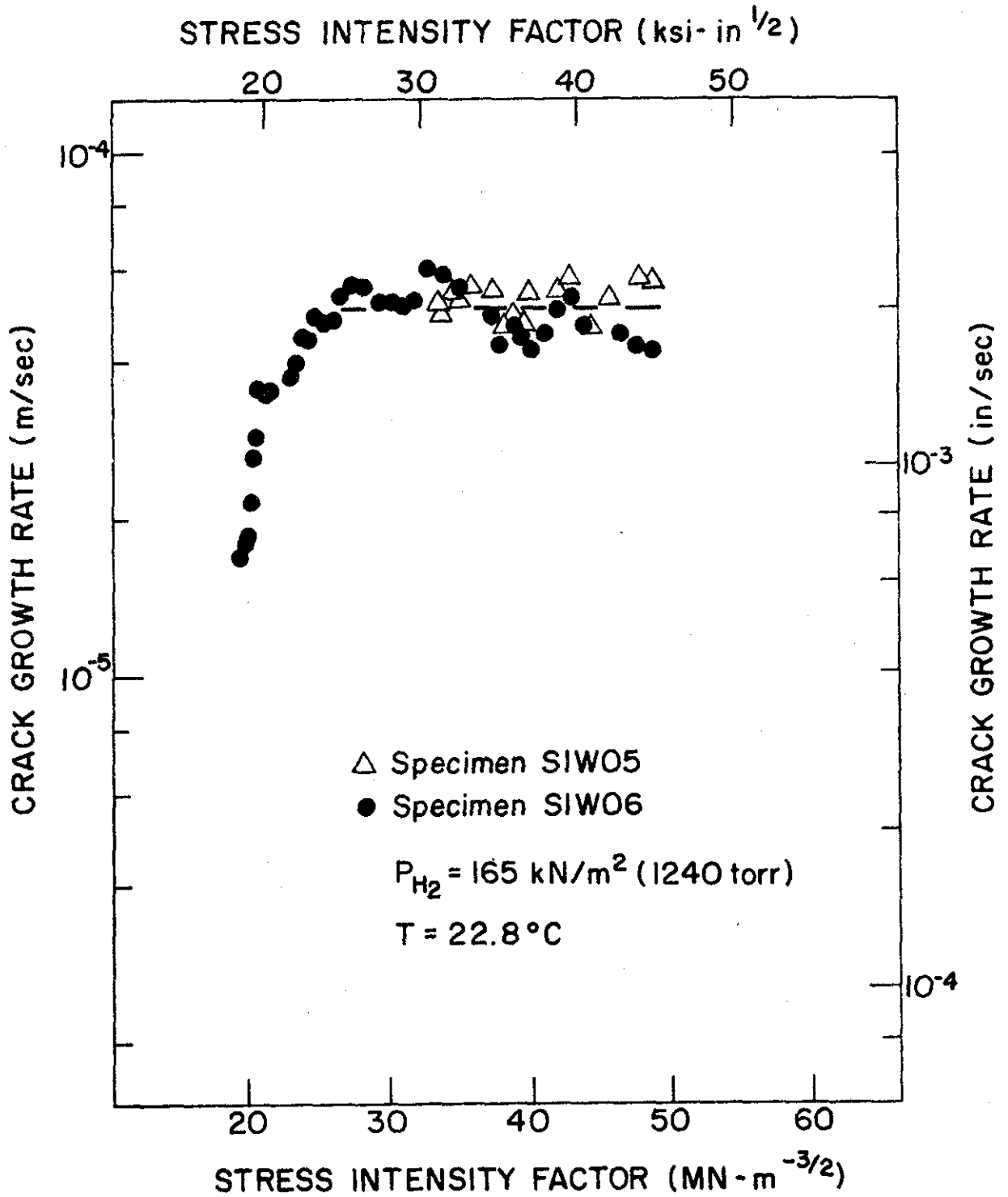


Figure 10: Sustained-load crack growth kinetics for replicate specimens of 18Ni(250) maraging steel tested in 165 kN/m² H₂ at 23°C.

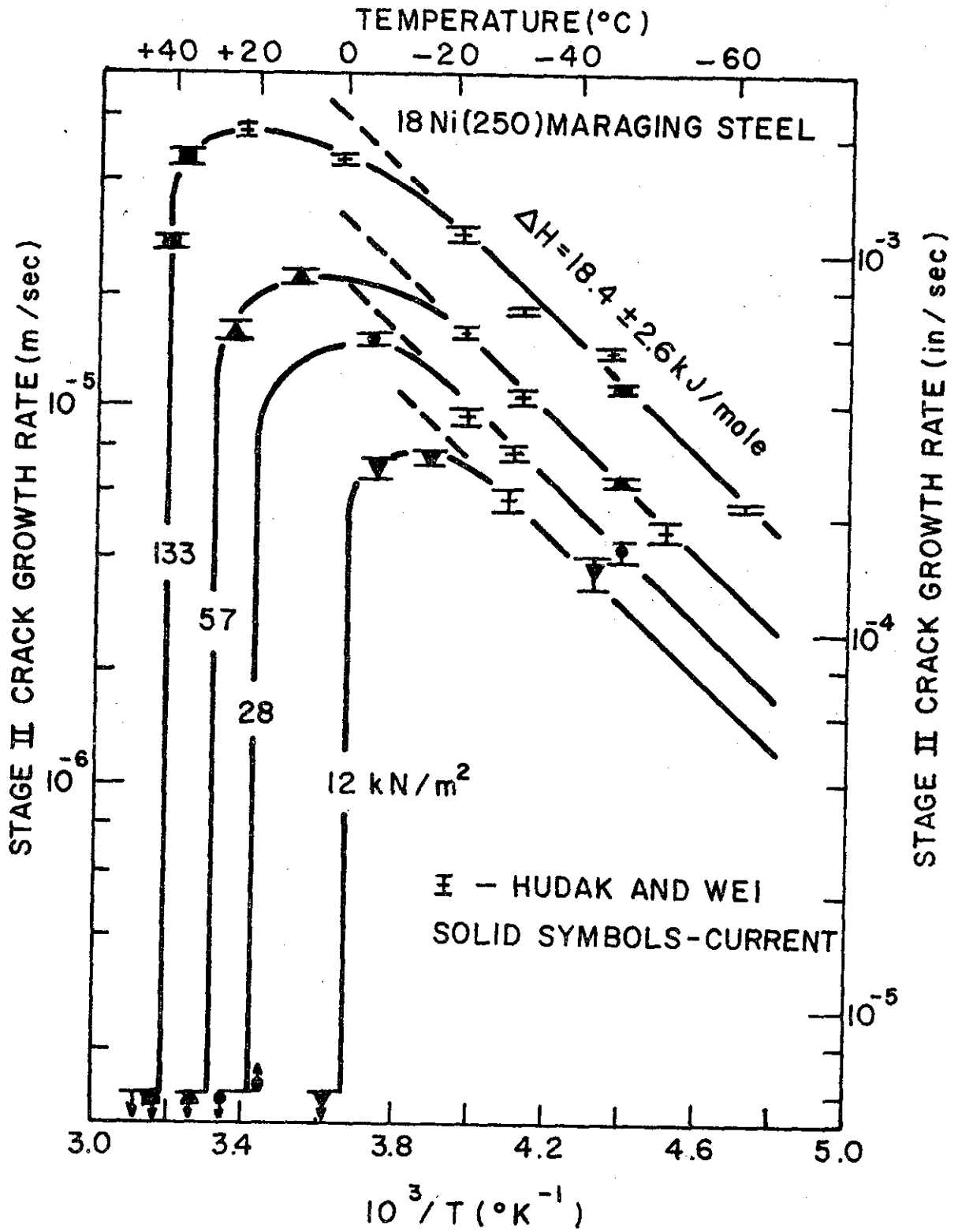


Figure 11: Effect of temperature on stage II (rate limited) crack growth rate for 18Ni(250) maraging steel tested over a range of gaseous hydrogen pressures.

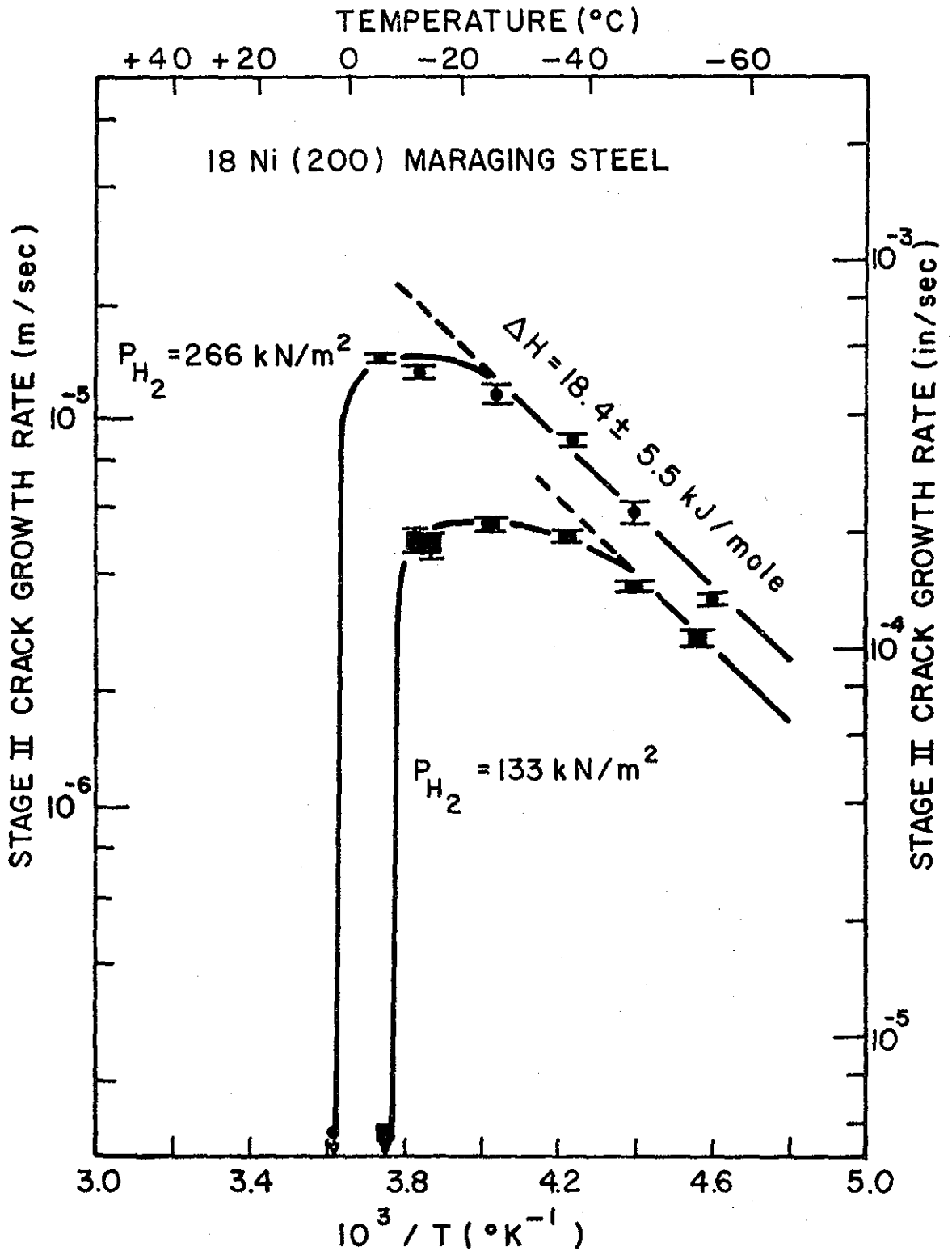


Figure 12: Effect of temperature on stage II (rate limited) crack growth rate for 18Ni(200) maraging steel tested at two hydrogen pressures.

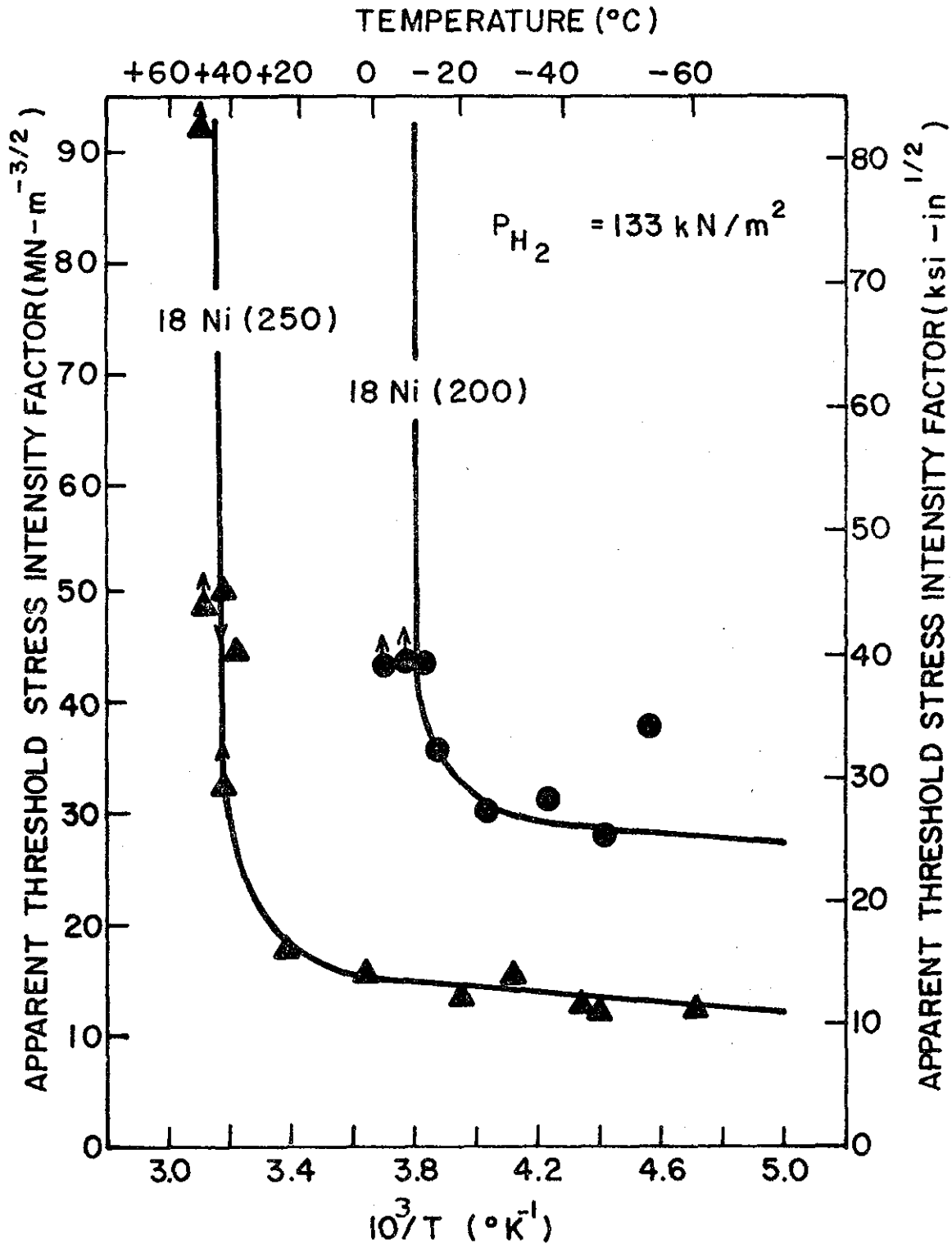


Figure 13: Effect of test temperature on the equilibrium threshold stress intensity factor exhibited by two grades of 18Ni maraging steel tested in $133 \text{ kN/m}^2 \text{ H}_2$.

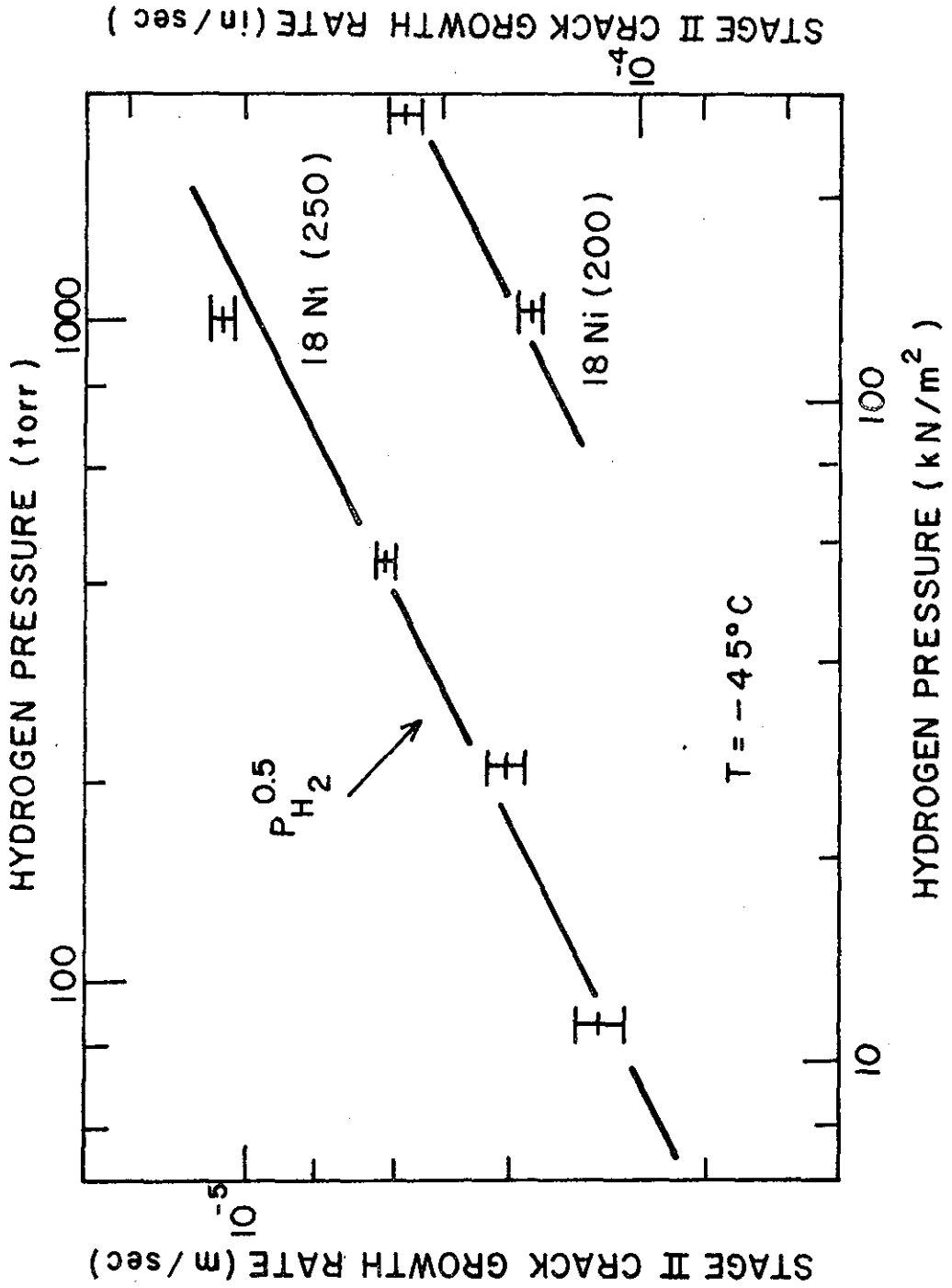


Figure 14: Effect of hydrogen pressure on the Region A ($T = -45^{\circ}\text{C}$), Stage II mean crack growth rate for two grades of 18Ni maraging steel.

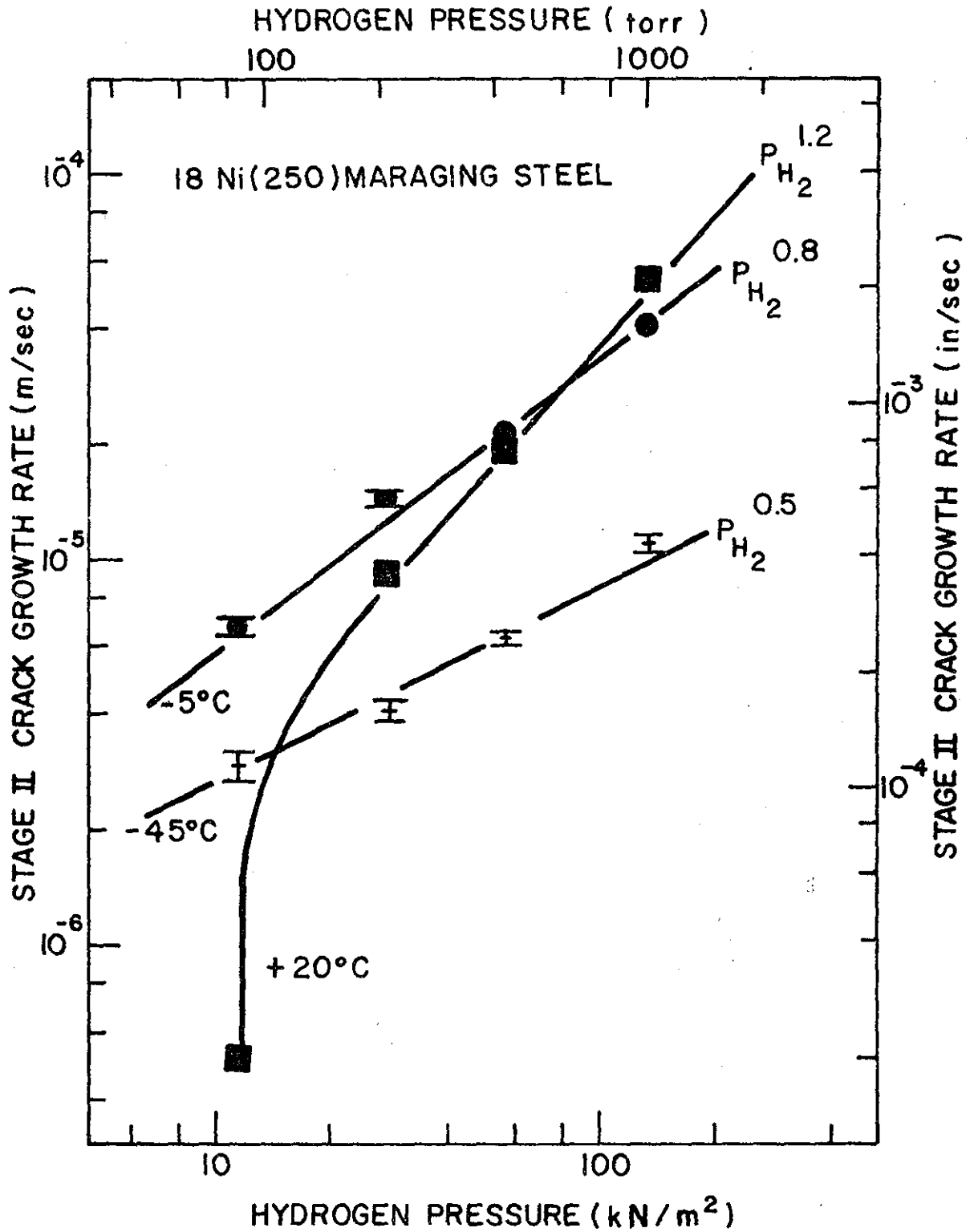


Figure 15: Effect of hydrogen pressure on the mean Stage II crack growth rate at three temperatures for 18Ni(250) maraging steel.

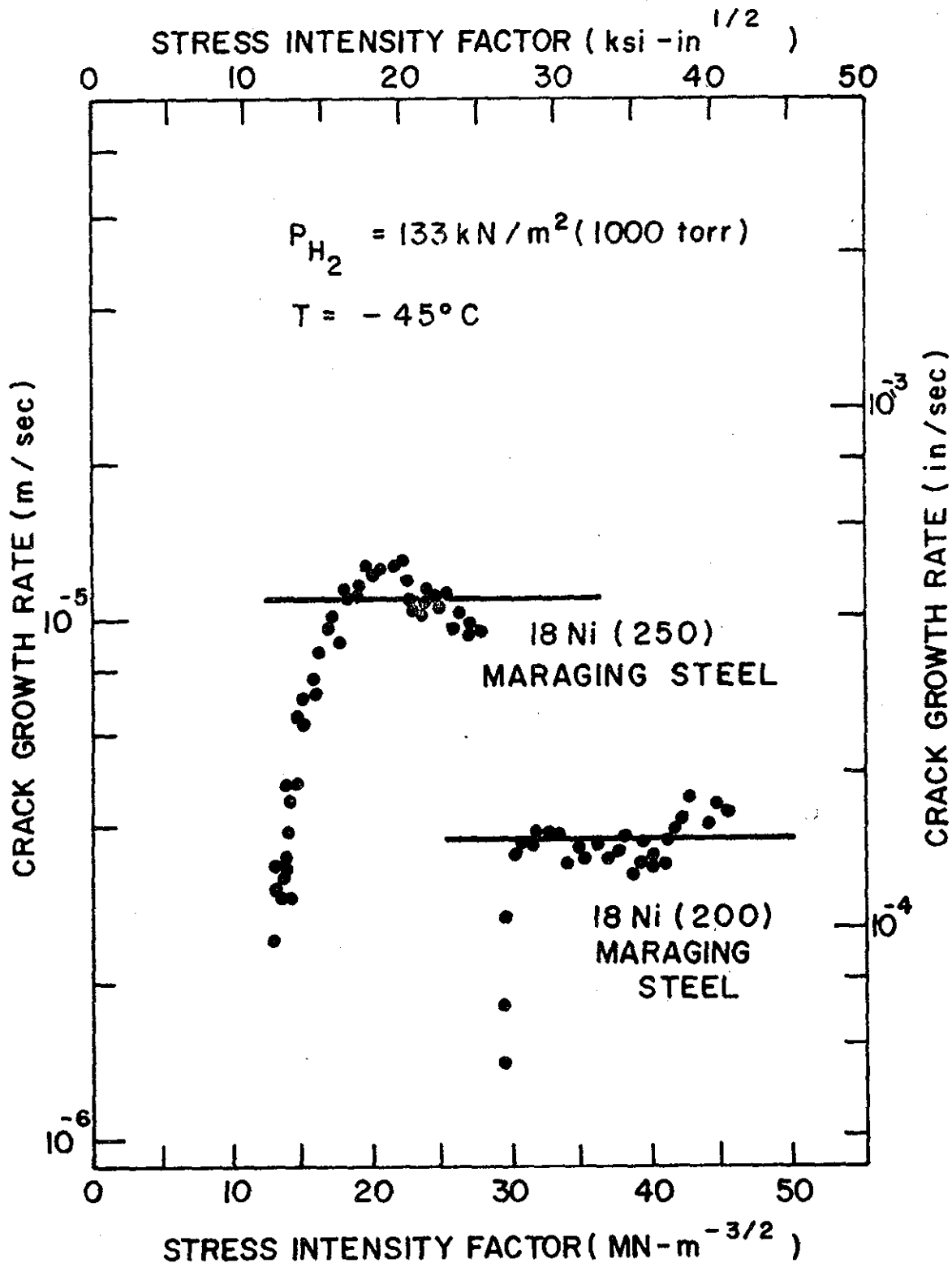


Figure 16: Comparison of crack growth kinetics at constant temperature and pressure for two strength levels of 18Ni maraging steel.

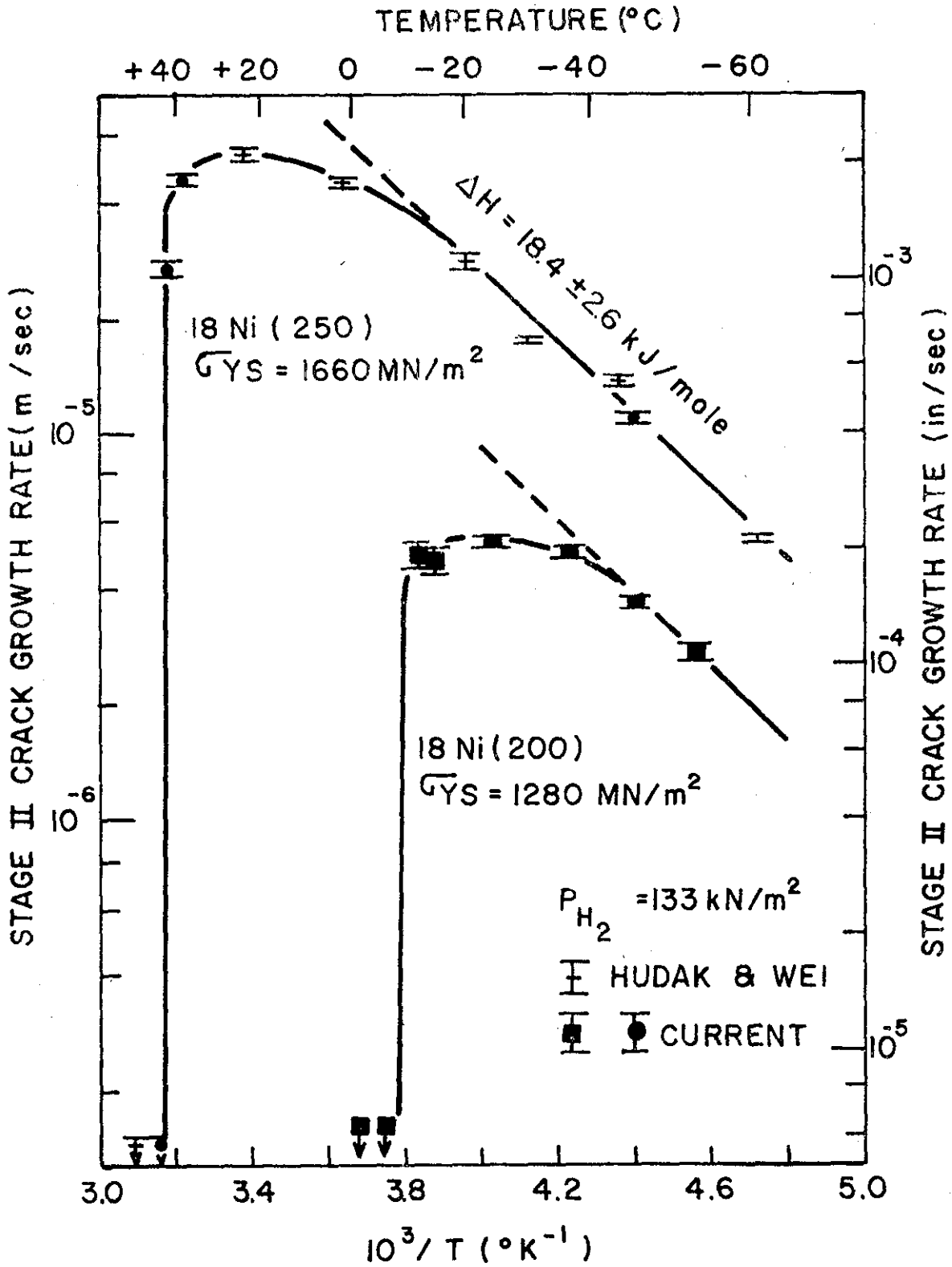


Figure 17: Effect of temperature on Stage II (rate limited) crack growth rate for two grades of 18Ni maraging steel tested in 133 kN/m² gaseous H₂.

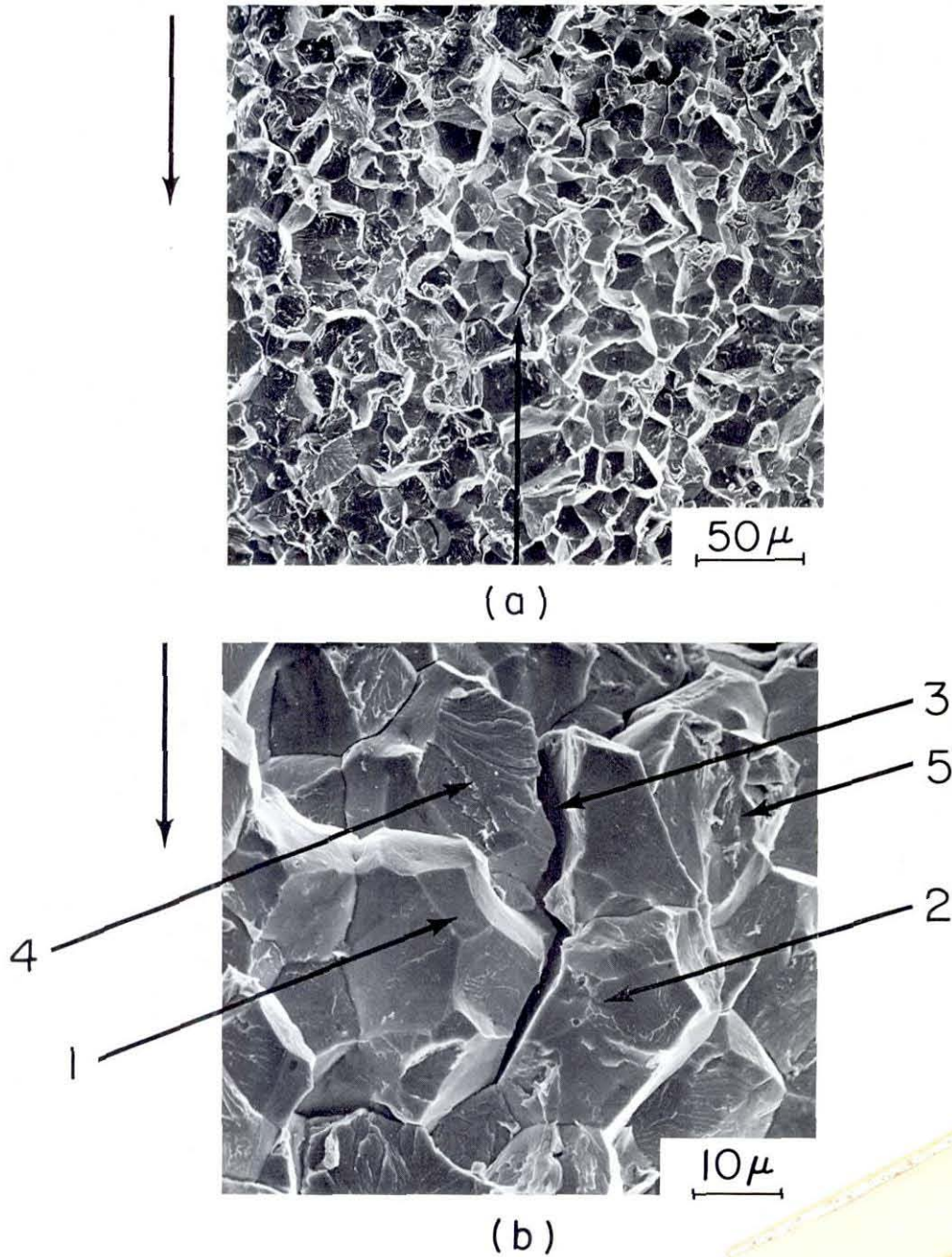


Figure 18: Matching scanning electron (SEM) fractographs of Stage II, Region A crack growth in an 18Ni(250) maraging steel specimen (S1W10). ($P_{H_2} = 57 \text{ kN/m}^2$, $T = -45^\circ\text{C}$, $K = 23 \text{ MN}\cdot\text{m}^{3/2}$. Magnifications: (a) 300X, (b) 1200X. (The arrow next to each fractograph indicates the macroscopic direction of crack growth.)

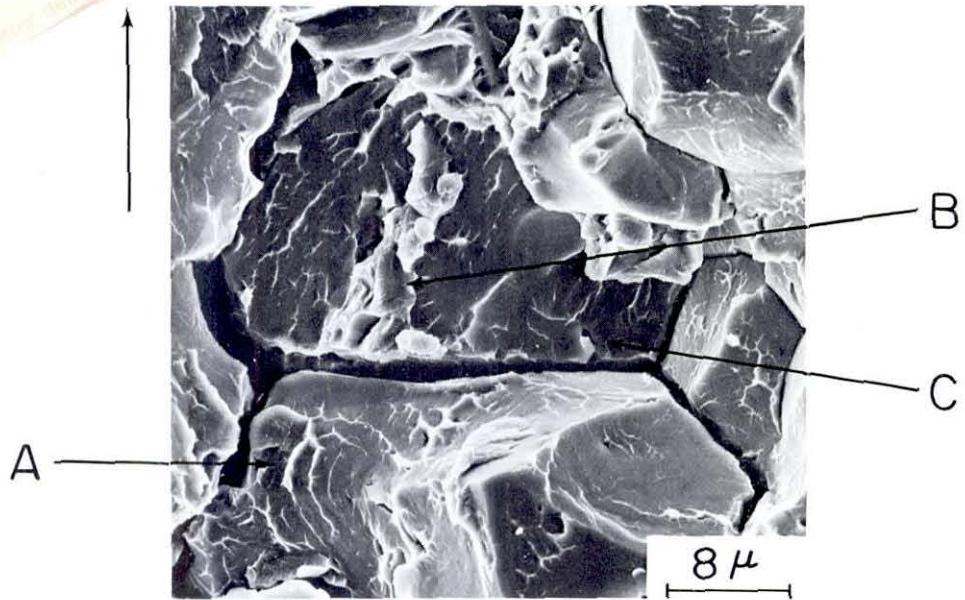


Figure 19: Fractograph of Stage II, Region A crack growth in an 18Ni(250) maraging steel specimen (S1W18). ($P_{H_2} = 12 \text{ kN/m}^2$, $T = -41^\circ\text{C}$, $K = 29 \text{ MN}\cdot\text{m}^{3/2}$). Magnification: 1980X.

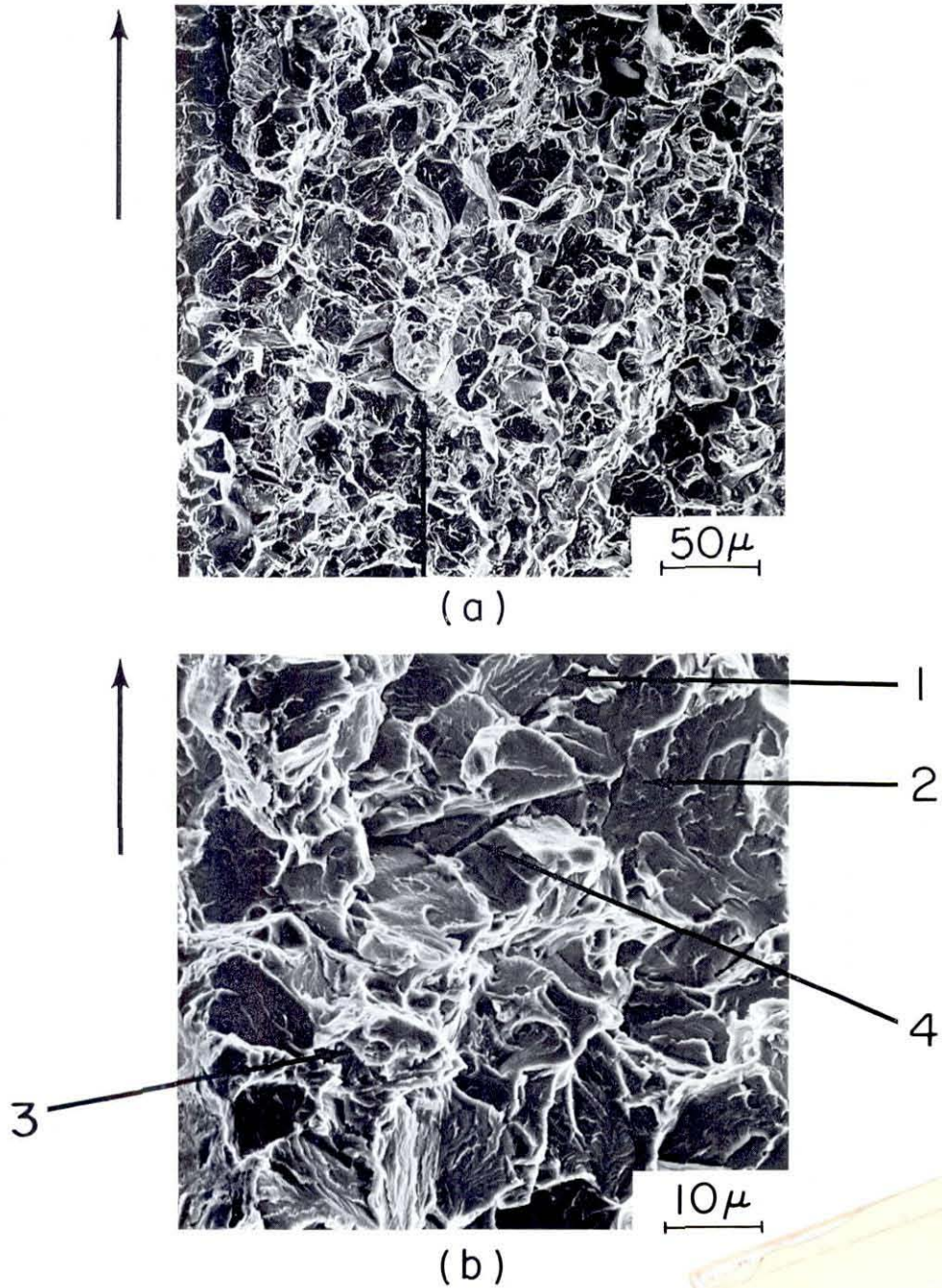


Figure 20: Fractographs of Stage II, Region B crack growth in an 18Ni(250) maraging steel specimen (S1W07). ($P_{H_2} = 133 \text{ kN/m}^2$, $T = +41^\circ\text{C}$, $K = 61 \text{ MN}\cdot\text{m}^{-3/2}$. Magnifications: (a) 260X, (b) 1300 X.

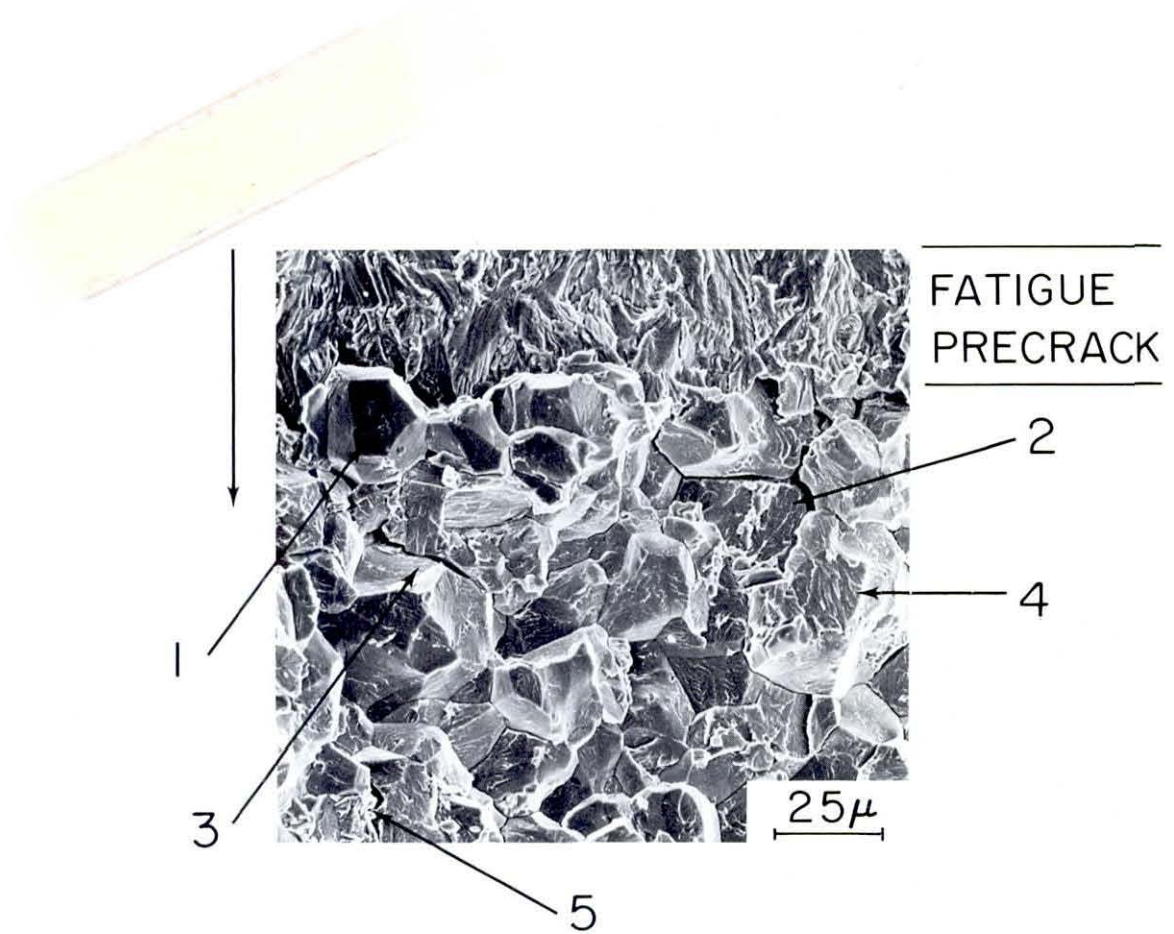


Figure 21: Fractograph showing the interface between fatigue precrack and hydrogen enhanced Stage II, Region A crack growth in an 18Ni(250) maraging steel specimen (S1W18). ($P_{H_2} = 12 \text{ kN/m}^2$, $T = -41^\circ\text{C}$, $K = 29 \text{ MN}\cdot\text{m}^{-3/2}$). Magnification: 560X.

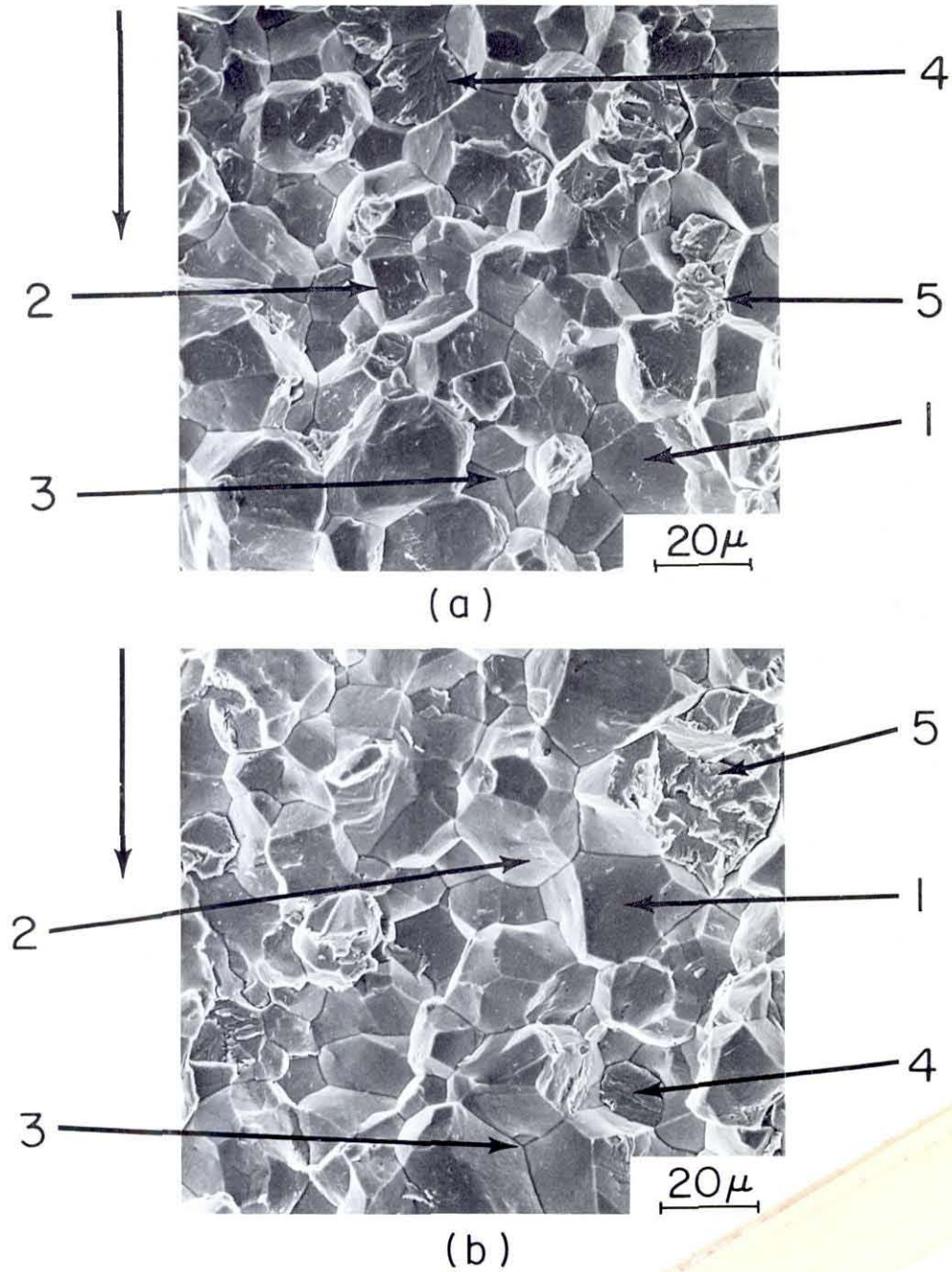


Figure 22: Comparison between fracture morphologies for Stage I and Stage II (Region A) crack growth in an 18Ni(250) maraging steel (S1W09). ($P_{H_2} = 133$ kN/m², $T = -45^\circ\text{C}$). (a) Stage I, $K = 13$ MN-m^{-3/2} (b) Stage II, $K = 28$ MN-m^{-3/2}. Magnification: 660X.

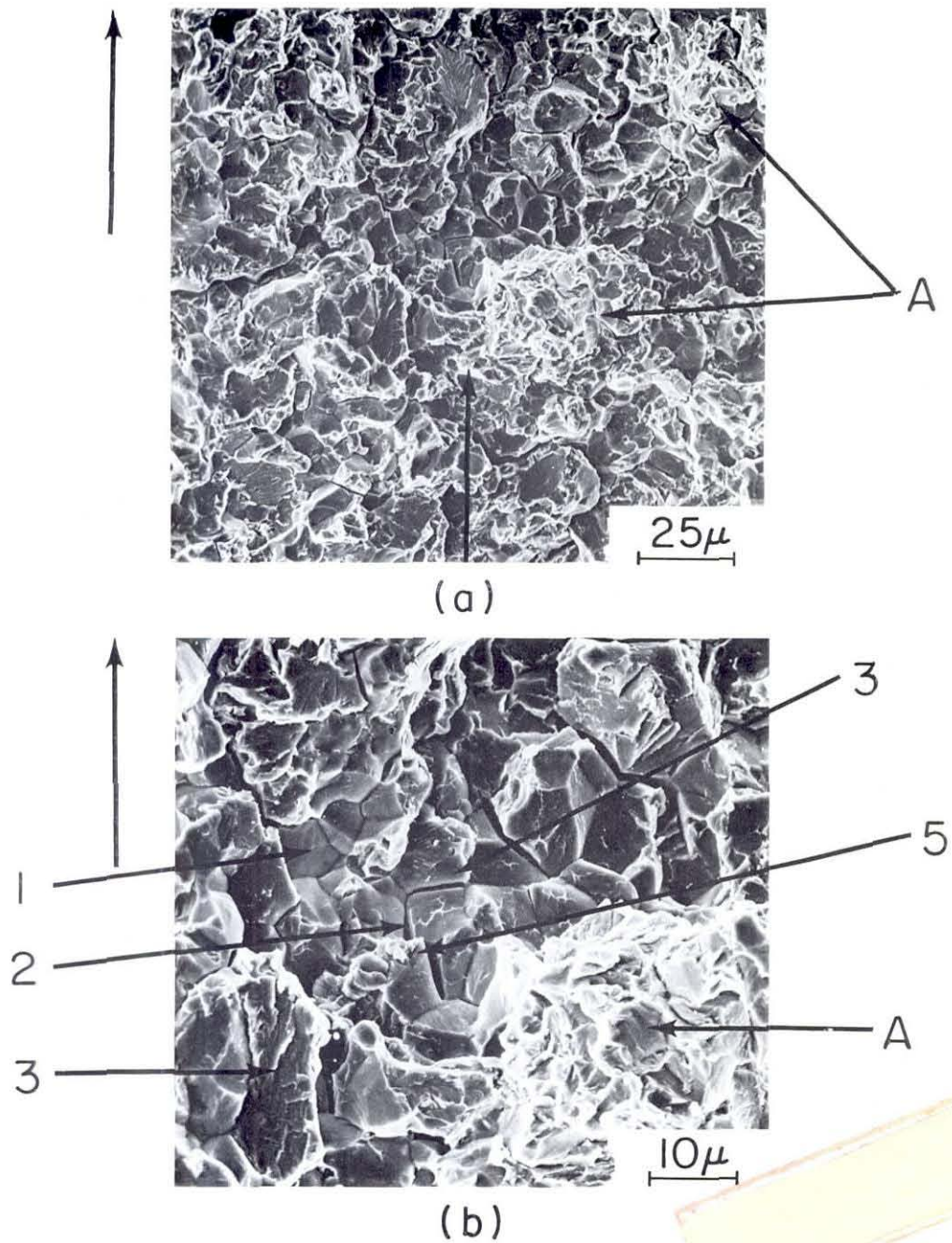


Figure 23: Fractographs of Stage II, Region A crack growth in an 18Ni(200) maraging steel specimen (S3W09). ($P_{H_2} = 133 \text{ kN/m}^2$, $T = -56^\circ\text{C}$, $K = 44 \text{ MN}\cdot\text{m}^{-3/2}$). Magnifications: (a) 520X, (b) 1200X.

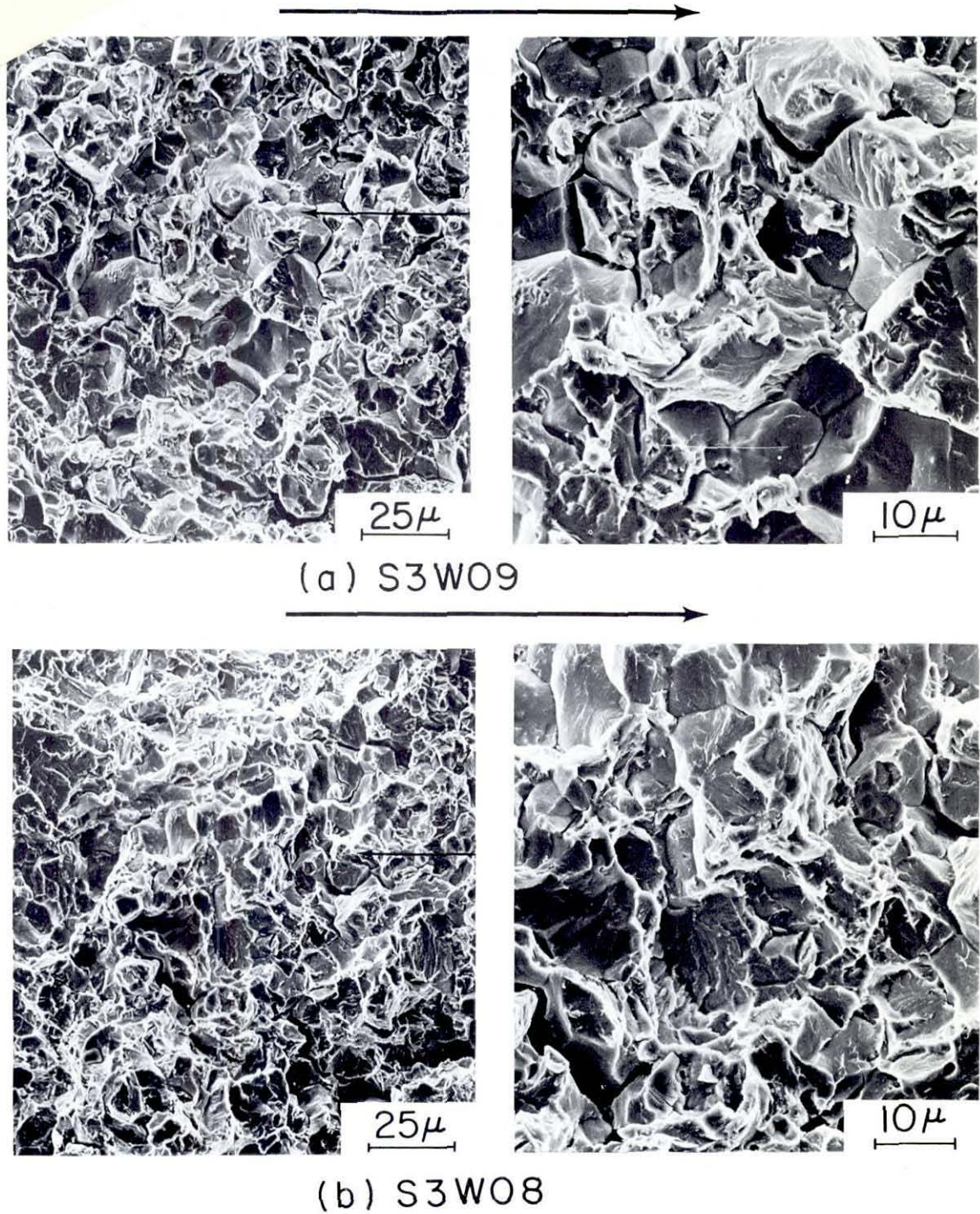


Figure 24: Comparison of Stage II fracture morphologies between Regions A and B for 18Ni(200) maraging steel tested in $133 \text{ kN/m}^2 \text{ H}_2$ at $K = 67 \text{ MN-m}^{-3/2}$, (a) Region A (-56°C) - 520X and 1280X, (b) Region B (-12°C) - 520X and 1200X.

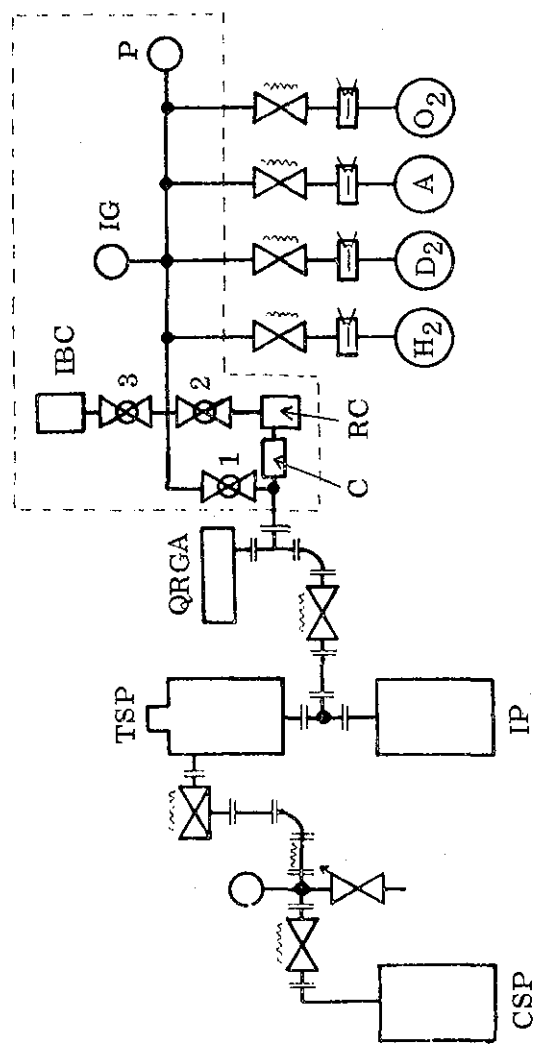


Figure 25: Block diagram of the UHV system for exchange measurements. Framed part is an all-glass apparatus with magnetically operated glass ball-to-socket valves 1, 2 and 3; ion and electron bombardment cell IBC; ionization gauge IG and Pirani gauge P as pressure sensors; reaction cell RC; and calibrated leak C. The sputter ion pump IP is a Varian 50 ls⁻¹ model, used conjointly with an air cooled 50 ls⁻¹ Varian titanium sublimation pump TSP; the cryosorbent, CSP, uses Linde Molecular Sieve 13X; the bellow valves are Granville-Phillips Type C metal valves; and a Varian quadrupole residual gas analyzer (QRGA) is used to monitor the exchange experiments.

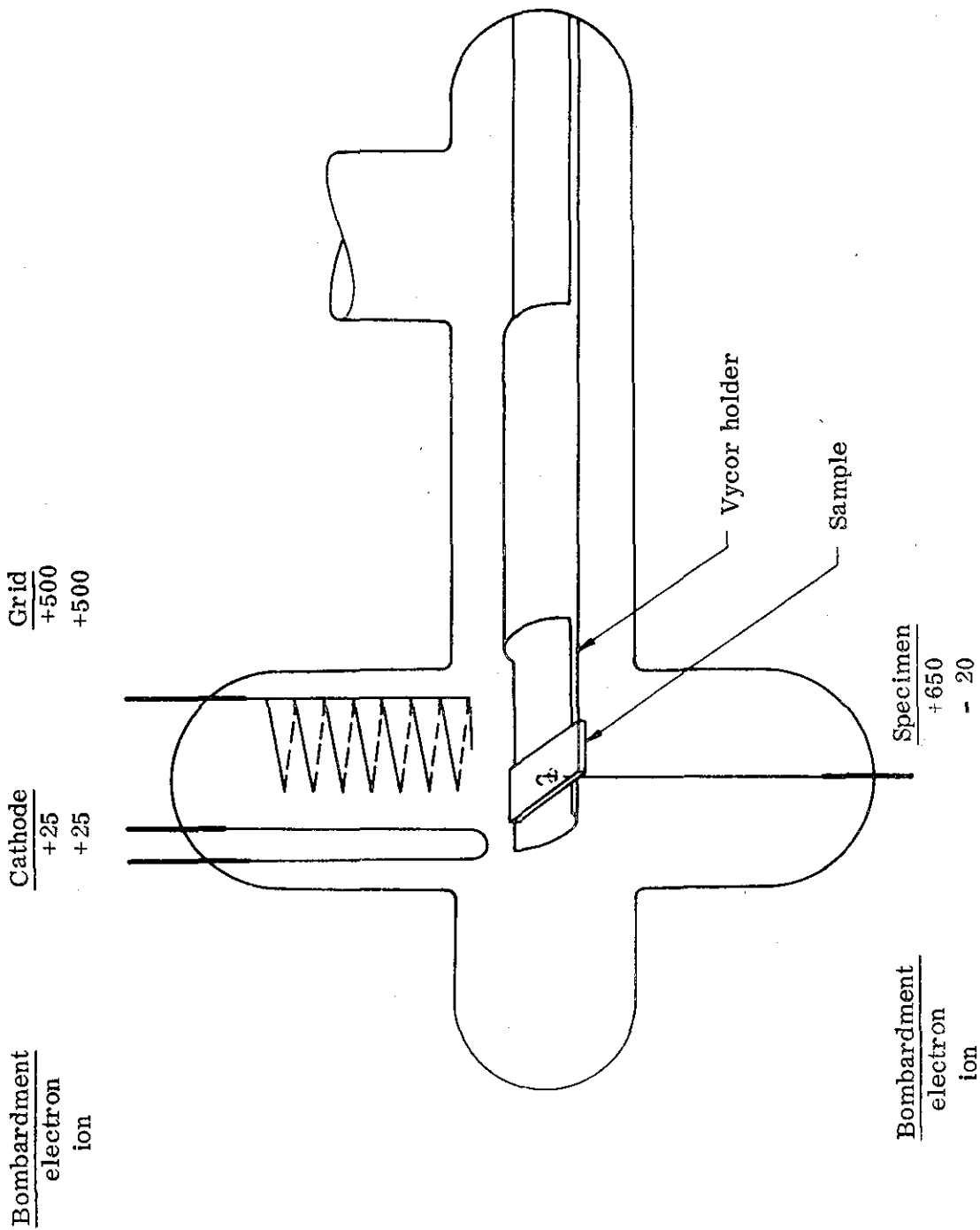


Figure 26: Schematic representation of the electron and ion bombardment cell IBC. The sample rests on a tungsten lead connected via a feedthrough to the potentials required for electron and ion bombardment. The specimen is placed in and removed from the bombarding position by an external magnet.

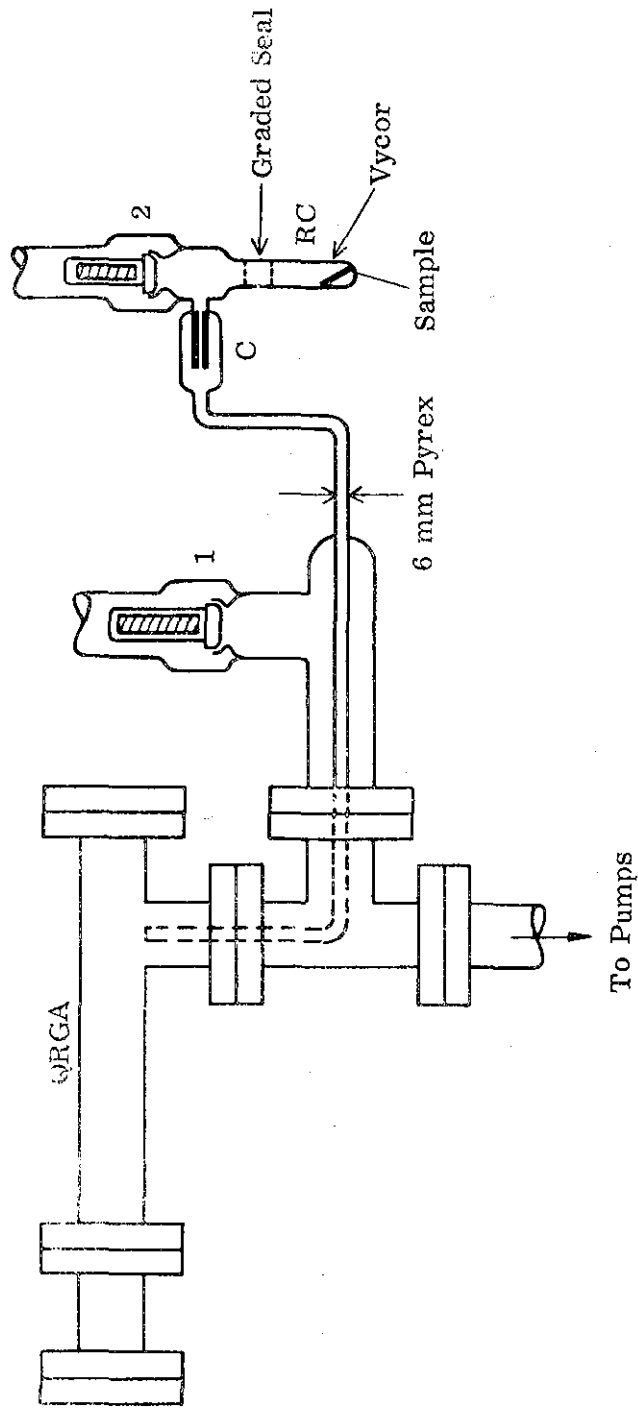
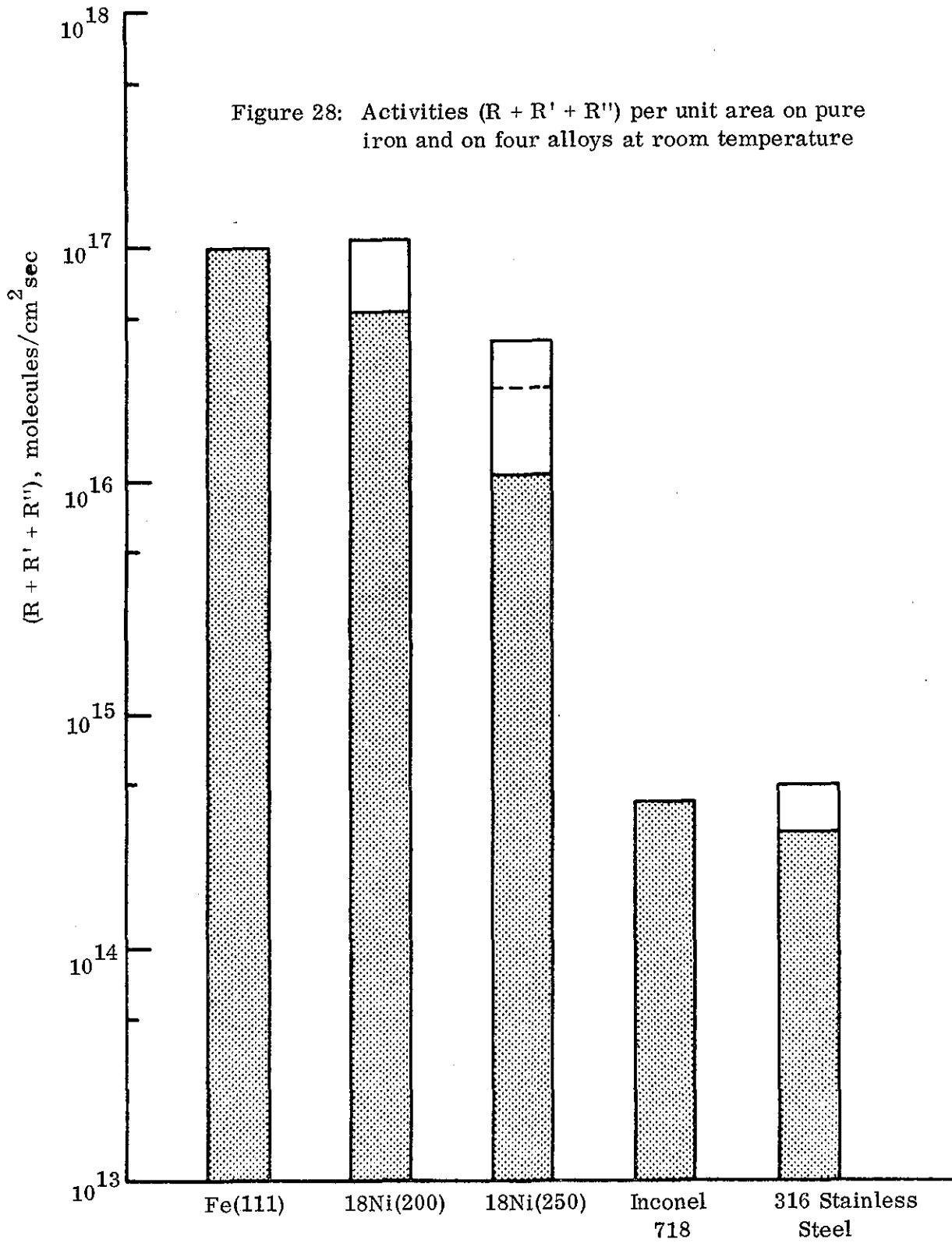


Figure 27: Arrangement between the reaction cell and the quadrupole. The calibrated conductance is a 0.002 inch capillary mounted on a Pyrex envelope. The reaction products reach the ionization chamber of the quadrupole via a 6 mm o. d. Pyrex tubing.

Figure 28: Activities ($R + R' + R''$) per unit area on pure iron and on four alloys at room temperature



APPENDIX I

KINETICS OF SUBCRITICAL CRACK GROWTH

Data on crack growth kinetics in the 18Ni maraging steels are compiled in tabular and graphical form in this Appendix. The stress intensity factor (K) is given in $\text{MN}\cdot\text{m}^{-3/2}$, and the crack growth rate (da/dt) in m/sec. Supplementary information given at the beginning of each Table is as follows:

- Line 1. Steel Type; Specimen Number
- Line 2. Hydrogen Pressure; Test Temperature
- Line 3. Mean Stage II Growth Rate; 95% Confidence Interval Estimate
- Line 4. Average Stage II Growth Rate ($\Delta a/\Delta t$); Percent Difference between Mean (Item 3) and Average Stage II Rates
- Line 5. Statement of Statistical K-Independence (if applicable)
- Line 6. Statement of Macroscopic Crack Branching (if applicable)

18 NI(250) MARAGING STEEL SPECIMEN S1405

HYDROGEN PRESSURE = 165 KN/M**2 TEMPERATURE = 22.6C
 MEAN STAGE II RATE = 5.19 E-5 M/S CONF INT = 0.23 E-5 M/S
 AVERAGE STAGE II RATE = 6.50 E-5 M/S 55 PCT DIFFERENCE = 25 PCT
 STAGE II RATE IS STATISTICALLY K-INDEPENDENT
 CRACK FRONT BRANCHING AT K = 50.6 MN/M**3/2

K	DA/DT	K	DA/DT	K	DA/DT
34.03	5.13E-05	37.90	5.15E-05	42.57	5.45E-05
34.46	4.91E-05	38.94	4.61E-05	43.37	5.82E-05
34.83	5.40E-05	39.35	4.83E-05	44.58	4.61E-05
35.39	5.19E-05	39.91	4.63E-05	46.10	5.25E-05
35.94	5.56E-05	40.55	5.38E-05	48.12	5.77E-05

49.24

5.68E-05

REPRODUCIBILITY OF THE ORIGINAL PAGE IS POOR

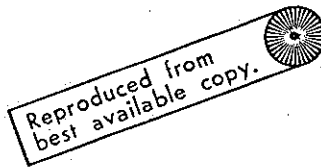
18 NI(250) MARAGING STEEL SPECIMEN S1406

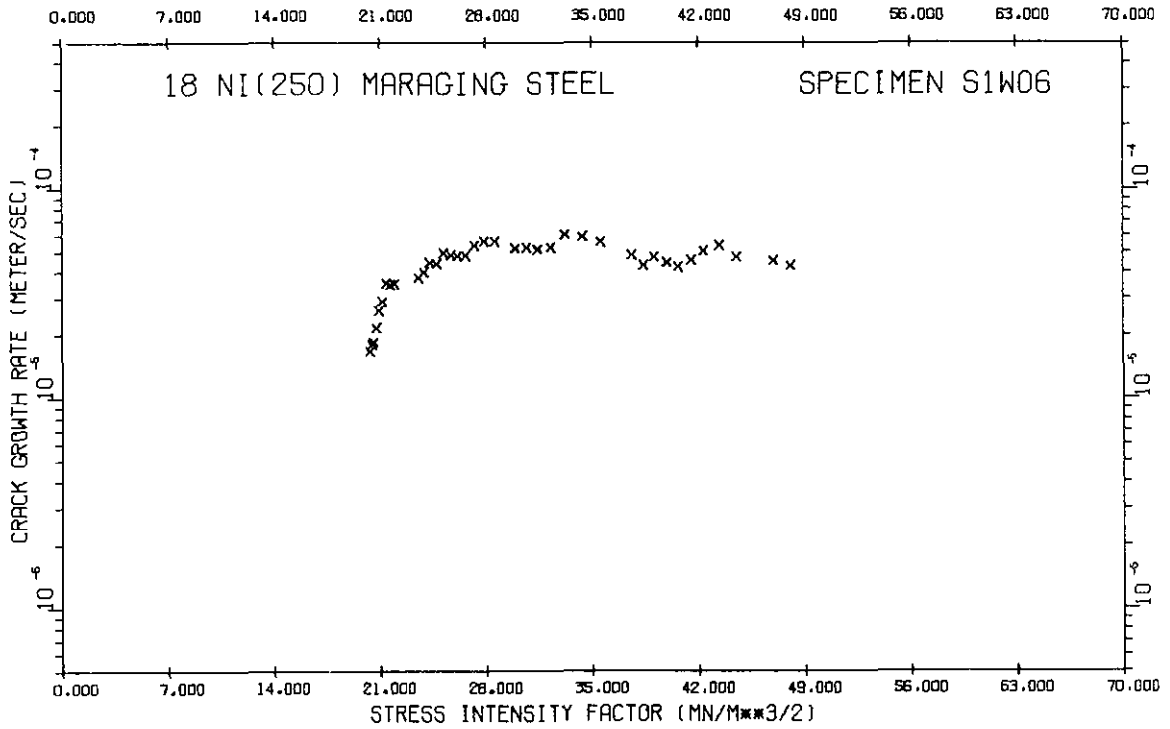
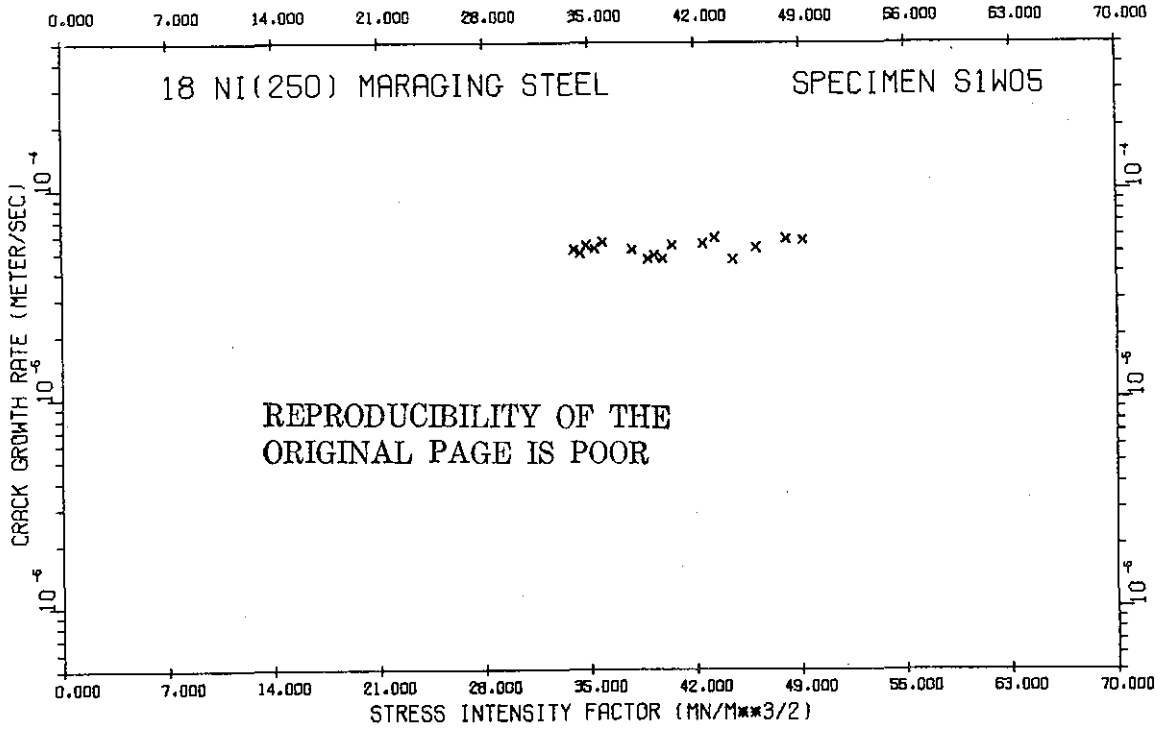
HYDROGEN PRESSURE = 165 KN/M**2 TEMPERATURE = 23.0C
 MEAN STAGE II RATE = 5.07 E-5 M/S CONF INT = 0.15 E-5 P/S
 AVERAGE STAGE II RATE = 4.54 E-5 M/S 55 PCT DIFFERENCE = 18 PCT
 STAGE II RATE IS STATISTICALLY K-INDEPENDENT
 CRACK FRONT BRANCHING AT K = 48.9 MN/M**3/2

K	DA/DT	K	DA/DT	K	DA/DT
20.34	1.68E-05	23.92	3.98E-05	29.92	5.19E-05
20.48	1.80E-05	24.32	4.44E-05	30.68	5.23E-05
20.60	1.84E-05	24.75	4.36E-05	31.38	5.12E-05
20.76	2.16E-05	25.18	4.92E-05	32.25	5.24E-05
20.92	2.62E-05	25.67	4.82E-05	33.21	6.05E-05
21.16	2.88E-05	26.10	4.74E-05	34.35	5.89E-05
21.41	3.53E-05	26.64	4.79E-05	35.53	5.55E-05
21.68	3.47E-05	27.23	5.35E-05	37.59	4.84E-05
21.96	3.49E-05	27.88	5.60E-05	38.37	4.30E-05
23.58	3.75E-05	28.54	5.58E-05	39.04	4.70E-05

39.93
40.65
41.51
42.33
43.41
44.54
46.94
48.07

4.42E-05
4.21E-05
4.53E-05
5.03E-05
5.37E-05
4.70E-05
4.52E-05
4.27E-05





Reproduced from best available copy.



18 NI(250) MARAGING STEEL SPECIMEN S1M07

HYDROGEN PRESSURE = 133 KN/M**2 TEMPERATURE = 41.6C
 MEAN STAGE II RATE = 2.72 E-5 M/S 95 PCT CONF INT = 0.10 E-5 M/S
 AVERAGE STAGE II RATE = 3.10 E-5 M/S DIFFERENCE = 15 PCT

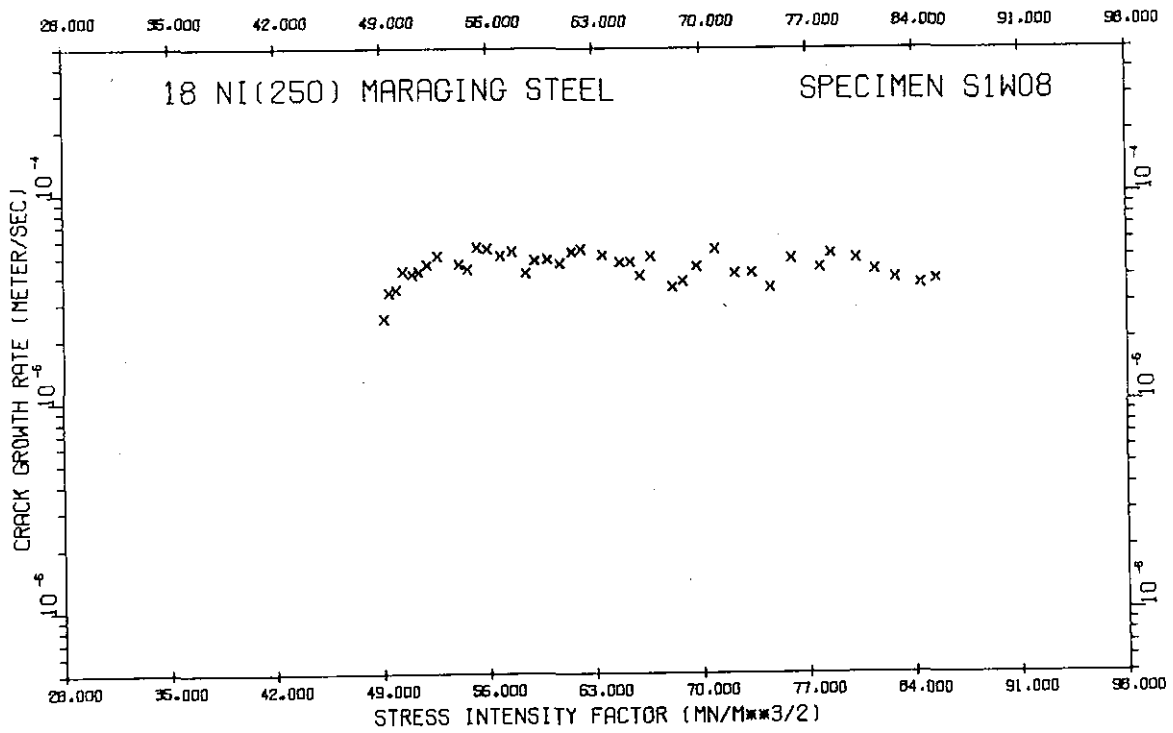
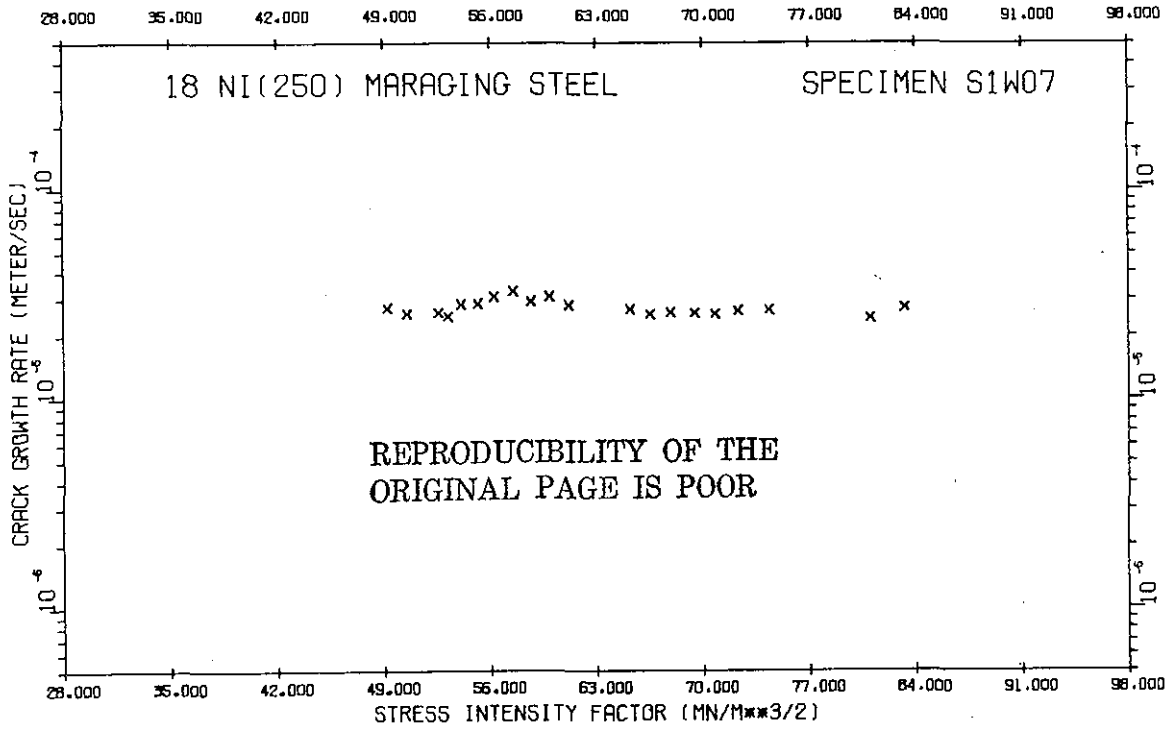
K	DA/DT	K	DA/DT	K	DA/DT
49.25	2.73E-05	55.21	2.86E-05	61.15	2.80E-05
50.53	2.55E-05	56.27	3.07E-05	65.24	2.66E-05
52.64	2.58E-05	57.51	3.25E-05	66.55	2.54E-05
53.24	2.48E-05	58.70	2.92E-05	67.92	2.15E-05
54.12	2.84E-05	59.93	3.07E-05	69.48	2.56E-05
				70.82	2.53E-05
				72.37	2.63E-05
				74.38	2.66E-05
				81.03	2.41E-05
				83.32	2.72E-05

REPRODUCIBILITY OF THE ORIGINAL PAGE IS POOR

18 NI(250) MARAGING STEEL SPECIMEN S1M08

HYDROGEN PRESSURE = 133 KN/M**2 TEMPERATURE = 37.3C
 MEAN STAGE II RATE = 4.58 E-5 M/S 95 PCT CONF INT = 0.22 E-5 M/S
 AVERAGE STAGE II RATE = 5.75 E-5 M/S DIFFERENCE = 26 PCT
 STAGE II RATE IS STATISTICALLY K-INDEPENDENT

K	DA/DT	K	DA/DT	K	DA/DT
49.12	2.52E-05	55.30	5.50E-05	63.59	5.07E-05
49.51	3.38E-05	55.97	5.45E-05	64.70	4.68E-05
49.95	3.48E-05	56.85	5.04E-05	65.40	4.70E-05
50.42	4.24E-05	57.60	5.27E-05	66.00	4.02E-05
51.01	4.11E-05	58.49	4.16E-05	66.71	4.96E-05
51.48	4.23E-05	59.10	4.79E-05	68.12	3.55E-05
52.02	4.57E-05	59.94	4.86E-05	68.78	3.78E-05
52.71	5.06E-05	60.71	4.63E-05	69.69	4.45E-05
54.10	4.61E-05	61.54	5.24E-05	70.90	5.48E-05
54.69	4.34E-05	62.15	5.39E-05	72.23	4.13E-05
				73.33	4.16E-05
				74.55	3.53E-05
				75.93	4.96E-05
				77.83	4.41E-05
				78.56	5.14E-05
				80.21	4.88E-05
				81.47	4.30E-05
				82.79	3.90E-05
				84.46	3.66E-05
				85.50	3.88E-05



Reproduced from best available copy. 

18 NI(250) MARAGING STEEL SPECIMEN SIM09

HYDROGEN PRESSURE = 133 KN/M**2 TEMPERATURE = -45.4C
 MEAN STAGE II RATE = 1.11 E-5 M/S 55 PCT CONF INT = 0.04 E-5 M/S
 AVERAGE STAGE II RATE = 0.70 E-5 M/S DIFFERENCE = 46 PCT

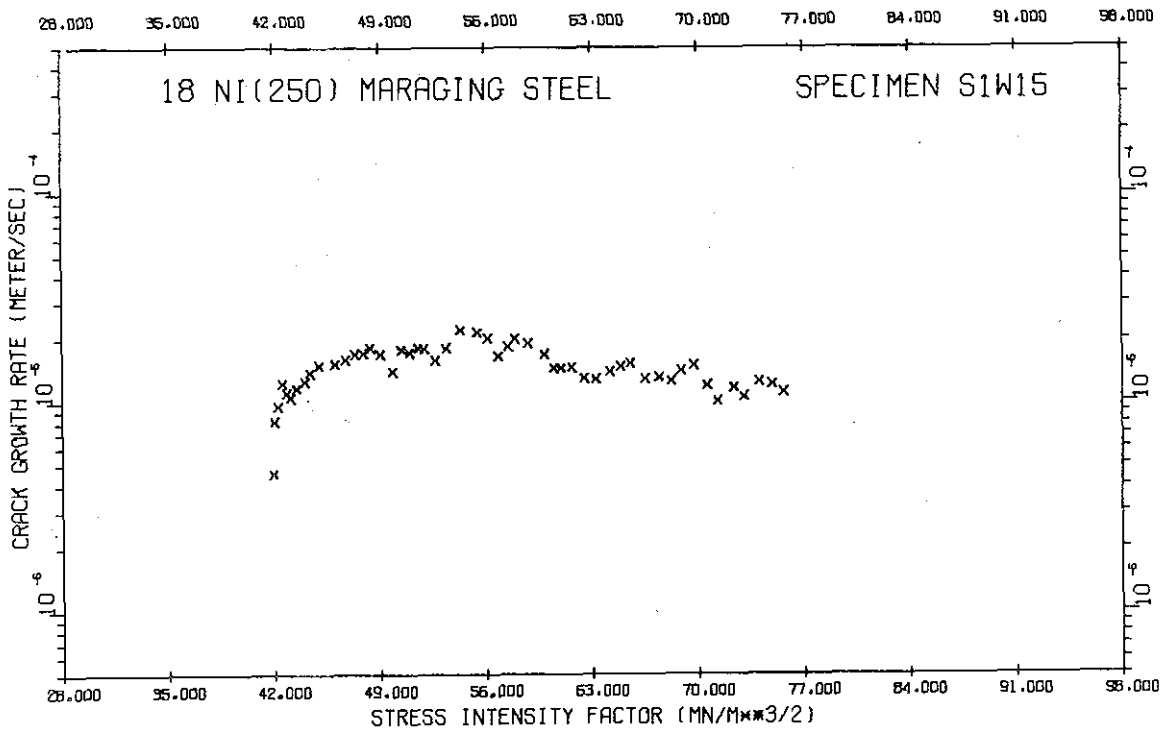
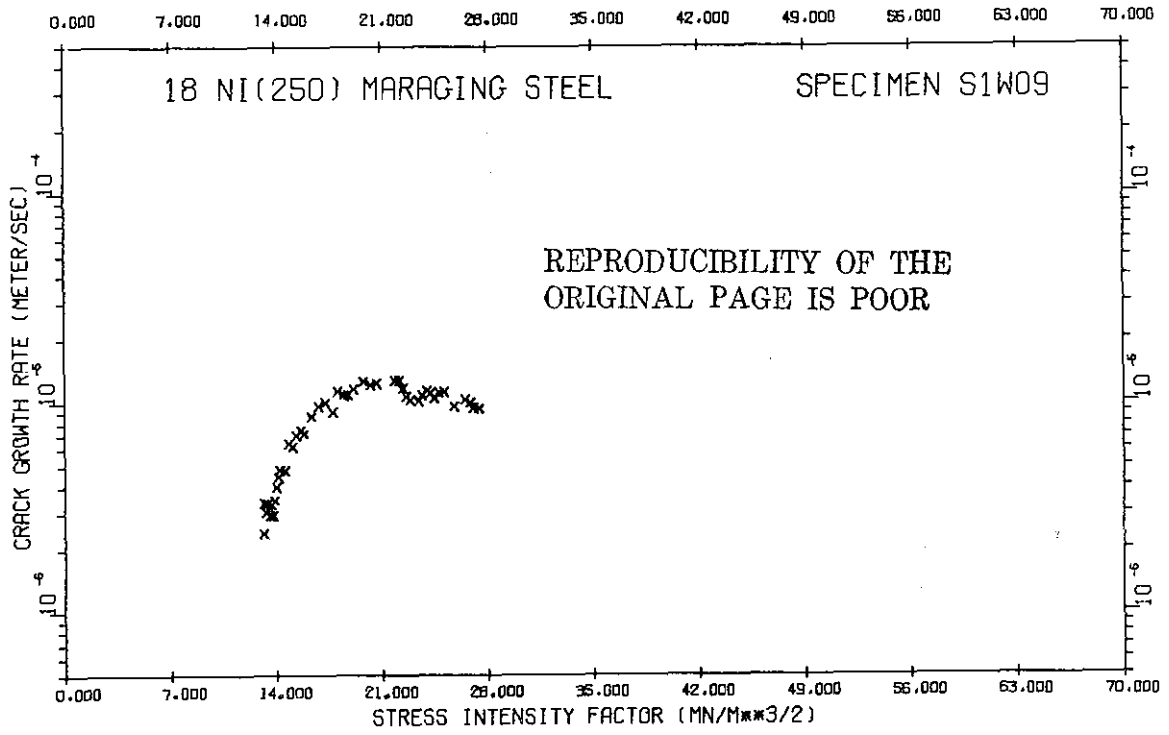
K	DA/DT	K	DA/DT	K	DA/DT	K	DA/DT
13.15	2.40E-06	14.54	4.77E-06	18.75	1.10E-05	23.99	1.14E-05
13.19	3.34E-06	14.85	6.38E-06	19.11	1.16E-05	24.25	1.11E-05
13.28	3.03E-06	15.10	6.20E-06	19.76	1.27E-05	24.52	1.05E-05
13.38	3.30E-06	15.35	7.02E-06	20.20	1.22E-05	24.79	1.12E-05
13.48	3.17E-06	15.63	7.47E-06	20.62	1.24E-05	25.10	1.12E-05
13.56	2.91E-06	15.85	7.12E-06	21.82	1.28E-05	25.82	9.62E-06
13.66	3.31E-06	16.34	8.67E-06	22.10	1.28E-05	26.52	1.04E-05
13.78	2.93E-06	16.77	9.68E-06	22.38	1.17E-05	26.86	1.00E-05
13.89	3.44E-06	17.24	1.01E-05	22.61	1.08E-05	27.08	9.43E-06
14.01	3.99E-06	17.77	9.08E-06	22.88	1.03E-05	27.47	9.44E-06
14.12	4.44E-06	18.04	1.14E-05	23.42	1.02E-05		
14.24	4.79E-06	18.46	1.09E-05	23.66	1.09E-05		

18 NI(250) MARAGING STEEL SPECIMEN SIM15

HYDROGEN PRESSURE = 57 KN/M**2 TEMPERATURE = 24.4C
 MEAN STAGE II RATE = 1.55 E-5 M/S 55 PCT CONF INT = 0.09 E-5 M/S
 AVERAGE STAGE II RATE = 1.53 E-5 M/S DIFFERENCE = 1 PCT

K	DA/DT	K	DA/DT	K	DA/DT	K	DA/DT
41.95	4.54E-06	47.88	1.72E-05	59.80	1.68E-05	66.52	1.29E-05
42.06	8.11E-06	48.35	1.83E-05	57.49	1.83E-05	67.44	1.32E-05
42.30	9.56E-06	49.01	1.70E-05	57.95	2.01E-05	68.22	1.26E-05
42.55	1.24E-05	49.81	1.40E-05	58.80	1.91E-05	68.86	1.42E-05
42.82	1.11E-05	50.42	1.79E-05	59.83	1.70E-05	69.72	1.50E-05
43.09	1.05E-05	50.93	1.73E-05	60.47	1.46E-05	70.60	1.20E-05
43.48	1.17E-05	51.55	1.62E-05	60.93	1.45E-05	71.30	1.01E-05
44.03	1.27E-05	51.94	1.81E-05	61.66	1.47E-05	72.41	1.17E-05
44.36	1.39E-05	52.65	1.59E-05	62.48	1.30E-05	73.05	1.06E-05
44.95	1.51E-05	53.38	1.82E-05	63.26	1.29E-05	74.07	1.25E-05
46.02	1.53E-05	54.34	2.22E-05	64.21	1.40E-05	74.92	1.21E-05
46.68	1.61E-05	55.46	2.16E-05	64.88	1.49E-05	75.65	1.11E-05
47.32	1.71E-05	56.13	2.03E-05	65.53	1.54E-05		

C-2



Reproduced from
best available copy.



18 NI(250) MARAGING STEEL SPECIMEN SIM11

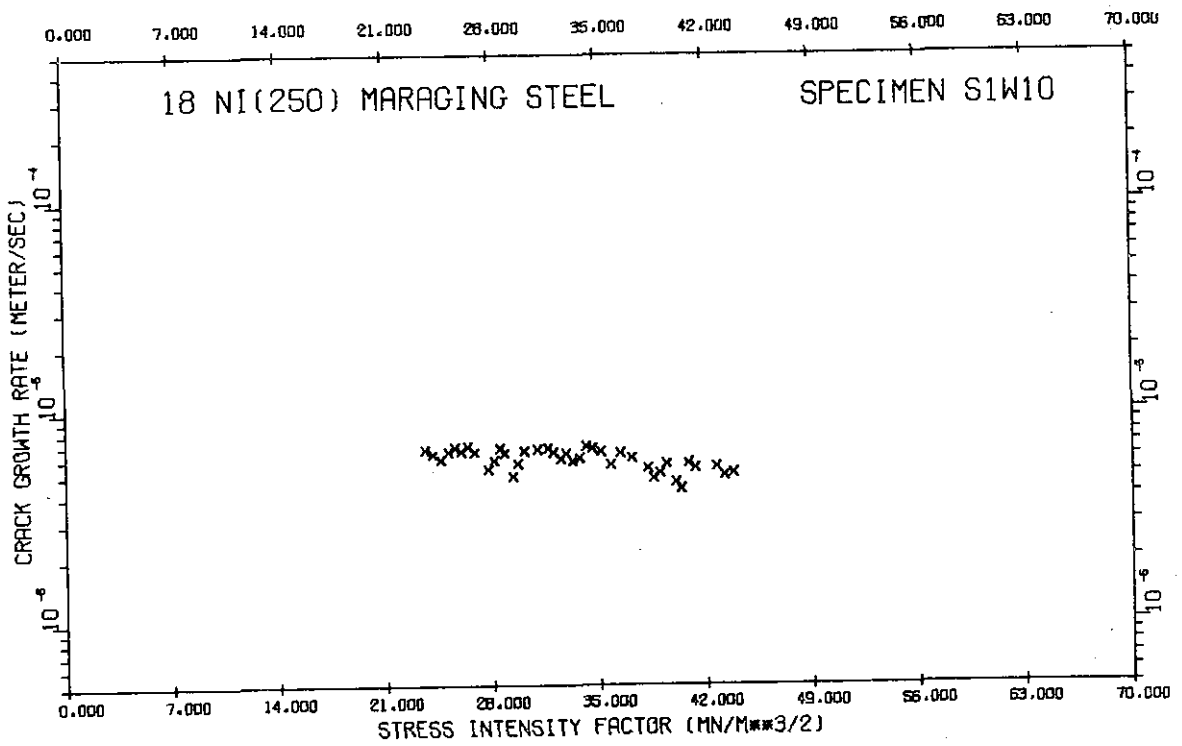
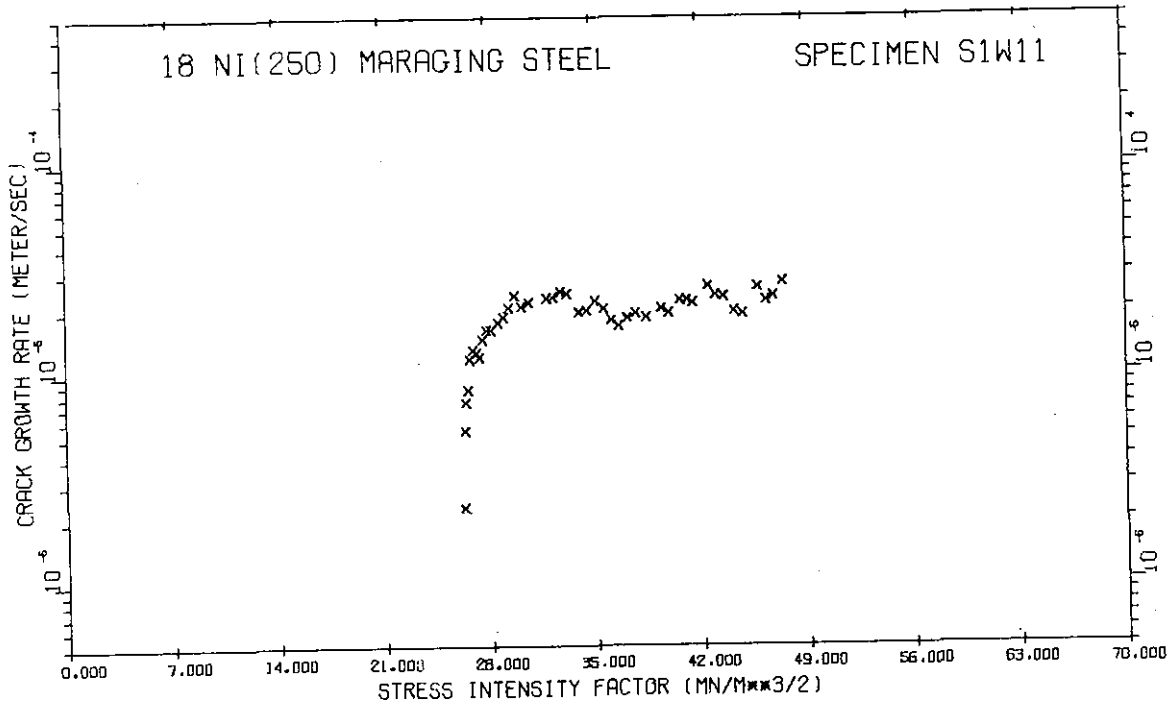
HYDROGEN PRESSURE = 57 KN/M**2 TEMPERATURE = 10.5C
 MEAN STAGE II RATE = 2.15 E-5 M/S 55 PCT CONF INT = 0.09 E-5 M/S
 AVERAGE STAGE II RATE = 1.86 E-5 M/S DIFFERENCE = 13 PCT
 STAGE II RATE IS STATISTICALLY K-INDEPENDENT


K	DA/DT	K	DA/DT	K	DA/DT	K	DA/DT
26.31	2.31E-06	28.62	1.76E-05	34.52	2.01E-05	41.12	2.23E-05
26.36	5.39E-06	28.98	1.87E-05	35.06	2.23E-05	41.48	2.17E-05
26.44	7.37E-06	29.31	2.07E-05	35.82	2.02E-05	42.52	2.60E-05
26.57	8.43E-06	29.73	2.38E-05	36.14	1.80E-05	42.99	2.35E-05
26.73	1.18E-05	30.17	2.09E-05	36.62	1.69E-05	43.51	2.31E-05
26.94	1.31E-05	30.66	2.21E-05	37.19	1.83E-05	44.21	1.98E-05
27.16	1.42E-05	31.85	2.30E-05	37.74	1.93E-05	44.80	1.91E-05
27.34	1.21E-05	32.27	2.33E-05	38.43	1.85E-05	45.80	2.57E-05
27.57	1.47E-05	32.75	2.47E-05	39.43	2.04E-05	46.34	2.33E-05
27.84	1.63E-05	33.20	2.40E-05	39.91	1.93E-05	46.85	2.32E-05
28.15	1.63E-05	33.98	1.97E-05	40.64	2.23E-05	47.44	2.73E-05

18 NI(250) MARAGING STEEL SPECIMEN SIM10

HYDROGEN PRESSURE = 57 KN/M**2 TEMPERATURE = -45.2C
 MEAN STAGE II RATE = 5.91 E-6 M/S 55 PCT CONF INT = 0.23 E-6 M/S
 AVERAGE STAGE II RATE = 5.85 E-6 M/S DIFFERENCE = 1 PCT

K	DA/DT	K	DA/DT	K	DA/DT	K	DA/DT
23.61	6.63E-06	28.50	6.74E-06	33.20	5.81E-06	39.01	5.09E-06
24.10	6.29E-06	28.80	6.34E-06	33.71	5.98E-06	39.42	5.61E-06
24.62	5.93E-06	29.34	4.92E-06	34.17	6.82E-06	40.03	4.57E-06
25.11	6.46E-06	29.66	5.65E-06	34.56	6.64E-06	40.36	4.25E-06
25.55	6.76E-06	30.08	6.49E-06	35.11	6.41E-06	40.85	5.67E-06
25.96	6.50E-06	30.94	6.59E-06	35.79	5.58E-06	41.31	5.38E-06
26.39	6.83E-06	31.61	6.69E-06	36.40	6.30E-06	42.69	5.42E-06
26.83	6.43E-06	31.98	6.38E-06	37.15	5.98E-06	43.23	4.92E-06
27.72	5.34E-06	32.48	5.96E-06	38.20	5.34E-06	43.82	5.10E-06
28.12	5.88E-06	32.83	6.29E-06	38.59	4.79E-06		



Reproduced from best available copy. 

REPRODUCIBILITY OF THE ORIGINAL PAGE IS POOR

18 NI(250) MARAGING STEEL SPECIMEN S1M14

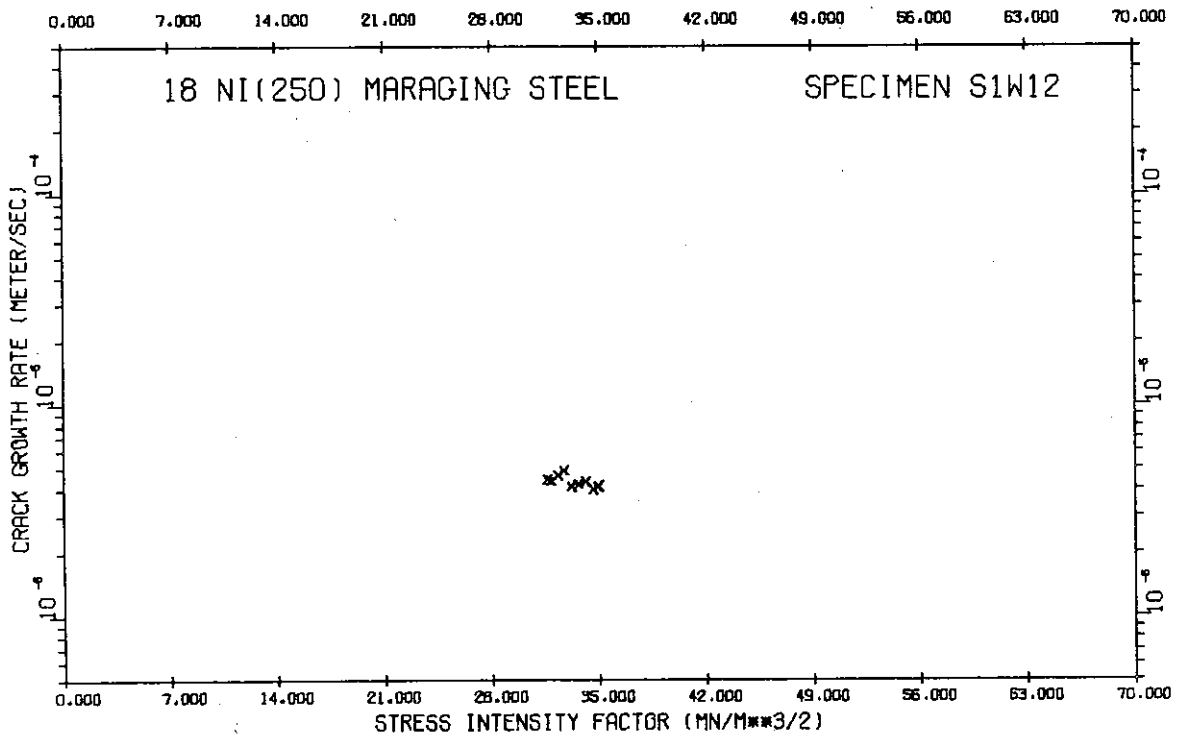
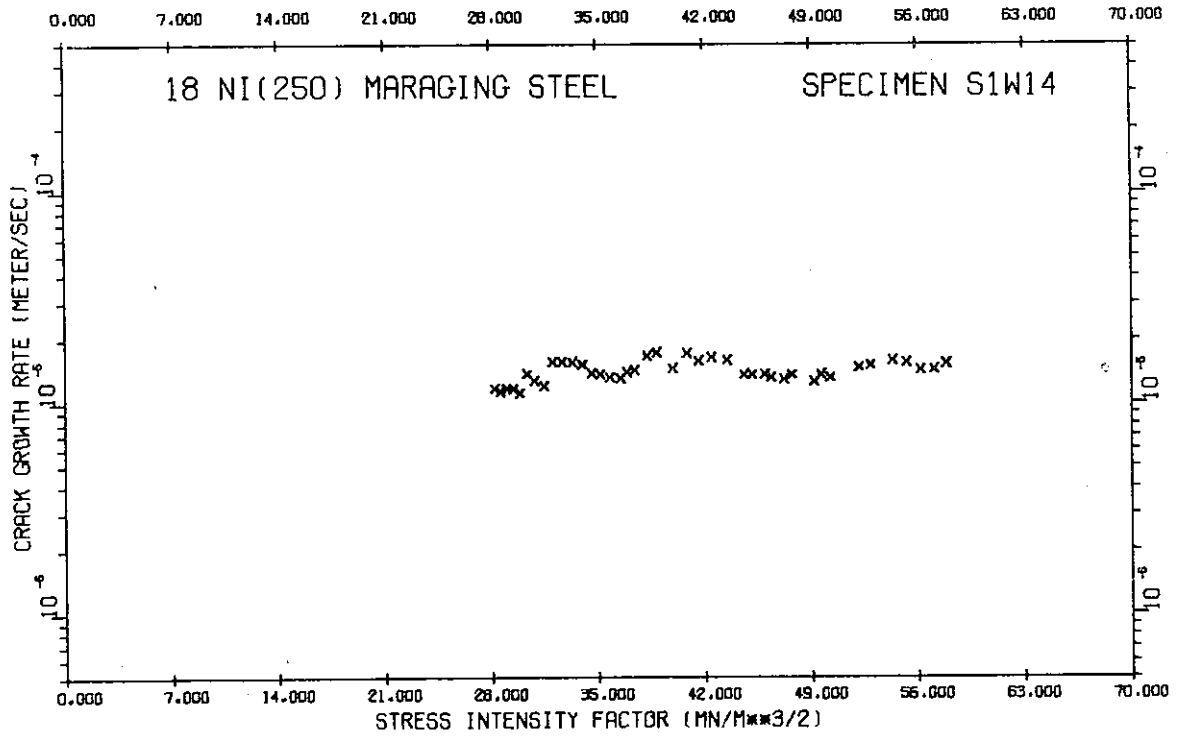
HYDROGEN PRESSURE = 28 KN/M**2 TEMPERATURE = -5.2C
 MEAN STAGE II RATE = 1.47 E-5 M/S 55 PCT CONF INT = 0.05 E-5 M/S
 AVERAGE STAGE II RATE = 1.44 E-5 M/S DIFFERENCE = 2 PCT
 STAGE II RATE IS STATISTICALLY K-INDEPENDENT


K	DA/DT	K	DA/DT	K	DA/DT	K	DA/DT
28.26	1.17E-05	34.04	1.52E-05	41.62	1.58E-05	50.28	1.31E-05
28.64	1.14E-05	34.65	1.39E-05	42.49	1.65E-05	52.18	1.47E-05
29.08	1.17E-05	35.20	1.37E-05	43.51	1.60E-05	52.94	1.51E-05
29.48	1.17E-05	35.86	1.33E-05	44.63	1.36E-05	54.39	1.58E-05
29.91	1.12E-05	36.55	1.30E-05	45.16	1.36E-05	55.30	1.56E-05
30.40	1.38E-05	36.95	1.40E-05	45.97	1.37E-05	56.22	1.44E-05
30.87	1.27E-05	37.45	1.44E-05	46.41	1.32E-05	57.11	1.44E-05
31.48	1.21E-05	38.26	1.68E-05	47.25	1.29E-05	57.89	1.53E-05
32.04	1.57E-05	38.89	1.74E-05	47.77	1.36E-05		
32.67	1.57E-05	39.94	1.46E-05	49.24	1.26E-05		
33.37	1.57E-05	40.88	1.73E-05	49.67	1.37E-05		

18 NI(250) MARAGING STEEL SPECIMEN S1M12

HYDROGEN PRESSURE = 32 KN/M**2 TEMPERATURE = -45.0C
 MEAN STAGE II RATE = 4.35 E-6 M/S 55 PCT CONF INT = 0.25 E-6 M/S
 AVERAGE STAGE II RATE = 4.27 E-6 M/S DIFFERENCE = 2 PCT
 STAGE II RATE IS STATISTICALLY K-INDEPENDENT

K	DA/DT	K	DA/DT	K	DA/DT	K	DA/DT
31.66	4.43E-06	32.74	4.89E-06	34.18	4.33E-06		
31.87	4.35E-06	33.22	4.10E-06	34.64	3.98E-06		
32.37	4.63E-06	33.70	4.18E-06	34.98	4.10E-06		



Reproduced from best available copy. 

18 NI(250) MARAGING STEEL SPECIMEN SIM17

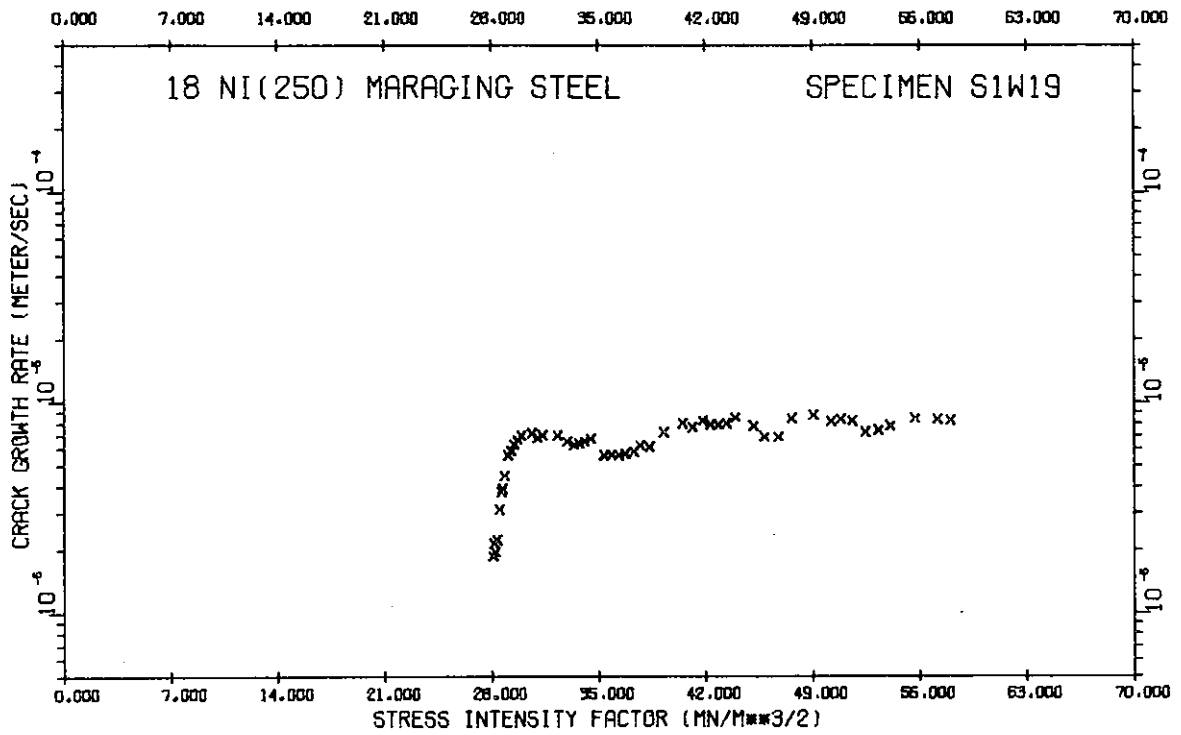
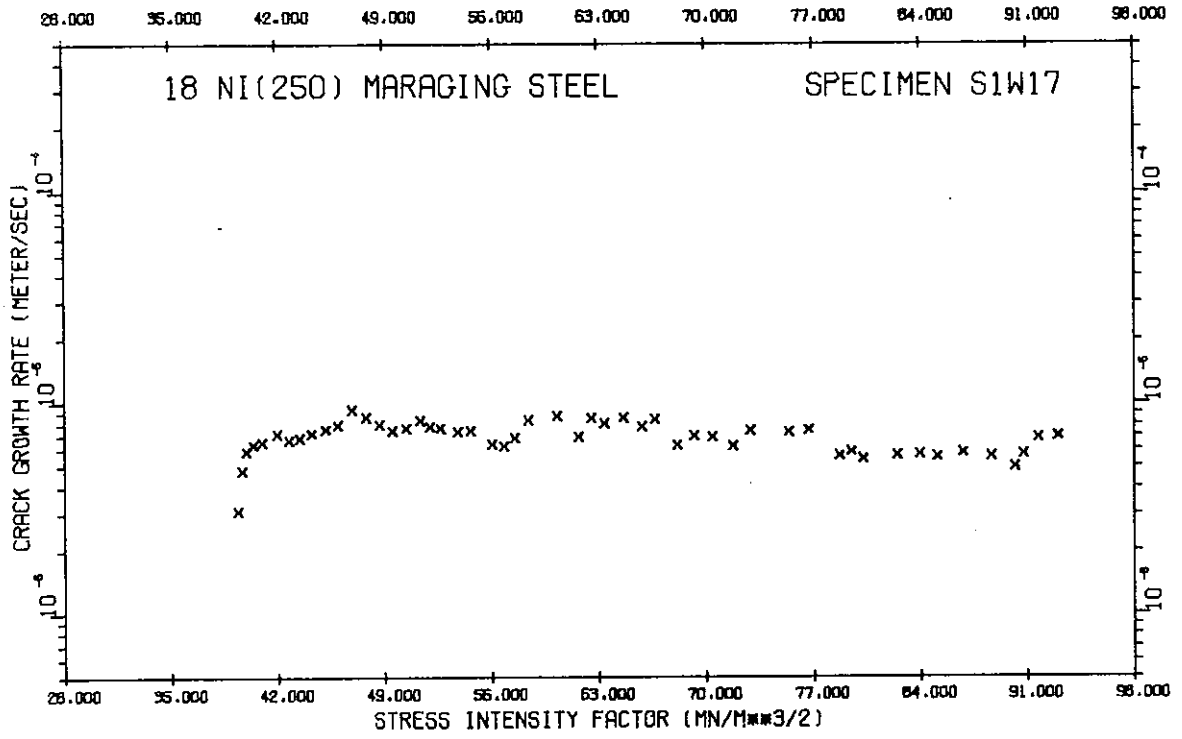
HYDROGEN PRESSURE = 13 KN/M**2 TEMPERATURE = -5.4C
 MEAN STAGE II RATE = 7.10 E-6 M/S 55 PCT CONF INT = 0.33 E-6 M/S
 AVERAGE STAGE II RATE = 7.14 E-6 M/S DIFFERENCE = 1 PCT

K	CA/DT	K	OA/DT	K	DA/DT	K	OA/DT
39.42	3.09E-06	48.71	7.96E-06	61.72	6.91E-06	78.78	5.62E-06
39.68	4.79E-06	49.54	7.44E-06	62.58	8.51E-06	79.54	5.87E-06
39.98	5.88E-06	50.46	7.64E-06	63.41	8.07E-06	80.32	5.42E-06
40.93	6.39E-06	51.37	8.35E-06	64.65	8.55E-06	82.56	5.63E-06
41.03	6.55E-06	52.00	7.76E-06	65.89	7.76E-06	83.98	5.69E-06
42.02	7.18E-06	52.70	7.63E-06	66.69	8.41E-06	85.15	5.55E-06
42.76	6.71E-06	53.80	7.34E-06	68.17	6.30E-06	86.82	5.80E-06
43.47	6.88E-06	54.67	7.40E-06	69.28	7.02E-06	88.68	5.57E-06
44.27	7.20E-06	56.05	6.40E-06	70.50	6.94E-06	90.23	4.96E-06
45.18	7.55E-06	56.86	6.26E-06	71.85	6.24E-06	90.78	5.72E-06
45.97	7.94E-06	57.56	6.86E-06	72.93	7.44E-06	91.79	6.87E-06
46.91	9.39E-06	58.46	8.31E-06	75.43	7.28E-06	93.06	6.95E-06
47.80	8.63E-06	60.35	8.76E-06	76.75	7.47E-06		

18 NI(250) MARAGING STEEL SPECIMEN SIM19

HYDROGEN PRESSURE = 12 KN/M**2 TEMPERATURE = -15.6C
 MEAN STAGE II RATE = 7.26 E-6 M/S 55 PCT CONF INT = 0.28 E-6 M/S
 AVERAGE STAGE II RATE = 6.44 E-6 M/S DIFFERENCE = 11 PCT

K	CA/DT	K	OA/DT	K	DA/DT	K	OA/DT
28.07	1.87E-06	29.96	7.05E-06	36.76	5.71E-06	45.88	6.90E-06
28.14	2.13E-06	30.68	7.17E-06	37.30	5.82E-06	46.78	6.87E-06
28.21	1.95E-06	31.04	6.79E-06	37.72	6.24E-06	47.64	8.43E-06
28.27	1.77E-07	31.36	7.04E-06	38.34	6.15E-06	49.00	8.71E-06
28.34	2.23E-06	32.36	7.03E-06	39.26	7.28E-06	50.20	8.11E-06
28.48	3.10E-06	32.98	6.56E-06	40.53	7.98E-06	50.89	8.33E-06
28.62	3.76E-06	33.40	6.28E-06	41.17	7.63E-06	51.65	8.19E-06
28.72	3.89E-06	33.71	6.40E-06	41.83	8.19E-06	52.49	7.24E-06
28.86	4.48E-06	34.09	6.56E-06	42.35	7.87E-06	53.37	7.39E-06
29.07	5.62E-06	34.50	6.79E-06	42.85	7.82E-06	54.12	7.74E-06
29.25	5.92E-06	35.38	5.60E-06	43.39	7.94E-06	55.74	8.39E-06
29.47	6.32E-06	35.86	5.66E-06	43.98	8.46E-06	57.19	8.35E-06
29.71	6.65E-06	36.33	5.60E-06	45.15	7.74E-06	58.03	8.21E-06



Reproduced from
best available copy.

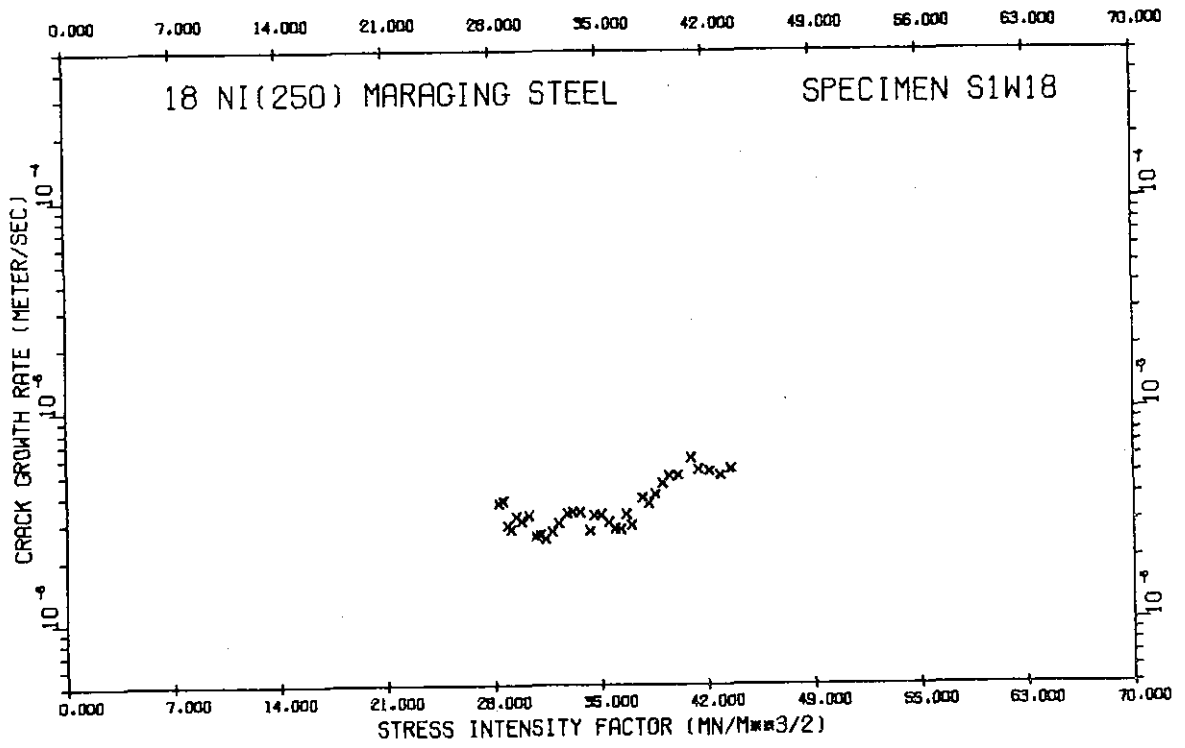


18 NI(250) MARAGING STEEL SPECIMEN SIM18

HYDROGEN PRESSURE = 12 KN/M**2 TEMPERATURE = -41.2C
 MEAN STAGE II RATE = 3.58 E-6 M/S 95 PCT CONF INT = 0.33 E-6 M/S
 AVERAGE STAGE II RATE = 3.62 E-6 M/S DIFFERENCE = 1 PCT

CRACK FRONT BRANCHING AT K = 43.5 MN/M**3/2

K	CA/DT	K	DA/DT	K	DA/DT	K	DA/DT
28.32	3.67E-06	31.42	2.49E-06	35.53	2.98E-06	39.56	4.90E-06
28.60	3.75E-06	31.88	2.69E-06	35.95	2.78E-06	40.12	4.93E-06
28.89	2.89E-06	32.29	2.95E-06	36.33	2.75E-06	40.99	5.97E-06
29.12	2.75E-06	32.82	3.28E-06	36.68	3.25E-06	41.50	5.28E-06
29.48	3.16E-06	33.17	3.31E-06	37.03	2.90E-06	42.24	5.17E-06
29.82	3.02E-06	33.68	3.31E-06	37.74	3.87E-06	42.94	4.95E-06
30.31	3.21E-06	34.32	2.71E-06	38.15	3.63E-06		
30.77	2.56E-06	34.59	3.20E-06	38.59	4.01E-06		
31.05	2.60E-06	35.06	3.22E-06	39.03	4.52E-06		



Reproduced from
best available copy.



REPRODUCIBILITY OF THE ORIGINAL PAGE IS POOR

18 NI(200) MARAGING STEEL SPECIMEN S3M10

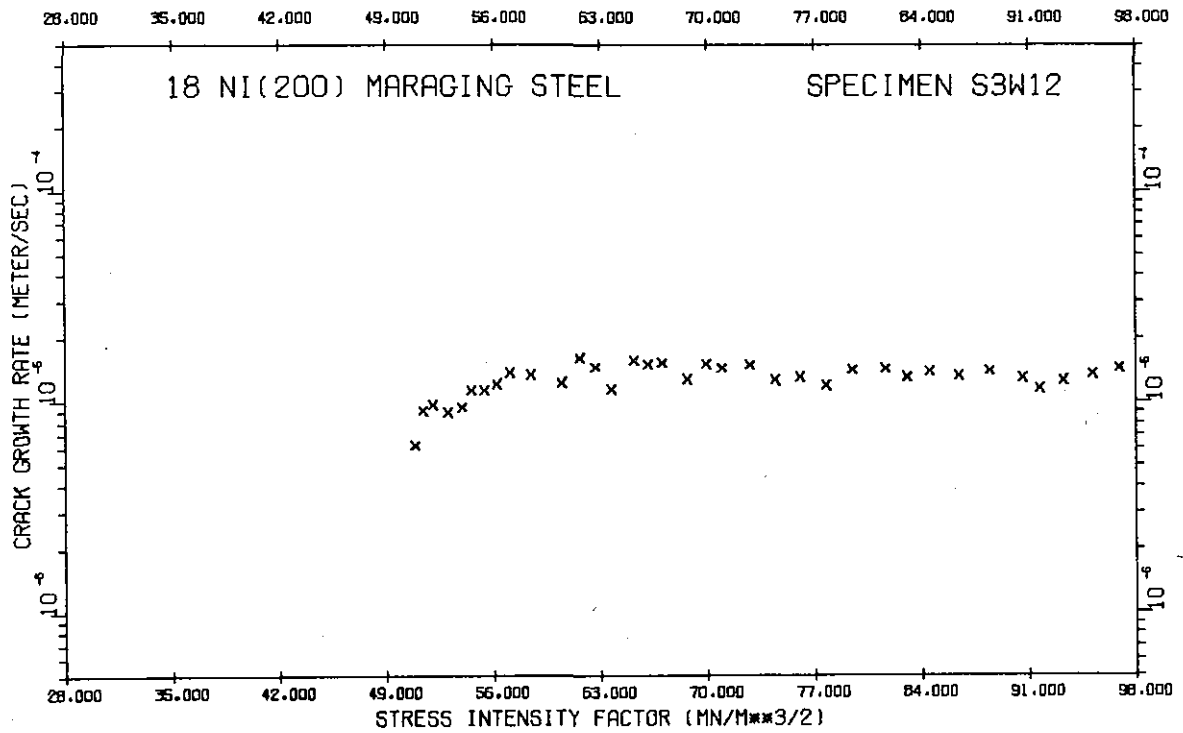
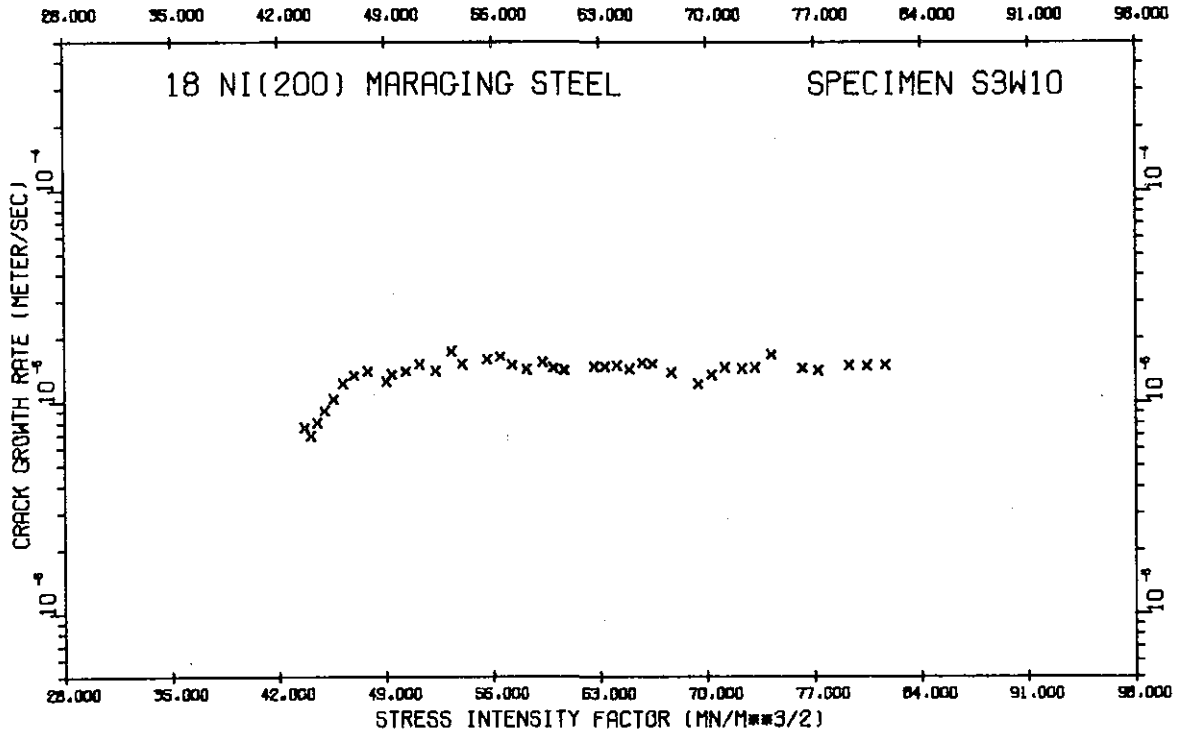
HYDROGEN PRESSURE = 268 KN/M**2 TEMPERATURE = -5.1C
 MEAN STAGE II RATE = 1.45 E-5 M/S 55 PCT CONF INT = 0.04 E-5 P/S
 AVERAGE STAGE II RATE = 1.36 E-5 M/S DIFFERENCE = 6 PCT
 STAGE II RATE IS STATISTICALLY K-INDEPENDENT

K	DA/DT	K	DA/DT	K	DA/DT	K	DA/DT
43.71	7.59E-06	50.35	1.39E-05	60.01	1.44E-05	70.32	1.34E-05
44.08	6.92E-06	51.23	1.50E-05	60.71	1.41E-05	71.19	1.45E-05
44.52	7.99E-06	52.29	1.41E-05	62.64	1.47E-05	72.30	1.43E-05
44.98	9.13E-06	53.31	1.74E-05	63.37	1.46E-05	73.17	1.45E-05
45.58	1.03E-05	54.01	1.50E-05	64.11	1.44E-05	74.23	1.68E-05
46.21	1.22E-05	55.65	1.60E-05	64.93	1.43E-05	74.26	1.44E-05
46.93	1.33E-05	56.52	1.63E-05	65.78	1.52E-05	77.26	1.40E-05
47.82	1.39E-05	57.29	1.49E-05	66.44	1.51E-05	79.32	1.49E-05
49.06	1.24E-05	58.23	1.43E-05	67.67	1.38E-05	80.47	1.48E-05
49.44	1.35E-05	59.31	1.53E-05	69.47	1.22E-05	81.68	1.49E-05

18 NI(200) MARAGING STEEL SPECIMEN S3M12

HYDROGEN PRESSURE = 272 KN/M**2 TEMPERATURE = -12.0C
 MEAN STAGE II RATE = 1.36 E-5 M/S 55 PCT CONF INT = 0.05 E-5 P/S
 AVERAGE STAGE II RATE = 1.27 E-5 M/S DIFFERENCE = 7 PCT
 STAGE II RATE IS STATISTICALLY K-INDEPENDENT

K	DA/DT	K	DA/DT	K	DA/DT	K	DA/DT
50.92	6.24E-06	60.52	1.23E-05	72.82	1.49E-05	90.65	1.30E-05
51.45	9.09E-06	61.71	1.62E-05	74.45	1.27E-05	91.77	1.16E-05
52.06	9.69E-06	62.74	1.46E-05	76.08	1.31E-05	93.29	1.26E-05
53.04	8.54E-06	63.76	1.16E-05	77.82	1.20E-05	95.17	1.34E-05
53.98	9.40E-06	65.25	1.57E-05	79.54	1.41E-05	96.95	1.44E-05
54.59	1.14E-05	66.15	1.50E-05	81.72	1.43E-05		
55.44	1.14E-05	67.08	1.53E-05	83.12	1.30E-05		
56.26	1.21E-05	68.74	1.28E-05	84.57	1.39E-05		
57.15	1.37E-05	69.98	1.51E-05	86.43	1.32E-05		
58.53	1.34E-05	71.00	1.44E-05	88.51	1.40E-05		



Reproduced from
best available copy.



18 NI(200) MARAGING STEEL SPECIMEN S3M17

HYDROGEN PRESSURE = 272 KN/M**2 TEMPERATURE = -25.4C
 MEAN STAGE II RATE = 1.17 E-5 M/S 55 PCT CONF INT = 0.07 E-5 M/S
 AVERAGE STAGE II RATE = 1.11 E-5 M/S DIFFERENCE = 6 PCT

CRACK FRONT BRANCHING AT K = 85.6 MN/M**3/2

K	CA/DT	K	DA/DT	K	DA/DT	K	DA/DT
51.93	6.35E-06	56.98	1.12E-05	64.65	1.13E-05	76.82	1.34E-05
52.36	7.48E-06	57.83	1.09E-05	65.76	1.04E-05	78.96	1.26E-05
52.90	8.84E-06	58.72	1.06E-05	66.91	1.04E-05	81.20	1.39E-05
53.52	1.06E-05	60.66	9.53E-06	68.16	1.13E-05	85.58	1.44E-05
54.32	1.16E-05	61.48	1.01E-05	69.39	1.19E-05		
55.16	1.22E-05	62.53	1.14E-05	72.14	1.22E-05		
56.06	1.19E-05	63.54	1.08E-05	74.06	1.52E-05		

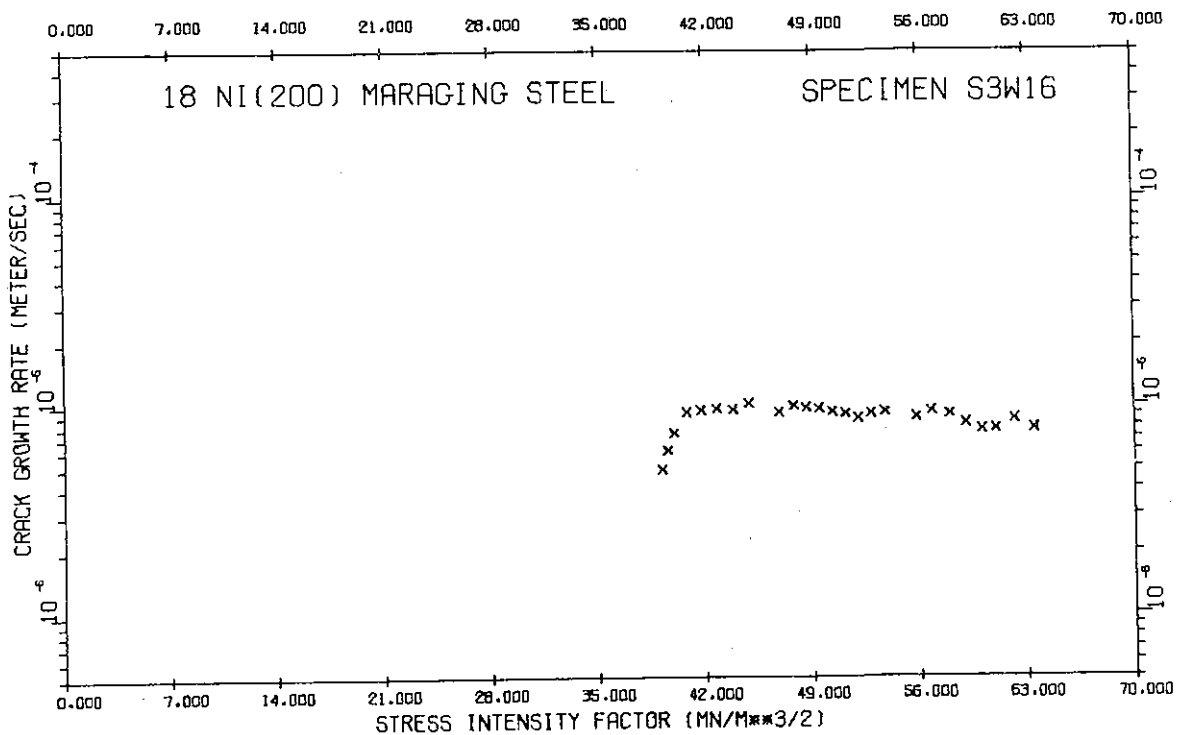
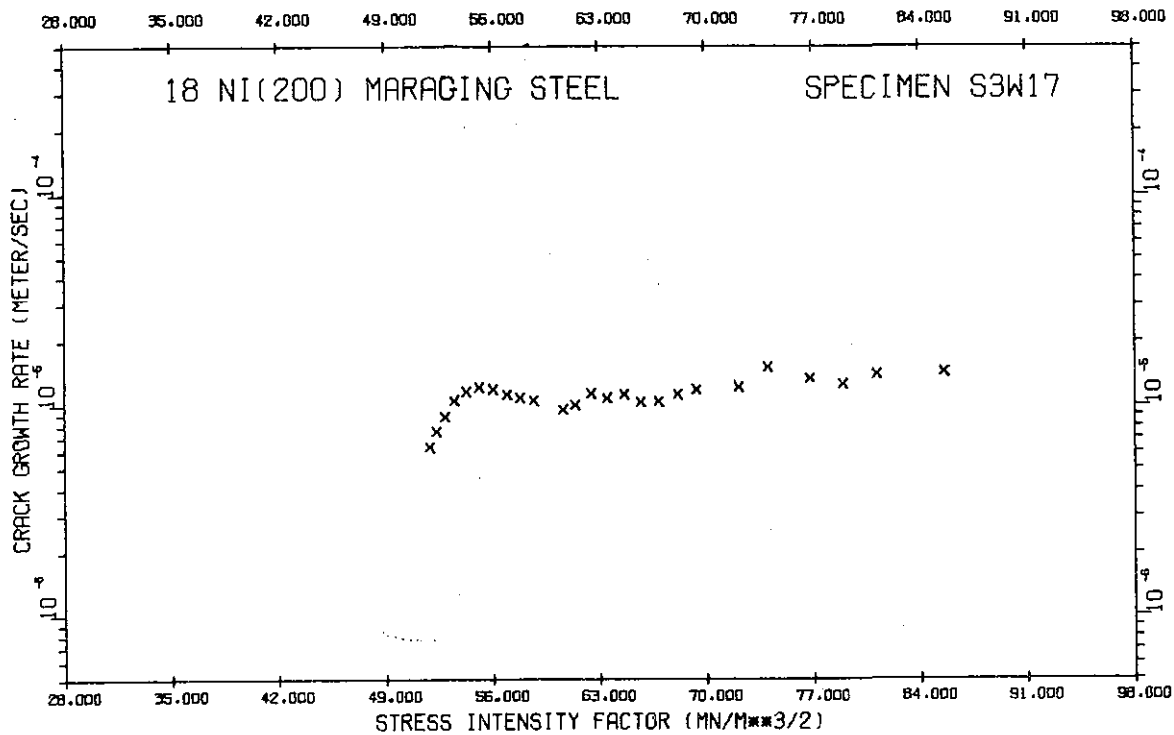
18 NI(200) MARAGING STEEL SPECIMEN S3M16

HYDROGEN PRESSURE = 272 KN/M**2 TEMPERATURE = -36.3C
 MEAN STAGE II RATE = 9.03 E-6 M/S 55 PCT CONF INT = 0.33 E-6 M/S
 AVERAGE STAGE II RATE = 8.64 E-6 M/S DIFFERENCE = 4 PCT

CRACK FRONT BRANCHING AT K = 63.2 MN/M**3/2

K	DA/DT	K	DA/DT	K	DA/DT	K	DA/DT
39.18	4.91E-06	44.92	1.03E-05	52.02	8.63E-06	60.05	7.58E-06
39.58	6.07E-06	46.80	9.24E-06	52.87	9.04E-06	61.00	7.67E-06
39.98	7.38E-06	47.82	9.95E-06	53.79	9.20E-06	62.21	8.51E-06
40.83	9.26E-06	48.63	9.75E-06	55.81	8.68E-06		
41.76	9.46E-06	49.46	9.65E-06	56.81	9.31E-06		
42.82	9.65E-06	50.31	9.27E-06	57.98	8.97E-06		
43.87	9.53E-06	51.19	9.10E-06	59.02	8.15E-06		

Reproduced from best available copy.



Reproduced from
best available copy.



18 NI(200) MARAGING STEEL SPECIMEN S3M25

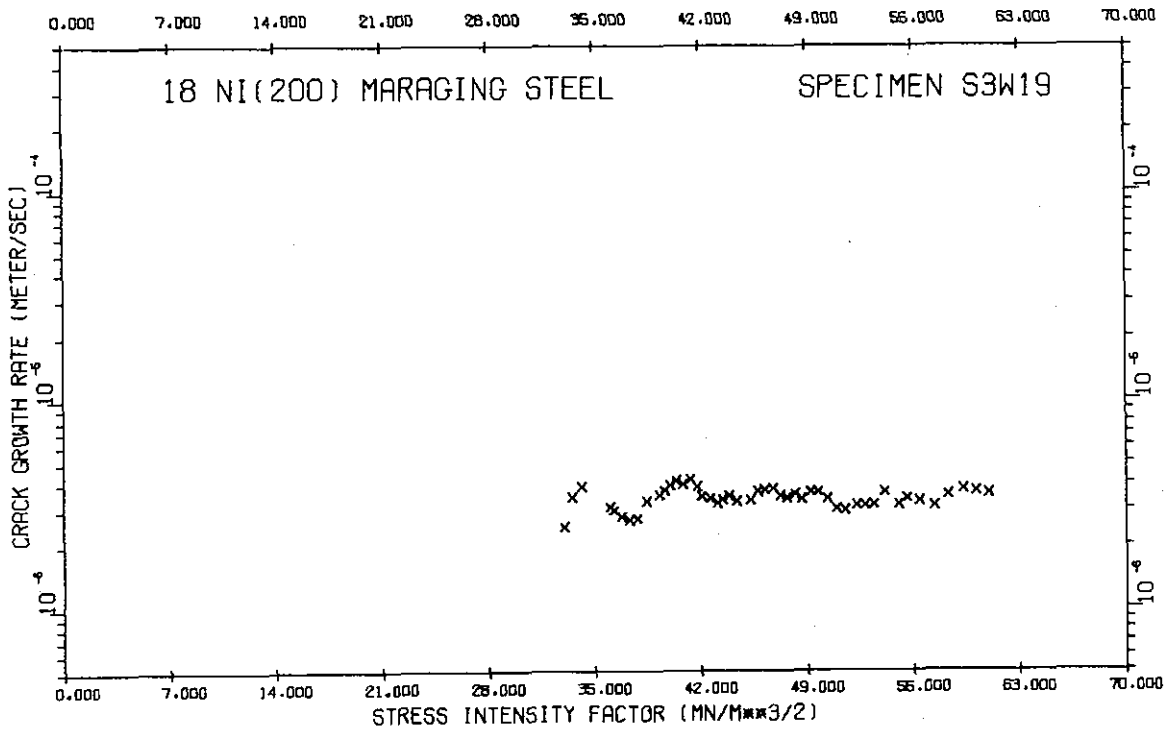
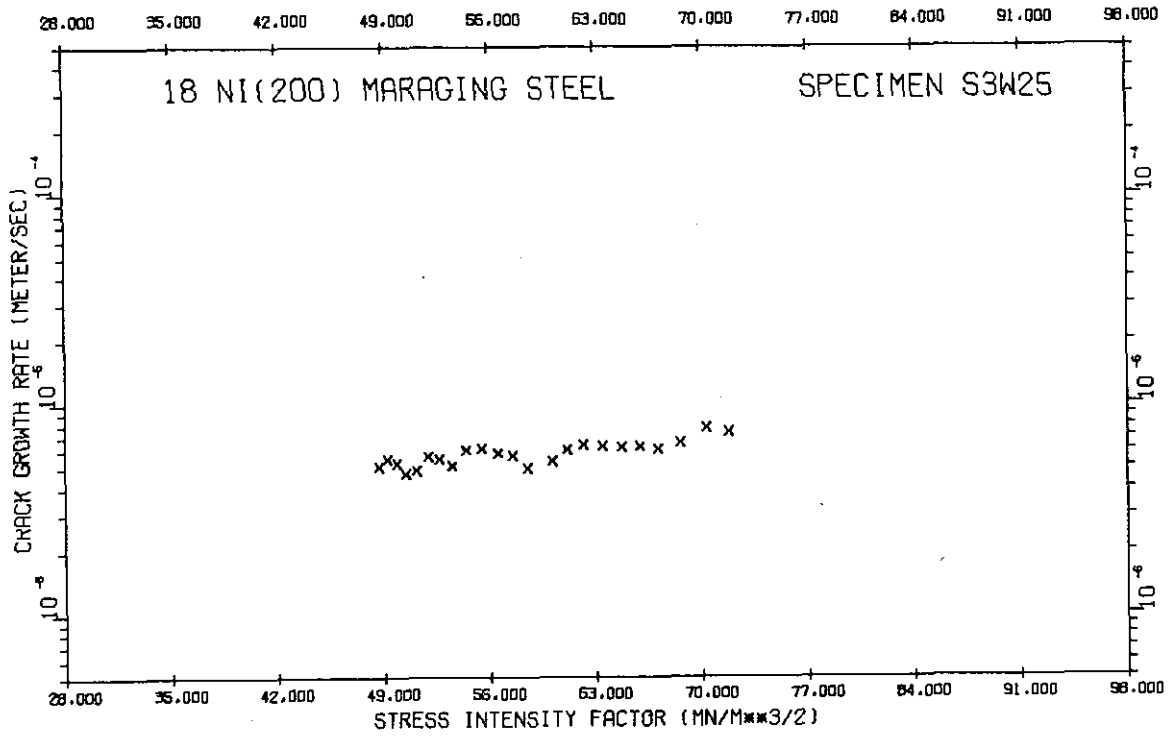
HYDROGEN PRESSURE = 270 KN/M**2 TEMPERATURE = -45.2C
 MEAN STAGE II RATE = 5.82 E-6 M/S 95 PCT CONF INT = 0.33 E-6 M/S
 AVERAGE STAGE II RATE = 5.19 E-6 M/S DIFFERENCE = 11 PCT
 CRACK FRONT BRANCHING AT K = 72.0 MN/M**3/2

K	DA/DT	K	DA/DT	K	DA/DT	K	DA/DT
48.70	5.07E-06	52.72	5.50E-06	58.53	4.98E-06	65.96	6.31E-06
49.26	5.51E-06	53.58	5.12E-06	60.19	5.34E-06	67.13	6.08E-06
49.94	5.25E-06	54.49	6.06E-06	61.15	6.07E-06	68.61	6.53E-06
50.51	4.70E-06	55.50	6.19E-06	62.20	6.40E-06	70.36	7.69E-06
51.21	4.86E-06	56.57	5.86E-06	63.49	6.31E-06	71.81	7.33E-06
51.99	5.65E-06	57.54	5.67E-06	64.74	6.23E-06		

18 NI(200) MARAGING STEEL SPECIMEN S3M19

HYDROGEN PRESSURE = 273 KN/M**2 TEMPERATURE = -55.7C
 MEAN STAGE II RATE = 3.48 E-6 M/S 95 PCT CONF INT = 0.10 E-6 M/S
 AVERAGE STAGE II RATE = 3.40 E-6 M/S DIFFERENCE = 2 PCT

K	DA/DT	K	DA/DT	K	DA/DT	K	DA/DT
33.02	2.47E-06	40.38	4.10E-06	46.23	3.71E-06	52.86	3.12E-06
33.54	3.44E-06	40.81	3.94E-06	46.74	3.77E-06	53.44	3.15E-06
34.15	3.85E-06	41.30	4.17E-06	47.25	3.47E-06	54.12	3.62E-06
36.02	3.08E-06	41.76	3.84E-06	47.66	3.39E-06	55.07	3.14E-06
36.27	2.97E-06	42.09	3.45E-06	48.20	3.52E-06	55.61	3.38E-06
36.79	2.76E-06	42.63	3.37E-06	48.64	3.34E-06	56.40	3.28E-06
37.33	2.66E-06	43.11	3.20E-06	49.23	3.60E-06	57.40	3.08E-06
37.82	2.71E-06	43.45	3.34E-06	49.73	3.61E-06	58.29	3.50E-06
38.43	3.28E-06	43.89	3.47E-06	50.32	3.36E-06	59.27	3.71E-06
39.27	3.52E-06	44.39	3.27E-06	50.94	3.08E-06	60.14	3.64E-06
39.59	3.67E-06	45.29	3.31E-06	51.50	2.95E-06	60.97	3.56E-06
39.99	3.88E-06	45.75	3.64E-06	52.31	3.13E-06		



Reproduced from
best available copy.



18 NI(200) MARAGING STEEL SPECIMEN S3M08

HYDROGEN PRESSURE = 133 KN/M**2 TEMPERATURE = -11.9C
 MEAN STAGE II RATE = 4.85 E-6 M/S 95 PCT CONF INT = 0.40 E-6 M/S
 AVERAGE STAGE II RATE = 3.86 E-6 M/S DIFFERENCE = 21 PCT
 STAGE II RATE IS STATISTICALLY K-INDEPENDENT

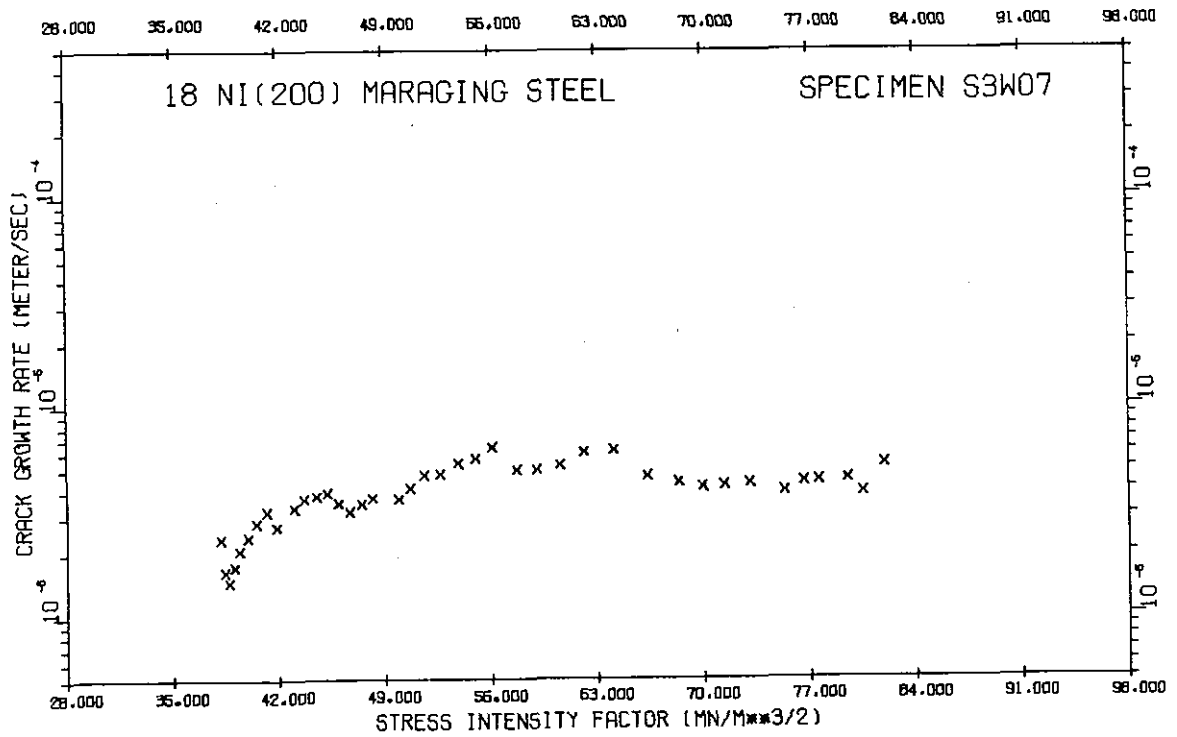
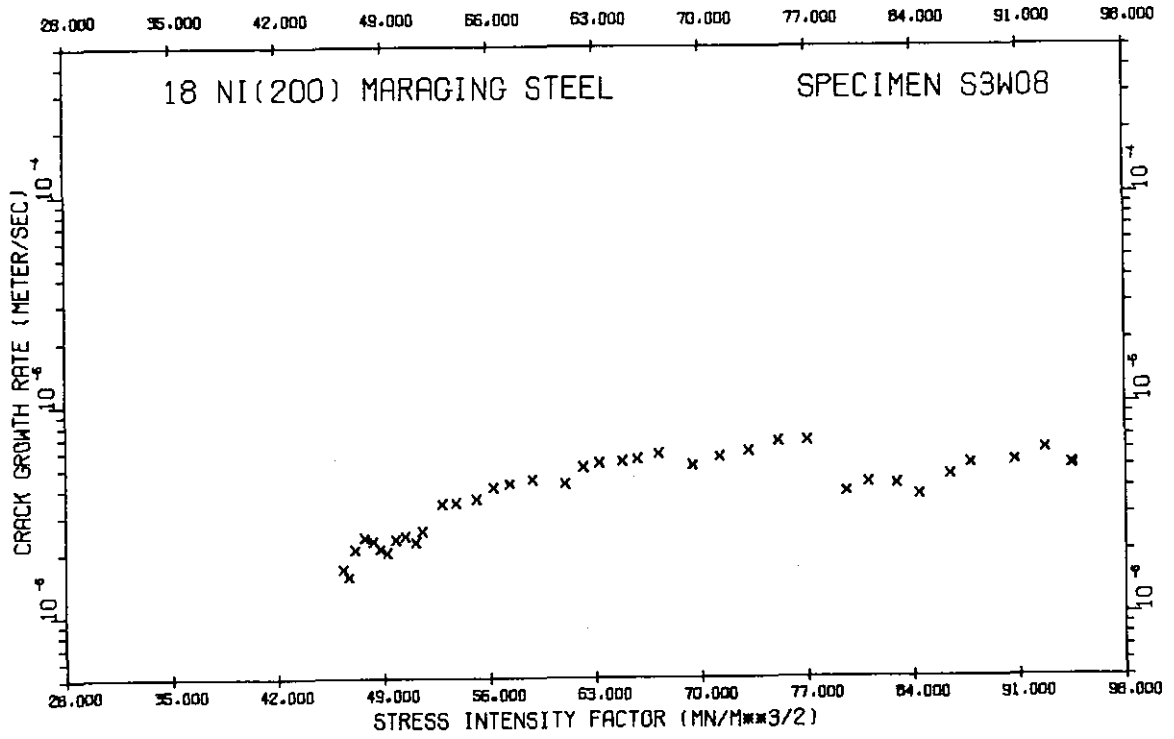
K	DA/DT	K	DA/DT	K	DA/DT	K	DA/DT
46.35	1.66E-06	51.59	2.51E-06	64.79	5.36E-06	82.93	4.15E-06
46.70	1.52E-06	52.89	3.37E-06	65.79	5.48E-06	84.41	3.68E-06
47.14	2.06E-06	53.81	3.42E-06	67.20	5.80E-06	86.42	4.50E-06
47.76	2.33E-06	55.16	3.56E-06	69.47	5.11E-06	87.81	5.16E-06
48.32	2.25E-06	56.28	4.02E-06	71.26	5.60E-06	90.74	5.28E-06
49.81	2.08E-06	57.34	4.20E-06	73.17	5.98E-06	92.75	6.04E-06
49.26	1.99E-06	58.85	4.39E-06	75.08	6.65E-06	94.50	5.11E-06
49.84	2.28E-06	61.01	4.19E-06	76.98	6.69E-06		
50.46	2.36E-06	62.20	5.01E-06	79.60	3.82E-06		
51.15	2.23E-06	63.28	5.26E-06	81.05	4.23E-06		

REPRODUCIBILITY OF THE ORIGINAL PAGE IS POOR

18 NI(200) MARAGING STEEL SPECIMEN S3M07

HYDROGEN PRESSURE = 133 KN/M**2 TEMPERATURE = -14.6C
 MEAN STAGE II RATE = 4.81 E-6 M/S 95 PCT CONF INT = 0.33 E-6 M/S
 AVERAGE STAGE II RATE = 3.78 E-6 M/S DIFFERENCE = 21 PCT
 STAGE II RATE IS STATISTICALLY K-INDEPENDENT

K	DA/DT	K	DA/DT	K	DA/DT	K	DA/DT
38.17	2.34E-06	43.70	3.64E-06	52.71	4.72E-06	68.42	4.30E-06
38.42	1.64E-06	44.50	3.74E-06	53.87	5.33E-06	69.98	4.10E-06
38.72	1.46E-06	45.20	3.88E-06	55.02	5.64E-06	71.39	4.16E-06
39.09	1.74E-06	45.94	3.46E-06	56.12	6.38E-06	73.08	4.27E-06
39.43	2.06E-06	46.66	3.15E-06	57.74	4.93E-06	75.35	3.69E-06
39.99	2.39E-06	47.44	3.43E-06	59.11	4.96E-06	76.64	4.33E-06
40.54	2.80E-06	48.17	3.65E-06	60.59	5.21E-06	77.65	4.37E-06
41.24	3.16E-06	49.93	3.62E-06	62.18	5.99E-06	79.57	4.45E-06
41.87	2.68E-06	50.70	4.09E-06	64.15	6.15E-06	80.50	3.87E-06
43.03	3.29E-06	51.65	4.69E-06	66.33	4.61E-06	81.97	5.24E-06



18 NI(200) MARAGING STEEL SPECIMEN S3M06

HYDROGEN PRESSURE = 133 KN/M**2 TEMPERATURE = -25.4C
 MEAN STAGE II RATE = 5.30 E-6 M/S 55 PCT CONF INT = 0.20 E-6 M/S
 AVERAGE STAGE II RATE = 4.96 E-6 M/S DIFFERENCE = 6 PCT

K	DA/DT	K	DA/DT	K	DA/DT	K	DA/DT
33.53	2.47E-06	40.48	5.14E-06	48.97	5.36E-06	60.82	4.05E-06
33.98	2.50E-06	41.15	5.43E-06	49.83	5.56E-06	62.52	5.18E-06
34.44	3.07E-06	41.90	5.00E-06	51.71	6.01E-06	65.24	4.58E-06
35.04	3.41E-06	42.80	5.56E-06	52.99	5.26E-06	66.73	4.59E-06
35.80	4.55E-06	43.85	5.01E-06	54.38	5.80E-06	68.29	5.39E-06
36.64	5.90E-06	45.52	5.08E-06	55.95	5.46E-06	69.73	4.84E-06
37.66	5.51E-06	46.67	5.88E-06	57.84	4.68E-06		
38.27	5.61E-06	47.89	6.44E-06	59.40	4.75E-06		

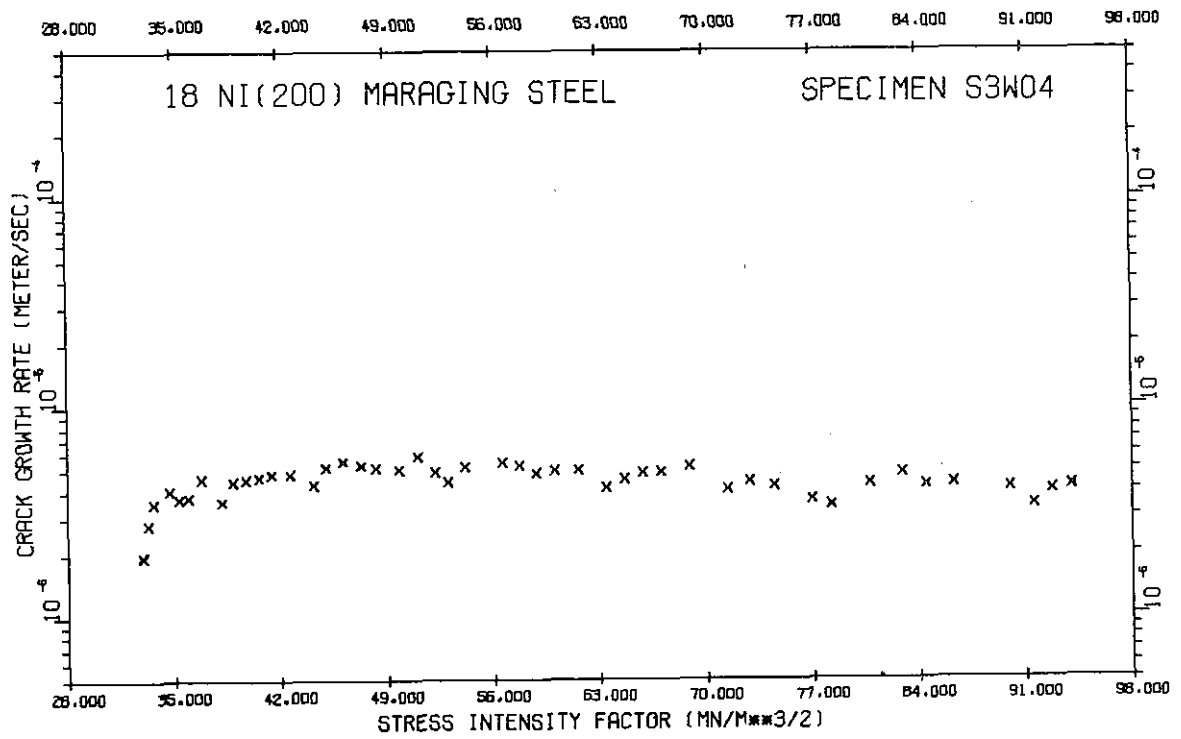
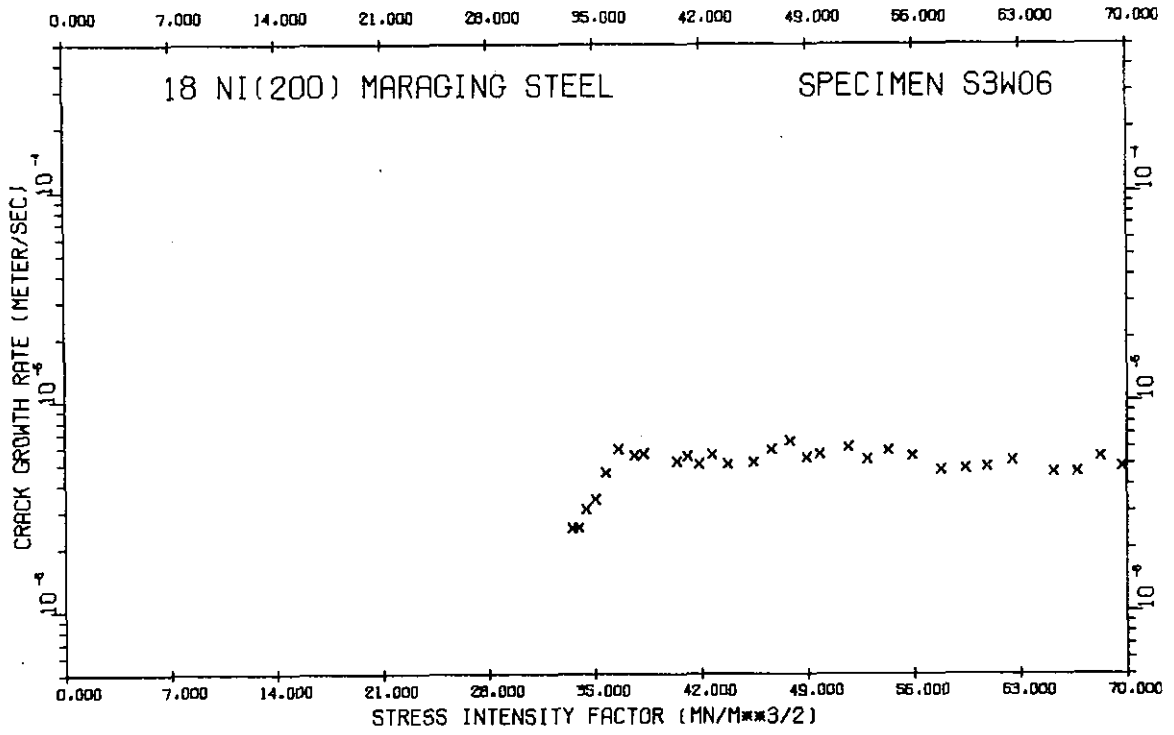
18 NI(200) MARAGING STEEL SPECIMEN S3M04

HYDROGEN PRESSURE = 133 KN/M**2 TEMPERATURE = -38.0C
 MEAN STAGE II RATE = 4.63 E-6 M/S 55 PCT CONF INT = 0.19 E-6 M/S
 AVERAGE STAGE II RATE = 4.75 E-6 M/S DIFFERENCE = 3 PCT

K	DA/DT	K	DA/DT	K	DA/DT	K	DA/DT
32.87	1.96E-06	41.47	4.82E-06	56.62	5.45E-06	74.54	4.20E-06
32.96	1.94E-06	42.69	4.82E-06	57.73	5.26E-06	76.98	3.60E-06
33.31	2.79E-06	44.21	4.28E-06	58.85	4.82E-06	78.28	3.34E-06
33.66	3.52E-06	45.02	5.16E-06	60.07	4.95E-06	80.33	4.29E-06
34.72	4.05E-06	46.14	5.53E-06	61.66	4.99E-06	82.93	4.60E-06
35.35	3.69E-06	47.35	5.31E-06	63.50	4.13E-06	84.52	4.20E-06
35.98	3.74E-06	48.33	5.14E-06	64.65	4.52E-06	86.30	4.27E-06
36.80	4.57E-06	49.81	5.80E-06	65.89	4.85E-06	90.01	4.09E-06
38.18	3.56E-06	51.08	5.85E-06	67.88	4.89E-06	91.62	3.37E-06
38.90	4.46E-06	52.23	4.91E-06	68.94	5.15E-06	92.81	3.97E-06
39.74	4.55E-06	53.05	4.41E-06	71.46	4.02E-06	94.08	4.11E-06
40.63	4.65E-06	54.18	5.18E-06	72.91	4.39E-06		

Reproduced from best available copy.





18 NI(200) MARAGING STEEL SPECIMEN S3M11

HYDROGEN PRESSURE = 137 KN/M**2 TEMPERATURE = -46.0C
 MEAN STAGE II RATE = 3.74 E-6 M/S 95 PCT CONF INT = 0.13 E-6 M/S
 AVERAGE STAGE II RATE = 3.55 E-6 M/S DIFFERENCE = 5 PCT
 STAGE II RATE IS STATISTICALLY K-INDEPENDENT

K	DA/DT	K	DA/DT	K	DA/DT	K	DA/DT
29.14	1.39E-06	32.83	3.88E-06	37.97	3.78E-06	41.61	3.96E-06
29.32	1.81E-06	33.26	3.84E-06	38.70	3.15E-06	42.12	4.10E-06
29.65	2.70E-06	34.12	3.38E-06	39.06	3.42E-06	42.72	4.54E-06
30.11	3.53E-06	34.71	3.59E-06	39.49	3.74E-06	43.89	4.05E-06
30.67	3.61E-06	35.40	3.49E-06	39.92	3.47E-06	44.52	4.36E-06
31.21	3.70E-06	36.08	3.70E-06	40.27	3.34E-06	45.18	4.28E-06
31.79	3.89E-06	36.78	3.50E-06	40.68	3.36E-06		
32.40	3.86E-06	37.46	3.54E-06	41.09	3.73E-06		

REPRODUCIBILITY OF THE ORIGINAL PAGE IS POOR

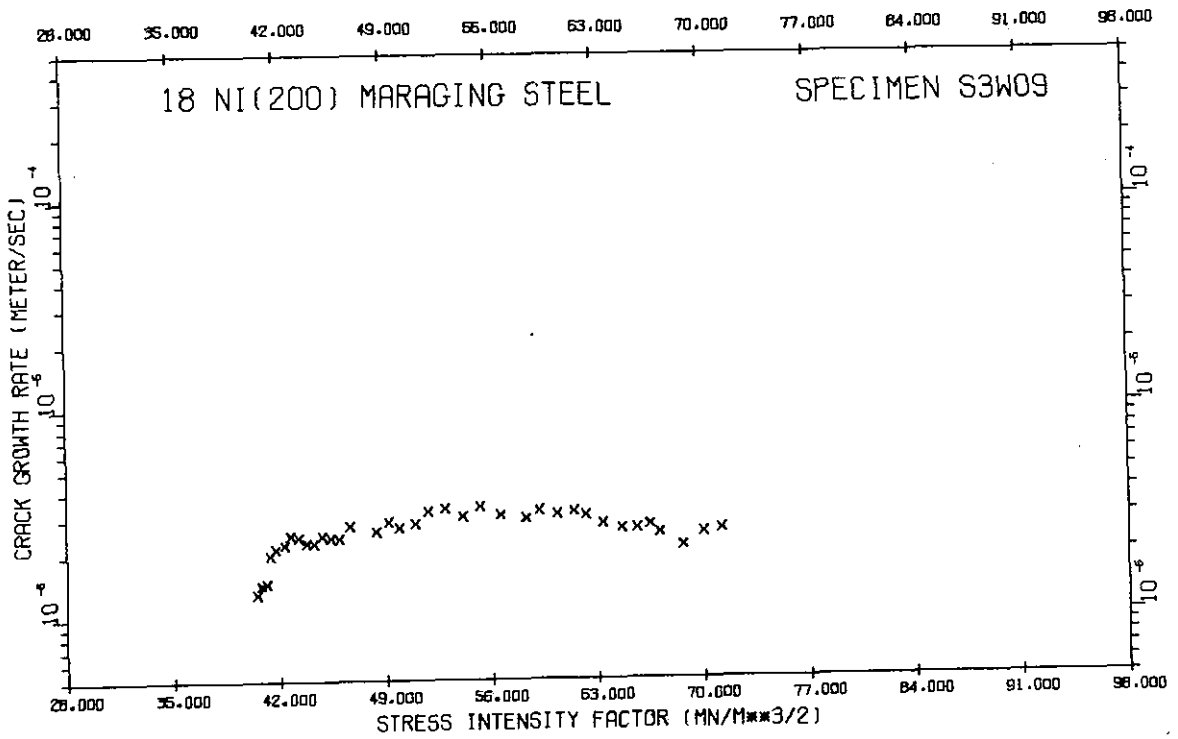
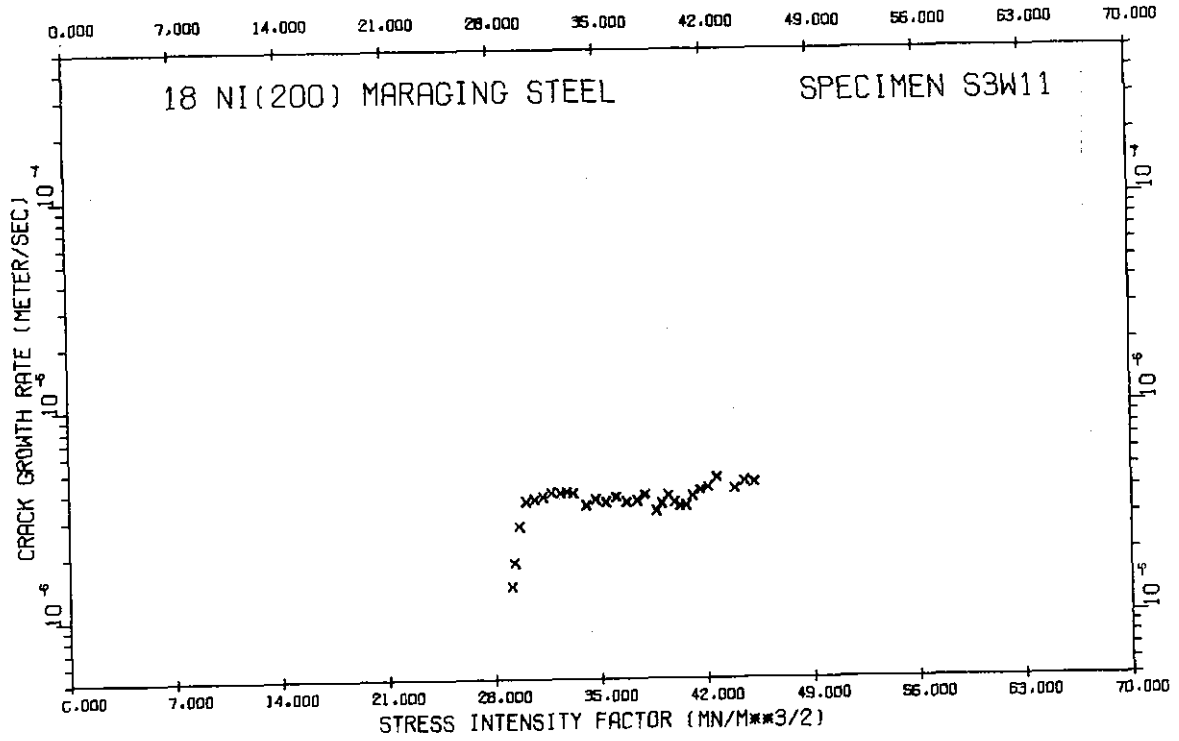
18 NI(200) MARAGING STEEL SPECIMEN S3M09

HYDROGEN PRESSURE = 133 KN/M**2 TEMPERATURE = -54.8C
 MEAN STAGE II RATE = 2.74 E-6 M/S 95 PCT CONF INT = 0.13 E-6 M/S
 AVERAGE STAGE II RATE = 2.67 E-6 M/S DIFFERENCE = 3 PCT
 STAGE II RATE IS STATISTICALLY K-INDEPENDENT
 CRACK FRONT BRANCHING AT K = 71.4 MN/M**3/2

K	DA/DT	K	DA/DT	K	DA/DT	K	DA/DT
40.51	1.30E-06	44.29	2.29E-06	51.87	3.23E-06	62.33	3.06E-06
40.83	1.43E-06	44.86	2.47E-06	52.99	3.30E-06	63.42	2.78E-06
41.15	1.46E-06	45.45	2.42E-06	54.15	3.03E-06	64.65	2.64E-06
41.46	2.00E-06	45.98	2.40E-06	55.30	3.40E-06	65.66	2.62E-06
41.82	2.16E-06	46.70	2.76E-06	56.65	3.08E-06	66.53	2.73E-06
42.39	2.24E-06	48.41	2.59E-06	58.32	2.98E-06	67.16	2.59E-06
42.80	2.49E-06	49.25	2.88E-06	59.19	3.23E-06	68.68	2.17E-06
43.31	2.54E-06	50.01	2.69E-06	60.41	3.09E-06	70.09	2.51E-06
43.84	2.30E-06	51.01	2.81E-06	61.51	3.19E-06	71.25	2.61E-06

Reproduced from best available copy.





APPENDIX II

HYDROGEN ADSORPTION AND DIFFUSION

The data on the time dependences of the concentrations of gaseous H_2 , D_2 , and HD molecules over various metal specimens investigated are given herein. The relative concentrations of the individual molecules at any given time are represented as molecular fractions, for example $\frac{[HD]}{[H_2] + [HD] + [D_2]}$ is the relative concentration of the HD molecules. The reduced concentrations are $\frac{[H_2] - [H_2]_\infty}{[H_2]_0 - [H_2]_\infty}$, $\frac{[HD] - [HD]_\infty}{[HD]_0 - [HD]_\infty}$, and $\frac{[D_2] - [D_2]_\infty}{[D_2]_0 - [D_2]_\infty}$, respectively. The derived quantity $K = \frac{[HD]^2}{[H_2][D_2]}$ is a measure of the mixing entropy in the gaseous phase, and is also plotted in some of the graphs. Its time dependence is a measure of the approach of the system metal-hydrogen to the equilibrium where K has a maximum value of 4. The data are presented in three separate sets, one for each material studied.

A. 18Ni(250) Maraging Steel

1. NAG-AB-NA (non-aged, argon bombarded, non-annealed) specimen.

The time dependences of the relative concentrations of H_2 , HD, and D_2 at pressures around 10^{-2} torr are given for the individual temperature runs in Figures 29-33. The variations in the pressure from one experiment to another were slight and did not significantly affect the measured rates. Also plotted in Figures 29-33 is the function $K = \frac{[HD]^2}{[H_2][D_2]}$. The rates of exchange are quantitatively evaluated by plotting the logarithms of the reduced concentrations of the D_2 and HD molecules against time. The slopes of the lines drawn through the experimental points in these coordinates give the rates of homomolecular exchange, $\frac{1}{a}(R + R' + R'')$, where $a = [H_2] + [HD] + [D_2]$.

An experimental check for the validity of this treatment is that the slopes for the reduced concentrations of H_2 , HD, and D_2 coincide. Figures 34-38 show the replotted data of Figures 29-33 for the reduced concentrations of the D_2 and HD molecules. The concentrations of D_2 and HD follow roughly the same lines, demonstrating that the true rates ($R + R' + R''$) are measured. The temperature dependence of the rates ($R + R' + R''$) is shown in Figure 39. The maximum exhibited on this temperature dependence was not found with other preparations of the 18Ni(250) maraging steel and is not understood at the present moment.

2. AG-AB-NA (aged, argon bombarded, non-annealed) specimen.

The rates of the H_2/D_2 exchange are represented as the time variations of the logarithms of the reduced concentrations of HD and D_2 in Figures 40-44. The temperatures and pressures at which these experiments were carried out are given in the figure captions.

The temperature dependence of the rates is presented in Figure 45, together with the temperature dependence on the AG-AB-A 18Ni(250) maraging steel.

3. AG-AB-A (aged, argon bombarded, -annealed) specimen.

The rates of the H_2/D_2 exchange are represented as the variations of the logarithms of the reduced concentrations of HD and D_2 in Figures 46-49. The temperatures and pressures at which these experiments were carried out are again given in the figure captions.

The temperature dependence of the rates is presented in Figure 45, together with the temperature dependence on the AG-AB-NA 18Ni(250) maraging steel.

B. 18Ni(200) Maraging Steel

1. AG-AB-NA (aged, argon bombarded, non-annealed) specimen.

The rates of the H_2/D_2 exchange are again represented as the time dependences of the logarithm of the reduced concentrations of HD and D_2 in Figures 50-55, with temperatures and pressures given in the figure captions.

The temperature dependence of the rates is represented in Figure 56, together with the temperature dependence of the exchange rates on the AG-AB-A 18Ni(200) maraging steel.

2. AG-AB-A (aged, argon bombarded, -annealed) specimen.

The rates of the H_2/D_2 exchange are again represented as the time dependences of the logarithms of the reduced concentrations of HD and D_2 in Figures 57-61, with temperatures and pressures given in the figure captions.

The temperature dependence of the rates is represented in Figure 56, along with the temperature dependence of the rates on the AG-AB-NA 18Ni(200) maraging steel.

C. Fe (111) Single Crystal

The iron single crystal was cut along the (111) plane, mechanically and chemically polished, and cleaned in the ultrahigh vacuum system by repeated argon ion and electron bombardments. The final treatment was electron bombardment annealing at 750-800°C. By this procedure, the (111) crystallographic orientation of iron crystal is restored. The data on iron crystal serve as a reference for comparison of the various ferrous alloys. The rates of the H_2/D_2 exchange on Fe (111) were the highest observed, and are presented in Table 6 and in Figure 28. The data on activation energies are not available since time limits permitted the experiments to be done only at room temperature.

The Time Dependence of the Rates on Iron and Maraging Steels

All rates measured in this work decayed with time by varying factors of 2-5 in 10 minutes (Table 6). The time dependence will certainly affect the slopes of the logarithms of the reduced concentrations vs. time, and therefore the calculated rates ($R + R' + R''$) are time averages over the duration of the experiment. It is unlikely that the time dependence is caused by poisoning of the surface by residual gases other than hydrogen since the clean surfaces retain their activity when kept in vacuum without the presence of hydrogen. The poisoning of the surface by the diffusion of impurities from the bulk is also unlikely since the time effects are little temperature dependent and since no time changes in surface chemical composition were observed by Auger spectroscopy at the temperatures of these experiments. A physical relaxation of the surface is ruled out on the annealed specimens which still show a similar time dependence as the non-annealed specimens. The remaining possibility is self-poisoning of the surface by hydrogen. At the present time this seems to be the best explanation of the time decay of the activity. Hydrogen may exist in the surface in various forms, one or more of which may be formed by a slow reaction. The question of time dependence of the reaction rates will require further attention.

D. Inconel 718

The Inconel 718 specimen was a 0.5 mm thick slab of total surface area 4.17 cm². After grinding and mechanical polishing with 1 μ m diamond paste, the specimen was chemically polished in 95% H₂O₂ (30 volume percent) and 5% HF solution for 1 min at 60°C, washed in distilled water and sealed into the vacuum apparatus. The background pressure after bakeout did not exceed 5×10^{-10} torr with all filaments hot. Argon

bombardment was generally at 50-100 μ A/cm² and was either done in five minute periods several times without intervening annealing (NA samples) or alternated with five minute annealing periods (A samples). In both cases, the sample was turned between successive bombardments so that both faces were equally bombarded, and for both procedures checks were made to ensure complete cleaning by continuing bombardment until there was no further increase in activity. Annealing temperatures were not allowed to rise above 600°C.

The rate of H₂/D₂ exchange was measured at room temperature only. The results are summarized in Table 6 and Figure 28.

E. 316 Stainless Steel

The specimen size and preparation was identical to that of Inconel 718. In the final stage of preparation, surface annealing temperature was about 650°C.

The rates of H₂/D₂ exchange were measured at room temperature, at 200°C, and at 300°C. The results are summarized in Table 6 and Figure 28. The temperature dependence of the rates normalized to unit area is shown in Figure 62 in the form of Arrhenius plot.

Figure 29: The time course of the concentrations of the H₂ (○), HD (●), and D₂ (◐) molecules over the ion-bombarded 18Ni(250) maraging steel at 1.4 x 10⁻² torr and 0°C. The time dependence of the function K is given as a dashed line.

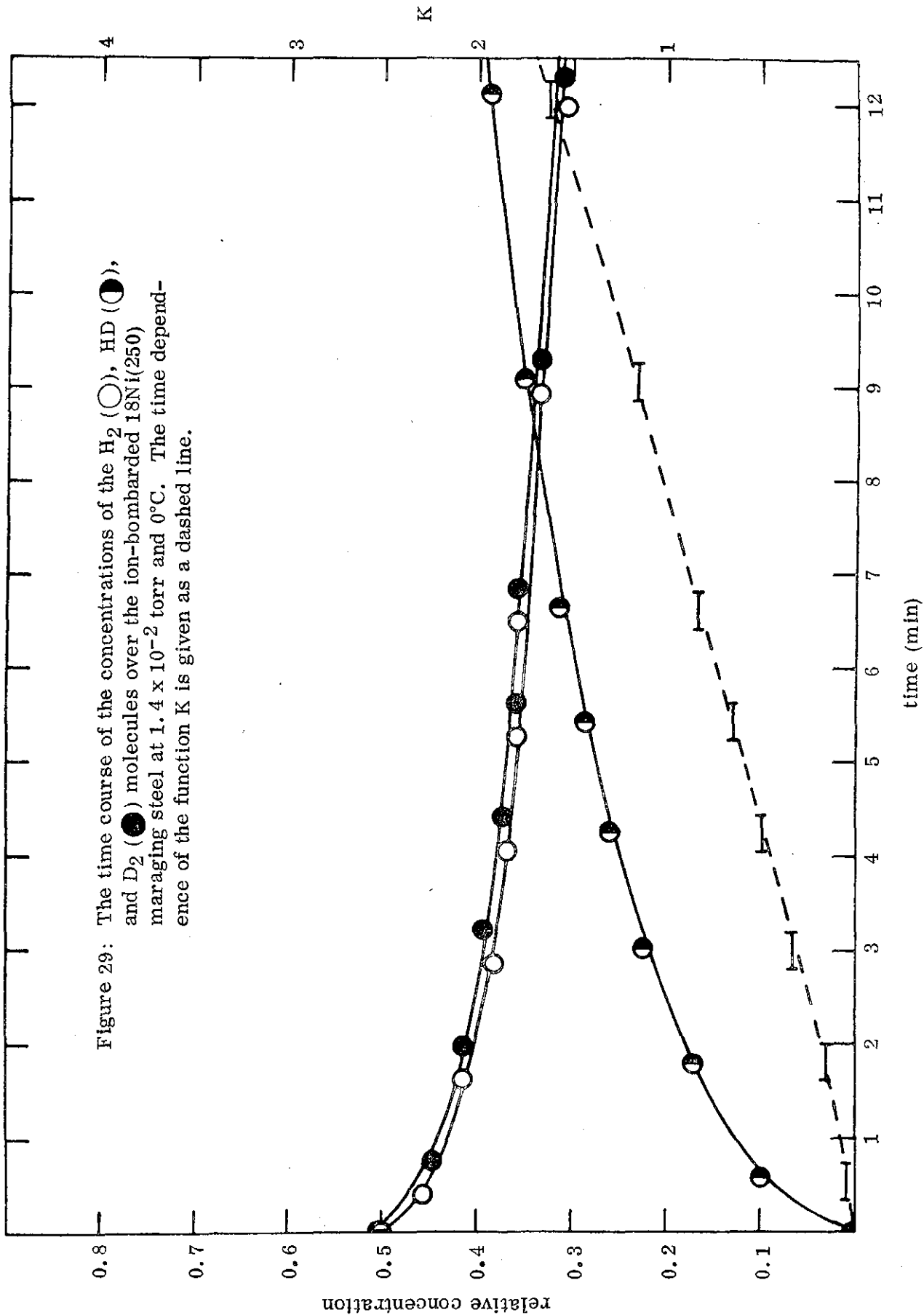
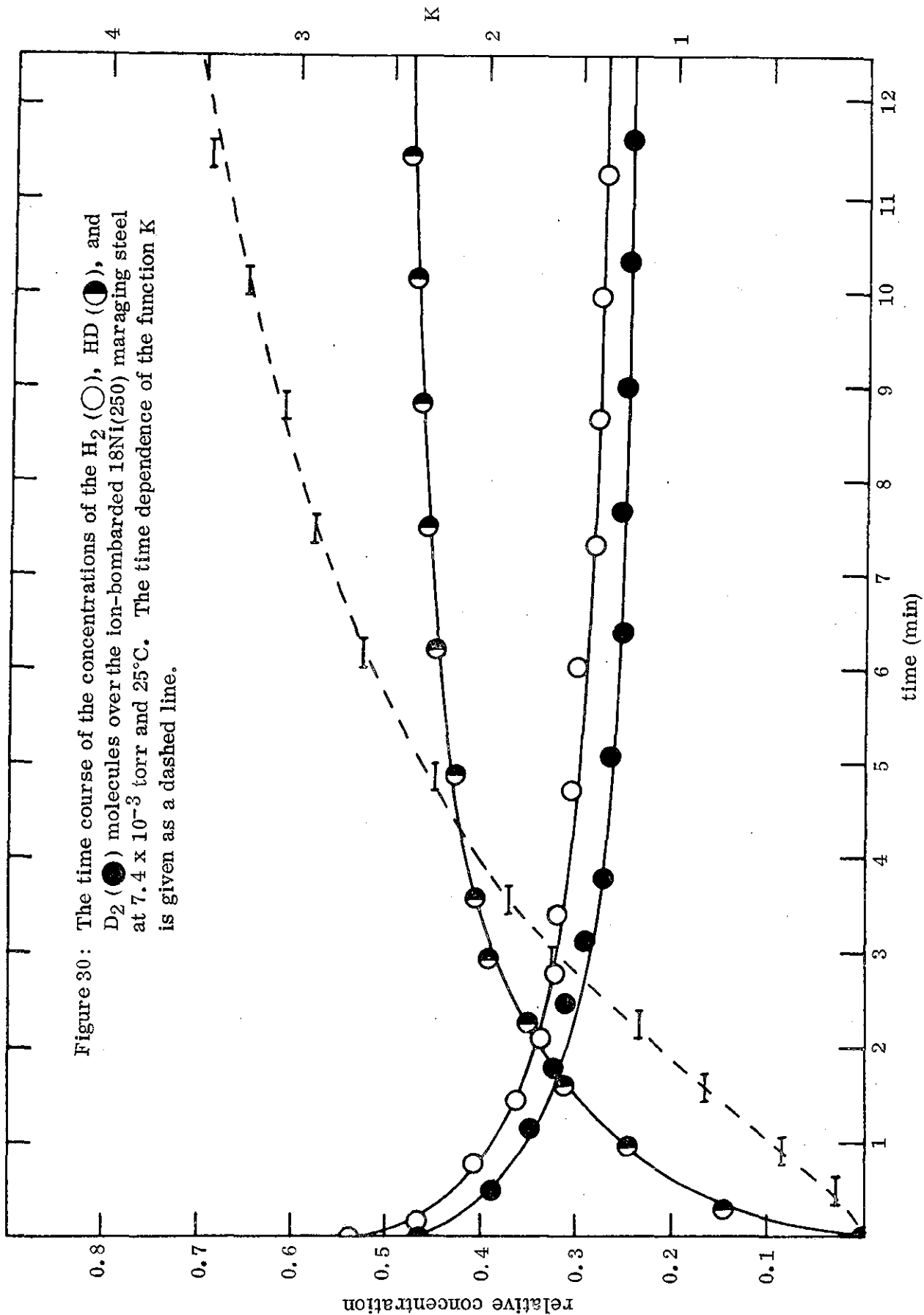


Figure 30: The time course of the concentrations of the H_2 (\circ), HD (\bullet), and D_2 (\bullet) molecules over the ion-bombarded $^{18}Ni(250)$ maraging steel at 7.4×10^{-3} torr and $25^\circ C$. The time dependence of the function K is given as a dashed line.



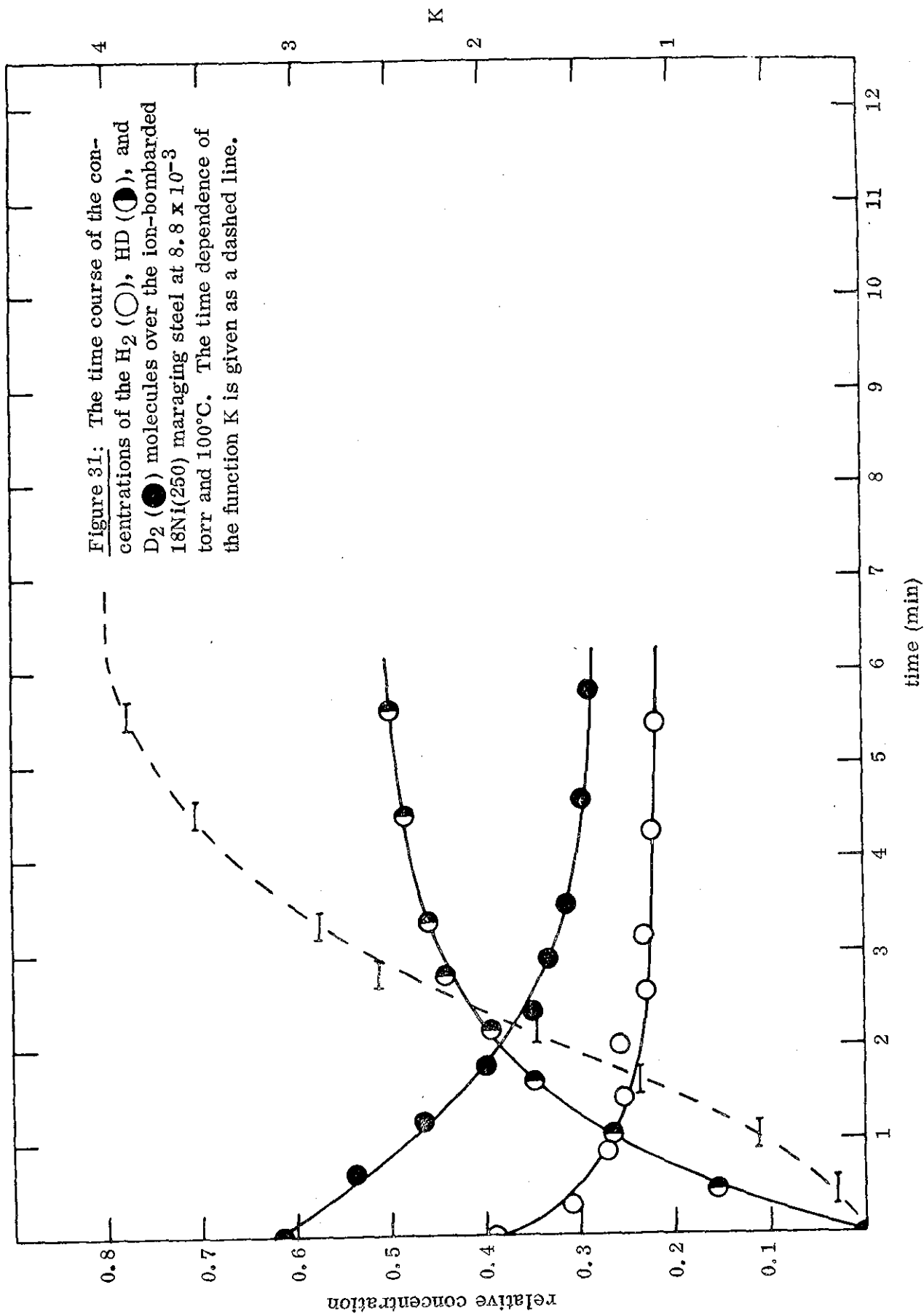


Figure 31: The time course of the concentrations of the H₂ (○), HD (◐), and D₂ (●) molecules over the ion-bombarded 18Ni(250) maraging steel at 8.8×10^{-3} torr and 100°C. The time dependence of the function K is given as a dashed line.

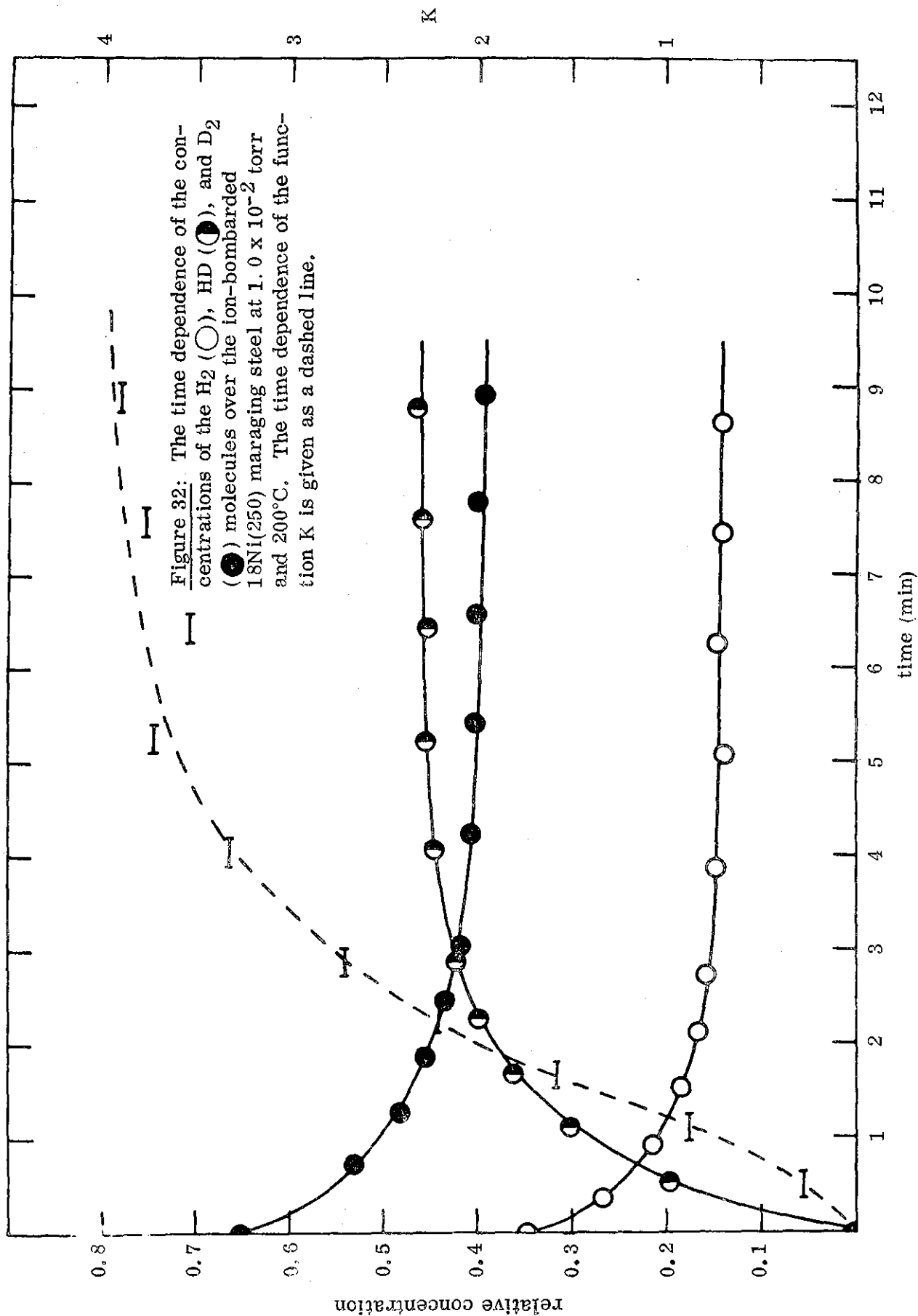


Figure 32: The time dependence of the concentrations of the H₂ (○), HD (●), and D₂ (●) molecules over the ion-bombarded ¹⁸Ni(250) maraging steel at 1.0 x 10⁻² torr and 200°C. The time dependence of the function K is given as a dashed line.

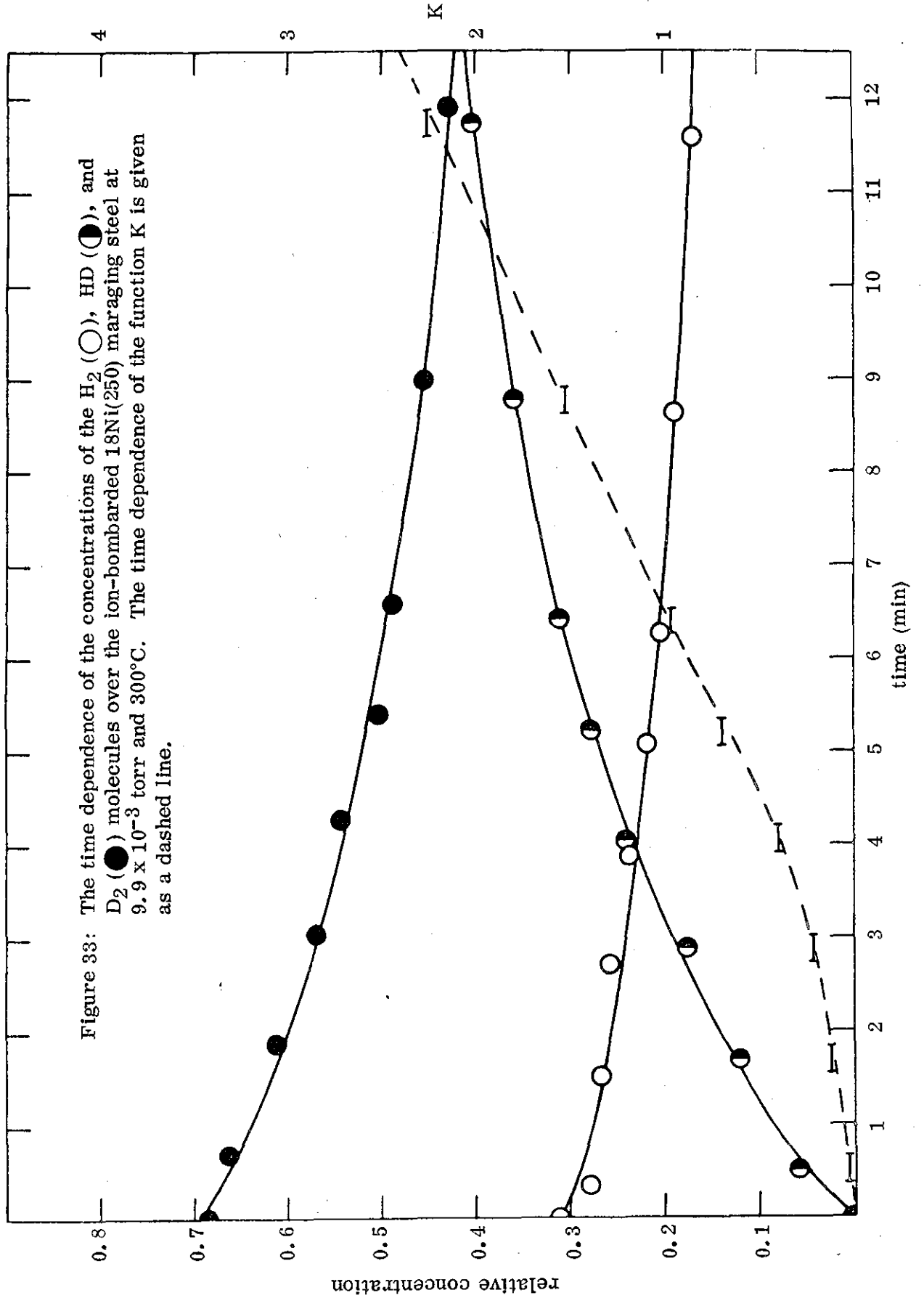
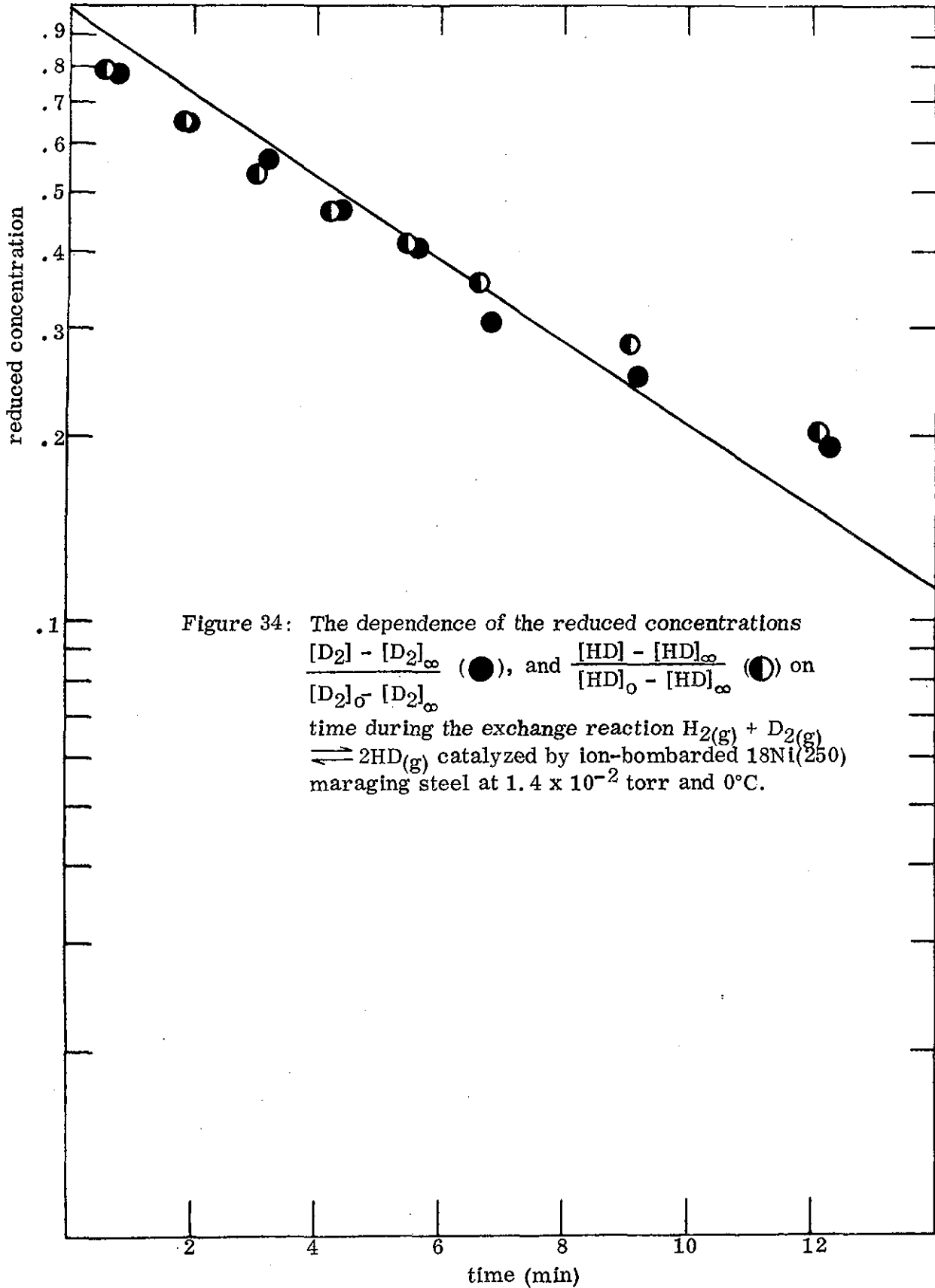
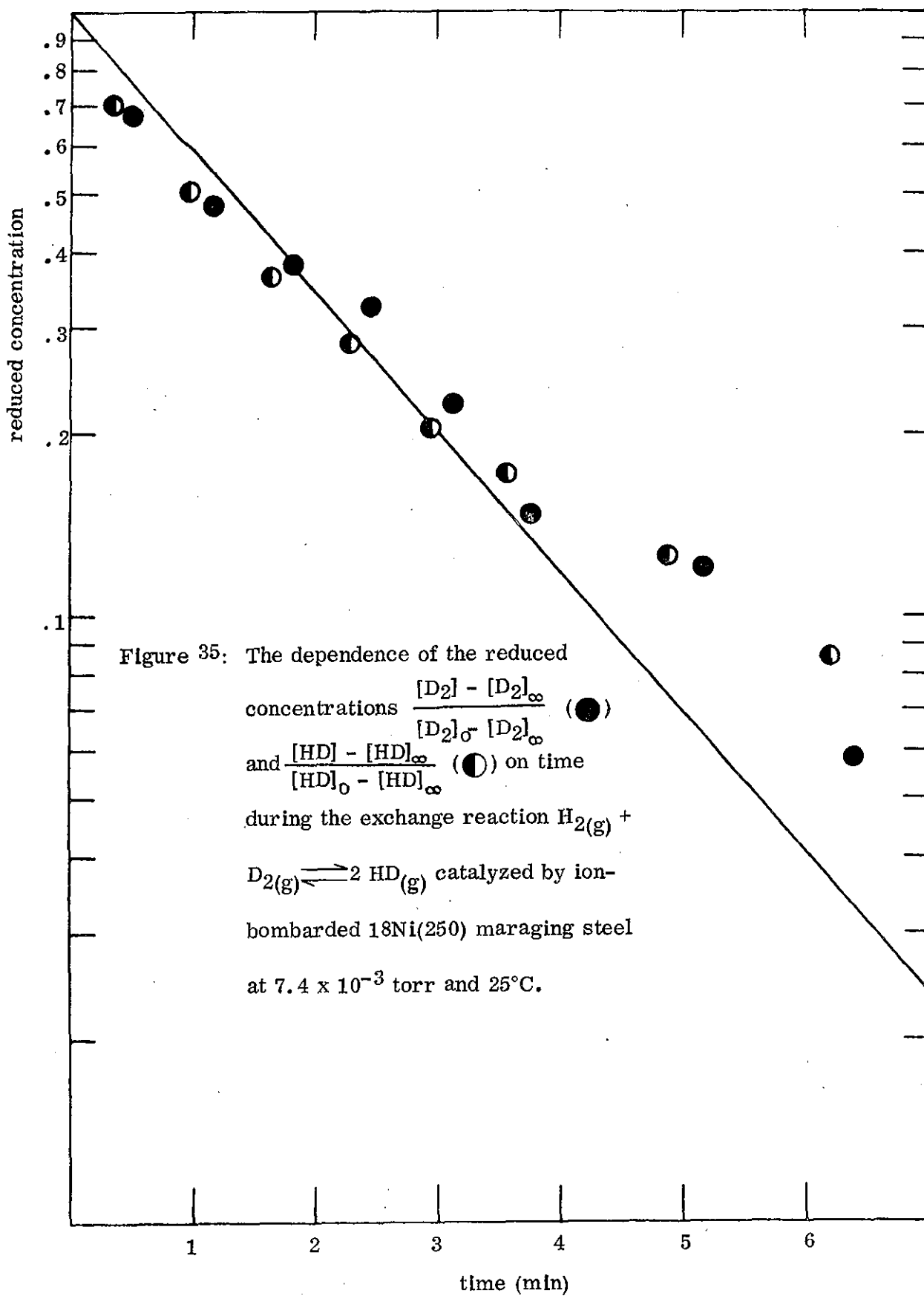
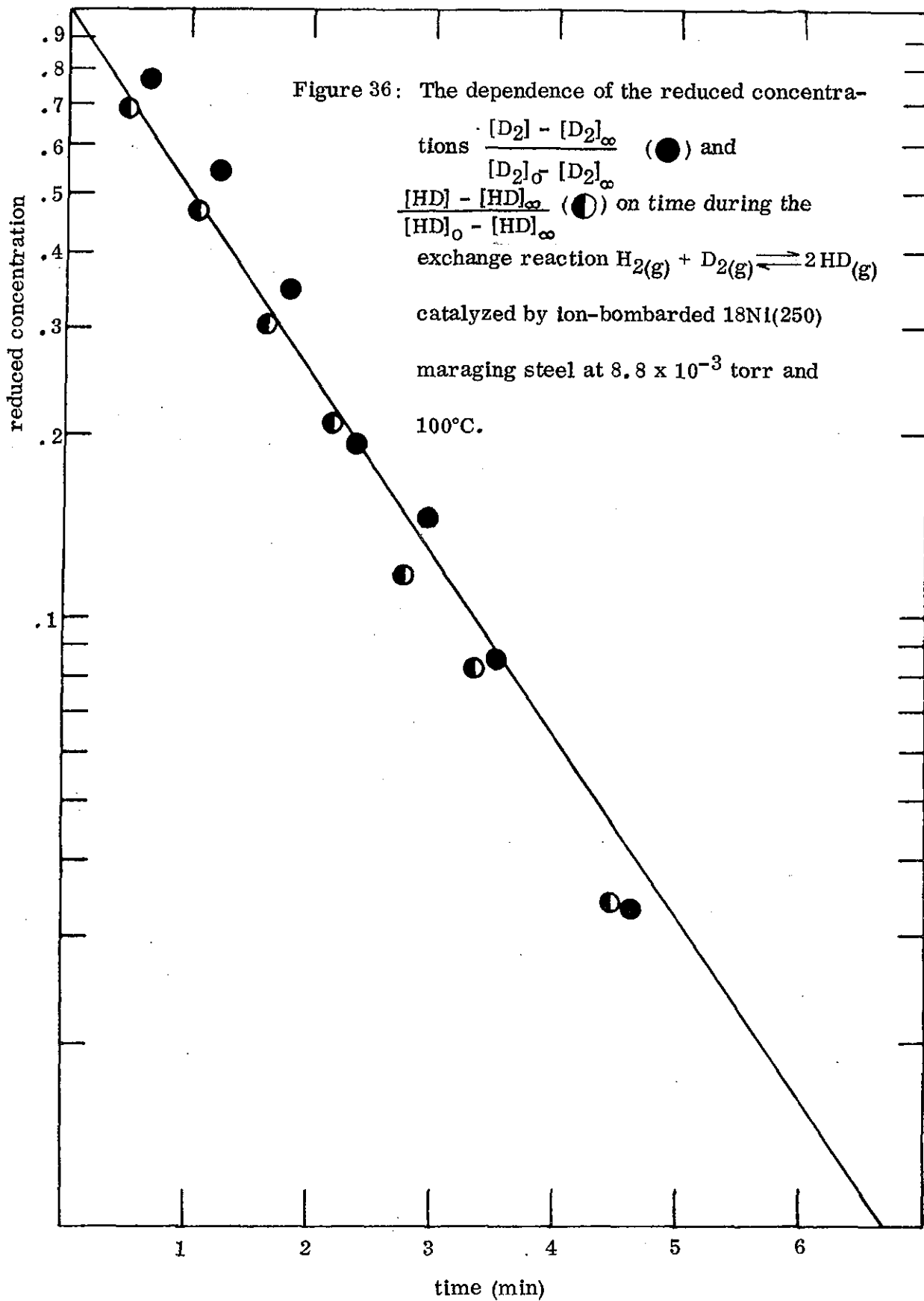
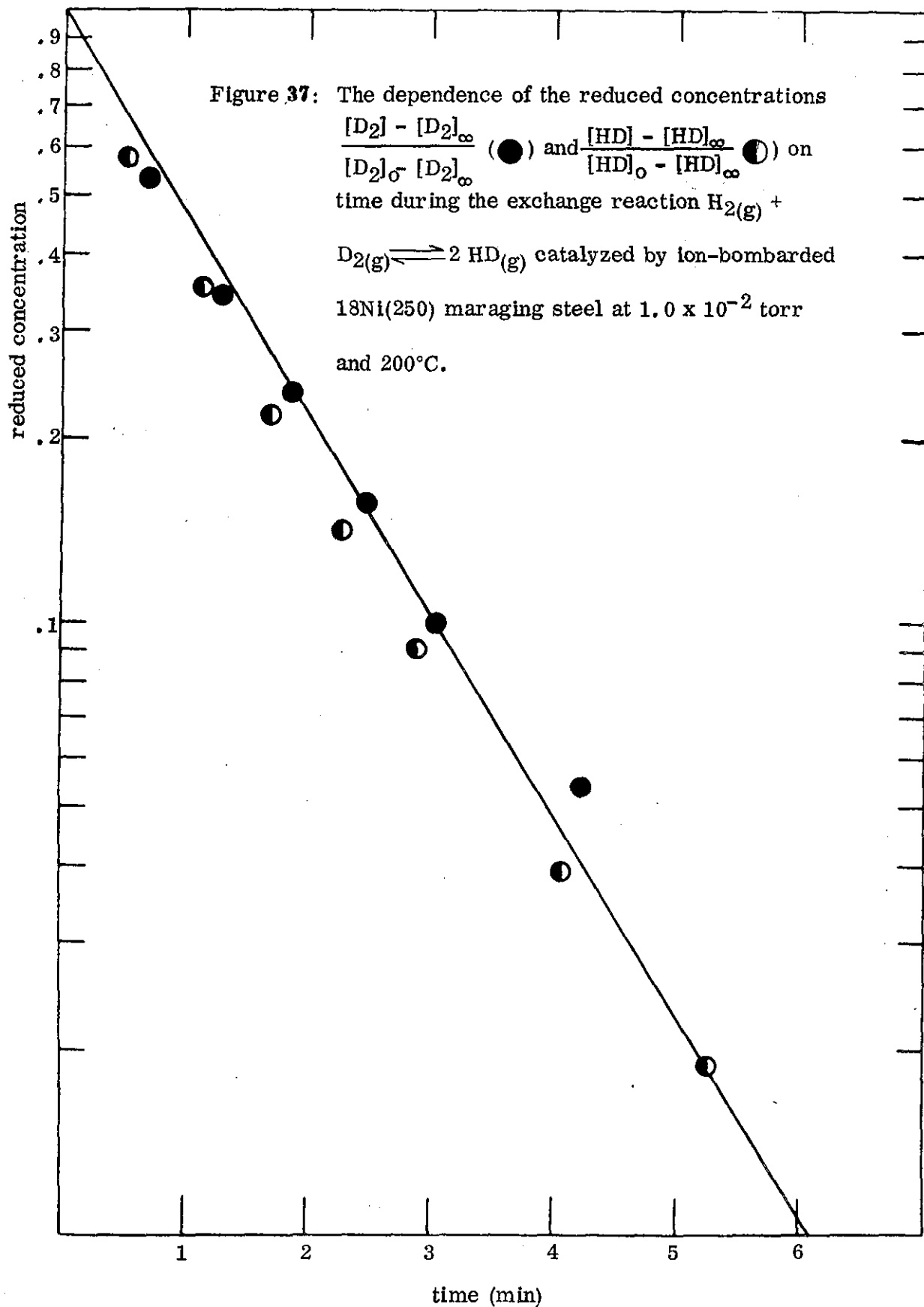


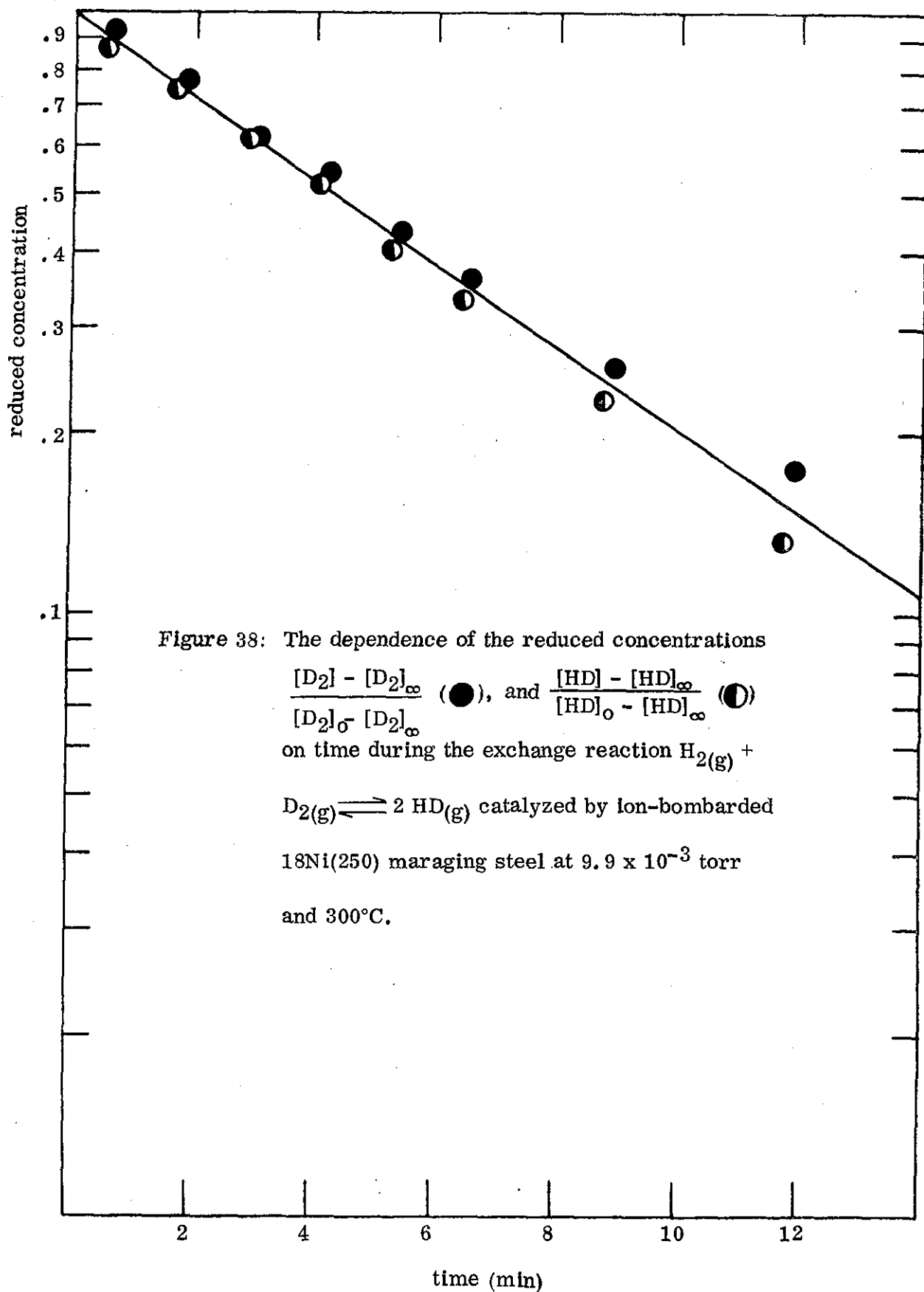
Figure 33: The time dependence of the concentrations of the H₂ (○), HD (●), and D₂ (●) molecules over the ion-bombarded 18Ni(250) maraging steel at 9.9 x 10⁻³ torr and 300°C. The time dependence of the function K is given as a dashed line.











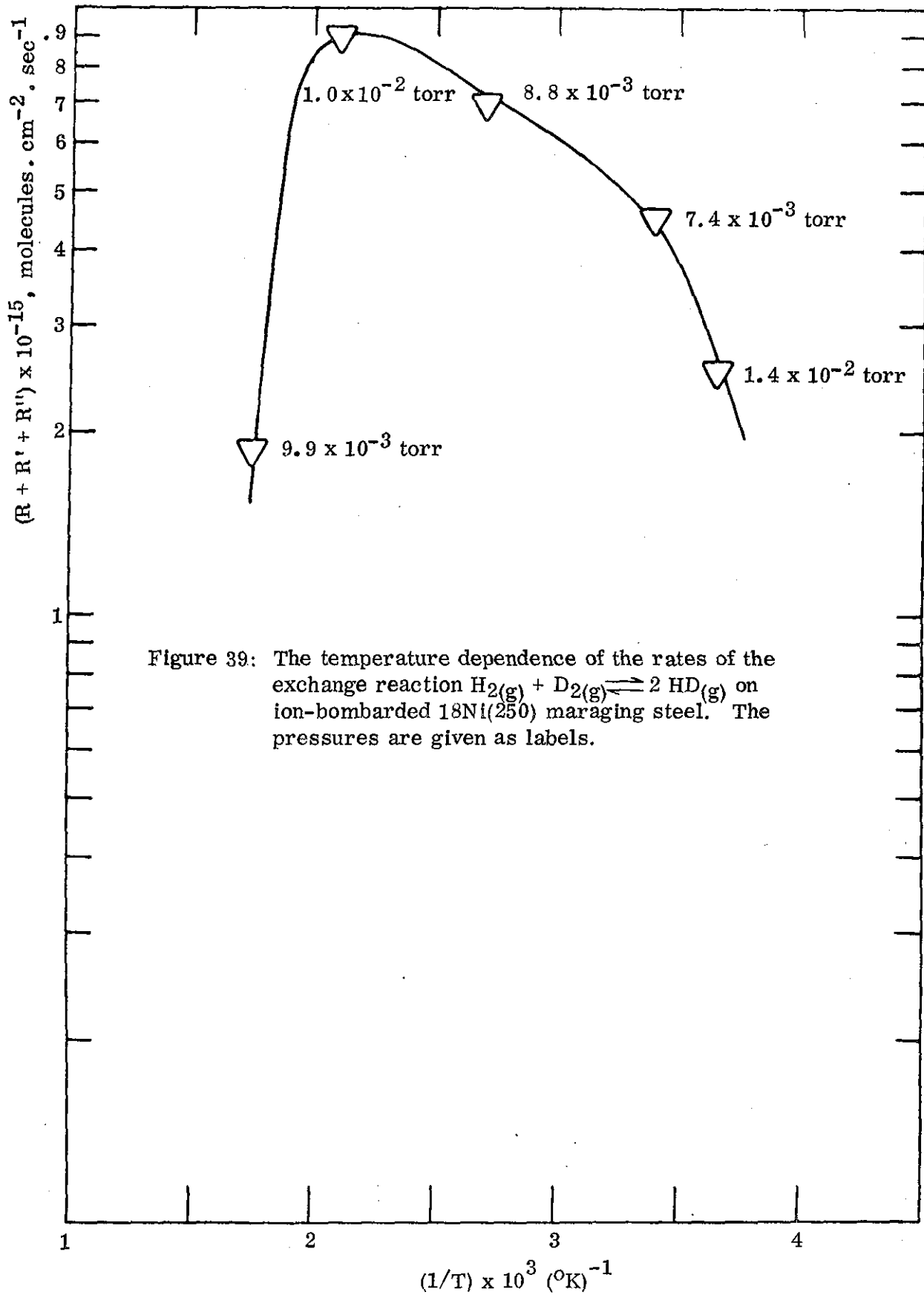
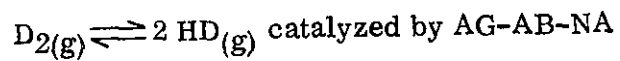


Figure 39: The temperature dependence of the rates of the exchange reaction $\text{H}_2(\text{g}) + \text{D}_2(\text{g}) \rightleftharpoons 2 \text{HD}(\text{g})$ on ion-bombarded $^{18}\text{Ni}(250)$ maraging steel. The pressures are given as labels.

Figure 40: The dependence of the reduced concentrations

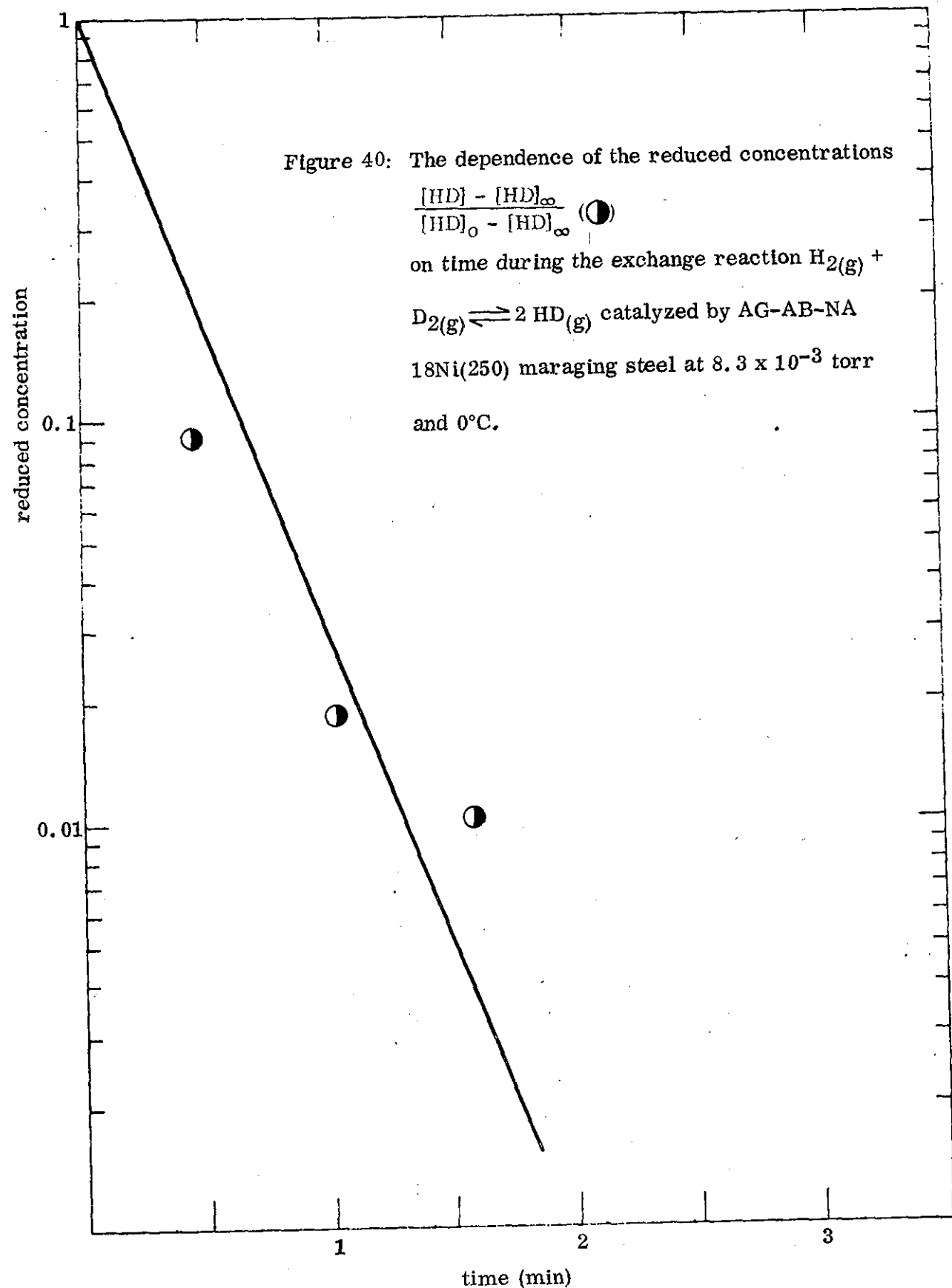
$$\frac{[HD] - [HD]_{\infty}}{[HD]_0 - [HD]_{\infty}} \quad (\bullet)$$

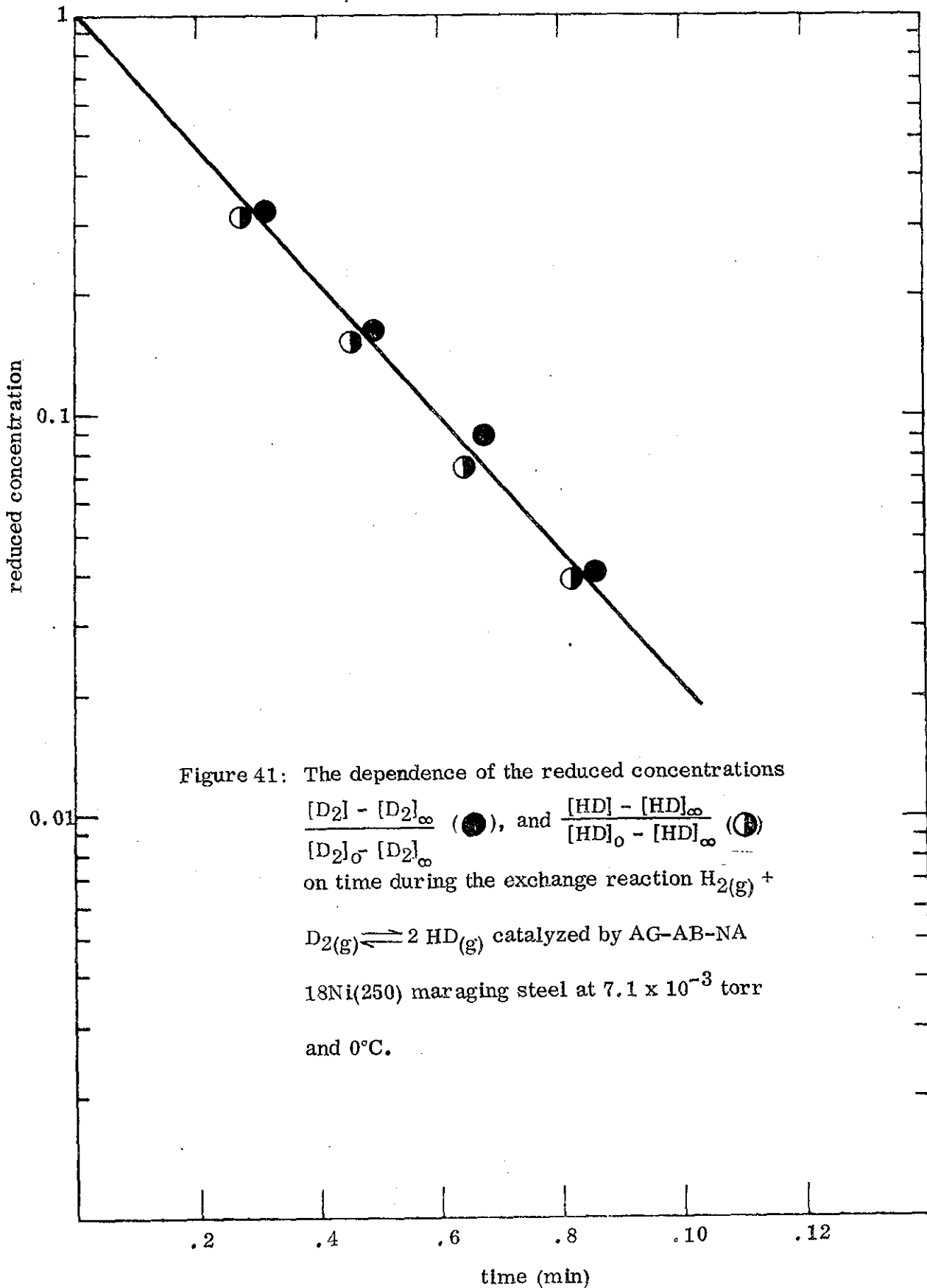
on time during the exchange reaction $H_2(g) +$

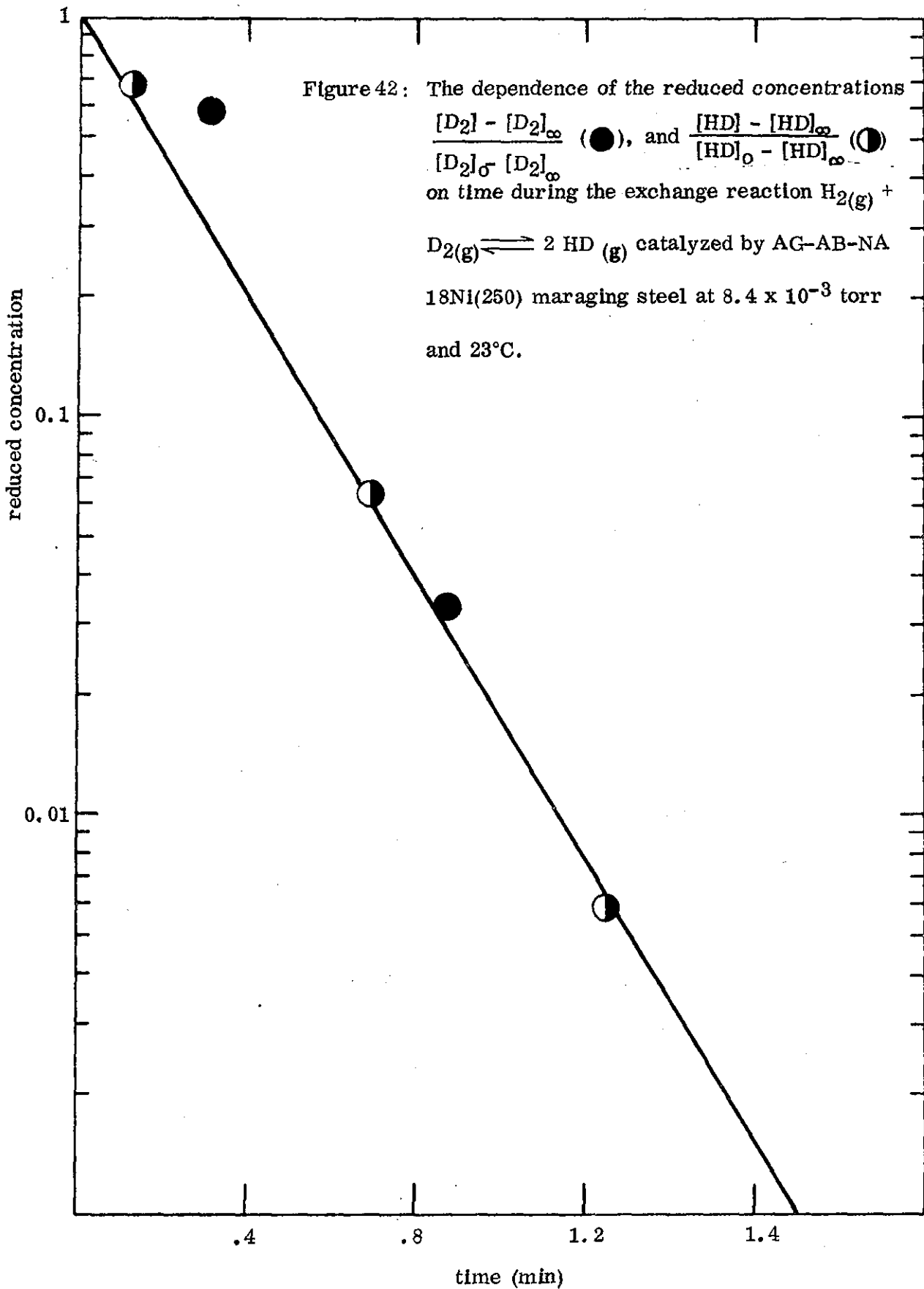


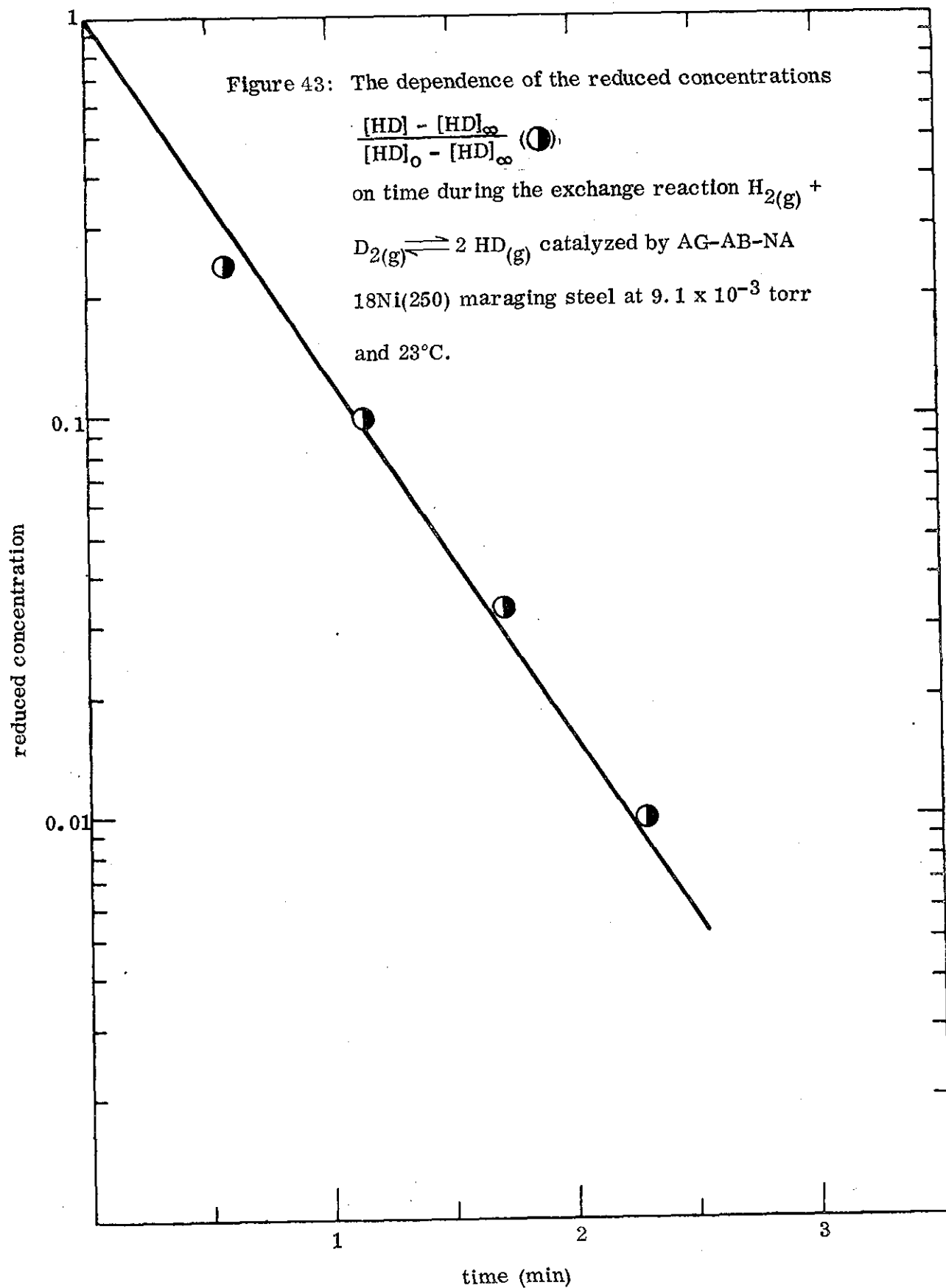
18Ni(250) maraging steel at 8.3×10^{-3} torr

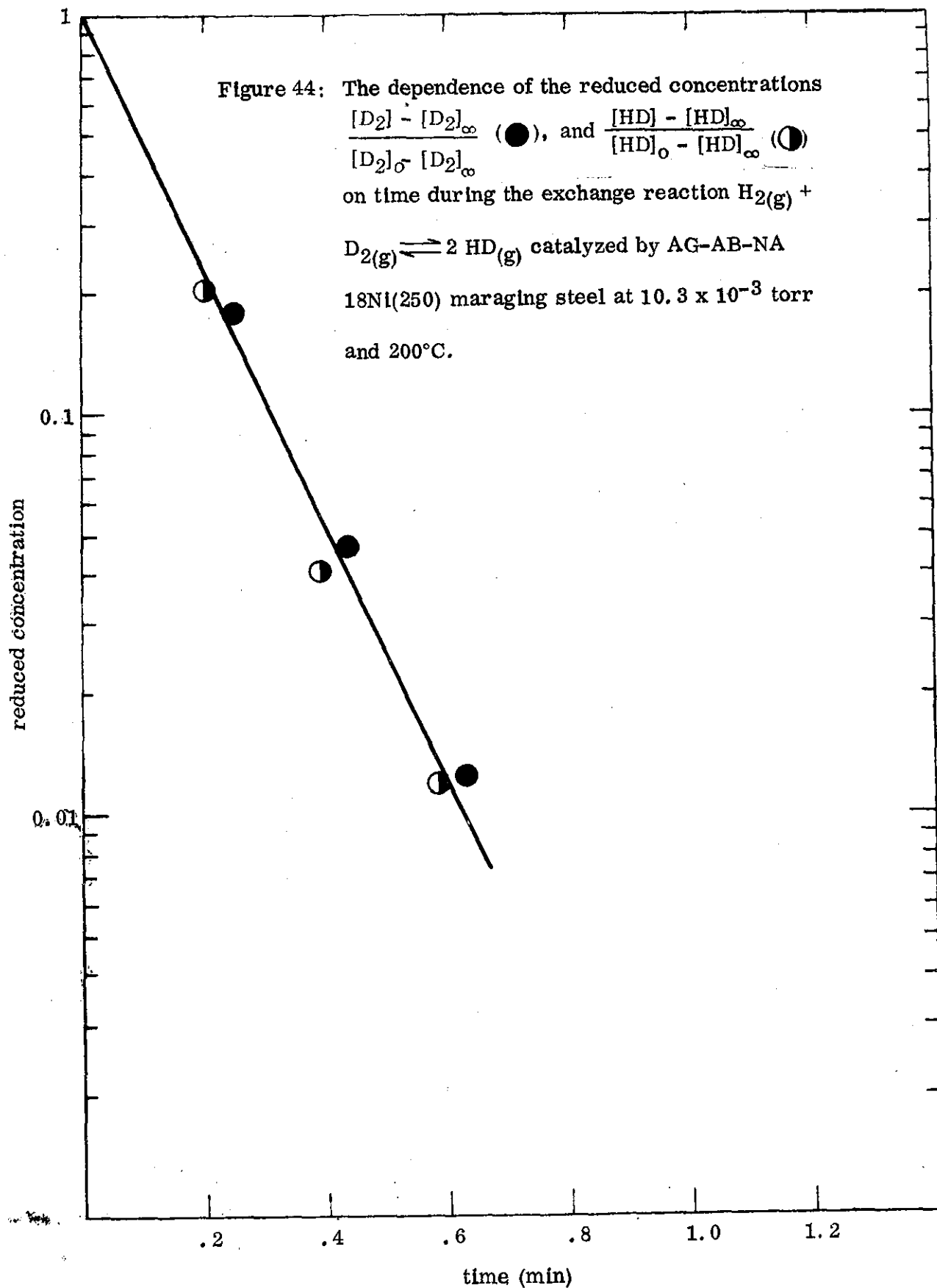
and $0^{\circ}C$.

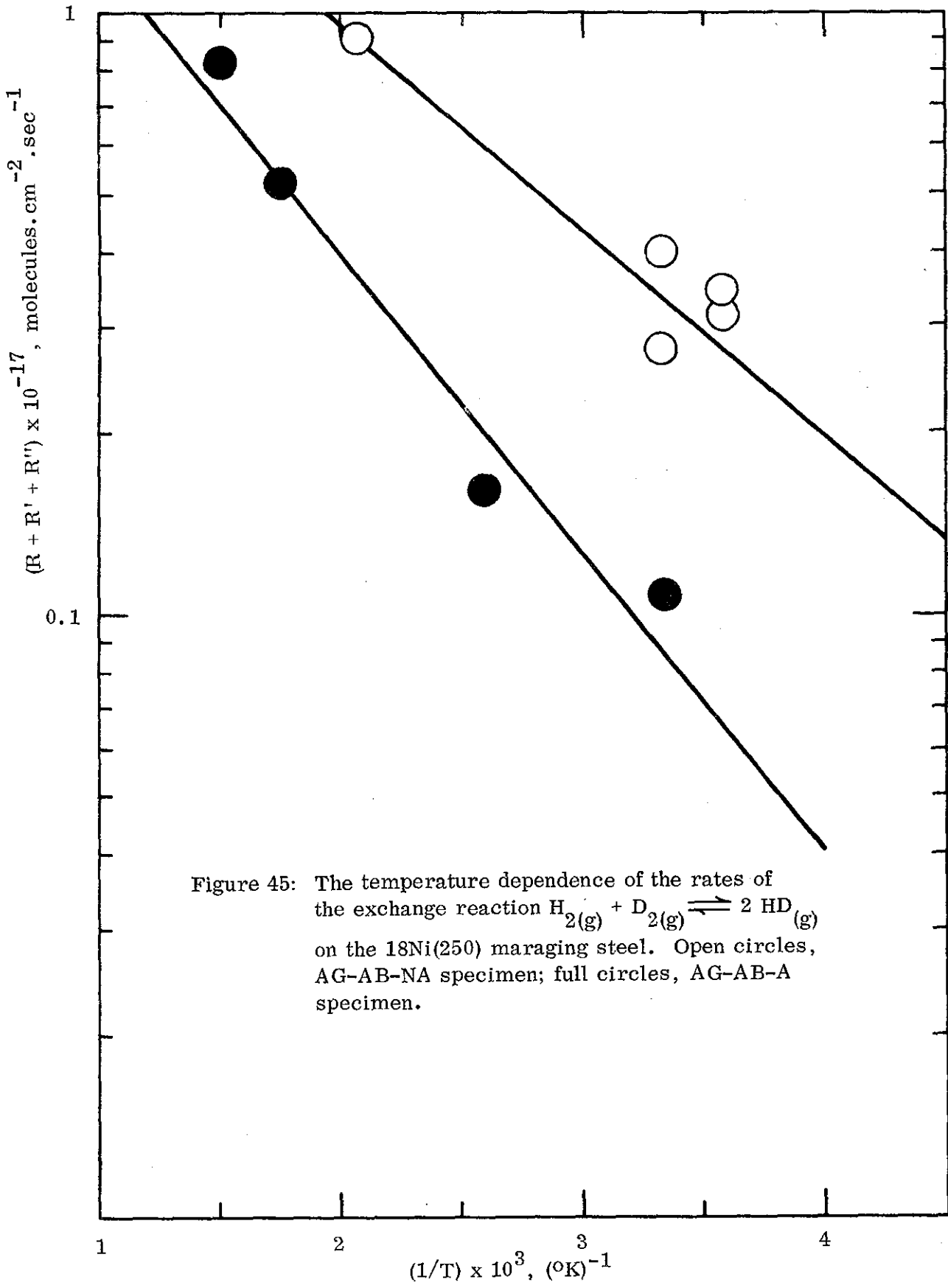


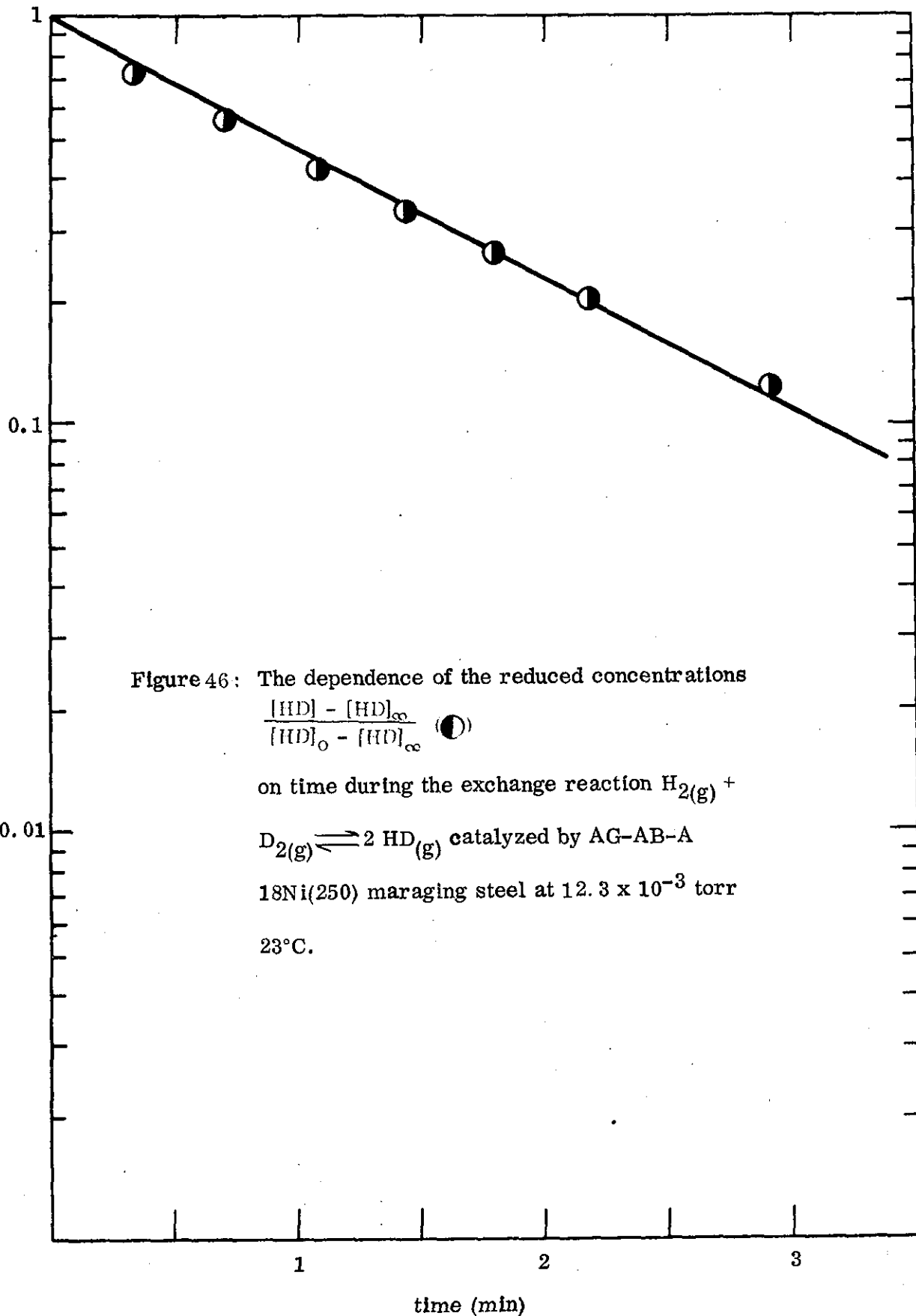


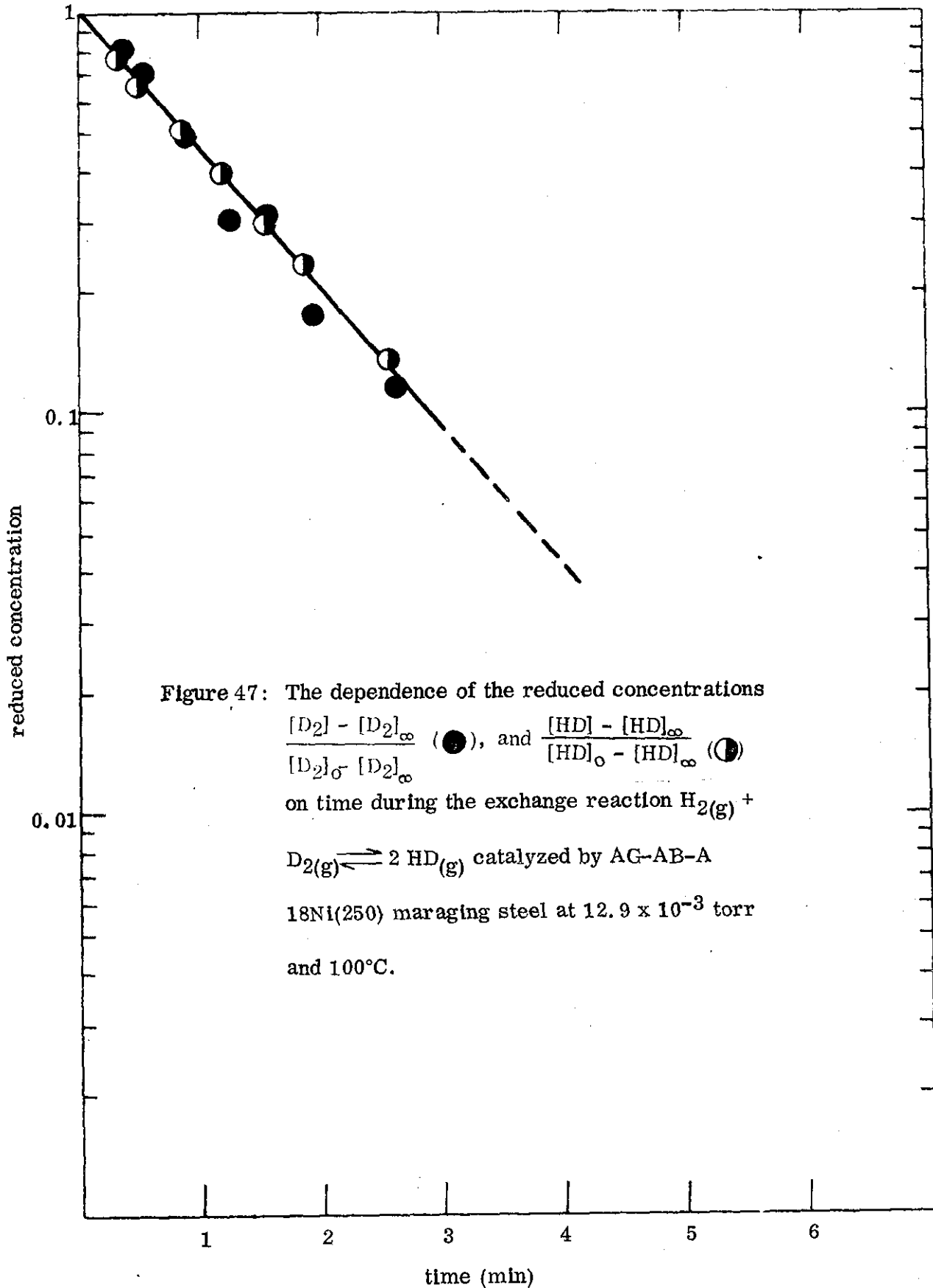


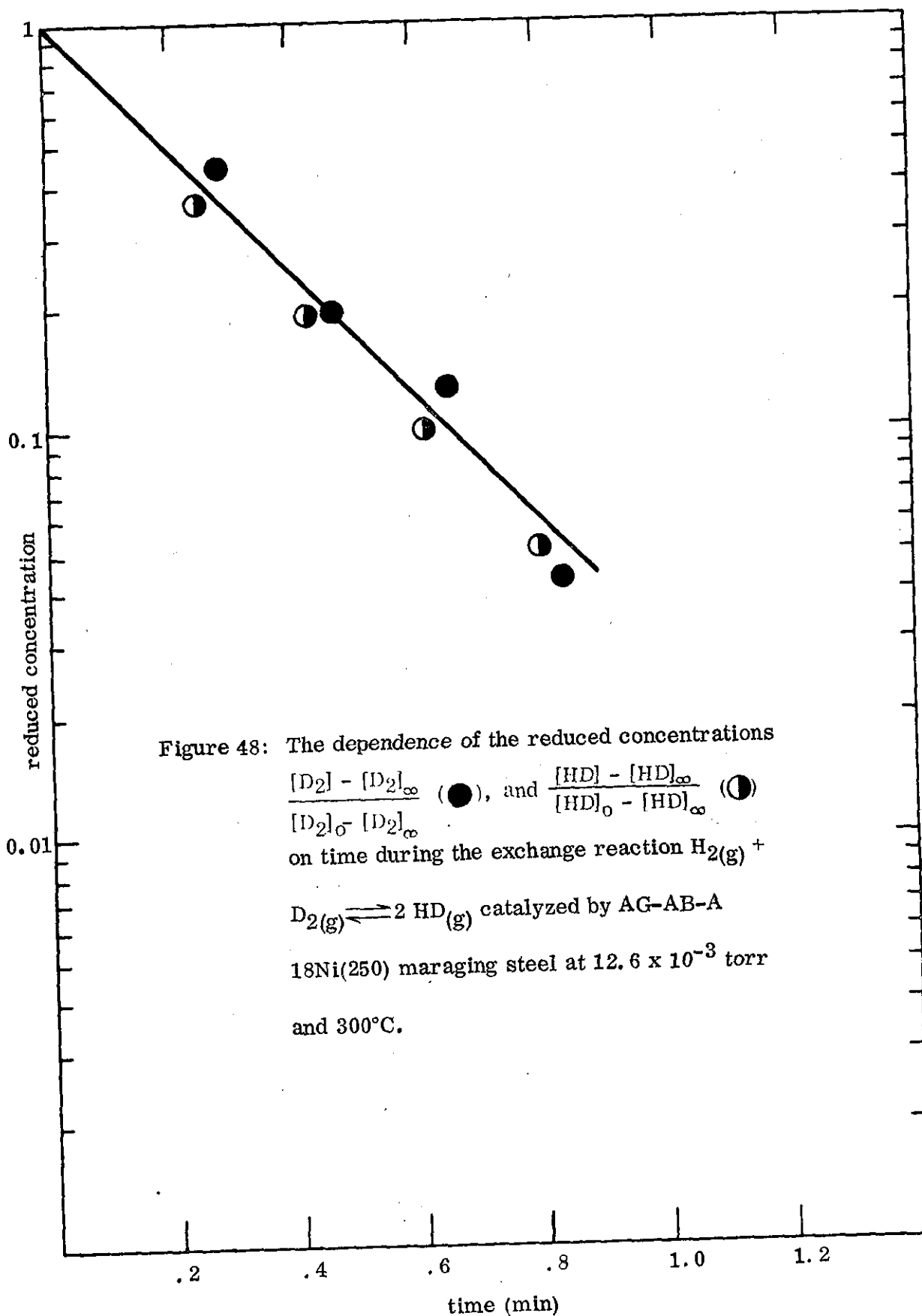


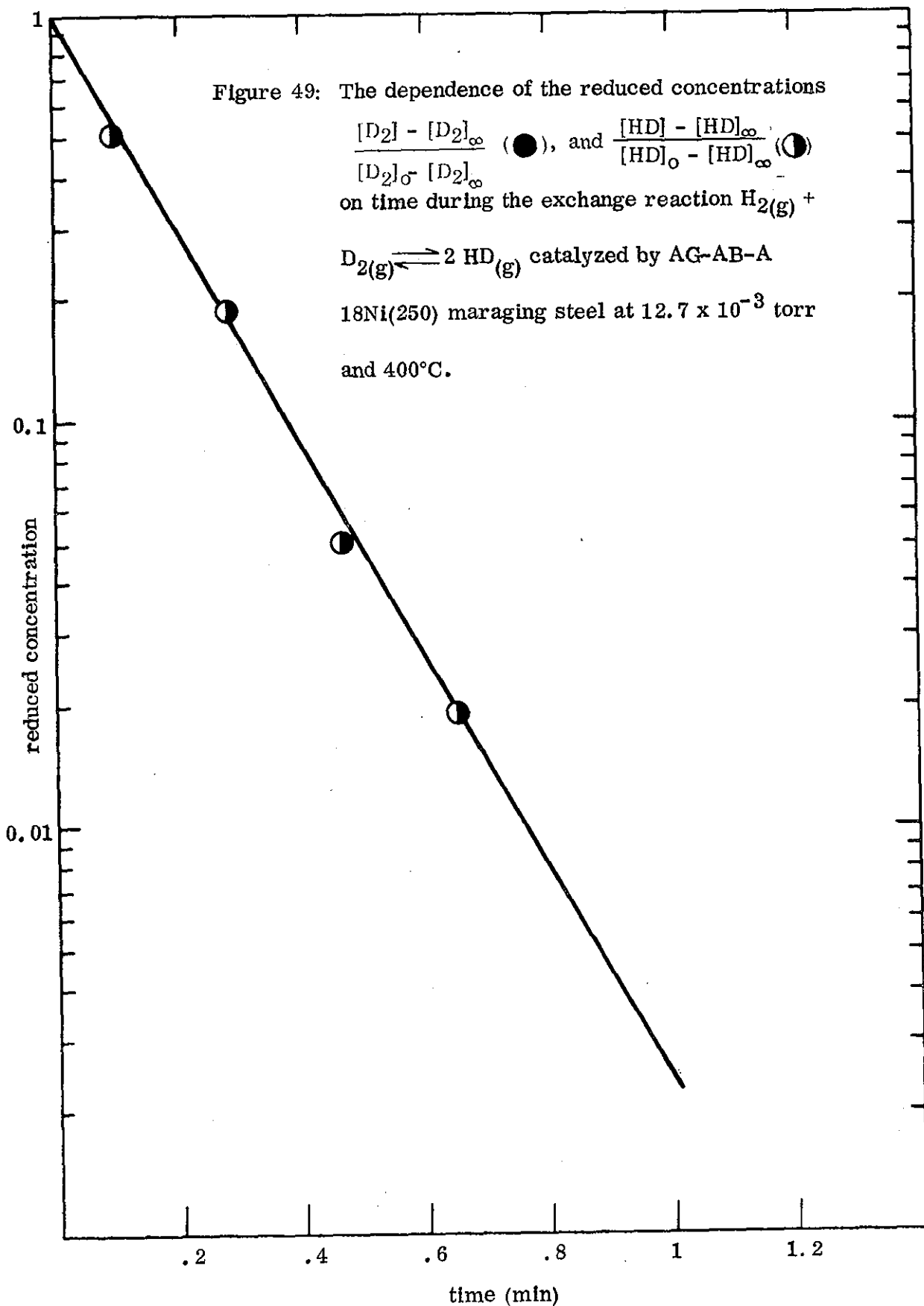


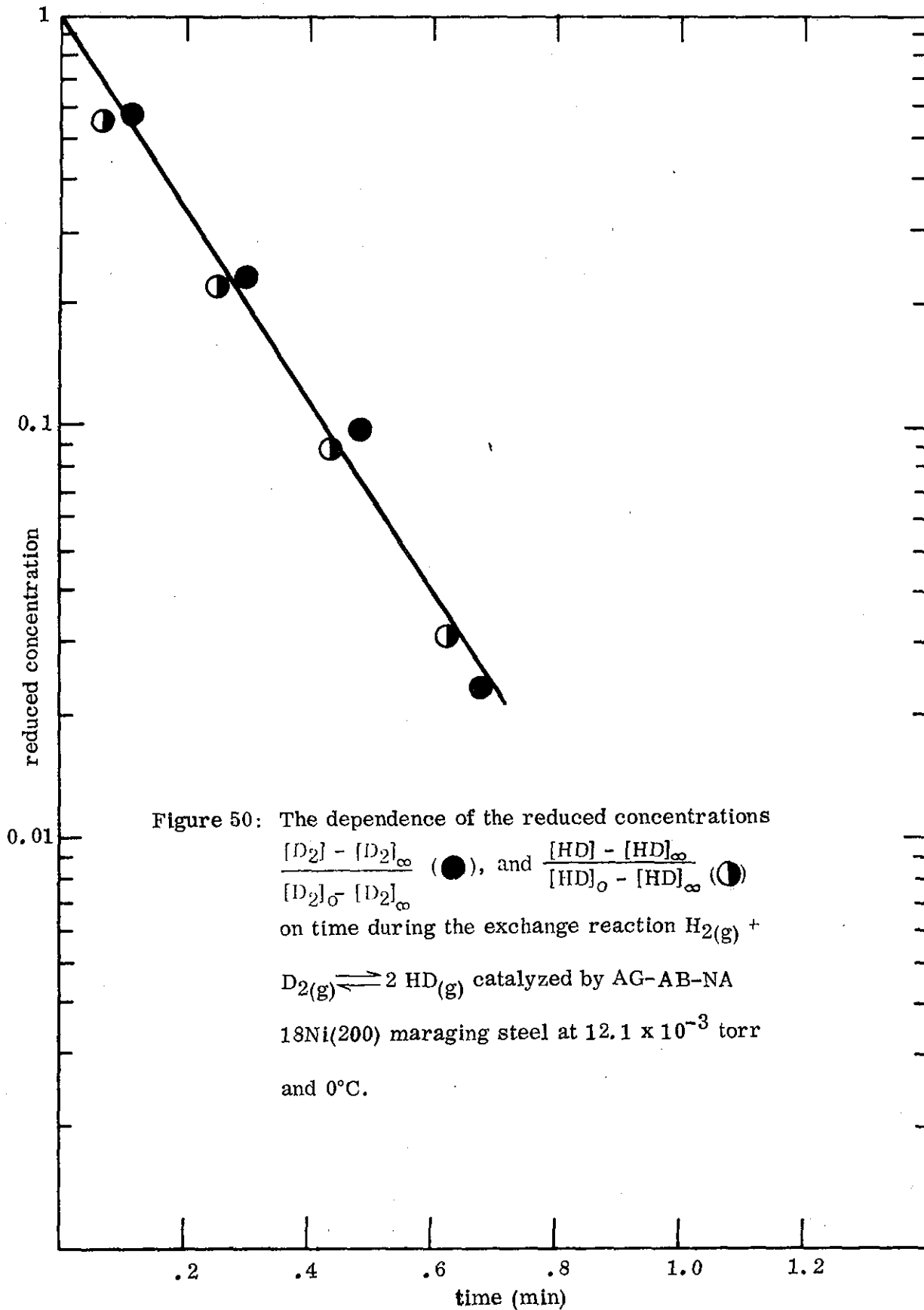


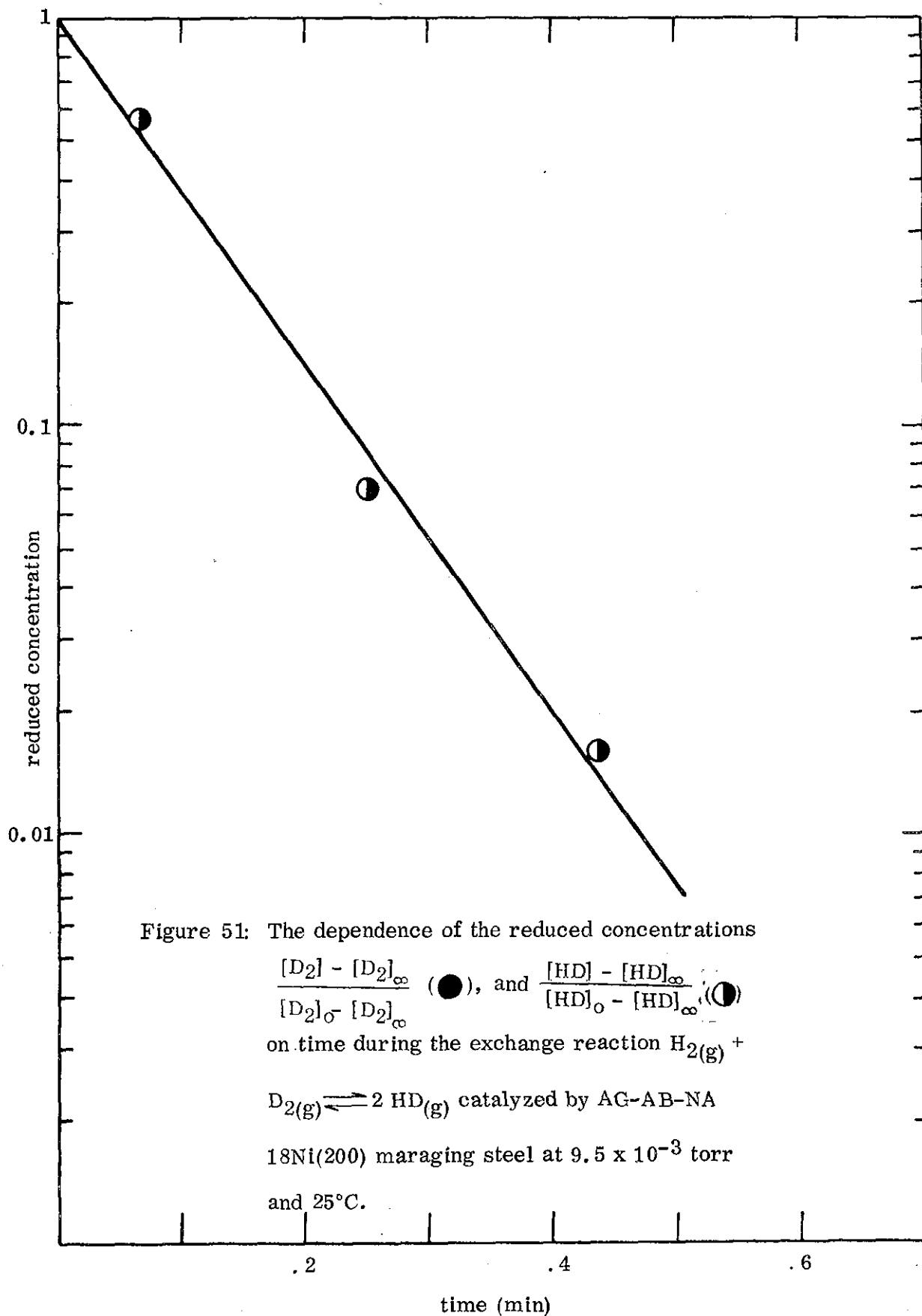


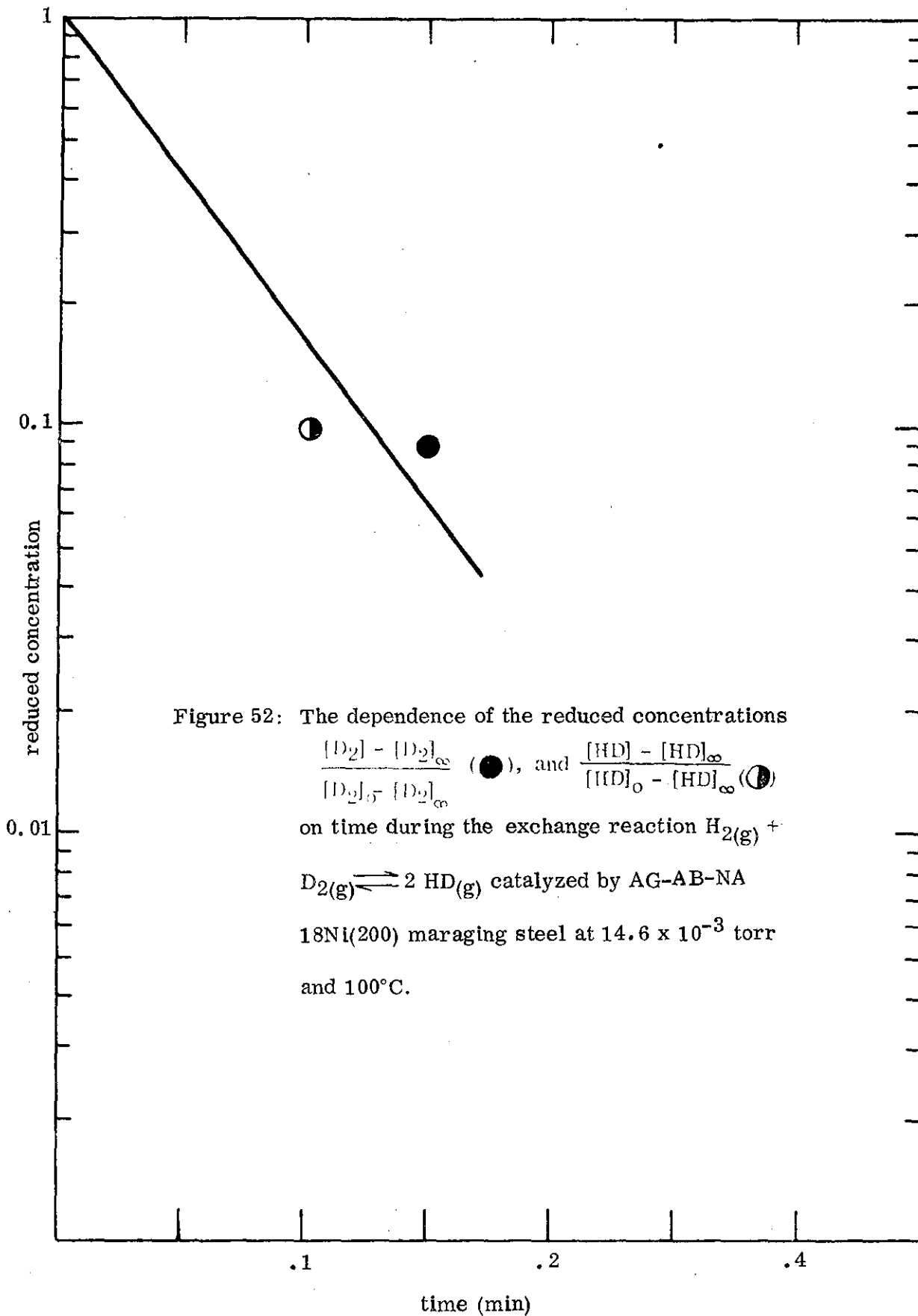


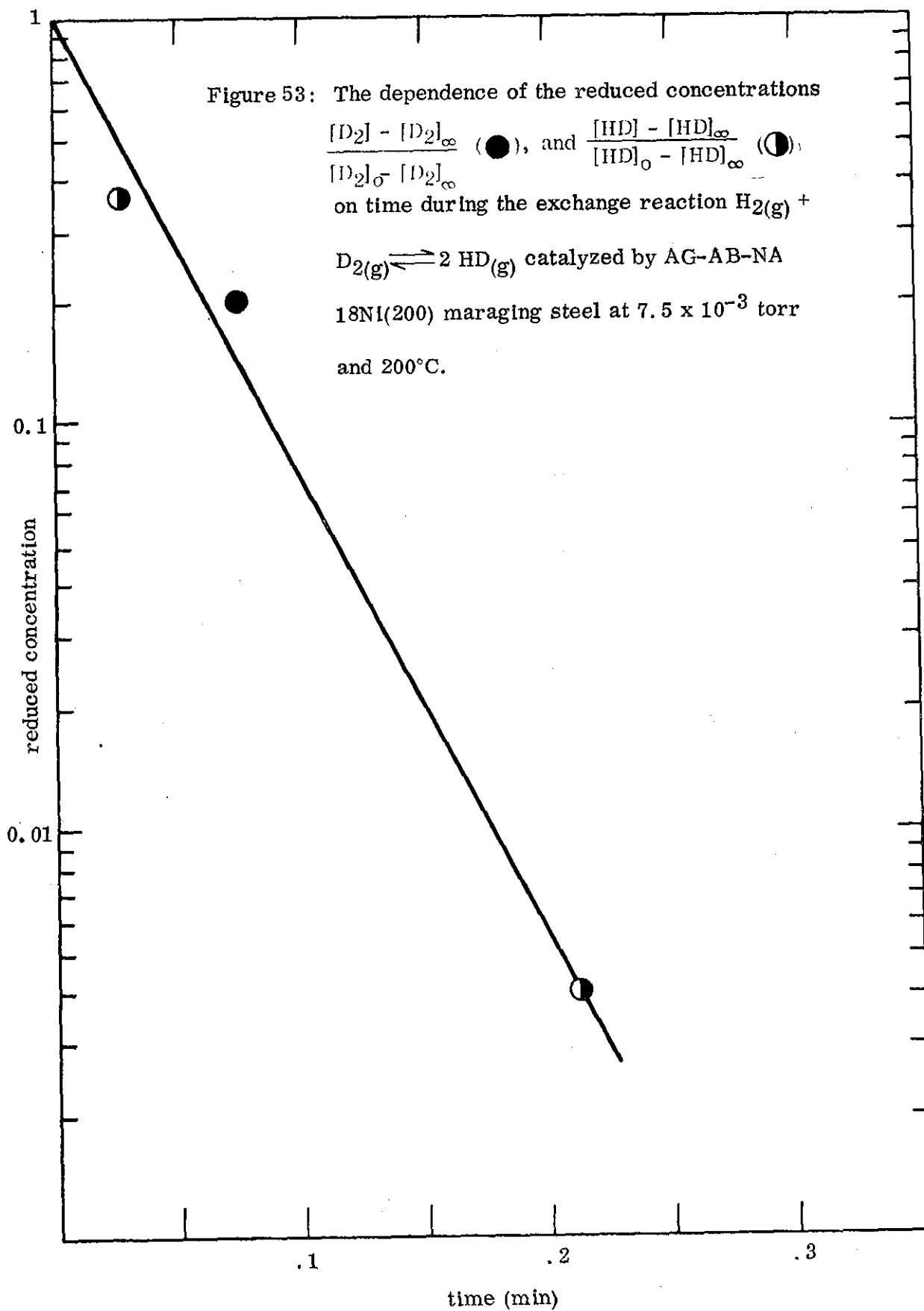


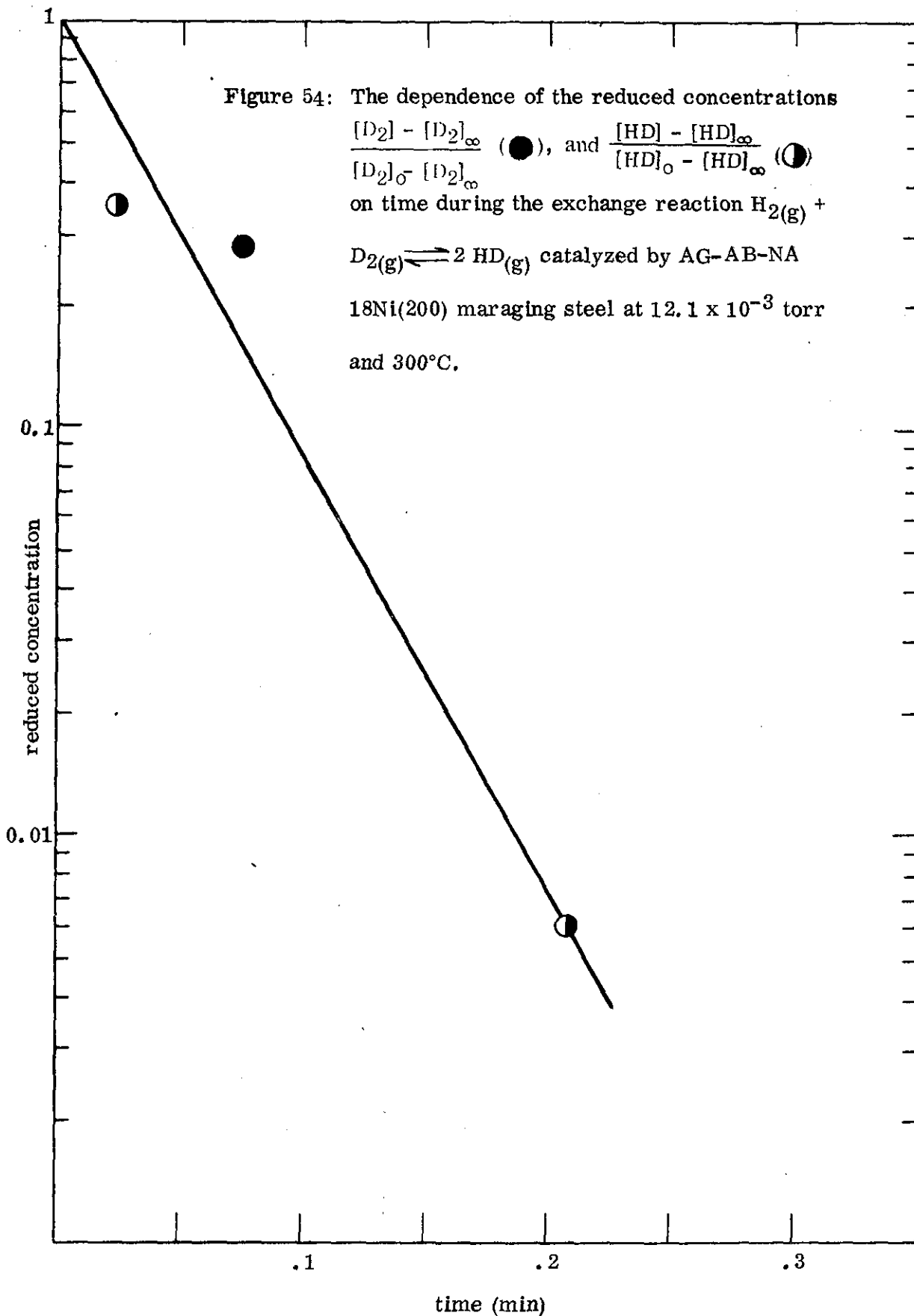


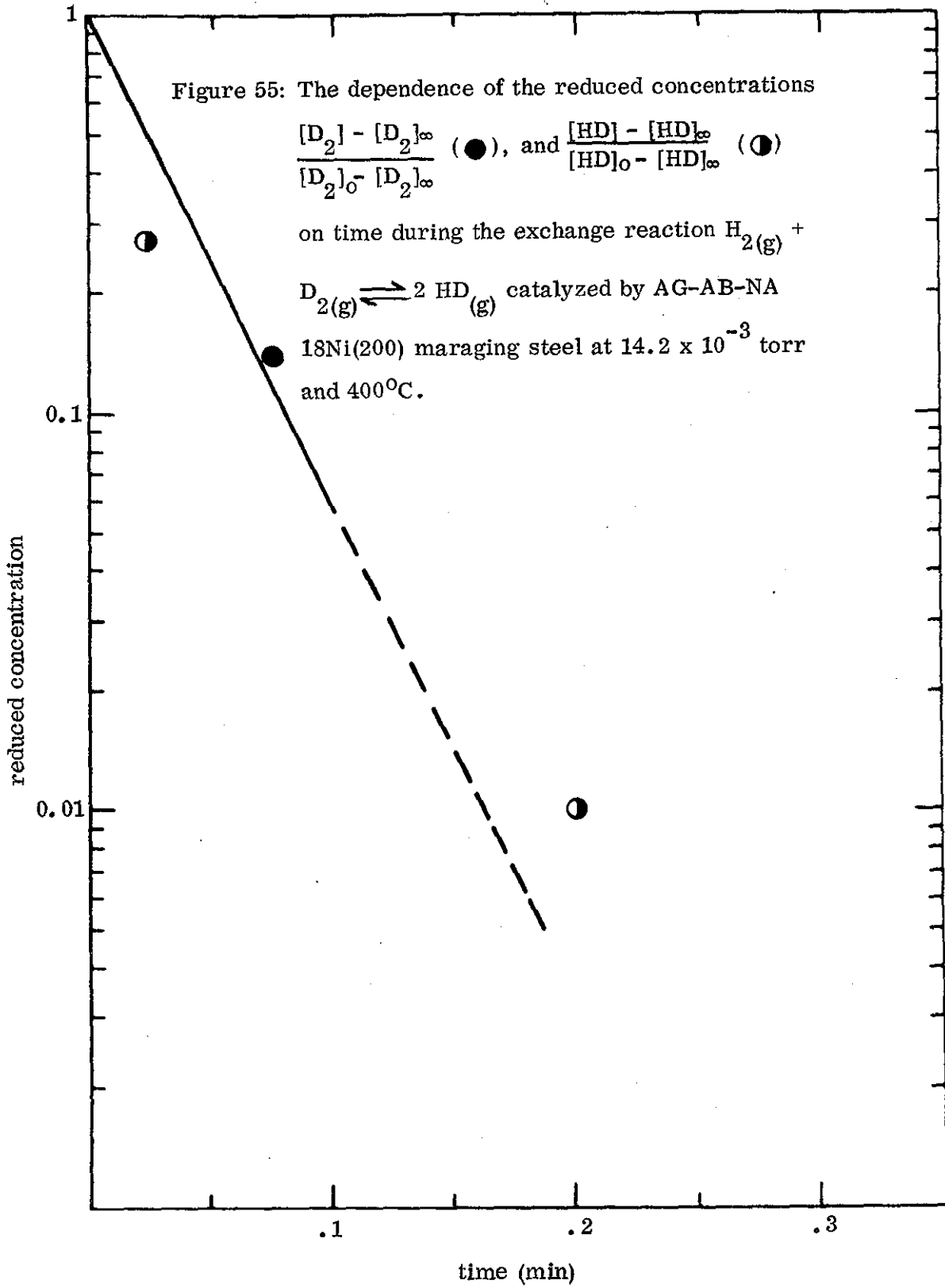


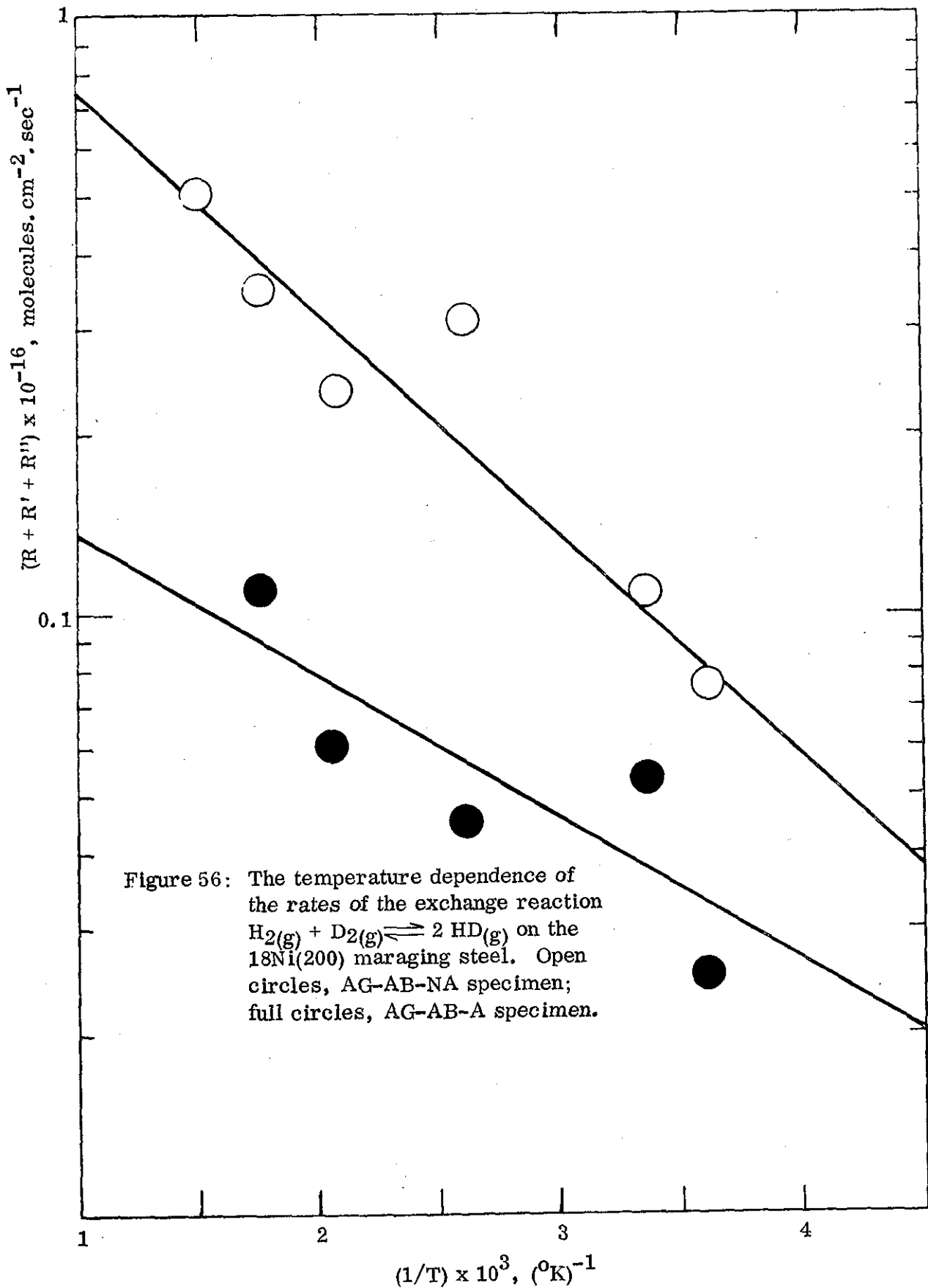


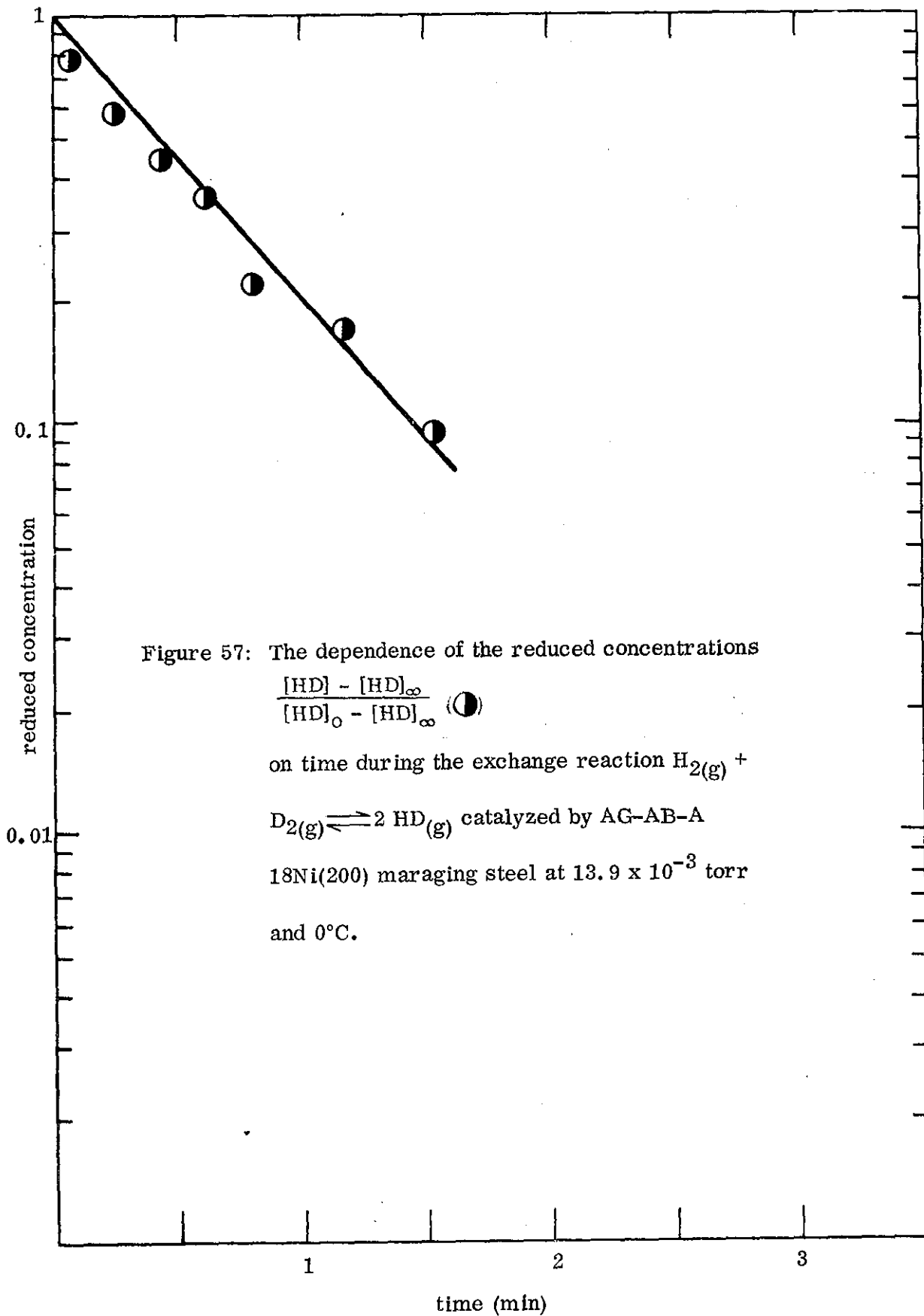












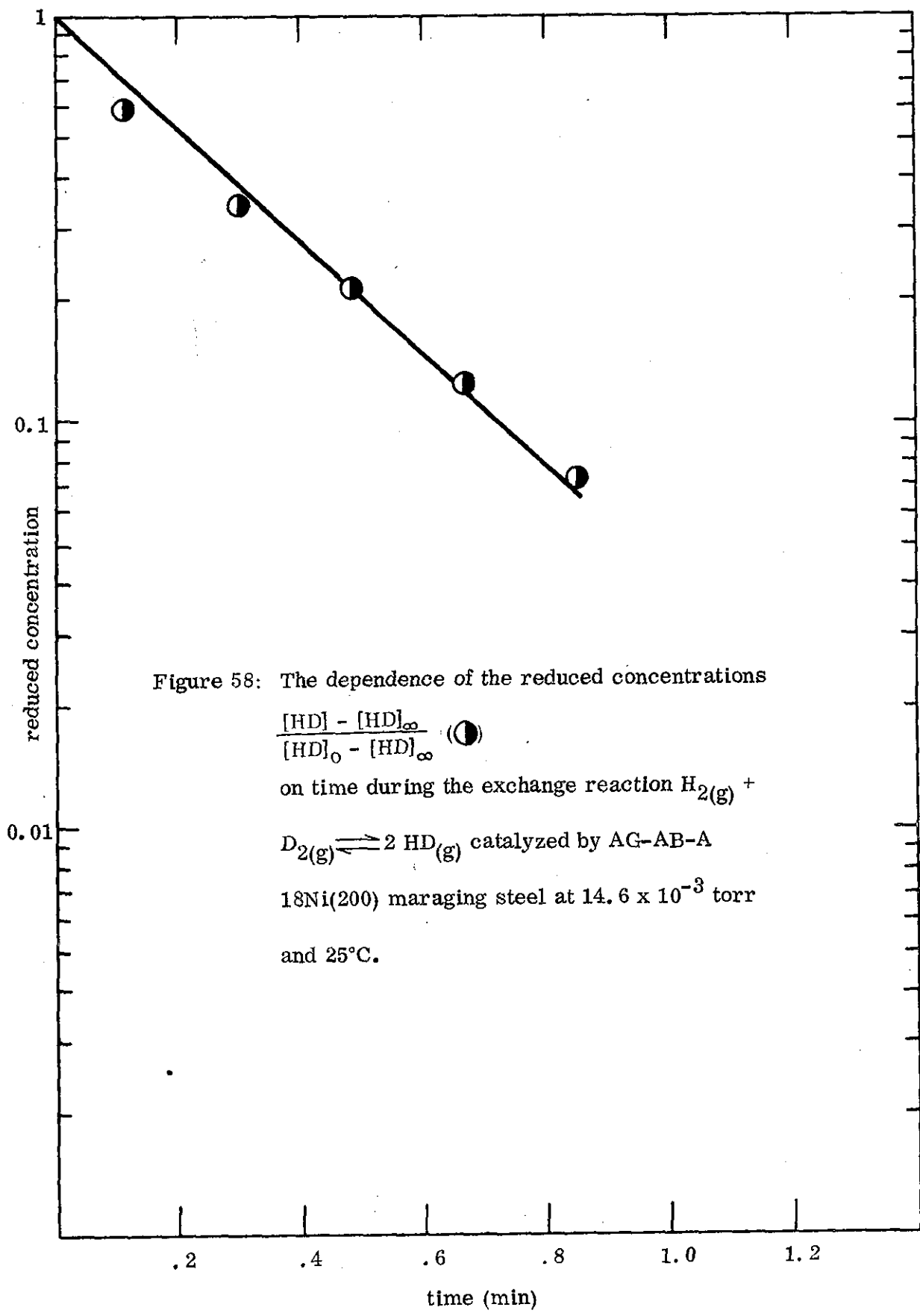
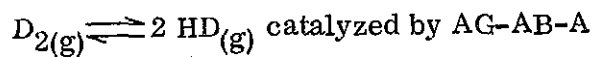


Figure 58: The dependence of the reduced concentrations

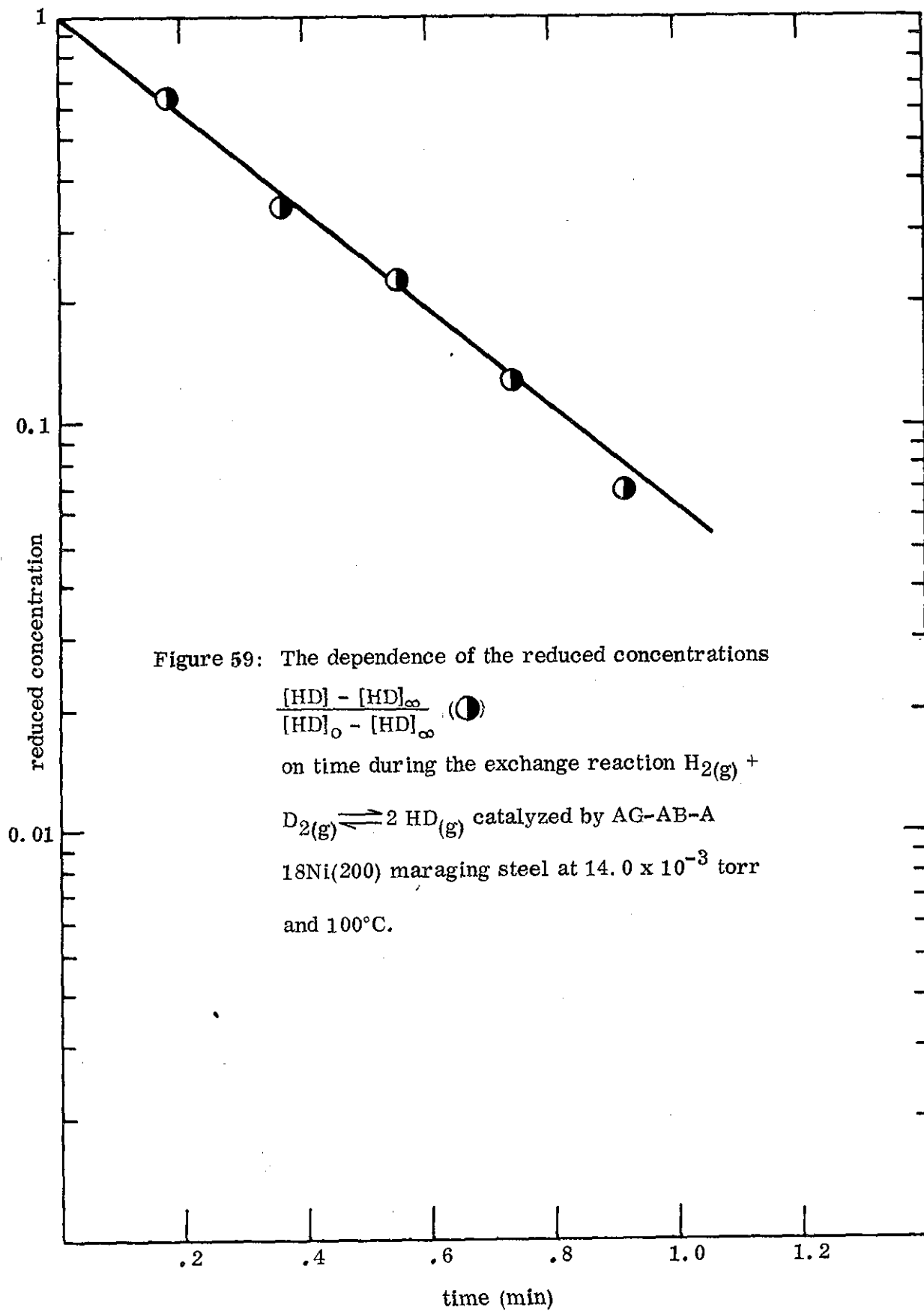
$$\frac{[HD] - [HD]_{\infty}}{[HD]_0 - [HD]_{\infty}} \quad (\bullet)$$

on time during the exchange reaction $H_{2(g)} +$



18Ni(200) maraging steel at 14.6×10^{-3} torr

and 25°C.



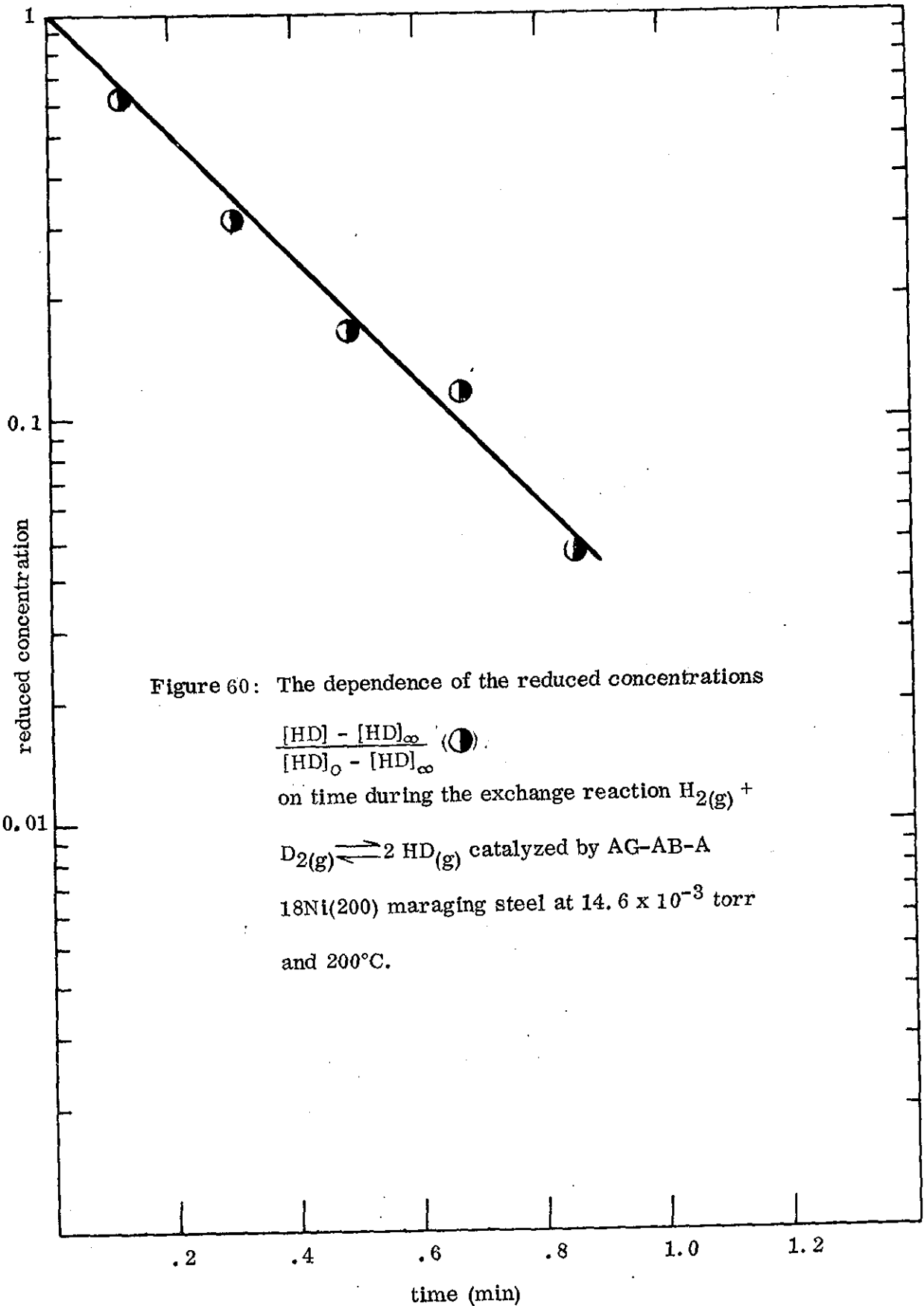
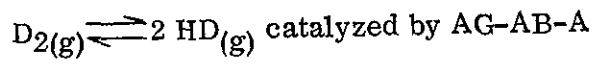


Figure 60: The dependence of the reduced concentrations

$$\frac{[HD] - [HD]_{\infty}}{[HD]_0 - [HD]_{\infty}} \quad (\bullet)$$

on time during the exchange reaction $H_2(g) +$



18Ni(200) maraging steel at 14.6×10^{-3} torr
and 200°C.

